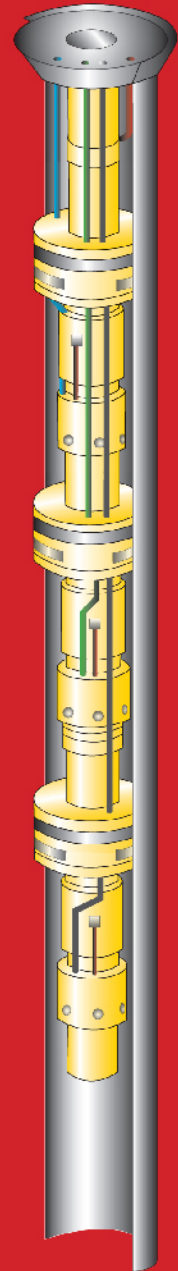
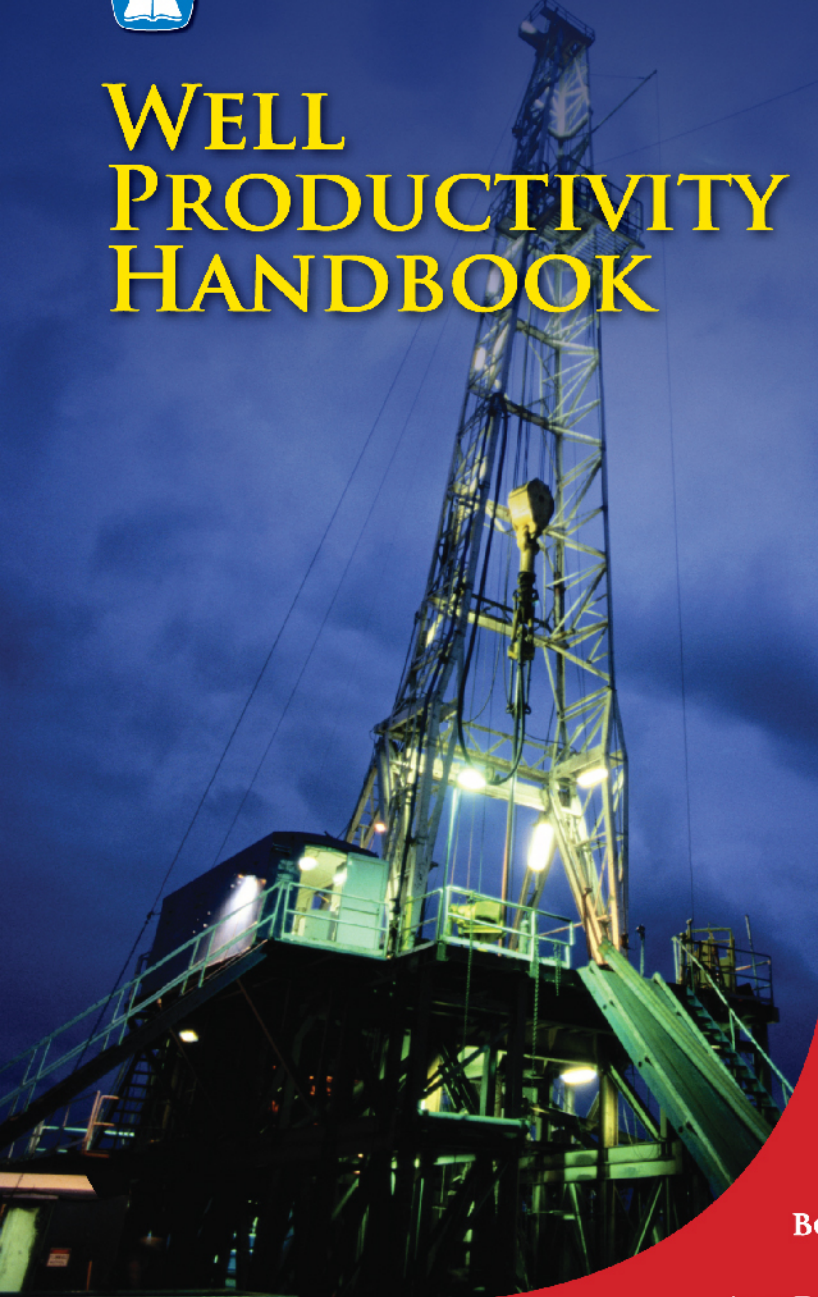




Gulf Publishing Company

WELL PRODUCTIVITY HANDBOOK



BOYUN GUO
KAI SUN
ALI GHALAMBOR

Well Productivity Handbook

**Vertical, Fractured, Horizontal,
Multilateral, and Intelligent Wells**

This page intentionally left blank

Well Productivity Handbook

Vertical, Fractured, Horizontal, Multilateral, and Intelligent Wells

Boyun Guo, Ph.D.

University of Louisiana at Lafayette

Kai Sun

Baker Oil Tools, Inc.

Ali Ghalambor, Ph.D.

University of Louisiana at Lafayette



Well Productivity Handbook: Vertical, Fractured, Horizontal, Multilateral,
and Intelligent Wells

Copyright © 2008 by Gulf Publishing Company, Houston, Texas. All rights reserved. No part of this publication may be reproduced or transmitted in any form without the prior written permission of the publisher.

Gulf Publishing Company
2 Greenway Plaza, Suite 1020
Houston, TX 77046

ISBN-10: 1-933762-32-2
ISBN-13: 978-1-933762-32-6

10 9 8 7 6 5 4 3 2

Library of Congress Cataloging-in-Publication Data in Progress

Guo, Boyun.

Well productivity handbook : vertical, fractured, horizontal, multilateral, and intelligent wells / Boyun Guo, Kai Sun, Ali Ghalambor.

p. cm.

Includes bibliographical references and index.

ISBN 1-933762-32-2 (978-1-933762-32-6 : alk. paper)

1. Oil wells—Handbooks, manuals, etc. 2. Gas wells—Handbooks, manuals, etc. 3. Oil reservoir engineering—Handbooks, manuals, etc. 4. Gas reservoirs—Handbooks, manuals, etc. 5. Petroleum engineering—Handbooks, manuals, etc. 6. Industrial productivity. I. Sun, Kai. II. Ghalambor, Ali. III. Title.

TN871.G7853 2008

622'.338—dc22

2008022304

Printed in the United States of America

Printed on acid-free paper. ∞

Text design and composition by TIPS Technical Publishing, Inc.

This book is dedicated to my wife Huimei for her understanding and encouragement that were as responsible as the experience and knowledge that have been inscribed herein.

—Boyun Guo

This page intentionally left blank

Contents

Preface xi

List of Symbols xv

List of Figures xxiii

List of Tables xxix

1	Introduction	1
1.1	Wells and Reservoirs	1
1.2	Well Productivity	10
1.3	About This Book	11
1.4	Summary	12
1.5	References	12
1.6	Problems	13
2	Properties of Petroleum Fluids	15
2.1	Introduction	15
2.2	Petroleum Fluids	15
2.3	Properties of Oil	16
2.4	Properties of Natural Gas	22
2.5	Properties of Produced Water	39
2.6	Summary	41
2.7	References	41
2.8	Problems	42
3	Properties of Petroleum Reservoirs	45
3.1	Introduction	45
3.2	Lithology	45
3.3	Reservoir Porosity	46
3.4	Reservoir Total Compressibility	47

3.5	Reservoir Permeability	48
3.6	Effective Permeability	50
3.7	Summary	60
3.8	References	60
3.9	Problems	62
4	Reservoir Deliverability	63
4.1	Introduction	63
4.2	Vertical Wells	64
4.3	Fractured Wells	70
4.4	Horizontal Wells	76
4.5	Inflow Performance Relationship (IPR)	77
4.6	Construction of IPR Curves Using Test Points	90
4.7	Composite IPR of Stratified Reservoirs	98
4.8	Predicting Future IPR	106
4.9	Summary	112
4.10	References	113
4.11	Problems	115
5	Wellbore Performance	119
5.1	Introduction	119
5.2	Single-Phase Liquid Flow	120
5.3	Multiphase Flow in Oil Wells	127
5.4	Single-Phase Gas Flow	147
5.5	Mist Flow in Gas Wells	154
5.6	Summary	154
5.7	References	154
5.8	Problems	157
6	Productivity of Wells with Simple Trajectories	161
6.1	Introduction	161
6.2	Principles of Well Productivity Analysis	161
6.3	Deliverability of Vertical Wells	162
6.4	Deliverability of Fractured Wells	185
6.5	Deliverability of Horizontal Wells	189

6.6	Summary	202
6.7	References	204
6.8	Problems	206
7	Productivity of Wells with Complex Trajectories	217
7.1	Introduction	217
7.2	Multi-Fractured Horizontal Wells	217
7.3	Multilateral Wells	226
7.4	Summary	241
7.5	References	241
7.6	Problems	242
8	Productivity of Intelligent Well Systems	247
8.1	Introduction	247
8.2	IWS Description	247
8.3	Performance of Down-Hole Flow Control Valves	257
8.4	Well Deliverability	292
8.5	Summary	305
8.6	References	308
A.	Unit Conversion Factors	313
B.	Minimum Performance Properties of API Tubing	315
C.	Mathematical Model for Obtaining Oil Rate Correction Factor F_o	321
C.1	Reference	323
D.	Mathematical Model for Obtaining Gas Rate Correction Factor F_g	325
D.1	Reference	328
	Index	329

This page intentionally left blank

Preface

Advances in digital computing technology in the past thirty years have revolutionized the petroleum industry. Computer reservoir simulation has become a must-have tool for planning oil and gas field development for all types and sizes of petroleum reservoirs. Several new types of wells with complex completions have been developed and used in the industry in the past decade, and all reservoir simulators require that representative well models be coded to simulate well production accurately. During several years of teaching professional and academic petroleum engineering courses, the authors realized that there is a real need for a book that documents the productivity models of both traditional and new well types. This motivated us to write this book.

This book is written primarily for reservoir and production engineers, and college students at senior and graduate levels. It is not the authors' intention to simply duplicate general information that can be found elsewhere. This book gathers the authors' experience gained through years of teaching production engineering and reservoir simulation courses in the petroleum industry and at the university level. The mission of the book is to provide reservoir and production engineers with a handy reference for modeling oil and gas production wells with simple and complex completions. The original manuscript of this book has been used as a petroleum engineering textbook for undergraduate and graduate students in Petroleum Engineering programs.

This book is intended to cover the full scope of the productivity of naturally flowing wells, with all types of completions. But the well inflow models presented here are also valid for wells that require artificial lift. Following a sequence from simple to complex well completions, this book presents its contents in eight chapters:

- Chapter 1 presents an introduction to petroleum production wells.
- Chapter 2 outlines methods for estimating fluid properties that are essential for analyzing oil and gas production wells.

- Chapter 3 addresses issues related to estimation of reservoir properties that are important for modeling of inflow performance of wells.
- Chapter 4 discusses modeling of inflow performance of wells producing different types of fluids.
- Chapter 5 presents and illustrates different mathematical models for describing wellbore/tubing performance when delivering single or multiphase production fluid.
- Chapter 6 describes the principle of well productivity analysis and shows how to predict productivity of wells with simple trajectories.
- Chapter 7 demonstrates methods for predicting productivity of wells with complex trajectories.
- Chapter 8 presents productivity of wells with intelligent completions.

Because the substance of this book is virtually boundless in depth, knowing what to omit was the greatest difficulty with its editing. The authors believe that it would require many books to fully cover the basics of well productivity modeling. To counter any deficiency that might arise from space limitations, the book contains a list of reference books and papers at the end of each chapter, so that readers should experience little difficulty in pursuing each topic beyond the presented scope.

Regarding presentation, this book focuses on presenting and illustrating the engineering principles used for well productivity modeling rather than covering in-depth theories. The derivation of mathematical models is beyond the scope of this book. Applications are illustrated by solving sample problems using computer spreadsheet programs except for very simple problems. All the computer programs are provided with the book. Although the U.S. field units are used in the text, the option of using SI units is provided in the computer spreadsheet programs.

This book is based on numerous documents, including reports and papers accumulated through years of industry and academic work by the authors. We are grateful to the University of Louisiana at Lafayette and to Baker Oil Tools, Inc., for permission to publish their material. Special thanks are due to Chevron Corporation for providing Chevron I and Chevron II professorships during the editing of this book. Our thanks are also due to Dr. Baojun Bai of the University of Missouri at Rola, who made a thorough

review of this book. On the basis of our collective experience, we expect this book to be of value to reservoir and production engineers in the petroleum industry.

—Boyun Guo, Ph.D.
January 18, 2008
Lafayette, Louisiana

This page intentionally left blank

List of Symbols

- A = cross-sectional area for fluid flow, or drainage area
- A_{in} = choke port area
- $^{\circ}API$ = API gravity of stock tank oil
- A_1 = upstream hydraulic flow area
- A_2 = downstream hydraulic flow area
- B_o = formation volume factor of oil
- B_g = formation volume factor of gas
- B_w = formation volume factor of water
- c = polytropic constant
- C_A = drainage area shape factor
- c_d = choke discharge coefficient
- c_L = specific heat of liquid
- c_t = total compressibility
- c_p = specific heat of gas at constant pressure
- C_v = control valve coefficient
- c_v = specific heat of gas at constant volume
- c_{vg} = gas heat capacity at constant volume
- c_{vo} = oil heat capacity at constant volume
- c_{vw} = water heat capacity at constant volume
- C_d = drag coefficient
- D = inner diameter in feet, or non-Darcy flow coefficient

d = inner diameter

d_{choke} = choke port ID

D_H = hydraulic diameter

d_h = equivalent diameter of the drain hole

$D\rho v$ = inertial force

d_1 = upstream hydraulic ID

E_k = kinetic energy per unit volume of gas

E_{km} = minimum required kinetic energy

F_{CD} = fracture conductivity

f_F = Fanning friction factor

F_g = correction factor for gas production rate

f_M = Darcy-Wiesbach (Moody) friction factor

F_o = correction factor for oil production rate

f_{2F} = two-phase friction factor

g = gravitational acceleration

g_c = gravitational conversion factor

G_2 = mass flux at downstream

h = pay zone thickness

I_{ani} = anisotropy index

J = productivity index

J^* = productivity index at and above bubble-point

J_o = productivity index of non-fractured well

k = effective horizontal permeability, or heat specific ratio

k_f = fracture permeability

k_H = horizontal permeability

k_V = vertical permeability

L = length

- ΔL = length change
- M = liquid mass flow rate
- m_i = mass flow rate from/into layer i
- M_{G2} = gas phase mass flow rate at downstream
- M_{L2} = liquid phase mass flow rate at downstream
- m_t = total mass flow rate
- M_w = molecular weight of gas
- m_{wh} = mass flow rate at wellhead
- M_2 = mixture mass flow rate at downstream
- n = polytropic exponent for gas
- N_D = pipe diameter number
- N_L = liquid viscosity number
- N_{Re} = Reynolds number
- N_{Vg} = gas velocity number
- N_{vL} = liquid velocity number
- p = pressure
- p_a = atmospheric pressure
- p_b = oil bubble-point pressure
- p_{dst} = downstream pressure
- p_e = reservoir pressure
- p_{hf} = wellhead flowing pressure
- p_i = initial reservoir pressure
- P_{kf} = pressure at kick-out point
- p_L = average pressure in the inner region
- p_m = pressure at the mid-depth
- P_{outlet} = pressure at choke outlet
- P_{pr} = pseudoreduced pressure

- p_{sc} = standard pressure
 P_{up} = upstream pressure
 p_{wf} = flowing bottom-hole pressure
 p_{wH} = pressure at the heel of drain hole
 \bar{p} = reservoir pressure
 Δp = pressure increment
 P_1 = pressure at point 1
 P_2 = pressure at point 2
 p_1 = upstream pressure
 p_2 = downstream pressure
 q = liquid flow rate
 q_g = gas production rate
 Q_{gpm} = liquid flow rate
 q_{gmin} = minimum gas flow rate
 q_i = flow rate from/into layer i
 q_o = critical oil rate
 q_s = sand production rate
 q_w = water production rate
 R = universal gas constant
 r_e = radius of drainage area of vertical well
 r_{eH} = radius of drainage area of horizontal well
 r_L = equivalent radius of the inner region
 R_s = solution gas-oil ratio
 r_w = wellbore radius
 S = skin factor
 S_o = skin factor of the non-fractured well
 T = temperature in °R

-
- t = temperature in °F
- T_{av} = average temperature
- T_{pr} = pseudoreduced temperature
- T_{sc} = standard temperature
- T_{up} = upstream gas temperature
- u = fluid velocity
- u_m = mixture velocity
- u_{SG} = superficial velocity of gas phase
- u_{SL} = superficial velocity of liquid phase
- u_1 = mixture fluid velocity at upstream
- u_2 = mixture fluid velocity at downstream
- V = volume of the pipe segment
- V_{G1} = upstream gas specific volume
- V_{G2} = downstream gas specific volume
- V_{gas} = gas volume in standard condition
- V_L = upstream liquid specific volume
- V_{oil} = oil volume in stock tank condition
- V_{sc} = gas volume in standard condition
- v_{sl} = terminal slip velocity
- V_{st} = oil volume in stock tank condition
- w = fracture width
- x_g = free gas in-situ quality at upstream
- x_o = oil in-situ quality at upstream
- x_w = water in-situ quality at upstream
- x_f = fracture half-length
- x_1 = free gas quality at upstream
- y = downstream-to-upstream pressure ratio

- y_a = actual downstream-to-upstream pressure ratio
 y_b = distance of boundary from drain hole
 y_c = critical downstream-to-upstream pressure ratio
 y_e = half drainage length perpendicular to horizontal wellbore
 y_L = liquid holdup
 z = gas compressibility factor
 \bar{z} = average gas compressibility factor
 z_e = half of the distance between fractures
 z_{up} = upstream gas compressibility factor
 Δz = elevation change
 β = upstream-downstream fluid velocity ratio
 ε = relative roughness
 ϕ = porosity
 γ = specific gravity of the liquid relative to water
 γ_g = gas specific gravity
 γ_o = oil specific gravity
 γ_s = specific gravity of produced solid
 γ_w = water specific gravity
 ρ = fluid density
 $\bar{\rho}$ = average mixture density
 ρ_{air} = density of air
 ρ_g = gas density
 ρ_{G1} = upstream gas density
 ρ_{G2} = downstream gas density
 ρ_i = density of fluid from/into layer i
 ρ_L = liquid density
 ρ_{m2} = mixture density

ρ_o = oil density

$\rho_{o,st}$ = density of stock tank oil

ρ_w = water density

ρ_{wh} = density of fluid at wellhead

$\Delta\rho$ = density difference

ρ_1 = mixture density at top of tubing segment

ρ_2 = mixture density at bottom of segment

λ = parameter group

σ = liquid-gas interfacial tension

μ = fluid viscosity

μ_G = gas viscosity

$\bar{\mu}_g$ = average gas viscosity

μ_J = Joule-Thomson coefficient

μ_L = liquid viscosity

μ_o = oil viscosity

This page intentionally left blank

List of Figures

- Figure 1–1 A naturally flowing well produces oil and gas by its own pressure. 2
- Figure 1–2 The hydrocarbon phase diagram shows how the liquid or gas phases of hydrocarbons are related to temperature and pressure. 3
- Figure 1–3 In a water-drive reservoir, pressure exerted at the water-oil contact (WOC) forces the oil up and toward the wellbore. 4
- Figure 1–4 In a gas-cap drive reservoir, pressure is exerted on the oil by the overlying gas cap, forcing it toward and into the wellbore. 5
- Figure 1–5 In a dissolved-gas drive reservoir, production pressure comes from the gas that emerges from the oil when reservoir pressure falls below the bubble point. 6
- Figure 1–6 A typical flowing oil well requires specific equipment from the bottom of the wellbore to the producing wellhead. 7
- Figure 1–7 The wellhead is the link between casing and tubing within the wellbore and the surface production equipment. 8
- Figure 1–8 A “Christmas Tree” is used to regulate well fluid flow passively, through surface chokes, or actively, through valves. 9
- Figure 1–9 Either wellhead or down-hole chokes can be used to regulate well fluid flow. 10
- Figure 2–1 A typical hydrocarbon phase diagram. 17
- Figure 3–1 Typical relative permeability data for a water-gas system. 51

- Figure 3–2 Parameters for a horizontal wellbore. 53
- Figure 3–3 Measured bottom-hole pressures and oil production rates during a pressure draw-down test. 58
- Figure 3–4 Log-log diagnostic plot of test data. 58
- Figure 3–5 Semi-log plot for vertical radial flow analysis. 59
- Figure 3–6 Square-root time plot for pseudo-linear flow analysis. 59
- Figure 3–7 Semi-log plot for horizontal pseudo-radial flow analysis. 61
- Figure 3–8 Model-match to the measured pressure response. 61
- Figure 4–1 A reservoir model illustrating radial flow: (a) lateral view, (b) top view. 65
- Figure 4–2 A reservoir model illustrating a constant-pressure boundary. 68
- Figure 4–3 Pressure and flow conditions of a reservoir with no-flow boundaries. 68
- Figure 4–4 Shape factors for closed drainage areas with low-aspect ratios. 70
- Figure 4–5 Shape factors for closed drainage areas with high-aspect ratios. 71
- Figure 4–6 An example of reservoir pressure distribution near a long fracture. 75
- Figure 4–7 A typical IPR curve for an oil well. 78
- Figure 4–8 Transient IPR curve for Sample Problem 4-2. 82
- Figure 4–9 Steady-state IPR curve for Sample Problem 4-2. 82
- Figure 4–10 Pseudosteady-state IPR curve for Sample Problem 4-2. 83
- Figure 4–11 IPR curve for Sample Problem 4-3. 87
- Figure 4–12 Generalized Vogel IPR model for partial two-phase reservoirs. 88

- Figure 4–13 IPR curve for Sample Problem 4-4. 91
- Figure 4–14 IPR curves for Sample Problem 4-5, Well A. 93
- Figure 4–15 IPR curves for Sample Problem 4-5, Well B. 94
- Figure 4–16 IPR curves for Sample Problem 4-6. 98
- Figure 4–17 IPR curves of individual oil-bearing strata. 104
- Figure 4–18 Composite IPR curve for all strata open to flow. 105
- Figure 4–19 IPR curves for Sample Problem 4-8. 109
- Figure 4–20 IPR curves for Sample Problem 4-9. 113
- Figure 5–1 Parameters used to characterize flow along a tubing string. 121
- Figure 5–2 Darcy-Wiesbach friction factor diagram. 123
- Figure 5–3 Pressure profile given by the spreadsheet program HagedornBrownCorrelation.xls for Sample Problem 5-5. 147
- Figure 5–4 Calculated tubing pressure profile for Sample Problem 5-6. 151
- Figure 6–1 IPR and TPR curves given by the spreadsheet program Transient Production Forecast.xls. 164
- Figure 6–2 IPR and TPR curves given by the spreadsheet program Pseudosteady-2Phase Production Forecast.xls. 167
- Figure 6–3 IPR and TPR curves given by the spreadsheet program Steady-2Phase Production Forecast.xls. 169
- Figure 6–4 IPR and TPR curves given by the spreadsheet program Dry Gas Production Forecast.xls. 174
- Figure 6–5 Curves given by the spreadsheet program Pseudosteady Production of Single-Fractured Well.xls. 188
- Figure 6–6 Curves given by the spreadsheet program Pseudosteady-2Phase Horizontal Well Production Forecast.xls. 193
- Figure 6–7 Calculated annular pressure distributions with and without ICD installations. 199

- Figure 6–8 Calculated oil influx distributions with and without ICD installations. 199
- Figure 6–9 Curves given by the spreadsheet program Horizontal Dry Gas Well Production Forecast.xls. 203
- Figure 7–1 A reservoir section drained by a multi-fractured horizontal wellbore. 219
- Figure 7–2 Fluid flow in a fracture to a horizontal wellbore. 219
- Figure 7–3 Curves given by spreadsheet program Pseudosteady Production of Multi-Fractured Well.xls. 224
- Figure 7–4 Schematic of a typical root well. 227
- Figure 7–5 Schematic of a reservoir section drained by a fishbone well. 227
- Figure 7–6 Curves given by the spreadsheet program Pseudosteady Production of Fishbone Oil Well.xls. 232
- Figure 7–7 A simplified multilateral well structure. 235
- Figure 7–8 Symbols used to describe a multilateral well. 235
- Figure 8–1 Intelligent well system components. 248
- Figure 8–2 Cash flow profile of IWS versus conventional. 249
- Figure 8–3 Single tubing string with selective control of production/injection in multiple zones. 251
- Figure 8–4 Single tubing string with selective control of production/injection in multi-laterals. 252
- Figure 8–5 Flow paths of a two-lateral IWS production well with shroud-unshroud valve configuration. 253
- Figure 8–6 Flow direction in shrouded control valve. 253
- Figure 8–7 Intelligent completion with sand control to selectively control production in multiple zones. 254
- Figure 8–8 Intelligent completion with Electric Submerge Pump (ESP) to selectively control production in multiple zones/laterals. 255

- Figure 8–9 Intelligent completion utilizing in-situ gas zone for auto-gas-lift. 256
- Figure 8–10 Intelligent completion utilizing in-situ water zone for dump-flooding. 257
- Figure 8–11 Down-hole control valve at fixed-open position. 259
- Figure 8–12 Down-hole control valve at fixed-open position. 259
- Figure 8–13 Typical choke flow performance of a down-hole control valve. 261
- Figure 8–14 Typical choke shapes at various open positions. 264
- Figure 8–15 Procedure for calculating free gas quality. 286
- Figure 8–16 A typical two-zone IWS system. 294
- Figure 8–17 Simplified node network of the two-zone IWS system. 296
- Figure 8–18 Integrated IPR of upper zone corresponding to the commingle point with the upper control valve 3% open. 297
- Figure 8–19 Integrated IPR of lower zone corresponding to the commingle point with the lower shrouded control valve 100% open. 298
- Figure 8–20 Combined inflow curve at the commingle point (upper control valve port). 299
- Figure 8–21 Operating point and production allocations. 299
- Figure 8–22 Determination of operating point using the integrated IPR approach. 303
- Figure 8–23 Flow contributions at the operating point (upper valve 1.4%, lower valve 100%, WHP 8000psi). 304
- Figure 8–24 Wellbore flowing pressure profile at the recommended operating point. 304
- Figure 8–25 Wellbore flowing temperature profile at the recommended operating point. 306

- Figure 8–26 Wellbore flowing velocity profile at the recommended operating point. 306
- Figure 8–27 Flow contributions with both valves 100% open (WHP 8800 psi). 307
- Figure 8–28 The effect of choking operations on liquid production contributions from individual zones. 307
- Figure 8–29 The effect of choking operation on oil contributions from individual zones. 308

List of Tables

Table 2–1	Composition of a Typical Petroleum Fluid.....	16
Table 2–2	Results Given by the Spreadsheet Program OilProperties.xls.....	23
Table 2–3	Results Given by the Spreadsheet Program MixingRule.xls.....	26
Table 2–4	Results Given by the Spreadsheet Program Carr-Kobayashi-Burrows-GasViscosity.xls.....	31
Table 2–5	Results Given by the Spreadsheet Program Brill-Beggs-Z.xls.....	34
Table 2–6	Results Given by the Spreadsheet Program Hall-Yarborough-z.xls	37
Table 4–1	Summary of Test Points for Eight Oil-Bearing Layers.....	104
Table 4–2	Comparison of Commingled and Strata-Grouped Productions.....	105
Table 5–1	Results given by Spreadsheet Program Poettmann- CarpenterBHP.xls for Sample Problem 5-3.....	133
Table 5–2	Results given by Spreadsheet Program Guo- GhalamborBHP.xls for Sample Problem 5-4.....	137
Table 5–3	Result Given by Spreadsheet Program HagedornBrownCorrelation.xls for Sample Problem 5-5.....	144
Table 5–4	Spreadsheet Program AverageTZ.xls—Data Input and Result Sections	150
Table 5–5	Spreadsheet Program Cullender-Smith.xls— Data Input and Result Sections	155

Table 6–1	Data Given by the Spreadsheet Program Transient Production Forecast.xls	164
Table 6–2	Data Generated by the Spreadsheet Program Pseudosteady-2Phase Production Forecast.xls	166
Table 6–3	Data Given by the Spreadsheet Program Steady-2Phase Production Forecast.xls	169
Table 6–4	Data Given by the Spreadsheet Program Dry Gas Production Forecast.xls	173
Table 6–5	Data Given by the Spreadsheet Program Wet Gas Pseudosteady Production Forecast.xls	176
Table 6–6	Result Given by the Spreadsheet Program TurnerLoading.xls	179
Table 6–7	Results Given by the Spreadsheet Program GasWellLoading.xls	185
Table 6–8	Data Given by the Spreadsheet Program Pseudosteady Production of Single-Fractured Well.xls	187
Table 6–9	Data Given by the Spreadsheet Program Fractured Gas Well Production Forecast.xls	190
Table 6–10	Data Given by the Spreadsheet Program Pseudosteady- 2Phase Horizontal Well Production Forecast.xls	193
Table 6–11	Designed ICD Locations and Sizes	200
Table 6–12	Data Given by the Spreadsheet Program Horizontal Dry Gas Well Production Forecast.xls	203
Table 7–1	Results Given by Spreadsheet Program Pseudosteady Production of Fishbone Gas Well.xls	234
Table 7–2	Reservoir Property Data	238
Table 7–3	Fluid Property Data	239
Table 7–4	Well Data for Vertical Sections	239
Table 7–5	Well Data for Curved Sections	240
Table 7–6	Well Data for Horizontal Sections	240

Table 7-7	Summary of Calculated Lateral and Well Production Rates.....	241
Table 8-1	Fluid Property Data.....	287
Table 8-2	Reservoir and Production Target Data.....	301
Table 8-3	Completion String and Reservoir/Operation Data of a Full Wellbore Model.....	302

This page intentionally left blank

Introduction

1.1 Wells and Reservoirs

Oil and gas wells are used for extracting crude oil and natural gas from oil and gas reservoirs. There are three types of wells: oil, gas condensate, and gas. Their classification depends on the producing gas-oil ratio (GOR). Gas wells produce at a GOR greater than 100,000 scf/stb; condensate wells produce at a GOR less than 100,000 scf/stb but greater than 5,000 scf/stb; and oil wells produce at a GOR less than 5,000 scf/stb. Unit conversion factors for the SI systems are provided in Appendix A.

A naturally flowing well consists of a reservoir segment, wellbore, and wellhead (Figure 1–1).

The reservoir segment supplies the wellbore with production fluids (crude oil and/or natural gas). The wellbore provides a path for the fluids to flow from bottom hole to the surface. The wellhead permits control of the fluid production rate.

An oil or gas reservoir is a single porous and permeable underground rock formation containing an individual bank of fluid hydrocarbons, and confined by impermeable rock or water barriers. It contains a single natural pressure system. An oil or gas field is an underground region consisting of one or more reservoirs, all related to the same structural feature. An oil or gas pool is a more extensive region containing one or more reservoirs, in isolated structures.

Engineers classify oil, gas condensate, and gas reservoirs on the basis of the initial reservoir condition and hydrocarbon composition. An oil that is at a pressure above its bubble point is called an undersaturated oil,

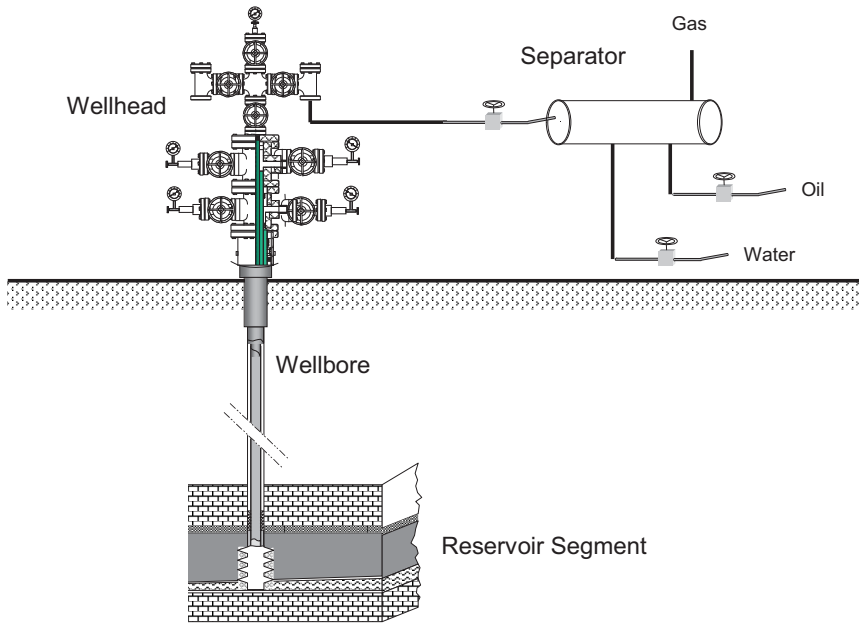


Figure 1–1 A naturally flowing well produces oil and gas by its own pressure.

because it can hold more dissolved gas at any given temperature (Figure 1–2). An oil that is at its bubble-point pressure is called a saturated oil because it can dissolve no more gas at any given temperature. In an undersaturated oil reservoir, single (liquid) phase flow occurs. Two-phase (liquid oil and free gas) flow occurs in a saturated oil reservoir.

Oil reservoirs are further classified on the basis of boundary type, which determines the driving mechanism. The three types of reservoirs are

- Water-drive
- Gas-cap drive
- Dissolved-gas drive

In water-drive reservoirs, the oil zone is connected through a continuous pressure path to a ground water system (aquifer). The pressure due to the water column forces the oil and gas to the top of the reservoir against the impermeable barrier that restricts further migration (the trap boundary). This pressure forces the oil and gas toward the wellbore. Under a constant

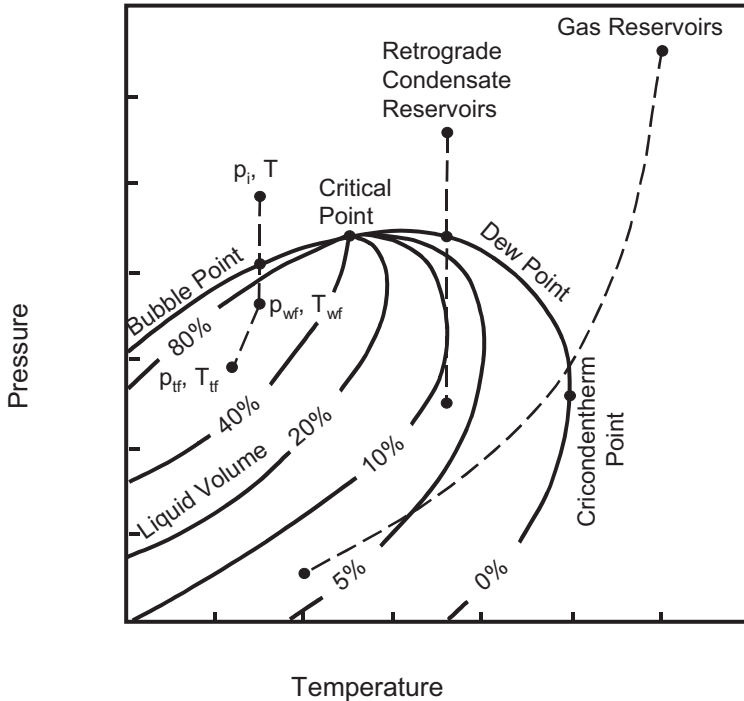


Figure 1–2 The hydrocarbon phase diagram shows how the liquid or gas phases of hydrocarbons are related to temperature and pressure.

oil production rate, an active water-drive reservoir will maintain reservoir pressure longer, compared to other driving mechanisms. Edge-water drive reservoirs are better producers than bottom-water drive reservoirs. The reservoir pressure remains at its initial value above bubble-point pressure for longer, maintaining single-phase liquid flow in the reservoir for maximum productivity. An edge-water drive reservoir can also maintain steady-state flow condition for a significantly longer time before water breakthrough into the well. Bottom-water drive reservoirs are more troublesome because of water-coning problems that affect oil production economics due to water treatment and disposal issues (Figure 1–3).

In gas-cap drive reservoirs, the gas in the gas cap expands and compensates for pressure depletion in the oil zone due to production (Figure 1–4). Thus, the oil below the gas cap will produce naturally, longer. If the gas in the gas cap is extracted early in field development, the reservoir pressure

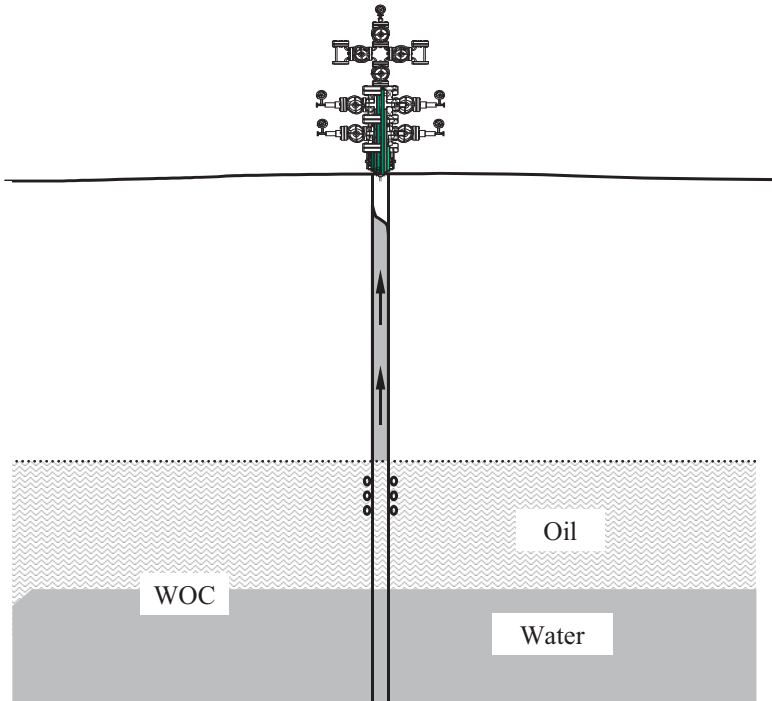


Figure 1–3 In a water-drive reservoir, pressure exerted at the water-oil contact (WOC) forces the oil up and toward the wellbore.

will decrease rapidly. Some oil reservoirs display both water and gas-cap driving mechanisms.

A dissolved-gas drive reservoir is also called a solution-gas drive reservoir (Figure 1–5). The oil reservoir has a fixed volume, bounded by impermeable structures or layers (faults or pinch-outs). In dissolved-gas drive oil reservoirs, the driving mechanism is gas held in solution in the oil (and water, if any). During production, the dissolved gas expands and partially compensates for the inevitable pressure decline in reservoir production. Dissolved-gas drive is a weaker mechanism in a volumetric reservoir than either water-drive or gas-drive. If the reservoir pressure drops to a value below the bubble-point pressure of the oil, gas escapes from the oil, and oil-gas two-phase competing flow begins. This reduces the effective permeability of the reservoir to the oil, increases the viscosity of the remaining oil, and thus reduces well productivity and ultimate oil

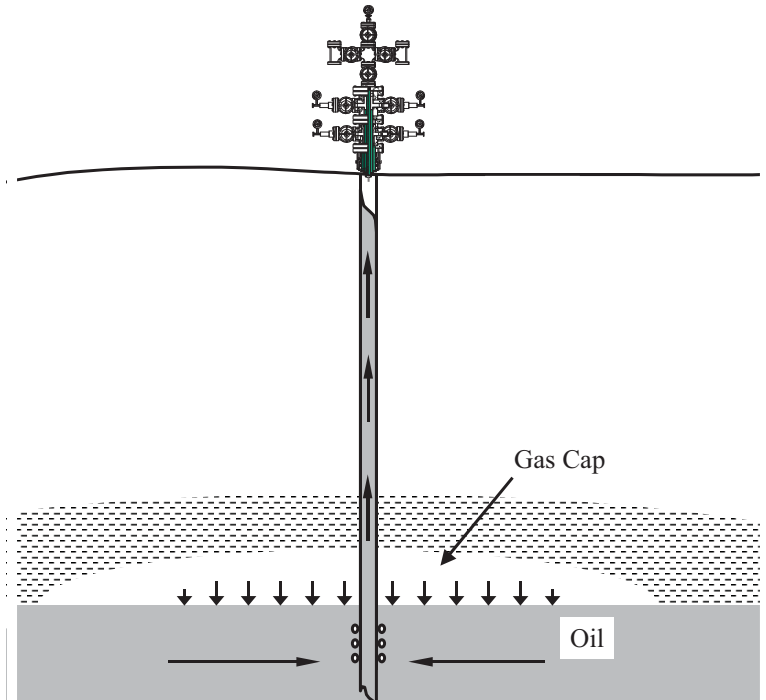


Figure 1–4 *In a gas-cap drive reservoir, pressure is exerted on the oil by the overlying gas cap, forcing it toward and into the wellbore.*

recovery. Early attention to pressure maintenance can increase ultimate oil recovery in the solution-gas drive reservoir.

For a typical oil well that delivers fluids to the surface solely due to the natural pressure of the reservoir, a completed wellbore is composed of casings, tubing, packers, and optional down-hole chokes (Figure 1–6).

A wellbore is like an upside-down telescope. The large diameter borehole section is at the top of the well. Each successive section of the wellbore is cased to the surface using narrower and narrower strings of nested casing. Lastly, a liner is inserted down the well that laps over the last casing at its upper end. Each casing or liner is cemented into the well (usually up to at least where the cement overlaps the previous cement job).

The final casing in the well is the production casing (or production liner). Once this casing has been cemented, production tubing is run down the well. A packer is usually used near the bottom of the tubing to isolate the

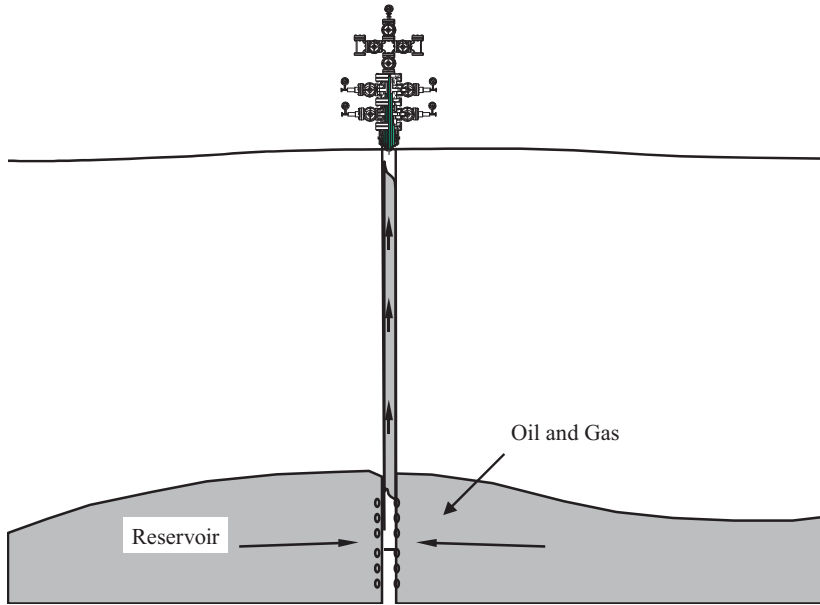


Figure 1–5 *In a dissolved-gas drive reservoir, production pressure comes from the gas that emerges from the oil when reservoir pressure falls below the bubble point.*

annulus between tubing and casing, and to guide the produced fluids into the tubing. Packers can be actuated mechanically or hydraulically. The production tubing is often provided with a bottom-hole choke (particularly during initial well flow) to control the well flow and restrict over-production.

Tubing strings are installed in most production wells. A tubing string provides a good seal and allows gas expansion to help lift the oil to the wellhead. The American Petroleum Institute (API) defines tubing size using nominal diameter and weight-per-foot. The nominal diameter refers to the inside diameter (I.D.) of the tubing. The tubing outside diameter (O.D.) determines the tubing's weight-per-foot. Steel grade used in tubing is designated H-40, J-55, C-75, L-80, N-80, C-90, and P-105, where the numbers represent minimum yield strength in units of 1,000 psi. The minimum performance properties of production tubing are given in Appendix B.

The wellhead is the surface equipment set below the master valve and includes multiple casing heads and a tubing head. A casing head is a

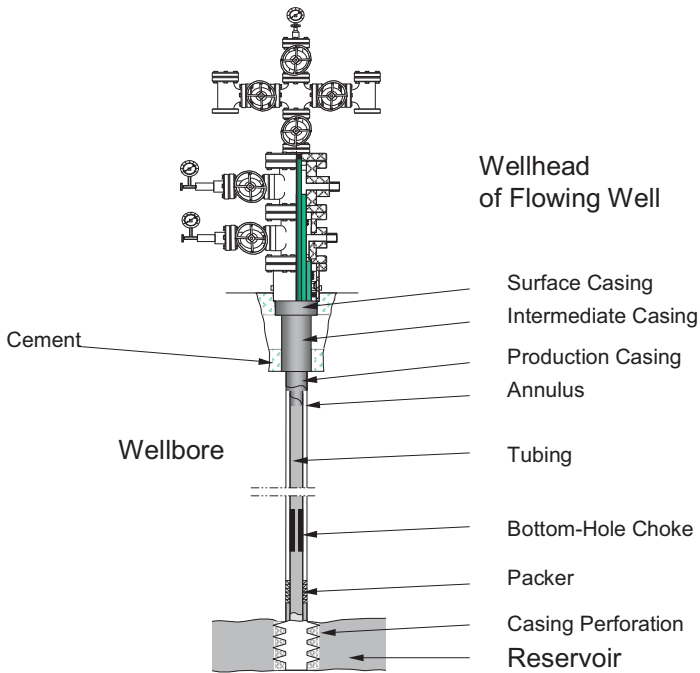


Figure 1-6 A typical flowing oil well requires specific equipment from the bottom of the wellbore to the producing wellhead.

mechanical assembly used for hanging a casing string. The lowermost casing head is threaded, flanged, or studded into the surface casing (Figure 1-7). Depending on the casing programs used during drilling, several casing heads might be installed. The casing head has a bowl which supports the casing hanger, which is threaded into the top of the production casing (or utilizes friction grips to hold the casing). As in the case of the production tubing, the production casing is suspended in tension so that the casing hanger actually supports it down to the freeze point. In a similar manner, the intermediate casings are supported by their respective casing hangers and bowls. The casing heads are all supported by the surface casing, which is in compression and cemented to the surface. A well completed with three casing strings will have two casing heads. The uppermost casing head supports the production casing, while the lowermost casing head is attached to and is supported by the surface casing.

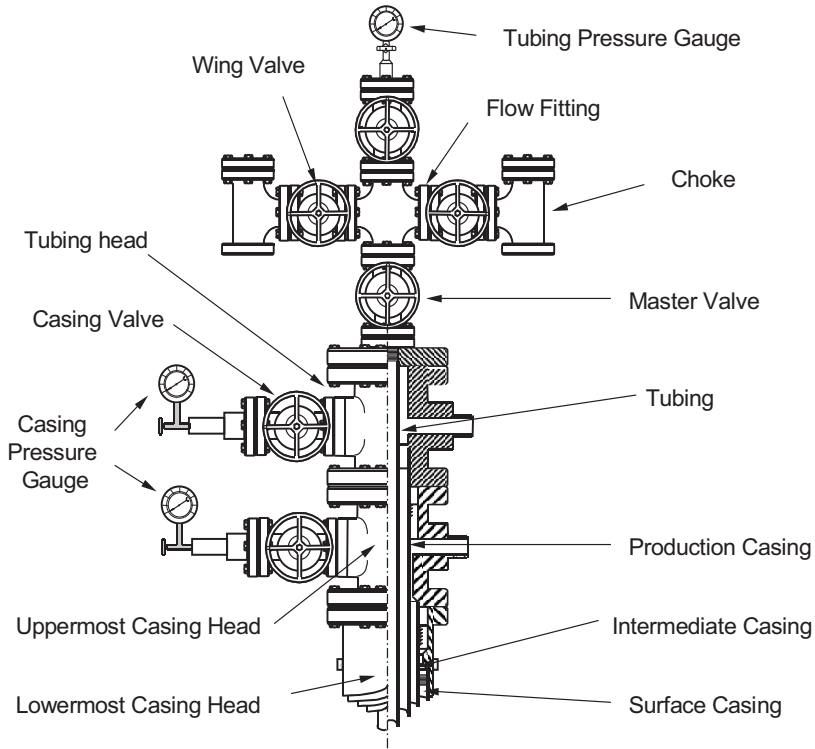


Figure 1-7 *The wellhead is the link between casing and tubing within the wellbore and the surface production equipment.*

The tubing string is supported at the surface by the tubing head, which is supported, in turn, by the production casing head. The tubing string is in tension all the way down to the packer.

The “Christmas Tree” is connected to the tubing head by an adaptor and regulates fluid flow from the well (Figure 1-8). The Christmas Tree may have one flow outlet (a tee) or two flow outlets (a cross). A typical Christmas Tree consists of a master valve, wing valves, and a needle valve, located just below the tubing pressure gauge. The master valve and wing valves can close the well partially or completely when needed, but to replace the master valve itself, the tubing must be plugged. At the top of the “Christmas Tree,” a pressure gauge indicates tubing pressure when the needle valve is open.

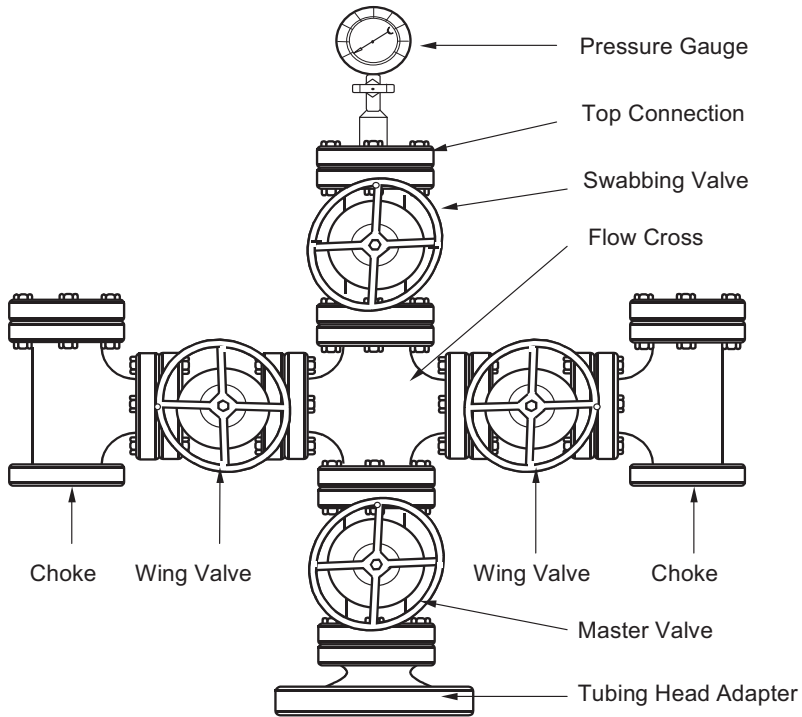


Figure 1–8 A “Christmas Tree” is used to regulate well fluid flow passively, through surface chokes, or actively, through valves.

Surface chokes are restrictions in the flow-line and control the flow rate in their respective lines (Figure 1–9). In most naturally flowing wells, the oil production rate is regulated by changing the choke size. The choke (plus any other restrictions in the flow-line) causes backpressure in the line, which increases the flowing bottom-hole pressure. Increasing this flowing bottom-hole pressure decreases the pressure drawdown from the reservoir to the wellbore, in turn decreasing the fluid production rate of the well.

In some wells, chokes are installed in the lower section of tubing strings. This arrangement reduces wellhead pressure and increases the oil production rate due to gas expansion in the tubing string. For gas wells, the use of down-hole chokes minimizes any gas hydrate problems in the well stream. A major disadvantage of the down-hole choke arrangement is that they are more expensive to replace than those chokes installed in the Christmas Tree.

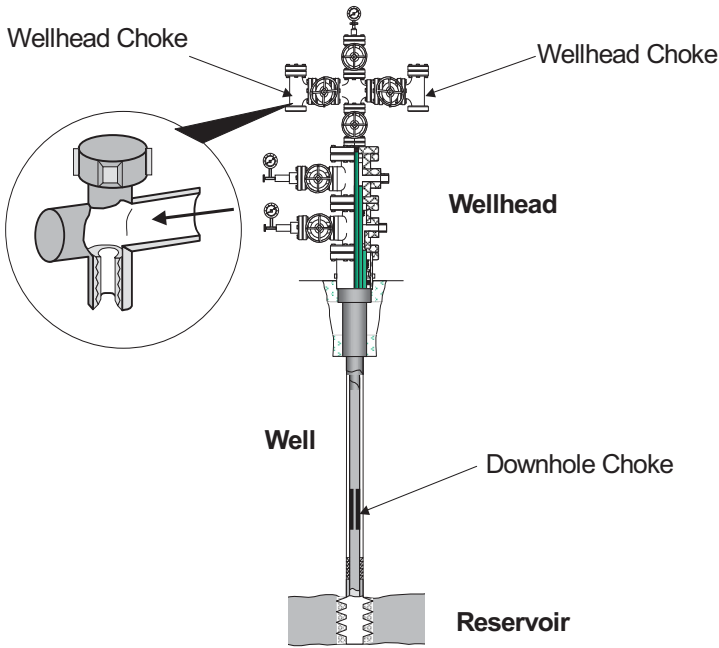


Figure 1–9 *Either wellhead or down-hole chokes can be used to regulate well fluid flow.*

1.2 Well Productivity

The past two decades have seen rapid changes in field development methods. The traditional way to develop oil and gas fields has been to drill and complete vertical wells with specific well spacing chosen to correspond with the properties of the specific oil and gas reservoirs being developed. New technologies in well construction and stimulation introduced over the last 30 years include horizontal well drilling (Joshi 1991), multilateral well drilling (SPE 2002), intelligent wells (Gao et al. 2007), enhanced oil recovery methods (Willhite 1986), and hydraulic fracturing (Economides and Nolte 2000). These newer technologies permit drilling fewer wells to develop oil and gas fields, with lower costs and improved oil and gas recovery.

Numerical reservoir simulators have revolutionized oil and gas field development. A development strategy targeting maximum oil and gas

recovery can be designed using reservoir simulation in a few days to a few weeks. However, reservoir simulators are subject to GIGO (garbage-in, garbage-out). They require realistic well models and reliable input data for the specific reservoir and fluid properties. This book addresses both the well model and input data quality issues and emphasizes the realistic well models that should be used in both reservoir and production simulation.

Reservoir productivity is not the same as well productivity. The former is usually described using the inflow performance relationship (IPR), which predicts the oil or gas production rate at a specified bottom-hole pressure. While reservoir productivity refers to the reservoir's ability to deliver oil and gas to the wellbore, well productivity refers to the production rate of oil or gas by a well against a specified wellhead pressure. Thus the well productivity is the well's ability to deliver oil and gas to the wellhead. Obviously, well productivity is determined by both reservoir productivity and wellbore performance (flow resistance). This book presents well models and productivities of various types of wells at designed wellhead pressures.

For simple well trajectories such as vertical and horizontal wells, NODAL analysis (a Schlumberger patent) can predict well productivity. Although NODAL analysis can be performed using any point in the system as a solution node, it is usually conducted using either the bottom hole or wellhead as the solution node. This is because measured pressure data are normally available at these two points and these data can be used for evaluating the predictions of NODAL analysis. This book illustrates the principle of NODAL analysis using bottom-hole as the solution node where IPR is readily available for predicting the productivities of wells with simple trajectories.

For more complicated well trajectories, such as multilateral wells, an iteration procedure proposed by Guo et al. (2006) can predict well productivity. It uses a trial-and-error method to couple pressures, flow rates, and fluid properties in different wellbore branches, and equipment such as down-hole chokes to estimate oil and gas production at the surface.

1.3 About This Book

This book provides realistic well models to use in reservoir and production simulations. The contents are arranged to make the material useful

for reservoir and production engineers at various levels. Chapters 2 and 3 describe the methods for obtaining fluid and reservoir properties that are necessary for building reservoir and production simulation models. Chapter 4 addresses IPR of wells with simple trajectories, including vertical, fractured, and horizontal wells. Chapter 5 discusses the performance of wellbores with different fluids. The coupling of IPR and wellbore performance for predicting the productivity of wells with simple trajectories is illustrated in Chapter 6. The productivity of wells with complex trajectories is illustrated in Chapter 7. Finally, intelligent well productivity is addressed in Chapter 8.

Although U.S. field units are used throughout the text of this book, all attached spreadsheet programs are coded with both U.S. field units and SI units. Unit conversion factors are presented in Appendix A.

1.4 Summary

This chapter provides an introduction to oil and gas wells and defines the concept of well productivity.

1.5 References

Economides, M. J. and Nolte, K.G.: *Reservoir Stimulation*, John Wiley & Sons Ltd., New York (2000).

Gao, C., Rajeswaran, T., and Nakagawa, E.: "A Literature Review on Smart Well Technology," paper SPE 106011, presented at the SPE Production and Operations Symposium (31 March–3 April 2007), Oklahoma City, OK.

Guo, B., Zhou, J., Ling, K., and Ghalambor, A.: "A Rigorous Composite-IPR Model for Multilateral Wells," paper SPE 100923, presented at the SPE Annual Technical Conference & Exhibition (24–27 September 2006), San Antonio, TX.

Joshi, S.D.: *Horizontal Well Technology*, PennWell Publishing Company, Tulsa, OK (1991).

SPE: *Multilateral Wells Reprint No. 53*, Richardson, Texas (2002).

Willhite, G.P.: *Waterflooding*, SPE, Vol. 3, Richardson, Texas (1986).

1.6 Problems

- 1-1 What are the advantages and disadvantages of using down-hole chokes rather than wellhead chokes?
- 1-2 What do the digits in the tubing specification represent (e.g. H-40, J-55, C-75, L-80, N-80, C-90, and P-105)?

This page intentionally left blank

Properties of Petroleum Fluids

2.1 Introduction

Crude oil, natural gas, and produced water are petroleum fluids, which are characterized by their physical and chemical properties. Understanding these properties is essential for predicting well productivity, which is the subject of this book. This chapter presents definitions of these fluid properties and non-experimental methods for obtaining their values. Applications of the fluid properties appear in the later chapters.

2.2 Petroleum Fluids

Any naturally-occurring petroleum is a fluid mixture of hundreds of different hydrocarbons and a few inorganic compounds. These components exist in gas, liquid, and solid phases. PVT laboratories usually report hydrocarbons as a number of groups, typically less than 20. Table 2–1 summarizes the composition of a typical petroleum fluid. Because methane (C_1), ethane (C_2), propane (C_3), and nitrogen (N_2) are gases at atmospheric and relatively low pressures, and the major component of the fluid mixture defined in the table is methane, this petroleum fluid is considered a natural gas.

Phase changes of a petroleum fluid are characterized by its pseudocritical point, bubble-point pressure locus, dewpoint pressure locus, and grade curves within a phase envelope (Figure 2–1). Petroleum fluids are further characterized by the properties of the oil, its dissolved gas, and the produced water.

Table 2–1 Composition of a Typical Petroleum Fluid

Component	Mole Fraction
C_1	0.775
C_2	0.083
C_3	0.021
$i-C_4$	0.006
$n-C_4$	0.002
$i-C_5$	0.003
$n-C_5$	0.008
C_6	0.001
C_{7+}	0.001
N_2	0.050
CO_2	0.030
H_2S	0.020

2.3 Properties of Oil

Oil properties include its solution gas-oil ratio, density, formation volume factor, viscosity, and compressibility. The latter four properties are inter-related through the first.

2.3.1 Solution Gas-Oil Ratio

The solution gas-oil ratio is the fundamental parameter used to characterize an oil. It is defined as the volume of gas, normalized to standard temperature and pressure (STP), which will dissolve in a unit volume of oil at the prevailing pressure and temperature of the actual reservoir. That is,

$$R_s = \frac{V_{gas}}{V_{oil}} \quad (2.1)$$

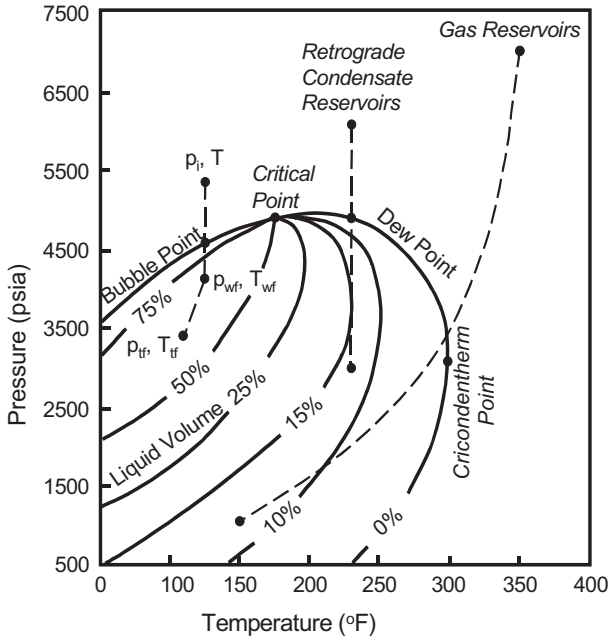


Figure 2-1 A typical hydrocarbon phase diagram.

where

R_s = solution gas-oil ratio (scf/stb)

V_{gas} = gas volume at STP (scf)

V_{oil} = oil volume at STP (stb)

In most states in the U.S., STP is defined as 14.7 psia and 60°F. At a given temperature, the solution gas-oil ratio of a particular oil remains constant at pressures greater than bubble-point pressure. In the pressure range less than the bubble-point pressure, the solution gas-oil ratio decreases as the pressure decreases.

PVT laboratories can provide actual solution gas-oil ratios from direct measurement, or empirical correlations can be made based on PVT laboratory data. One of the correlations is expressed as

$$R_s = \gamma_g \left[\frac{p}{18} \frac{10^{0.0125(^{\circ}API)}}{10^{0.00091t}} \right]^{1.2048} \quad (2.2)$$

where γ_g and $^{\circ}API$ are gas-specific gravity and oil-API gravity (defined in later sections of this chapter), and p and t are pressure and temperature in psia and $^{\circ}F$, respectively.

Solution gas-oil ratios are often used for volumetric oil and gas calculations in reservoir engineering, and as a base parameter for estimating other fluid properties such as oil density.

2.3.2 Oil Density

Oil density is defined as the mass of oil per unit volume, or lb_m/ft^3 in U.S. field units. It is widely used in hydraulics calculations, such as those for wellbore performance (see Chapter 5).

Because of the dissolved gas content, oil density is pressure and temperature-dependent. Oil density at STP (stock tank oil or dead oil) is evaluated using its API gravity. The relationship between the density of a stock tank oil and its API gravity is given by

$$^{\circ}API = \frac{141.5}{\gamma_o} - 131.5 \quad (2.3)$$

and

$$\gamma_o = \frac{\rho_{o,st}}{\rho_w} \quad (2.4)$$

where

$^{\circ}API$ = API gravity of stock tank oil (fresh water equals 10)

γ_o = specific gravity of stock tank oil (fresh water equals 1)

$\rho_{o,st}$ = density of stock tank oil (lb_m/ft^3)

ρ_w = density of fresh water ($62.4 \text{ lb}_m/\text{ft}^3$)

The density of oil at elevated temperatures and pressures can be estimated based on empirical correlations developed by a number of investigators, summarized by Ahmed (1989). Engineers should select and validate the

correlations carefully against actual measurements before adopting any of them.

Standing (1981) presented a correlation for estimating the oil formation volume factor as a function of solution gas-oil ratio, specific gravity of stock tank oil, specific gravity of solution gas, and temperature. By coupling the mathematical definition of the oil formation volume factor with Standing's correlation, Ahmed (1989) proposed the following expression for the density of live oil at elevated pressures and temperatures:

$$\rho_o = \frac{62.4\gamma_o + 0.0136R_s\gamma_g}{0.972 + 0.000147 \left[R_s \sqrt{\frac{\gamma_g}{\gamma_o}} + 1.25t \right]^{1.175}} \quad (2.5)$$

where

- t = temperature (°F)
- γ_g = specific gravity of gas (air equals 1)

2.3.3 Oil Formation Volume Factor

The formation volume factor of an oil is defined as the volume occupied by the oil in the reservoir at the prevailing pressure and temperature by the volume of oil in stock tank conditions (STP) plus its dissolved gas. That is,

$$B_o = \frac{V_{res}}{V_{st}} \quad (2.6)$$

where

- B_o = formation volume factor of oil (rb/stb)
- V_{res} = oil volume under reservoir conditions (rb)
- V_{st} = oil volume under stock tank conditions (STP, stb)

The formation volume factor of oil is always greater than one because an oil will dissolve more gas under prevailing reservoir conditions than under stock tank conditions (STP). At a given reservoir temperature, the

oil formation volume factor remains nearly constant at pressures greater than its bubble-point pressure. In pressure ranges less than the bubble-point pressure, the oil formation volume factor decreases as pressure decreases due to released gas.

PVT laboratories also measure the formation volume factor of oil, and numerous empirical correlations are available based on accumulated experimental data. One correlation was developed by Standing (1981):

$$B_o = 0.9759 + 0.00012 \left(R_s \sqrt{\frac{\gamma_g}{\gamma_o}} + 1.25t \right)^{1.2} \quad (2.7)$$

The formation volume factor of an oil is often used for oil volumetric calculations and well inflow performance calculations, as well as a base parameter for estimating other oil properties.

2.3.4 Oil Viscosity

Viscosity is an empirical parameter that describes the resistance of a fluid to flow. Oil viscosity is used in well inflow and hydraulics calculations in reservoir and production engineering. While PVT laboratories can measure actual oil viscosity, it is often estimated using empirical correlations developed by a number of investigators, including Beal (1946), Beggs and Robinson (1975), Standing (1981), Glaso (1985), Khan (1987), and Ahmed (1989), who also provides a summary. As with oil density, engineers should select and validate a correlation with actual measurements before using it. Standing's (1981) correlation for dead oil is expressed as

$$\mu_{od} = \left(0.32 + \frac{1.8 \times 10^7}{API^{4.53}} \right) \left(\frac{360}{t + 200} \right)^A \quad (2.8)$$

where

$$A = 10^{\left(0.43 + \frac{8.33}{API} \right)} \quad (2.9)$$

and μ_{od} is the viscosity of dead oil in cp.

Standing's (1981) correlation for **gas-saturated crude oil** is expressed as

$$\mu_{ob} = 10^a \mu_{od}^b \quad (2.10)$$

where μ_{ob} is the viscosity of saturated crude oil in cp, and

$$a = R_s \left(2.2 \times 10^{-7} R_s - 7.4 \times 10^{-4} \right) \quad (2.11)$$

$$b = \frac{0.68}{10^c} + \frac{0.25}{10^d} + \frac{0.062}{10^e} \quad (2.12)$$

$$c = 8.62 \times 10^{-5} R_s \quad (2.13)$$

$$d = 1.10 \times 10^{-3} R_s \quad (2.14)$$

$$e = 3.74 \times 10^{-3} R_s \quad (2.15)$$

Standing's (1981) correlation for **undersaturated crude oil** is expressed as

$$\mu_o = \mu_{ob} + 0.001(p - p_b) \left(0.024 \mu_{ob}^{1.6} + 0.38 \mu_{ob}^{0.56} \right) \quad (2.16)$$

where p_b is bubble-point pressure in psi.

2.3.5 Oil Compressibility

Oil compressibility is defined as

$$c_o = -\frac{1}{V} \left(\frac{\partial V}{\partial p} \right)_T \quad (2.17)$$

where T and V denote temperature and volume, respectively. Oil compressibility is measured in PVT laboratories and is often used in modeling well inflow performance and reservoir simulation. Its value is in the order of 10^{-5} psi^{-1} .

2-1 SAMPLE PROBLEM

The solution gas-oil ratio of an oil is 600 scf/stb at 4,475 psia and 140°F. Given the following PVT data, estimate density and viscosity of the crude oil at the following pressure and temperature:

Bubble-point pressure: 2.745 (psia)

Oil gravity: 35 (°API)

Gas specific gravity: 0.77 (air equals 1)

SOLUTION

This problem may be quickly solved using spreadsheet program **OilProperties.xls** in which Standing's correlation for oil viscosity has been coded. Input data and program output are shown in Table 2-2.

2.4 Properties of Natural Gas

Natural gas properties include gas specific gravity, gas pseudocritical pressure and temperature, gas viscosity, gas compressibility factor, gas density, gas formation volume factor, and gas compressibility. The first three depend on natural gas composition. The remainder depend on composition, pressure, and temperature.

2.4.1 Gas Specific Gravity

Gas specific gravity is defined as the ratio of the apparent molecular weight of the gas to that of air. The molecular weight of air is usually taken as 28.97 (approximately 79% nitrogen and 21% oxygen). Therefore, the gas specific gravity can be expressed as

$$\gamma_g = \frac{MW_a}{28.97} \quad (2.18)$$

where MW_a is the apparent molecular weight of the gas, which can be calculated on the basis of its composition. Gas composition is usually determined in laboratories and is reported in mole fractions of the gas components. For example, if y_i is the mole fraction of component i , the

Table 2–2 Results Given by the Spreadsheet Program
OilProperties.xls

OilProperties.xls	
Description: This spreadsheet calculates density and viscosity of a crude oil.	
Instruction: 1) Click a unit-box to choose a unit system; 2) Update parameter values in the “Input Data” section; 3) View result in the “Solution” section.	
Input Data:	US Field Units
Pressure (p):	4475 psia
Temperature (t):	140 °F
Bubble-point pressure (p _b):	2745 psia
Stock tank oil gravity (API):	35 °API
Solution gas-oil ratio (R _g):	600 scf/stb
Gas specific gravity (γ _g):	0.77 air = 1
Solution:	
$\gamma_o = \frac{141.5}{API + 131.5}$	= 0.8498 H ₂ O=1
$\rho_o = \frac{62.4\gamma_o + 0.0136R_s\gamma_g}{0.972 + 0.000147 \left[R_s \sqrt{\frac{\gamma_g}{\gamma_o}} + 1.25t \right]^{1.175}}$	= 44.90 lb _m /ft ³
$A = 10^{(0.43+8.33/API)}$	= 4.6559
$\mu_{od} = \left(0.32 + \frac{1.8 \times 10^7}{API^{4.53}} \right) \left(\frac{360}{t + 200} \right)^A$	= 2.7956 cp

Table 2–2 Results Given by the Spreadsheet Program **OilProperties.xls** (Continued)

$a = R_s (2.2 \times 10^{-7} R_s - 7.4 \times 10^{-4})$	= -0.3648
$c = 8.62 \times 10^{-5} R_s$	= 0.0517
$d = 1.10 \times 10^{-3} R_s$	= 0.6600
$e = 3.74 \times 10^{-3} R_s$	= 2.2440
$b = \frac{0.68}{10^c} + \frac{0.25}{10^d} + \frac{0.062}{10^e}$	= 0.6587
$\mu_{ob} = 10^a \mu_{od}^b$	= 0.8498 cp
$\mu_o = \mu_{ob} + 0.001(p - p_b) (0.024\mu_{ob}^{1.6} + 0.38\mu_{ob}^{0.56})$	= 1.4819 cp

apparent molecular weight of the gas can be calculated using the mixing rule:

$$MW_a = \sum_{i=1}^{N_c} y_i MW_i \quad (2.19)$$

where MW_i is the molecular weight of component i , and N_c is the number of components in the gas. The necessary molecular weights of compounds can be found in textbooks on organic chemistry or petroleum fluids, such as that by Ahmed (1989). Gas specific gravity varies between 0.55 and 0.9.

2.4.2 Gas Pseudocritical Pressure and Temperature

In a similar way to determining gas apparent molecular weight by using the gas composition data, the mixing rule can also be used to estimate the critical properties of a gas on the basis of the critical properties of the compounds it contains. The gas critical properties determined in such a

way are called pseudocritical properties. Gas pseudocritical pressure (p_{pc}) and pseudocritical temperature (T_{pc}) are, respectively, expressed as

$$p_{pc} = \sum_{i=1}^{N_c} y_i p_{ci} \quad (2.20)$$

and

$$T_{pc} = \sum_{i=1}^{N_c} y_i T_{ci} \quad (2.21)$$

where p_{ci} and T_{ci} are the critical pressure and the critical temperature of compound i , respectively.

2-2 SAMPLE PROBLEM

For the gas composition given in Table 2–1, estimate the gas apparent molecular weight, specific gravity, pseudocritical pressure, and pseudocritical temperature of the gas.

SOLUTION

This problem may be solved using the spreadsheet program **MixingRule.xls**, as shown in Table 2–3.

If the gas composition is not known, but gas-specific gravity is given, the pseudocritical pressure and temperature can be estimated using various charts or correlations that have been developed empirically. Two simple correlations are

$$p_{pc} = 709.604 - 58.718\gamma_g \quad (2.22)$$

$$T_{pc} = 170.491 + 307.344\gamma_g \quad (2.23)$$

which are valid for sweet gases—that is, those in which $\text{H}_2\text{S} < 3\%$, $\text{N}_2 < 5\%$ and the total content of inorganic compounds is less than 7%.

Table 2–3 Results Given by the Spreadsheet Program **MixingRule.xls**

MixingRule.xls							
Description: This spreadsheet calculates gas apparent molecular weight, specific gravity, pseudo-critical pressure, and pseudo-critical temperature based on gas composition.							
Instruction: 1) Update gas composition data (y_i); 2) view result.							
Compound	y_i	MW_i	$y_i MW_i$	P_{ci} (psia)	$y_i P_{ci}$ (psia)	T_{ci} (°R)	$y_i T_{ci}$ (°R)
C_1	0.775	16.04	12.43	673	521.58	344	266.60
C_2	0.083	30.07	2.50	709	58.85	550	45.65
C_3	0.021	44.10	0.93	618	12.98	666	13.99
$i-C_4$	0.006	58.12	0.35	530	3.18	733	4.40
$n-C_4$	0.002	58.12	0.12	551	1.10	766	1.53
$i-C_5$	0.003	72.15	0.22	482	1.45	830	2.49
$n-C_5$	0.008	72.15	0.58	485	3.88	847	6.78
C_6	0.001	86.18	0.09	434	0.43	915	0.92
C_{7+}	0.001	114.23	0.11	361	0.36	1024	1.02
N_2	0.050	28.02	1.40	227	11.35	492	24.60
CO_2	0.030	44.01	1.32	1073	32.19	548	16.44
H_2S	0.020	34.08	0.68	672	13.45	1306	26.12
	1.000	$MW_a =$	20.71	$p_{pc} =$	661	$T_{pc} =$	411
		$\gamma_g =$	0.71				

Corrections for impurities in sour gases are always necessary and can be determined using either charts or correlations. One is the Wichert-Aziz (1972) correction, expressed as

$$A = y_{H_2S} + y_{CO_2} \quad (2.24)$$

$$B = y_{H_2S} \quad (2.25)$$

$$\epsilon_3 = 120(A^{0.9} - A^{1.6}) + 15(B^{0.5} - B^{4.0}) \quad (2.26)$$

$$T_{pc}' = T_{pc} - \epsilon_3 \quad (\text{corrected } T_{pc}) \quad (2.27)$$

$$P_{pc}' = \frac{P_{pc} T_{pc}'}{T_{pc} + B(1-B)\epsilon_3} \quad (\text{corrected } P_{pc}) \quad (2.28)$$

Other correlations with impurity corrections to compensate for inorganic components are also available (Ahmed 1989):

$$P_{pc} = 678 - 50(\gamma_g - 0.5) - 206.7y_{N_2} + 440y_{CO_2} + 606.7y_{H_2S} \quad (2.29)$$

$$T_{pc} = 326 + 315.7(\gamma_g - 0.5) - 240y_{N_2} - 83.3y_{CO_2} + 133.3y_{H_2S} \quad (2.30)$$

Applications of the pseudocritical pressure and temperature are normally found in petroleum engineering using pseudoreduced pressure and temperature, defined as

$$P_{pr} = \frac{P}{P_{pc}} \quad (2.31)$$

$$T_{pr} = \frac{T}{T_{pc}} \quad (2.32)$$

2.4.3 Gas Viscosity

Petroleum engineers usually measure dynamic viscosity (μ_g) in centipoises (cp). Dynamic viscosity is related to kinematic viscosity (ν_g) through density (ρ_g):

$$\nu_g = \frac{\mu_g}{\rho_g} \quad (2.33)$$

For a new gas, engineers prefer to measure gas viscosity directly. If the gas composition (y_i) and the viscosities of the gas components are known, the mixing rule can be used to estimate the viscosity of the mixed gas:

$$\mu_g = \frac{\sum (\mu_{gi} y_i \sqrt{MW_i})}{\sum (y_i \sqrt{MW_i})} \quad (2.34)$$

Gas viscosity is often estimated using charts or correlations derived experimentally. The gas viscosity correlation of Carr, Kobayashi, and Burrows (1954) involves a two-step procedure. First, the gas viscosity at STP is estimated from the specific gravity of the gas and its inorganic compound content. The STP value is then adjusted to local pressure conditions using a correction factor that compensates for the increased gas temperature and pressure. Gas viscosity at atmospheric pressure (μ_1) can be expressed as

$$\mu_1 = \mu_{1HC} + \mu_{1N_2} + \mu_{1CO_2} + \mu_{1H_2S} \quad (2.35)$$

where

$$\begin{aligned} \mu_{1HC} = & 8.188 \times 10^{-3} - 6.15 \times 10^{-3} \log(\gamma_g) \\ & + (1.709 \times 10^{-5} - 2.062 \times 10^{-6} \gamma_g) T \end{aligned} \quad (2.36)$$

$$\mu_{1N_2} = [9.59 \times 10^{-3} + 8.48 \times 10^{-3} \log(\gamma_g)] y_{N_2} \quad (2.37)$$

$$\mu_{1CO_2} = [6.24 \times 10^{-3} + 9.08 \times 10^{-3} \log(\gamma_g)] y_{CO_2} \quad (2.38)$$

$$\mu_{1H_2S} = [3.73 \times 10^{-3} + 8.49 \times 10^{-3} \log(\gamma_g)] y_{H_2S} \quad (2.39)$$

Dempsey (1965) developed the following correlation for determining gas viscosity at elevated pressures:

$$\begin{aligned} \mu_r = \ln \left(\frac{\mu_g}{\mu_1} T_{pr} \right) = & a_0 + a_1 p_{pr} + a_2 p_{pr}^2 + a_3 p_{pr}^3 \\ & + T_{pr} (a_4 + a_5 p_{pr} + a_6 p_{pr}^2 + a_7 p_{pr}^3) \\ & + T_{pr}^2 (a_8 + a_9 p_{pr} + a_{10} p_{pr}^2 + a_{11} p_{pr}^3) \\ & + T_{pr}^3 (a_{12} + a_{13} p_{pr} + a_{14} p_{pr}^2 + a_{15} p_{pr}^3) \end{aligned} \quad (2.40)$$

where

$$\begin{aligned} a_0 &= -2.46211820 \\ a_1 &= 2.97054714 \\ a_2 &= -0.28626405 \\ a_3 &= 0.00805420 \\ a_4 &= 2.80860949 \\ a_5 &= -3.49803305 \\ a_6 &= 0.36037302 \\ a_7 &= -0.01044324 \\ a_8 &= -0.79338568 \\ a_9 &= 1.39643306 \\ a_{10} &= -0.14914493 \\ a_{11} &= 0.00441016 \\ a_{12} &= 0.08393872 \\ a_{13} &= -0.18640885 \\ a_{14} &= 0.02033679 \\ a_{15} &= -0.00060958 \end{aligned}$$

Once the value of μ_r is determined using the right-hand side of the equation, the gas viscosity at an elevated pressure can be readily calculated using the following relation:

$$\mu_g = \frac{\mu_1}{T_{pr}} e^{\mu_r} \quad (2.41)$$

Other correlations for gas viscosity include those of Dean-Stiel (1958) and Lee-Gonzalez-Eakin (1966).

2-3 SAMPLE PROBLEM

A natural gas has a specific gravity of 0.65 and contains 10% nitrogen, 8% carbon dioxide, and 2% hydrogen sulfide. Estimate the viscosity of the gas at 10,000 psia and 180°F.

SOLUTION

This problem may be solved using the spreadsheet program **Carr-Kobayashi-Burrows-Gas Viscosity.xls**, as shown in Table 2-4.

2.4.4 Gas Compressibility Factor

The gas compressibility factor is also called the deviation factor, or z -factor. Its value reflects how much the real gas behavior deviates from that of an ideal gas at a given pressure and temperature. The compressibility factor is expressed as

$$z = \frac{V_{actual}}{V_{ideal\ gas}} \quad (2.42)$$

Introducing the z -factor to the gas law for an ideal gas results in the gas law for a real gas as

$$pV = nzRT \quad (2.43)$$

where n is the number of moles of gas. When pressure p is entered in psia, volume V in ft^3 , and temperature in $^{\circ}\text{R}$, the gas constant R is equal to:

$$10.73 \frac{\text{psia} - \text{ft}^3}{\text{mole} - ^{\circ}\text{R}}$$

PVT laboratories can determine the gas compressibility factor from measurements. For a given amount of gas, if temperature is kept constant and

Table 2-4 Results Given by the Spreadsheet Program
Carr-Kobayashi-Burrows-GasViscosity.xls

Carr-Kobayashi-Burrows-GasViscosity.xls	
Description: This spreadsheet calculates gas viscosity with correlation of Carr, Kobayashi, and Burrows.	
Instruction: 1) Select a unit system; 2) Update data in the “Input Data” section; 3) Review result in the “Solution” section.	
Input Data:	US Field Units
Pressure:	10000 psia
Temperature:	180 °F
Gas specific gravity:	0.65 air =1
Mole fraction of N ₂ :	0.1
Mole fraction of CO ₂ :	0.08
Mole fraction of H ₂ S:	0.02
Solution:	
Pseudocritical pressure	= 697.164 psia
Pseudocritical temperature	= 345.357 °R
Uncorrected gas viscosity at 14.7 psia	= 0.012174 cp
N ₂ correction for gas viscosity at 14.7 psia	= 0.000800 cp
CO ₂ correction for gas viscosity at 14.7 psia	= 0.000363 cp
H ₂ S correction for gas viscosity at 14.7 psia	= 0.000043 cp
Corrected gas viscosity at 14.7 psia (μ_I)	= 0.013380 cp
Pseudo-reduced pressure	= 14.34
Pseudo-reduced temperature	= 1.85
$\ln(\mu_g/\mu_1 * T_{pr})$	= 1.602274
Gas viscosity	= 0.035843 cp

the volume is measured both at 14.7 psia and at an elevated pressure p_1 , the z -factor can be determined using the following formula:

$$z = \frac{p_1}{14.7} \frac{V_1}{V_0} \quad (2.44)$$

where V_0 and V_1 are the gas volumes measured at 14.7 psia and p_1 , respectively.

Very often the z -factor is estimated using a chart developed by Standing and Katz (1954), which has been adapted for computer solution by a number of individuals. Brill and Beggs's correlation (1974) gives z -factor values accurate enough for many engineering calculations. The correlation is expressed as

$$A = 1.39(T_{pr} - 0.92)^{0.5} - 0.36T_{pr} - 0.10 \quad (2.45)$$

$$B = (0.62 - 0.23T_{pr})p_{pr} + \left(\frac{0.066}{T_{pr} - 0.86} - 0.037 \right) p_{pr}^2 + \frac{0.32p_{pr}^6}{10^E} \quad (2.46)$$

$$C = 0.132 - 0.32 \log(T_{pr}) \quad (2.47)$$

$$D = 10^F \quad (2.48)$$

$$E = 9(T_{pr} - 1) \quad (2.49)$$

$$F = 0.3106 - 0.49T_{pr} + 0.1824T_{pr}^2 \quad (2.50)$$

and

$$z = A + \frac{1-A}{e^B} + Cp_{pr}^D \quad (2.51)$$

2-4 SAMPLE PROBLEM

A natural gas with a specific gravity of 0.65 contains 10% N₂, 8% CO₂, and 2% H₂S. Estimate z-factor of the gas at 5,000 psia and 180°F using the Brill and Beggs' correlation.

SOLUTION

This problem may be solved using the spreadsheet program **Brill-Beggs-Z.xls**, as shown in Table 2-5.

Hall and Yarborough (1973) presented a more accurate correlation to estimate the z-factor of natural gases, which may be summarized as

$$t_r = \frac{1}{T_{pr}} \quad (2.52)$$

$$A = 0.06125 t_r e^{-1.2(1-t_r)^2} \quad (2.53)$$

$$B = t_r (14.76 - 9.76t_r + 4.58t_r^2) \quad (2.54)$$

$$C = t_r (90.7 - 242.2t_r + 42.4t_r^2) \quad (2.55)$$

$$D = 2.18 + 2.82t_r \quad (2.56)$$

and

$$z = \frac{Ap_{pr}}{Y} \quad (2.57)$$

where Y is the reduced density, determined from

$$f(Y) = \frac{Y + Y^2 + Y^3 - Y^4}{(1 - Y)^3} - Ap_{pr} - BY^2 + CY^D = 0 \quad (2.58)$$

Table 2–5 Results Given by the Spreadsheet Program
Brill-Beggs-Z.xls

Results Given by the Spreadsheet Program Brill-Beggs-Z.xls	
Description: This spreadsheet calculates gas compressibility factor based on Brill and Beggs correlation.	
Instruction: 1) Select a unit system; 2) Update data in the “Input Data” section; 3) Review result in the “Solution” section.	
Input Data:	US Field Units
Pressure:	5000 psia
Temperature:	180 °F
Gas specific gravity:	0.65 air = 1
Mole fraction of N ₂ :	0.1
Mole fraction of CO ₂ :	0.08
Mole fraction of H ₂ S:	0.02
Solution:	
Pseudocritical pressure =	697 psia
Pseudocritical temperature =	345 °R
Pseudo-reduced pressure =	7.17
Pseudo-reduced temperature =	1.95
<i>A</i> =	0.6063
<i>B</i> =	2.4604
<i>C</i> =	0.0395
<i>D</i> =	1.1162
Gas compressibility factor <i>z</i> =	0.9960

If Newton-Raphson's iterative method is used to solve Equation (2.58) for Y , the following derivative is needed:

$$\frac{df(Y)}{dY} = \frac{1 + 4Y + 4Y^2 - 4Y^3 + Y^4}{(1 - Y)^4} - 2BY + CDY^{D-1} \quad (2.59)$$

An example of using the Hall and Yarborough's correlation is shown in the next section, covering gas density prediction.

2.4.5 Gas Density

Because gas is compressible, its density is a function of its pressure and temperature. In addition to direct laboratory measurement, gas density can be predicted from the gas law for real gases with acceptable accuracy:

$$\rho_g = \frac{m}{V} = \frac{MW_a p}{zRT} \quad (2.60)$$

where m is mass of gas and ρ_g is gas density. Taking air molecular weight as 29, and the gas constant R as equal to

$$10.73 \frac{\text{psia} - \text{ft}^3}{\text{mole} - ^\circ R}$$

Equation (2.60) may be rearranged to yield

$$\rho_g = \frac{2.7\gamma_g p}{zT} \quad (2.61)$$

where the gas density is expressed in lb_m/ft^3 .

2-5 SAMPLE PROBLEM

A gas with a specific gravity of 0.65 contains 10% N_2 , 8% CO_2 , and 2% H_2S . Estimate the z -factor and gas density at 5,000 psia and 180°F.

SOLUTION

This problem may be solved using the spreadsheet program **Hall-Yarborough-Z.xls**, as shown in Table 2-6.

2.4.6 Gas Formation Volume Factor

Gas formation volume factor is defined as the ratio of gas volume under reservoir conditions to the gas volume at STP, expressed as

$$B_g = \frac{V}{V_{sc}} = \frac{p_{sc}}{p} \frac{T}{T_{sc}} \frac{z}{z_{sc}} = 0.0283 \frac{zT}{p} \quad (2.62)$$

where

B_g = formation volume factor of gas (ft³/scf)

V = gas volume under reservoir conditions (ft³)

V_{sc} = gas volume under standard conditions (STP, ft³)

p = pressure (psia)

p_{sc} = standard pressure (psia)

T = temperature (°R)

T_{sc} = standard temperature (°R)

z = gas compressibility factor

z_{sc} = 1.0, gas compressibility factor under standard conditions (STP)

If expressed in rb/scf, Equation (2.62) can be simplified to:

$$B_g = 0.00504 \frac{zT}{p} \quad (2.63)$$

The gas formation volume factor is frequently used in mathematical modeling of the gas well inflow performance relationship (IPR). Another way to express this parameter is to use the gas expansion factor, defined in scf/ft³ as

Table 2–6 Results Given by the Spreadsheet Program
Hall-Yarborough-z.xls

Hall-Yarborough-z.xls	
Instruction: This spreadsheet computes gas compressibility factor with Hall-Yarborough method.	
Instruction: 1) Select a unit system; 2) Update data in the “Input Data” section; 3) Click “Solution” button; 4) View result.	
Input Data:	US Field Units
Temperature:	180 °F
Pressure:	5000 psia
Gas specific gravity:	0.65 air = 1
Nitrogen mole fraction:	0.1
Carbon dioxide fraction:	0.08
Hydrogen sulfite fraction:	0.02
Solution:	
$T_{pc} = 326 + 315.7(\gamma_g - 0.5) - 240y_{N_2} - 83.3y_{CO_2} + 133.3y_{H_2S}$	$= 345.357 \text{ °R}$
$p_{pc} = 678 - 50(\gamma_g - 0.5) - 206.7y_{N_2} + 440y_{CO_2} + 606.7y_{H_2S}$	$= 697.164 \text{ psia}$
$T_{pr} = \frac{T}{T_{pc}}$	$= 1.853155$
$t_r = \frac{1}{T_{pr}}$	$= 0.53962$
$p_{pr} = \frac{p}{p_{pc}}$	$= 7.171914$
$A = 0.06125 t_r e^{-1.2(1-t_r)^2}$	$= 0.025629$
$B = t_r (14.76 - 9.76t_r + 4.58t_r^2)$	$= 5.842446$

Table 2–6 Results Given by the Spreadsheet Program
Hall-Yarborough-z.xls (Continued)

$C = t_r (90.7 - 242.2t_r + 42.4t_r^2)$	= -14.9203
$D = 2.18 + 2.82t_r$	= 3.701729
Y = Result in trial-and-error	= 0.183729
$f(Y) = \frac{Y + Y^2 + Y^3 - Y^4}{(1 - Y)^3} - Ap_{pr} - BY^2 + CY^D = 0$	= -2.6E-05
$z = \frac{Ap_{pr}}{Y}$	= 1.000445
$\rho_g = \frac{2.7\gamma_g P}{zT}$	= 13.70484 lb _m /ft ³

$$E = \frac{1}{B_g} = 35.3 \frac{P}{ZT} \quad (2.64)$$

or in scf/rb as

$$E = 198.32 \frac{P}{zT} \quad (2.65)$$

The gas expansion factor is normally used for estimating gas reserves.

2.4.7 Gas Compressibility

Gas compressibility is defined as

$$c_g = -\frac{1}{V} \left(\frac{\partial V}{\partial p} \right)_T \quad (2.66)$$

Because the gas law for real gases gives $V = \frac{nzRT}{p}$,

$$\left(\frac{\partial V}{\partial p}\right) = nRT \left(\frac{1}{p} \frac{\partial z}{\partial p} - \frac{z}{p^2}\right) \quad (2.67)$$

Substituting Equation (2.67) into Equation (2.66) yields

$$c_g = \frac{1}{p} - \frac{1}{z} \frac{\partial z}{\partial p} \quad (2.68)$$

Because the second term in the right-hand-side is usually small, gas compressibility is approximately equal to the reciprocal of pressure.

2.5 Properties of Produced Water

Water properties that are frequently used in oil and gas field management include density, specific gravity, salinity, viscosity, formation volume factor, and compressibility. These properties are easy to measure in laboratories.

2.5.1 Density, Specific Gravity, and Salinity

The density of pure water (H₂O) is 62.4 lbm/ft³ at STP. The density of produced water is higher than this value due to impurities, mostly salts. Water specific gravity is defined as the ratio of density of the produced water to that of pure water. In practice, the water density, specific gravity, and salinity are inter-convertible, as their relationships depend on the types of salts dissolved in the water. For typical oil-field brines, the data from McCain (1973) provides the following correlation:

$$\rho_w = 62.4 + 0.48C_s \quad (2.69)$$

where

$$\begin{aligned}\rho_w &= \text{density of brine (lbm/ft}^3\text{)} \\ C_s &= \text{total dissolved solids (\%)}\end{aligned}$$

2.5.2 Water Viscosity

The viscosity of water is affected by its salinity, dissolved gas content, pressure, and temperature, with temperature being the most significant factor. For typical oil-field brines, the data from McCain (1973) provides the following correlation:

$$\mu_w = \frac{70.42}{t} \quad (2.70)$$

where

$$\begin{aligned}\mu_w &= \text{viscosity of brine (cp)} \\ t &= \text{temperature (}^\circ\text{F)}\end{aligned}$$

2.5.3 Water Formation Volume Factor

Like oil, the formation volume factor of produced water is defined as the volume occupied in the reservoir at the prevailing reservoir pressure and temperature, divided by the volume of water plus its dissolved gas at surface conditions (STP), expressed as

$$B_w = \frac{V_{res}}{V_{st}} \quad (2.71)$$

where

$$\begin{aligned}B_w &= \text{formation volume factor of water (rb/stb)} \\ V_{res} &= \text{water volume in reservoir condition (rb)} \\ V_{st} &= \text{water volume at surface conditions (STP, stb)}\end{aligned}$$

For typical oil-field brines, formation volume factors are very close to one.

2.5.4 Water Compressibility

Water compressibility is defined as

$$c_w = -\frac{1}{V} \left(\frac{\partial V}{\partial p} \right)_T \quad (2.72)$$

Water compressibility is measured in laboratories, with values in the order of 10^{-6} psi^{-1} . Water compressibility is often used in modeling well inflow performance and in reservoir simulation.

2.6 Summary

This chapter defined relevant properties of oil, natural gas, and produced water, and provided several techniques for using empirical correlations to estimate their values. These correlations are coded in spreadsheet programs included with this book. Applications of these fluid properties will be presented in later chapters.

2.7 References

Ahmed, T.: *Hydrocarbon Phase Behavior*, Gulf Publishing Company, Houston, 1989.

Beal, C.: "The Viscosity of Air, Water, Natural Gas, Crude Oils and Its Associated Gases at Oil Field Temperatures and Pressures," *Trans. AIME* 165 (1946): 94–112.

Beggs, H.D. and Robinson, J.R.: "Estimating the Viscosity of Crude Oil Systems," *Journal of Petroleum Technology* (September 1975): 1140–1141.

Brill, J. P., and Beggs, H.D.: "Two-Phase Flow in Pipes," INTERCOMP Course, The Hague, 1974.

Carr, N.L., Kobayashi, R. and Burrows, D.B.: "Viscosity of Hydrocarbon Gases under Pressure," *Trans. AIME* 201 (1954): 264–72.

Dempsey, J. R.: "Computer Routine Treats Gas Viscosity as a Variable," *Oil & Gas Journal* (16 August 1965): 141.

Dean, D. E. and Stiel, L. I.: "The Viscosity of Non-polar Gas Mixtures at Moderate and High Pressures," *AIChE Journal* 4 (1958): 430–436.

Glaso, O.: "Generalized Pressure-Volume-Temperature Correlations," *Journal of Petroleum Technology* (May 1985): 785–795.

Hall, K. R. and Yarborough, L.: "A New Equation of State for Z-Factor Calculations," *Oil & Gas Journal* (18 June 1973): 82.

Khan, S.A.: "Viscosity Correlations for Saudi Arabian Crude Oils," paper SPE 15720, presented at the 50th Middle East Conference and Exhibition (7–10 March 1987), Manama, Bahrain.

Lee, A. L., Gonzalez, M.H. and Eakin, B.E.: "The Viscosity of Natural Gases," *Journal of Petroleum Technology* (August 1966): 997–1000.

McCain, W.D., Jr.: *Properties of Petroleum Fluids*, PennWell Books, Tulsa (1973).

Standing, M. B.: *Volume and Phase Behavior of Oil Field Hydrocarbon Systems*, Society of Petroleum Engineers, 9th ed., Dallas (1981).

Standing, M. B. and Katz, D.L.: "Density of Natural Gases," *Trans. AIME* 146 (1954): 140–9.

Wichert, E. and Aziz, K.: "Calculate Zs for Sour Gases," *Hydrocarbon Processing* 51 (May 1972): 119.

2.8 Problems

- 2-1 Estimate the density of a 35 API gravity dead oil at 90°F.
- 2-2 The solution gas-oil ratio of a crude oil is 800 scf/stb at 3,000 psia and 110°F. Given the following PVT data

Bubble-point pressure: 2,550 psia

Oil gravity: 45 °API

Gas specific gravity: 0.70 air = 1

estimate the density and viscosity of the crude oil at 110°F: at 2,550 psia and at 3,000 psia.

- 2-3 For the gas composition given below, determine the apparent molecular weight, specific gravity, pseudocritical pressure, and pseudocritical temperature of the gas.

Component	Mole Fraction
C_1	0.665
C_2	0.123
C_3	0.071
$i-C_4$	0.006
$n-C_4$	0.002
$i-C_5$	0.003
$n-C_5$	0.008
C_6	0.001
C_{7+}	0.001
N_2	0.060
CO_2	0.040
H_2S	0.020

- 2-4 Estimate the gas viscosity of a 0.72 specific gravity gas at 150°F: at 100 psia, 1,000 psia, 5,000 psia, and 10,000 psia.
- 2-5 Use the Hall-Yarborough method to estimate the gas compressibility factor and density of a 0.75 specific gravity gas at 150°F: at 50 psia, 500 psia, and 5,000 psia. Compare the results with those given by the Brill and Beggs' correlation. What is your conclusion?
- 2-6 Estimate the density of a 0.8 specific gravity dead oil at 45°C.
- 2-7 The solution gas-oil ratio of a crude oil is 4,200 sm^3/m^3 at 20 MPa and 50°C. Given the following PVT data
- Bubble-point pressure: 15 MPa
 Oil specific gravity: 0.8 water = 1
 Gas specific gravity: 0.72 air = 1
- estimate density and viscosity of the crude oil at 50°C: at 15 MPa and at 20 MPa.

- 2-8 For the gas composition given below, determine the apparent molecular weight, specific gravity, pseudocritical pressure, and pseudocritical temperature of the gas.

Component	Mole Fraction
C_1	0.715
C_2	0.093
C_3	0.031
$i-C_4$	0.006
$n-C_4$	0.002
$i-C_5$	0.003
$n-C_5$	0.008
C_6	0.001
C_{7+}	0.001
N_2	0.070
CO_2	0.050
H_2S	0.020

- 2-9 Estimate the gas viscosity of a 0.75 specific gravity gas at 85°C: at 1 MPa, 5 MPa, 10 MPa, and at 50 MPa.
- 2-10 Using the Hall-Yarborough method, calculate the gas compressibility factor and density of a 0.73 specific gravity gas at 80°C: at 1 MPa, 5 MPa, 10 MPa, and at 50 MPa. Compare the results with those given by the Brill and Beggs' correlation. What is your conclusion?

Properties of Petroleum Reservoirs

3.1 Introduction

Petroleum reservoirs may contain oil, natural gas, or both. Their important properties include pay zone thickness, lithology, rock porosity, rock total compressibility, and rock permeability. These properties affect fluid flow within the reservoir and thus well productivity. Reservoir engineers must understand these properties to simulate reservoir behavior and to predict well productivity. Reservoir pay zone thickness is usually determined from open-hole logs, which are not addressed in this book. This chapter presents definitions of the remaining reservoir properties and the methods for obtaining their values. Applications of reservoir properties will be covered in Chapters 5 through 8, which deal with reservoir deliverability.

3.2 Lithology

Lithology is a geological term used to describe the types of formation rocks. Three main types are commonly defined: sedimentary, metamorphic, and igneous. In reservoir analysis, the lithology is identified by geologists using core samples taken from the exploration wells.

Sedimentary rocks are rocks formed after compaction of settled solid particles in water. For millions of years, the earth has been eroded—broken down and worn away by wind and water. The resulting small particles are washed downstream where they settle to the bottom of the rivers, lakes,

and oceans in layer after layer. These layers are pressed down through time, until heat and pressure slowly turn the lower layers into rock. Gravels, sandstones, siltstones, shales, and mudstones are some of the subclasses of sedimentary rocks. These subclasses are generally porous and can contain water and hydrocarbons. Geologists believe that most hydrocarbons formed in shales and subsequently migrated into sandstones over geologic time.

Carbonate rocks are a subclass of sedimentary rocks composed primarily of carbonate minerals. Two major types of carbonate rocks are limestone and dolomite, composed of calcite (CaCO_3) and the mineral dolomite ($\text{CaMg}(\text{CO}_3)_2$), respectively. Chalk and tufa are minor sedimentary carbonates. Carbonate rocks are very tight—that is, they display low porosity and permeability—but are highly fractured and may contain water and hydrocarbons.

Igneous rocks may be formed either underground or at the surface by the freezing or crystallization of molten rock. Subsurface molten rock is called magma and becomes igneous rock as it is trapped underground and crystallizes slowly. Igneous rocks are also formed as volcanoes erupt. When the magma rises to the surface, it is called lava, both as a molten and a solid rock. Igneous rocks are very tight and are not usually reservoir-rocks. Exceptions include naturally fractured igneous rocks.

Metamorphic rocks are composed of sedimentary, igneous, or even previously-metamorphosed rocks that have been chemically altered by heat, pressure and deformation while buried deep in the earth's crust. These rocks show changes in mineral composition, texture, or both. This area of rock classification is highly specialized and complex. Marble and quartz are typical metamorphic rocks. These types of rocks are not porous and thus do not form hydrocarbon-bearing reservoirs.

3.3 Reservoir Porosity

Porosity of reservoir rock is defined as the pore fraction of the rock—that is, the ratio of pore space volume to bulk volume of the rock. Porosity is usually expressed as a percentage:

$$\varphi = \frac{V_{pore}}{V_{bulk}} \quad (3.1)$$

Fluid-productive sandstones display porosities ranging between 0.05 to 0.4, or 5% to 40%. Although the porosity of carbonate base material is practically zero, the overall porosity of carbonate rocks can be significant due to natural fractures within the rocks. The base materials of igneous rocks have no porosity, but their natural fractures form some degree of overall porosity in which hydrocarbons have been discovered in recent years.

Reservoir rock porosity can be measured in laboratories through core sample analysis. It may also be estimated using open-hole well logs. The porosity factor is often used to estimate hydrocarbon reserves.

3.4 Reservoir Total Compressibility

Total reservoir compressibility is defined as

$$c_t = -\frac{1}{V} \left(\frac{\partial V}{\partial p} \right)_T \quad (3.2)$$

For gas reservoirs, its value is close to gas compressibility, as defined by Equation (2.68). For undersaturated oil reservoirs, its value can be estimated using fluid saturations and the compressibilities of reservoir fluids, expressed as

$$c_t = c_o S_o + c_w S_w + c_f \quad (3.3)$$

where c_f is formation rock compressibility, and S_o and S_w are oil and water saturations in the pore space, respectively. The following values are typical:

$$c_o = 10 \times 10^{-6} \text{ psi}^{-1}$$

$$c_w = 3 \times 10^{-6} \text{ psi}^{-1}$$

$$c_f = 6 \times 10^{-6} \text{ psi}^{-1}$$

The most reliable way to determine total reservoir compressibility is by using pressure transient test analysis. Total reservoir compressibility data is crucial for well productivity during the transient flow period.

3.5 Reservoir Permeability

Permeability refers to a rock's ability to transmit fluids. Permeable formations are those that transmit fluids readily, such as sandstones, and tend to have many large, well-connected pores. Impermeable formations, such as shales and siltstones, tend to be finer grained or of mixed grain size, with smaller, fewer, or less interconnected pores.

Consider a fluid with viscosity μ flowing horizontally in a cylindrical rock body of length ΔL and cross-sectional area A . The relationship between the pressure drop Δp across the rock and volumetric flow rate q obeys Darcy's law:

$$q = k \frac{A\Delta p}{\mu\Delta L} \quad (3.4)$$

where the proportionality factor k is called permeability.

If the pore space in the rock is filled with one fluid such as water, the permeability is called the *absolute* permeability (k_a). Thus the absolute permeability is equal to the measured permeability when a single fluid, or fluid phase, is present in the rock. The absolute permeability of rock sample can therefore be determined experimentally. If μ , ΔL , A , Δp , and q are measured in cp, cm, cm², Atm, and cm³/s, respectively, the absolute permeability of the rock sample in darcies can be calculated from the measurements by

$$k_a = \frac{q\mu\Delta L}{A\Delta p} \quad (3.5)$$

The absolute permeability may be different when different types of fluids (water, oil, or gas, etc.) are used in the experiments. This is due to rock's wetting preference for different fluids, and the Klinkenberg effect for gas flow.

If more than one fluid or fluid phase is present in the pore space, Darcy's law applies to each phase. The permeability parameter is called the *effec-*

tive permeability. The effective permeability is the ability to preferentially flow or transmit a particular fluid through a rock when other immiscible fluids are also present. If water, oil, and gas are present in the pore space, the relationship is expressed as

$$q_w = k_w \frac{A\Delta p}{\mu_w \Delta L} \quad (3.6)$$

$$q_o = k_o \frac{A\Delta p}{\mu_o \Delta L} \quad (3.7)$$

$$q_g = k_g \frac{A\Delta p}{\mu_g \Delta L} \quad (3.8)$$

where k_w , k_o , and k_g are the effective permeability to water, oil, and gas, respectively. The effective permeability of the rock to any phase is proportional to the absolute permeability of the rock, where the proportionality factor is called the *relative permeability*. The effective permeabilities to water, oil, and gas, respectively, are expressed as

$$k_w = k_{rw} k_a \quad (3.9)$$

$$k_o = k_{ro} k_a \quad (3.10)$$

$$k_g = k_{rg} k_a \quad (3.11)$$

where k_{rw} , k_{ro} , and k_{rg} are the relative permeabilities to water, oil, and gas, respectively. In addition to the nature of the rock, the relative saturations (pore volume fractions) of the fluids also influence effective permeability. That is,

$$k_{rw} = f(S_w) \quad (3.12)$$

$$k_{ro} = \phi(S_o) \quad (3.13)$$

$$k_{rg} = \psi(S_g) \quad (3.14)$$

where S_w , S_o , and S_g are saturations of water, oil, and gas, respectively. If a single fluid is present in a rock, its relative permeability is 1.0. Generally, relative permeability increases with the corresponding phase saturation, but the relationship between them must be established experimentally for any given rock. Figure 3–1 shows a typical set of relative permeability data as measured in a laboratory for a water-gas system.

Calculating relative permeabilities permits comparison of the abilities of different fluids to flow in multi-fluid systems, because the presence of more than one fluid generally inhibits flow.

3.6 Effective Permeability

The effective permeabilities determined by using laboratory measurement of the absolute permeability and relative permeability from well cores are only accurate at the small scale of the well core. Their accuracy breaks down at the larger scales of well and field levels. The effective permeability data required for well productivity prediction are often obtained by analyzing pressure transient data from actual well testing.

In pressure transient data analyses, the effective reservoir permeability controlling a well's deliverability should be derived from the flow regime that prevails in the reservoir for long-term production. To better understand the flow regimes, the commonly used equations describing flow in oil reservoirs are summarized first in the following subsection. Similar equations for gas reservoirs can be found in the literature.

3.6.1 Flow Regimes

3.6.1.1 Horizontal Radial Flow

For vertical wells that fully penetrate non-fractured reservoirs, horizontal radial flow can be mathematically described in consistent units as

$$p_{wf} = p_i - \frac{qB\mu}{4\pi k_h h} \left[\ln \left(\frac{k_h t}{\phi \mu c_i r_w^2} \right) + 2S + 0.80907 \right] \quad (3.15)$$

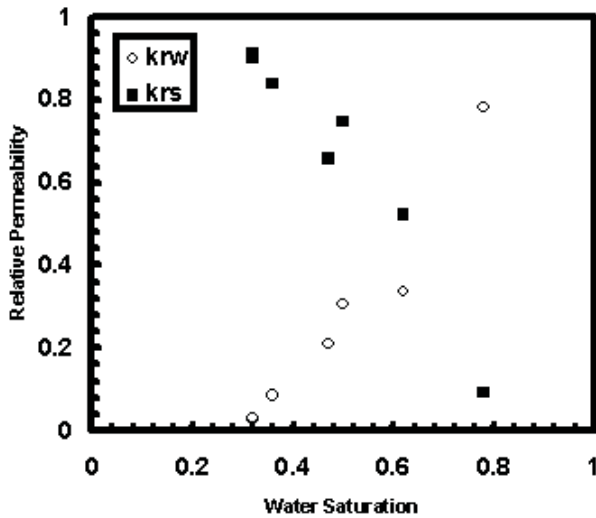


Figure 3–1 Typical relative permeability data for a water-gas system.

where

- p_{wf} = flowing bottom-hole pressure
- p_i = initial reservoir pressure
- q = volumetric liquid production rate
- B = formation volume factor
- μ = fluid viscosity
- k_h = average horizontal permeability
- h = pay zone thickness
- t = flow time
- ϕ = initial reservoir pressure
- c_t = total reservoir compressibility
- r_w = wellbore radius
- S = total skin factor

3.6.1.2 Horizontal Linear Flow

For hydraulically-fractured wells, horizontal linear flow can be mathematically described in consistent units as

$$p_{wf} = p_i - \frac{qB\mu}{2\pi k_y h} \left[\sqrt{\frac{\pi k_y t}{\phi \mu c_t x_f^2}} + S \right] \quad (3.16)$$

where x_f is fracture half-length, and k_y is the permeability in the direction perpendicular to the fracture surface.

3.6.1.3 Vertical Radial Flow

For the horizontal well depicted in Figure 3–2, initial vertical radial flow can be mathematically described in consistent units as

$$p_{wf} = p_i - \frac{qB\mu}{4\pi k_{yz} L} \left[\ln \left(\frac{k_{yz} t}{\phi\mu c_i r_w^2} \right) + 2S + 0.80907 \right] \quad (3.17)$$

where L is the horizontal wellbore length and k_{yz} is the arithmetic mean of horizontal and vertical permeabilities, expressed as

$$k_{yz} = \sqrt{k_y k_z} \quad (3.18)$$

3.6.1.4 Horizontal Pseudo-Linear Flow

Pseudo-linear fluid flow toward a horizontal wellbore can be mathematically described in consistent units as

$$p_{wf} = p_i - \frac{qB\mu}{2\pi k_y (h - Z_w)} \left[\sqrt{\frac{4\pi k_y t}{\phi\mu c_i L^2}} + S \right] \quad (3.19)$$

3.6.1.5 Horizontal Pseudo-Radial Flow

Pseudo-radial fluid flow toward a horizontal wellbore can be mathematically described in consistent units as

$$p_{wf} = p_i - \frac{qB\mu}{4\pi k_h h} \left[\ln \left(\frac{k_h t}{\phi\mu c_i r_w^2} \right) + 2S + 0.80907 \right] \quad (3.20)$$

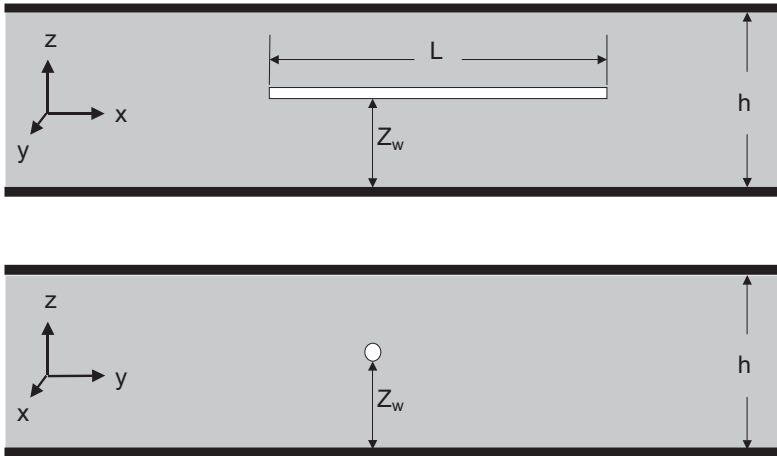


Figure 3–2 Parameters for a horizontal wellbore.

3.6.2 Permeability Determination

For vertical wells fully-penetrating non-fractured reservoirs, it is usually the average (geometric mean) of horizontal permeabilities, k_h , that dominates long-term production performance. The average horizontal permeability may be derived from data obtained during the horizontal radial flow regime. For wells draining relatively small portions of hydraulically-fractured reservoir segments, it is usually the permeability in the direction perpendicular to the fracture surface that controls long-term production performance. This permeability may be derived from the horizontal linear flow regime. For horizontal wells draining relatively large portions of non-fractured reservoir segments, it is usually again the geometric mean of horizontal permeabilities that dominates long-term production performance. This average horizontal permeability can be derived from the pseudo-radial flow regime. For vertical wells partially-penetrating non-fractured reservoirs, both horizontal and vertical permeabilities influence long-term production performance. These permeabilities can usually be derived from the so-called hemispherical flow regime.

Flow regimes are usually identified using the diagnostic pressure derivative p' , expressed as

$$p' = \frac{d\Delta p}{d\ln(t)} = t \frac{d\Delta p}{dt} \quad (3.21)$$

where t is time, and Δp is defined as

$$\Delta p = p_i - p_{wf} \quad (3.22)$$

for drawdown tests where p_i and p_{wf} are initial reservoir pressure and flowing bottom-hole pressure, respectively. For pressure buildup tests, the Δp is defined as

$$\Delta p = p_{sw} - p_{wfe} \quad (3.23)$$

where p_{ws} and p_{wfe} are shut-in bottom-hole pressure and the flowing bottom-hole pressure at the end of flow (before shut-in), respectively.

For any type of radial flow—that is, horizontal radial flow, vertical radial flow, and horizontal pseudo-radial flow—the diagnostic derivative is derived from Equations (3.15), (3.17), and (3.20) as

$$p' = \frac{d\Delta p}{d \ln(t)} = \frac{qB\mu}{4\pi\bar{k}H_R} \quad (3.24)$$

where \bar{k} is the average permeability in the flow plane (k_h or k_{yz}), and H_R is the distance of radial flow (h or L). Apparently, the diagnostic derivative is constant over the radial flow time regime. The plot of p' versus t data should show a straight line parallel to the t -axis.

For linear flow—that is, flow toward a hydraulic fracture—the diagnostic derivative is derived from Equation (3.16) as

$$p' = \frac{d\Delta p}{d \ln(t)} = \frac{qB}{4hx_f} \sqrt{\frac{\mu t}{\pi\phi c_i k_y}} \quad (3.25)$$

For pseudo-linear flow—that is, flow toward a horizontal well—the diagnostic derivative is derived from Equation (3.19) as

$$p' = \frac{d\Delta p}{d \ln(t)} = \frac{qB}{2L(h - z_w)} \sqrt{\frac{\mu t}{\pi\phi c_i k_y}} \quad (3.26)$$

Taking the logarithm of Equations (3.25) and (3.26) gives

$$\log(p') = \frac{1}{2} \log(t) + \log\left(\frac{qB}{4hx_f} \sqrt{\frac{\mu}{\pi\phi c_t k_y}}\right) \quad (3.27)$$

and

$$\log(p') = \frac{1}{2} \log(t) + \log\left(\frac{qB}{2L(h-z_w)} \sqrt{\frac{\mu}{\pi\phi c_t k_y}}\right) \quad (3.28)$$

Equations (3.27) and (3.28) indicate that the defining characteristic of a linear flow regime is the half slope on the log-log plot of diagnostic derivative versus time.

Once the flow regimes are identified, slope analysis can be used to calculate reservoir permeabilities. For any type of radial flow, Equations (3.15), (3.17), and (3.20) indicate that plotting bottom-hole pressure against time on a semi-log scale will show a trend with constant slope m_R , where

$$m_R = -\frac{qB\mu}{4\pi\bar{k}H_R} \quad (3.29)$$

The average permeability in the flow plane (k_h or k_{yz}) can then be estimated by

$$\bar{k} = -\frac{qB\mu}{4\pi H_R m_R} \quad (3.30)$$

For any type of linear flow, Equations (3.16) and (3.19) indicate that plotting bottom-hole pressure against the square-root of time will show a trend of constant slope m_L where

$$m_L = -\frac{qB}{H_L X_L} \sqrt{\frac{\mu}{\pi\phi c_t k_y}} \quad (3.31)$$

where $H_L = h$ and $X_L = 2x_f$ for linear flow, and $H_L = h - Z_w$ and $X_L = L$ for pseudo-linear flow, respectively. The permeability in the flow direction can then be estimated by

$$k_y = \frac{\mu}{\pi\phi c_t} \left(\frac{qB}{m_L H_L X_L} \right)^2 \quad (3.32)$$

If a horizontal well is tested for long enough for a pseudo-radial flow regime to become established then it is possible to estimate other directional permeabilities by

$$k_x = \frac{k_h^2}{k_y} \quad (3.33)$$

and

$$k_z = \frac{k_{yz}^2}{k_y} \quad (3.34)$$

Although k_x and k_z are not used in well productivity analysis, they can provide insight about reservoir anisotropy and can also be used in petroleum reservoir simulation.

3.6.2.1 Skin Factor

Skin factor is a constant used to adjust flow equations derived from theoretically ideal conditions of homogeneous and isotropic porous media to suit applications under non-ideal conditions. It is a general factor designed to account for the lumped effects of several real-world variables not included in the derivation of the ideal flow equations. The skin factor can be derived from pressure transient test analysis using Equations (3.15), (3.16), (3.17), (3.19) and (3.20). But the practical definition of S is not the same under different flow regimes. A general expression of the skin factor is

$$S = S_D + S_{C+\theta} + S_P + \sum S_{PS} \quad (3.35)$$

where S_D is the damage skin component created during drilling, cementing, well completion, fluid injection, and even oil and gas production, due to physical plugging of pore space by external or internal solid particles and fluids. This component of skin factor can be removed or prevented in well stimulation operations. The $S_{C+\theta}$ is the skin component due to partial completion and deviation angle, which modify the flow pattern near the wellbore from an ideal radial flow pattern. This skin component is not removable in water-coning and gas-coning systems. The S_p is the skin component due to non-ideal flow conditions near the perforations made during cased-hole completion. It depends on a number of parameters, including perforation density, phase angle, perforation depth, diameter, compacted zone, etc. This component can be minimized by optimizing perforating techniques. The ΣS_{PS} represents pseudo-skin components due to non-Darcy flow effects, multiphase effects, and flow convergence near the wellbore. These components cannot be eliminated.

It is essential to know the magnitude of the components of the skin factor S derived from pressure transient test data analysis. Commercial software packages are available for decomposition of the skin factor for different well completion methods, such as WellFlo (EPS 2005).

3-1 SAMPLE PROBLEM

A horizontal wellbore is placed in a 100-ft thick oil reservoir of 0.23 porosity. Oil formation volume factor and viscosity are 1.25 rb/stb and 1 cp, respectively. The total reservoir compressibility factor is 10^{-5} psi⁻¹. The well is tested following the schedule shown in Figure 3-3, which also shows the measured flowing bottom-hole pressures. Estimate the directional permeabilities and the skin factors from the test data.

SOLUTION

Figure 3-4 presents a log-log diagnostic plot of well test data. It clearly indicates initial vertical radial flow, intermediate pseudo-linear flow, and the beginning of final pseudo-radial flow.

The semi-log analysis for the vertical radial flow is shown in Figure 3-5, which gives $k_{yz} = 0.9997$ md and near-wellbore skin factor $S = -0.0164$.

The square-root time-plot analysis for the pseudo-linear flow is shown in Figure 3-6, which gives the effective wellbore length of $L = 1,082.75$ ft and a skin factor due to convergence of $S = 3.41$.

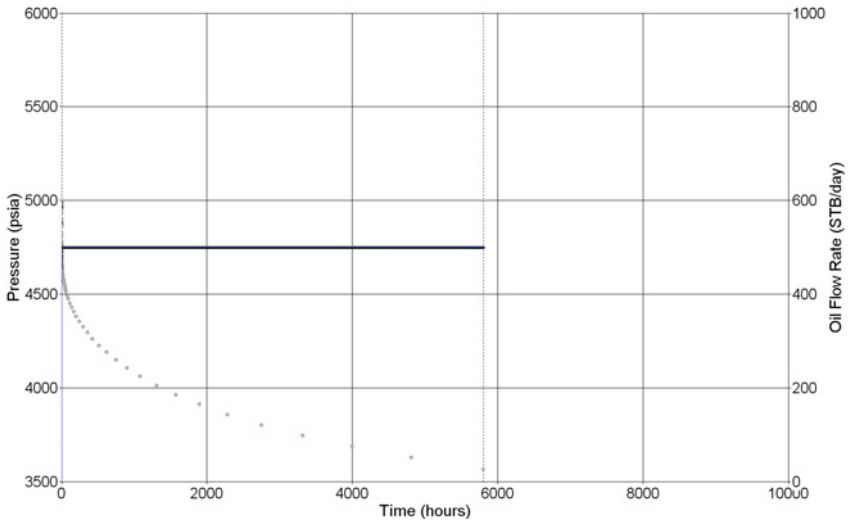


Figure 3–3 Measured bottom-hole pressures and oil production rates during a pressure draw-down test.

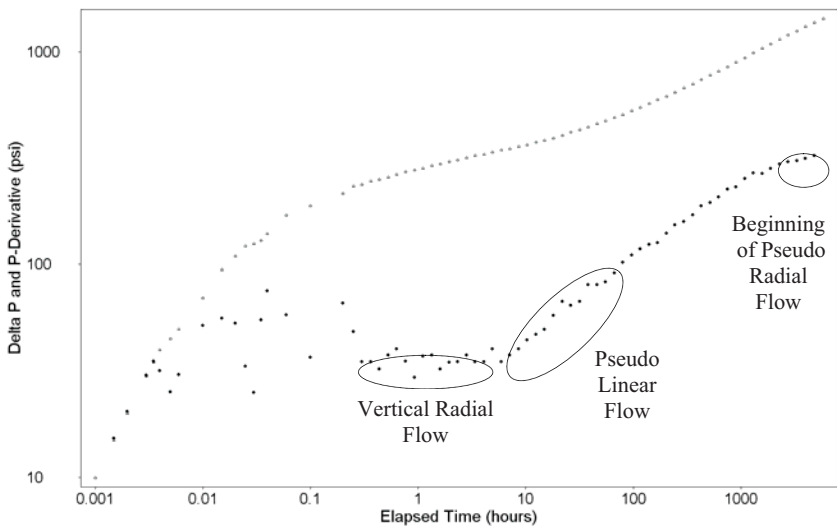


Figure 3–4 Log-log diagnostic plot of test data.

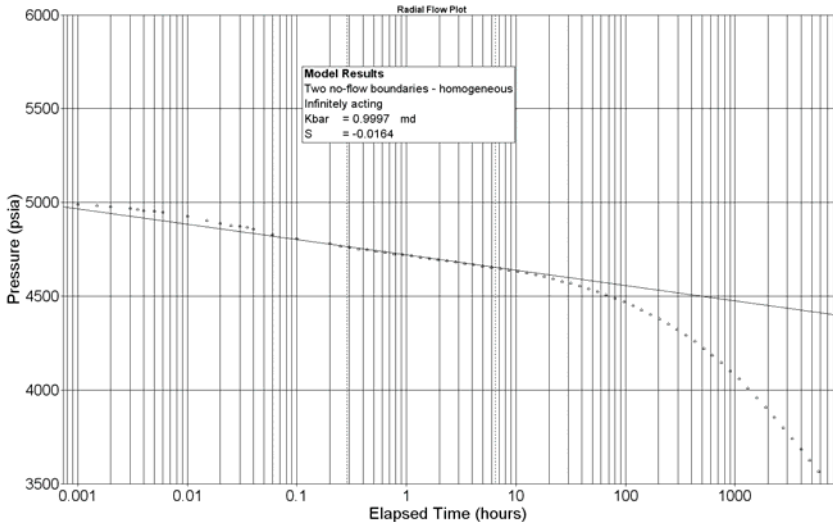


Figure 3-5 Semi-log plot for vertical radial flow analysis.

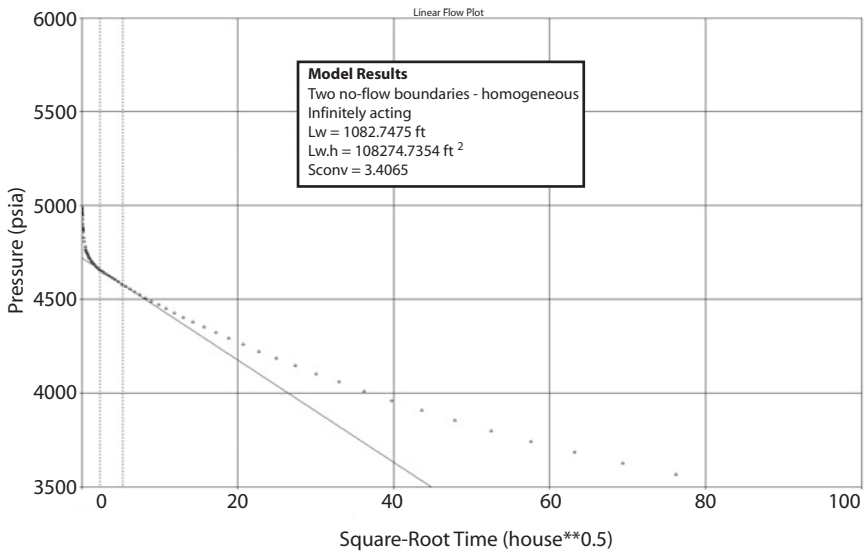


Figure 3-6 Square-root time plot for pseudo-linear flow analysis.

The semi-log analysis for the horizontal pseudo-radial flow is shown in Figure 3–7, which gives $k_h = 1.43$ md and a pseudo-skin factor $S = -6.17$.

Figure 3–8 shows a match between measured and predicted pressures, obtained using the following parameter values:

$$k_h = 1.29 \text{ md}$$

$$k_z = 0.80 \text{ md}$$

$$S = 0.06$$

$$L = 1,243 \text{ ft}$$

To estimate the long-term productivity of this horizontal well, the $k_h = 1.29$ md and $S = 0.06$ should be used in the well inflow equation to be presented in Chapter 5.

3.7 Summary

This chapter defined parameters used for characterizing reservoir properties. The effective permeabilities determined on the basis of absolute permeability and relative permeability from core measurements are only accurate at the small scale of the well core. The effective permeability data required to predict well productivity are often obtained by analyzing pressure transient data obtained by actual well testing. In pressure transient data analyses, the effective reservoir permeability that controls a well's deliverability should be derived from the flow regime that prevails in the reservoir for best long-term production.

3.8 References

Chaudhry, A. C.: *Oil Well Testing Handbook*, Gulf Professional Publishing, Burlington (2004).

Dake, L.P.: *Fundamentals of Reservoir Engineering*, Elsevier, Amsterdam (2002).

Economides, M.J., Hill, A.D., and Ehlig-Economides, C.: *Petroleum Production Systems*, Prentice Hall PTR, New Jersey (1994).

EPS: *FloSystem User Manual*, E-Production Services, Inc., Edinburgh (2005).

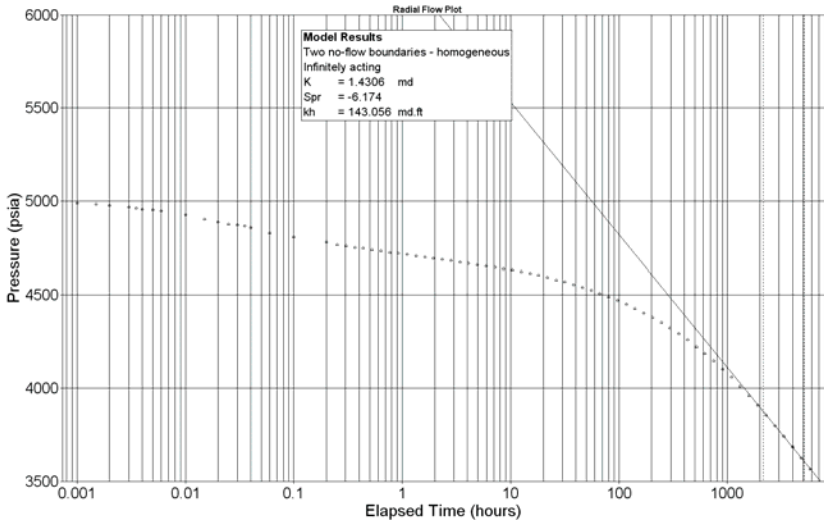


Figure 3-7 Semi-log plot for horizontal pseudo-radial flow analysis.

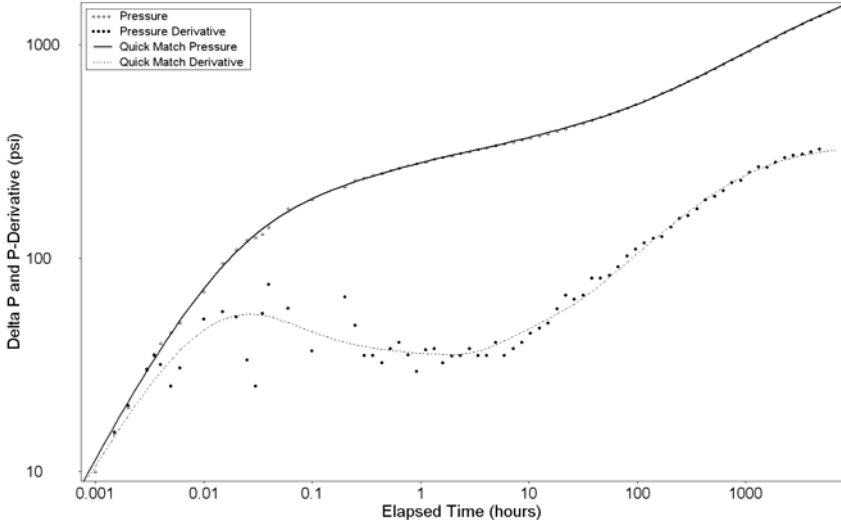


Figure 3-8 Model-match to the measured pressure response.

EPS: *PanSystem User Manual*, E-Production Services, Inc., Edinburgh (2004).

Fekete: *F.A.S.T. WellTest User Manual*, Fekete Associates, Inc., Calgary (2003).

Horne, R.N.: *Modern Well Test Analysis: A Computer-Aided Approach*, Petroway Publishing, New York (1995).

Lee, J.W., Rollins, J.B., and Spivey, J.P.: *Pressure Transient Testing*, Society of Petroleum Engineers, Richardson (2003).

3.9 Problems

- 3-1 What are the major differences between sandstone and carbonate rocks?
- 3-2 What is the maximum possible value of sandstone porosity?
- 3-3 What is the difference between absolute permeability and effective permeability?
- 3-4 What flow regimes should be used to determine effective horizontal permeability using pressure transient test data?
- 3-5 How would you determine the practical value for skin factor that truly reflects formation damage?

Reservoir Deliverability

4.1 Introduction

Reservoir deliverability is the oil or gas production rate that can be achieved from a reservoir at a given bottom-hole pressure, and is a major factor affecting well deliverability. Reservoir deliverability determines which types of completion and which artificial lift methods must be used. A thorough understanding of it is essential for accurately predicting well productivity.

Reservoir deliverability depends on several factors, including

- Reservoir pressure
- Pay zone thickness
- Effective permeability
- Reservoir boundary type and distance
- Wellbore radius
- Reservoir fluid properties
- Near-wellbore conditions

Reservoir engineers assume transient flow, steady-state flow, and pseudosteady-state flow to construct mathematical models predicting reservoir deliverability. Knowing the flow pattern permits engineers to formulate an analytical relationship between bottom-hole pressure and production rate, called inflow performance relationship (IPR). This chapter addresses the procedures used to establish the IPR of vertical, fractured, and horizontal wells producing oil and gas from reservoirs.

4.2 Vertical Wells

As a vertical well produces oil at production rate q , it creates a pressure funnel of radius r around the wellbore, as illustrated by the dotted curve in Figure 4–1(a). In this reservoir model, h is the reservoir thickness, k is the effective horizontal reservoir permeability to oil, μ_o is oil viscosity, B_o is oil formation volume factor, r_w is the wellbore radius, p_{wf} is the flowing bottom-hole pressure, and p is the pressure in the reservoir at the distance r from the wellbore center line. The flow stream lines in the cylindrical region form the horizontal radial flow pattern depicted in Figure 4–1(b).

4.2.1 Transient Flow

Transient flow is defined as a flow condition under which the radius of pressure wave propagation from the wellbore has not reached the boundaries of the reservoir. During transient flow the developing pressure funnel is small, relative to the reservoir size. Therefore, the transient pressure behaves as if the reservoir were infinitely large.

Assuming single-phase oil flow in the reservoir, several analytical solutions have been developed for describing transient flow behavior. These are available from classic textbooks, such as Dake (1978). A constant-rate solution expressed by Equation (4.1) is frequently used in reservoir engineering:

$$p_{wf} = p_i - \frac{162.6qB_o\mu_o}{kh} \left(\log t + \log \frac{k}{\phi\mu_o c_t r_w^2} - 3.23 + 0.87S \right) \quad (4.1)$$

where

p_{wf} = flowing bottom-hole pressure (psia)

p_i = initial reservoir pressure (psia)

q = oil production rate (stb/day)

μ_o = viscosity of oil (cp)

k = effective horizontal permeability to oil (md)

h = reservoir thickness (ft)

t = flow time (hours)

ϕ = porosity (fractional)

c_t = total compressibility (psi^{-1})

r_w = wellbore radius to the sand face (ft)

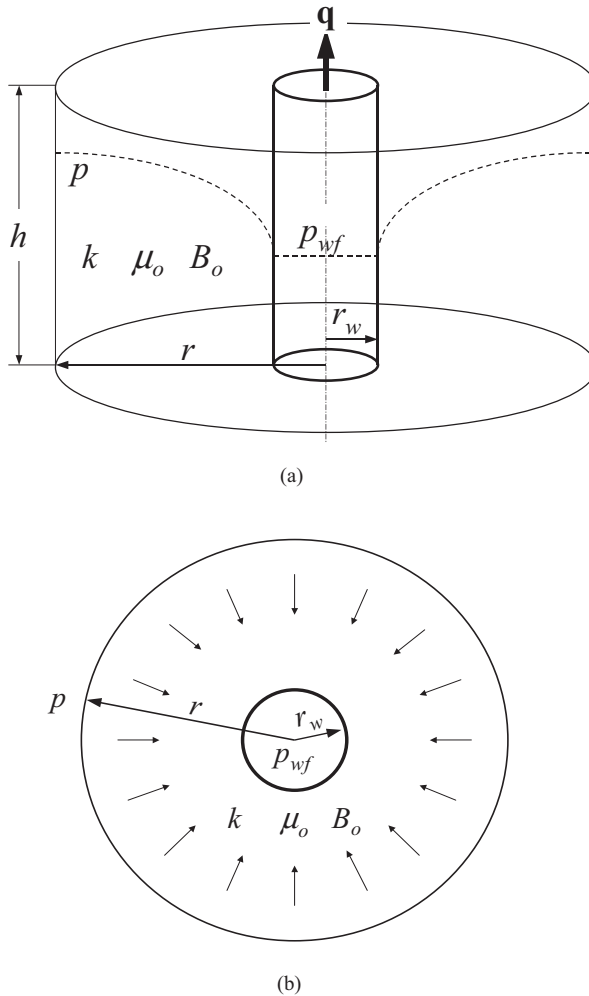


Figure 4-1 A reservoir model illustrating radial flow: (a) lateral view, (b) top view.

S = skin factor

Log = 10-based logarithm (\log_{10})

The fixed choke size used in typical production oil wells results in constant wellhead pressure, which, in turn, results in constant bottom-hole pressure. A constant-bottom-hole pressure solution is therefore more desirable for well inflow performance analysis. Using an appropriate inner boundary

condition arrangement, Earlougher (1977) developed a constant-bottom-hole pressure solution, which is similar to Equation (4.1), expressed as

$$q = \frac{kh(p_i - p_{wf})}{162.6B_o\mu_o \left(\log t + \log \frac{k}{\phi\mu_o c_t r_w^2} - 3.23 + 0.87S \right)} \quad (4.2)$$

which is used for transient well performance analysis in reservoir engineering.

Equation (4.2) indicates that at a constant bottom-hole pressure, the oil production rate decreases with flow time. This is because the radius of the pressure funnel (over which the pressure drawdown $(p_i - p_{wf})$ acts) increases with time. In other words, the overall pressure gradient in the drainage area decreases with time.

For gas wells, the transient solution is expressed as

$$q_g = \frac{kh[m(p_i) - m(p_{wf})]}{1638T \left(\log t + \log \frac{k}{\phi\mu_g c_t r_w^2} - 3.23 + 0.87S \right)} \quad (4.3)$$

where q_g is production rate in Mscf/d, k is the effective permeability to gas in md, T is temperature in °R, μ_g is gas viscosity in cp, and $m(p)$ is real-gas pseudo-pressure, defined as

$$m(p) = \int_{p_b}^p \frac{2p}{\mu_g z} dp \quad (4.4)$$

where p_b is the base pressure, usually taken as 14.7 psia. The real-gas pseudo-pressure can be readily determined using spreadsheet program **PseudoPressure.xls**.

4.2.2 Steady-State Flow

Steady-state flow is defined as a flow condition under which the pressure at any point in the reservoir remains constant over time. This flow condition prevails when the pressure funnel shown in Figure 4–1 has propagated to a constant-pressure boundary. The constant-pressure boundary might be the edge of an aquifer, or the region surrounding a water injection well. A sketch of this reservoir model is shown in Figure 4–2, where p_e represents the pressure at the constant-pressure boundary. Under steady-state flow conditions due to a circular constant-pressure boundary at distance r_e from the wellbore centerline, assuming single-phase flow, the following theoretical relationship for an oil reservoir can be derived from Darcy’s law:

$$q = \frac{kh(p_e - p_{wf})}{141.2B_o\mu_o \left(\ln \frac{r_e}{r_w} + S \right)} \quad (4.5)$$

where “ln” denotes 2.718-based natural logarithm (\log_e). The derivation of Equation (4.5) is left to the reader as an exercise.

4.2.3 Pseudosteady-State Flow

Pseudosteady-state flow is defined as a flow condition under which the pressure at any point in the reservoir declines at the same constant rate over time. This flow condition prevails after the pressure funnel shown in Figure 4–1 has propagated to all adjacent no-flow boundaries. A no-flow boundary can be a sealing fault, a pinch-out of the reservoir pay zone, or the boundaries of drainage areas of production wells. A sketch of this reservoir model is shown in Figure 4–3 where p_e represents the pressure at the no-flow boundary at time t_d . Under pseudosteady-state flow conditions due to a circular no-flow boundary at distance r_e from wellbore centerline, assuming single-phase flow, the following theoretical relationship for an oil reservoir can be derived from Darcy’s law:

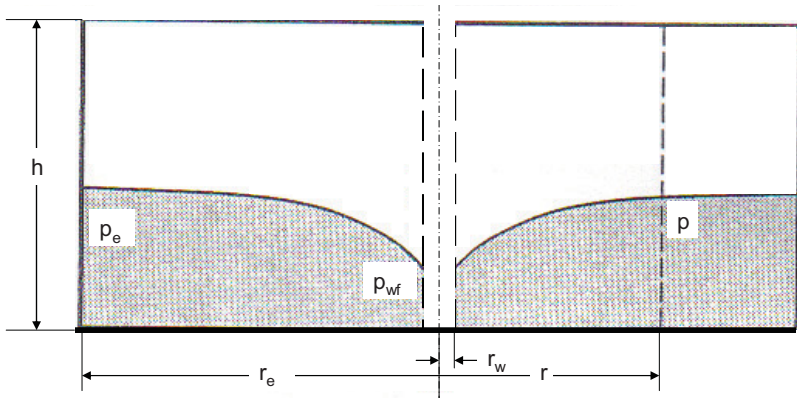


Figure 4-2 A reservoir model illustrating a constant-pressure boundary.

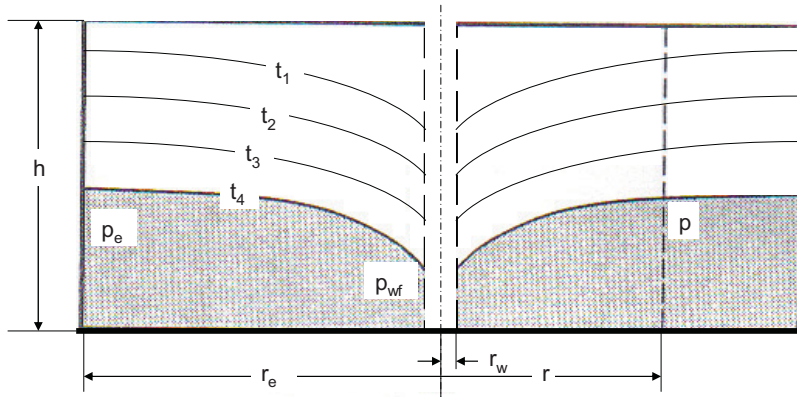


Figure 4-3 Pressure and flow conditions of a reservoir with no-flow boundaries.

$$q = \frac{kh(p_e - p_{wf})}{141.2B_o\mu_o \left(\ln \frac{r_e}{r_w} - \frac{1}{2} + S \right)} \quad (4.6)$$

The flow time required for the pressure funnel to reach the circular boundary can be expressed as

$$t_{pss} = 1200 \frac{\phi\mu_o c_t r_e^2}{k} \quad (4.7)$$

Since the value of reservoir pressure, p_e , in Equation (4.6) is usually not known, the following expression using the average reservoir pressure is more useful:

$$q = \frac{kh(\bar{p} - p_{wf})}{141.2B_o\mu_o \left(\ln \frac{r_e}{r_w} - \frac{3}{4} + S \right)} \quad (4.8)$$

where \bar{p} is the average reservoir pressure, estimated by pressure transient data analysis or predicted by reservoir simulation. The derivations of Equations (4.6) and (4.8) are left to the reader as an exercise.

If the no-flow boundaries delineate a non-circular drainage area, use the following equation to predict the pseudosteady-state flow:

$$q = \frac{kh(\bar{p} - p_{wf})}{141.2B_o\mu_o \left(\frac{1}{2} \ln \frac{4A}{\gamma C_A r_w^2} + S \right)} \quad (4.9)$$

where

A = drainage area (ft²)

$\gamma = 1.78 = e^{0.5572}$ (where 0.5572 is Euler's constant)

C_A = drainage area shape factor (31.6 for a circular boundary)

An appropriate value of the shape factor C_A can be found from Figures 4-4 and 4-5.

For a gas well located at the center of a circular drainage area, the pseudosteady-state solution is expressed as

$$q_g = \frac{kh \left[m(\bar{p}) - m(p_{wf}) \right]}{1424T \left(\ln \frac{r_e}{r_w} - \frac{3}{4} + S + Dq_g \right)} \quad (4.10)$$

where

D = non-Darcy flow coefficient, d/Mscf


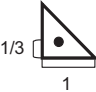
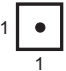
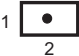

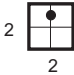

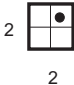
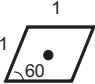

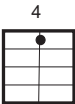

Reservoir Shape & Well Location	Shape Factor C_A	Reservoir Shape & Well Location	Shape Factor C_A
	31.6		21.9
	30.9		22.6
	31.6		12.9
	27.6		4.5
	27.1		In water-drive reservoirs 19.1
	3.39		In reservoirs of unknown production character 25

Figure 4-4 Shape factors for closed drainage areas with low-aspect ratios.

4.3 Fractured Wells

Hydraulically-created fractures receive fluids from the reservoir matrix and provide channels for it to flow into the wellbore. Apparently, the productivity of fractured wells depends on two stages: (1) receiving fluids from the formation by the fractures, and (2) transporting the received fluid to wellbore along the fractures. Usually one of the stages is a lim-

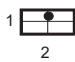
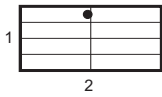
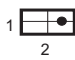
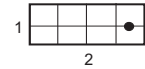
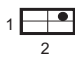
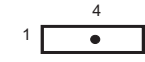
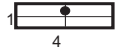
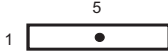
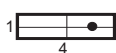
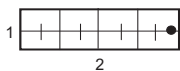
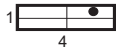

Reservoir Shape & Well Location	Shape Factor C_A	Reservoir Shape & Well Location	Shape Factor C_A
	10.8		3.13
	4.86		0.607
	2.07		5.38
	2.72		2.36
	0.232		0.111
	0.115		0.098

Figure 4-5 Shape factors for closed drainage areas with high-aspect ratios.

iting factor that controls well production rate. The efficiency of the first stage depends on fracture dimension (length and height), and the efficiency of the second stage depends on fracture permeability. The relative importance of each can be analyzed using the concept of fracture conductivity (Argawal et al. 1979; Cinco-Ley and Samaniego 1981) defined as

$$F_{CD} = \frac{k_f w}{k x_f} \tag{4.11}$$

where

F_{CD} = fracture conductivity (dimensionless)

k_f = fracture permeability (md)

w = fracture width (ft)

x_f = fracture half-length (ft)

In situations where the fracture length is much smaller compared to the drainage area of the well, the long-term productivity of a fractured well can be estimated assuming pseudo-radial flow in the reservoir. In that case, the inflow equation for steady-state flow can be expressed as

$$q = \frac{kh(p_e - p_{wf})}{141.2B\mu \left(\ln \frac{r_e}{r_w} + S_f \right)} \quad (4.12)$$

where S_f is the equivalent skin factor for the fractured well, and takes negative values. The factor of increase in reservoir deliverability can be expressed as

$$\frac{J}{J_o} = \frac{\ln \frac{r_e}{r_w}}{\ln \frac{r_e}{r_w} + S_f} \quad (4.13)$$

where

J = productivity of fractured well (stb/d-psi)

J_o = productivity of non-fractured well (stb/d-psi)

The effective skin factor S_f can be determined based on fracture conductivity. Cinco-Ley and Samanigo (1981) showed that the parameter $S_f + \ln(x_f / r_w)$ approaches a constant value of about 0.7 in the range of $F_{CD} > 100$ —that is,

$$S_f \approx 0.7 - \ln(x_f / r_w) \quad (4.14)$$

This indicates that the equivalent skin factor of fractured wells depends only on fracture length for high-conductivity fractures, not fracture permeability and width. This is the situation where the first stage is the limiting factor. On the other hand, their chart indicates that the parameter $S_f + \ln(x_f / r_w)$ declines linearly with $\log(F_{CD})$ in the range of $F_{CD} < 1$ —that is,

$$S_f + \ln(x_f / r_w) \approx 1.52 - 1.545 \log(F_{CD}) \quad (4.15)$$

which gives

$$S_f \approx 1.52 + 2.31 \log(r_w) - 1.545 \log\left(\frac{k_f w}{k}\right) - 0.765 \log(x_f) \quad (4.16)$$

Comparing the coefficients of the last two terms in this relation indicates that the equivalent skin factor of a fractured well is more sensitive to fracture permeability and width than to fracture length for low-conductivity fractures. This is the situation in which the second stage is the limiting factor.

The previous analyses reveal that low-permeability reservoirs would benefit most from increased fracture length, while high-permeability reservoirs benefit more from increased fracture permeability and width.

Valko et al. (1997) converted Cinco-Ley and Samanigo's (1981) chart in the whole range of fracture conductivity to the following correlation:

$$S_f + \ln(x_f / r_w) = \frac{1.65 - 0.328u + 0.116u^2}{1 + 0.180u + 0.064u^2 + 0.05u^3} \quad (4.17)$$

where $u = \ln(F_{CD})$.

4-1 SAMPLE PROBLEM

A gas reservoir has a permeability of 1 md. A vertical well with a radius of 0.328 ft drains a reservoir area of 160 acres. If the well is hydraulically fractured to create a 2,000 ft long, 0.12 inch wide fracture of 200,000 md permeability around the center of the drainage area, what is the expected factor of increase in reservoir deliverability?

SOLUTION

Radius of the drainage area:

$$r_e = \sqrt{\frac{A}{\pi}} = \sqrt{\frac{(43,560)(160)}{\pi}} = 1,490 \text{ ft}$$

Fracture conductivity:

$$F_{CD} = \frac{k_f w}{k x_f} = \frac{(200,000)(0.12 / 12)}{(1)(2,000 / 2)} = 2$$

Equation (4.17) yields

$$S_f + \ln(x_f / r_w) \approx 1.2$$

which gives

$$S_f \approx 1.2 - \ln(x_f / r_w) = 1.2 - \ln(1,000 / 0.328) = -6.82$$

The factor of increase in reservoir deliverability is therefore:

$$\frac{J}{J_o} = \frac{\ln \frac{r_e}{r_w}}{\ln \frac{r_e}{r_w} + S_f} = \frac{\ln \frac{1,490}{0.328}}{\ln \frac{1,490}{0.328} - 6.82} = 5.27$$

The above principle is also valid for pseudosteady flow, in which the average reservoir pressure should be used. In that case, Equation (4.12) becomes

$$q = \frac{kh(\bar{p} - p_{wf})}{141.2 B_o \mu_o \left(\frac{1}{2} \ln \frac{4A}{\gamma C_A r_w^2} + S_f \right)} \quad (4.18)$$

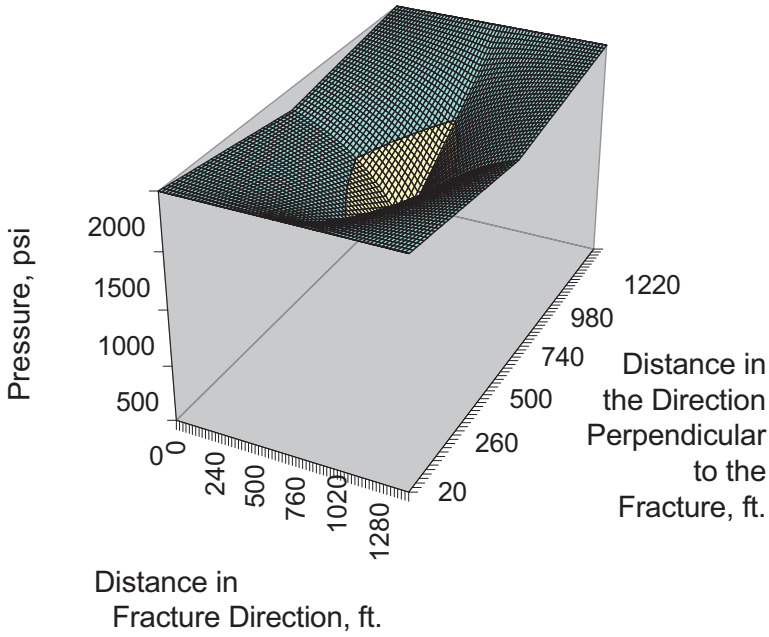


Figure 4-6 An example of reservoir pressure distribution near a long fracture.

Equation (4.13) assumes radial flow and may result in significant error if used in situations where the fracture length is comparable to the drainage area of the well ($x_f > 0.5r_e$). In these cases, long-term reservoir deliverability may be estimated assuming bilinear flow in the reservoir and fracture. Pressure distribution in a linear-flow reservoir with linear flow in a fracture of finite conductivity is illustrated in Figure 4-6. An analytical solution for estimating the factor of increase in reservoir deliverability was presented by Guo and Schechter (1999), as follows:

$$\frac{J}{J_o} = \frac{0.72 \left(\ln \frac{r_e}{r_w} - \frac{3}{4} + S_o \right)}{z_e \sqrt{c} \left(\frac{1}{1 - e^{-\sqrt{c}x_f}} - \frac{1}{2x_f \sqrt{c}} \right)} \quad (4.19)$$

where $c = \frac{2k}{z_e w k_f}$ and

$J =$ productivity index of fractured well (stb/d-psi)

$J_o =$ productivity index of non-fractured well (stb/d-psi)

$S_o =$ skin factor of the non-fractured well (dimensionless)

$z_e =$ distance between the fracture and the flow boundary (ft)

4.4 Horizontal Wells

The transient flow, steady-state flow, and pseudosteady-state flow can also exist in reservoirs penetrated by horizontal wells. Different mathematical models are available from literature. Joshi (1988) presented a mathematical model considering steady-state flow of oil in the horizontal plane and pseudosteady-state flow in the vertical plane. Joshi's equation was modified by Economides et al. (1991) to include the effect of reservoir anisotropy. Guo et al. (2007) pointed out that Joshi's equation is optimistic for high-productivity reservoirs due to neglecting the effect of frictional pressure in the horizontal wellbore. Guo et al. (2007) suggests that the following modified Joshi equations be applied to estimating horizontal well inflow performance.

For oil wells,

$$q = \frac{k_H h (p_e - p_{wf})}{141.2 B_o \mu_o \left\{ \ln \left[\frac{a + \sqrt{a^2 - (L/2)^2}}{L/2} \right] + \frac{I_{ani} h}{L} \ln \left[\frac{I_{ani} h}{r_w (I_{ani} + 1)} \right] + s \right\}} F_o \quad (4.20)$$

For gas wells,

$$q_g = \frac{k_H h (p_e^2 - p_{wf}^2)}{1424 \bar{\mu}_g \bar{z} T \left\{ \ln \left[\frac{a + \sqrt{a^2 - (L/2)^2}}{L/2} \right] + \frac{I_{ani} h}{L} \ln \left[\frac{I_{ani} h}{r_w (I_{ani} + 1)} \right] + s + Dq_g \right\}} F_g \quad (4.21)$$

where

$$a = \frac{L}{2} \sqrt{\frac{1}{2} + \sqrt{\left[\frac{1}{4} + \left(\frac{r_{eH}}{L/2} \right)^4 \right]}} \quad (4.22)$$

and

q = oil production rate (stb/day)

q_g = gas production rate (Mscf/day)

$$I_{ani} = \sqrt{\frac{k_H}{k_V}}$$

k_H = the average horizontal permeability (md)

k_V = vertical permeability (md)

r_{eH} = radius of drainage area of horizontal well (ft)

L = length of horizontal wellbore ($L/2 < 0.9r_{eH}$) (ft)

F_o = correction factor for oil production rate (dimensionless)

F_g = correction factor for gas production rate (dimensionless)

T = reservoir temperature ($^{\circ}\text{R}$)

$\bar{\mu}_g$ = average gas viscosity (cp)

\bar{z} = average gas compressibility factor (dimensionless)

s = skin factor (dimensionless)

D = non-Darcy flow coefficient (day/Mscf)

The methods for obtaining the correction factors F_o and F_g will be presented in Appendix C and Appendix D, respectively.

4.5 Inflow Performance Relationship (IPR)

Engineers use the inflow performance relationship (IPR) to evaluate reservoir deliverability in reservoir and production engineering. The IPR curve is a graphical presentation of the relationship between the flowing bottom-hole pressure and the liquid production rate. A typical IPR curve is shown in Figure 4–7. The magnitude of the slope of IPR curve is called productivity index (PI or J), expressed as

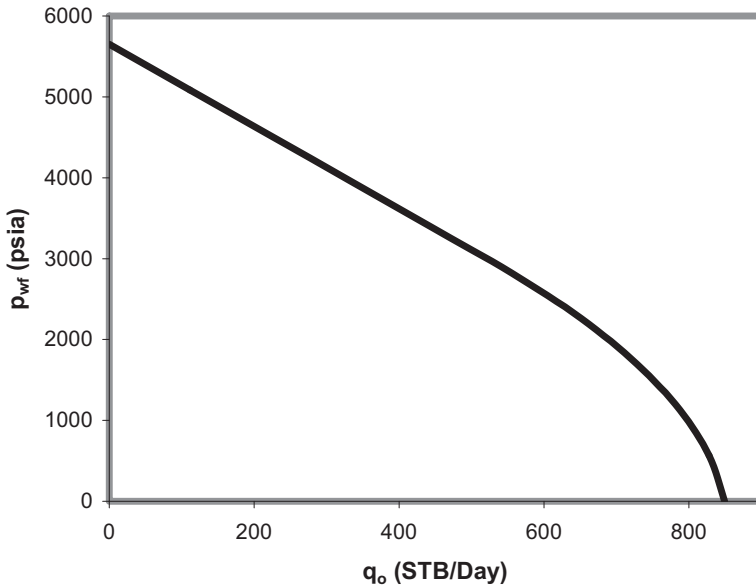


Figure 4–7 A typical IPR curve for an oil well.

$$J = \frac{q}{(p_e - p_{wf})} \quad (4.23)$$

where J is productivity index. Apparently J is not a constant in a two-phase flow reservoir.

The well IPR curves are usually constructed using reservoir inflow models, which can be derived theoretically or from empirical formulation. It is essential to validate these models with test points in field applications.

4.5.1 IPR for Single (Liquid) Phase Reservoirs

All reservoir inflow models presented earlier in this chapter were derived assuming single-phase flow. This assumption is valid for undersaturated oil reservoirs or for reservoir regions where the pressure is greater than the bubble-point pressure. The following equations define the productivity index (J^*) for flowing bottom-hole pressures greater than the bubble-point pressure.

For **radial transient** flow around a **vertical** well,

$$J^* = \frac{q}{(p_i - p_{wf})} = \frac{kh}{162.6B_o\mu_o \left(\log t + \log \frac{k}{\phi\mu_o c_t r_w^2} - 3.23 + 0.87S \right)} \quad (4.24)$$

For **radial steady-state** flow around a **vertical** well,

$$J^* = \frac{q}{(p_e - p_{wf})} = \frac{kh}{141.2B_o\mu_o \left(\ln \frac{r_e}{r_w} + S \right)} \quad (4.25)$$

For **pseudosteady-state** flow around a **vertical** well,

$$J^* = \frac{q}{(\bar{p} - p_{wf})} = \frac{kh}{141.2B_o\mu_o \left(\frac{1}{2} \ln \frac{4A}{\gamma C_A r_w^2} + S \right)} \quad (4.26)$$

For **steady-state** flow around a **fractured** well,

$$J^* = \frac{q}{(p_e - p_{wf})} = \frac{kh}{141.2B_o\mu_o \left(\ln \frac{r_e}{r_w} + S_f \right)} \quad (4.27)$$

For **steady-state** flow around a **horizontal** well,

$$J^* = \frac{q}{(p_e - p_{wf})} = \frac{k_H h}{141.2B_o\mu_o \left\{ \ln \left[\frac{a + \sqrt{a^2 - (L/2)^2}}{L/2} \right] + \frac{I_{ani} h}{L} \ln \left[\frac{I_{ani} h}{r_w (I_{ani} + 1)} \right] \right\}} \quad (4.28)$$

Because the productivity index (J^*) above the bubble-point pressure is independent of production rate, the IPR curve for single (liquid) phase reservoir is a straight line. If the bubble-point pressure is 0 psig, the absolute open flow (AOF) is equal to the productivity index (J^*) multiplied by the reservoir pressure.

4-2 SAMPLE PROBLEM

Calculate and graph the IPR for a vertical well in an oil reservoir. Consider: 1) transient flow at 30 days, 2) steady-state flow, and 3) pseudosteady-state flow. The following data are given:

Porosity: $\phi = 0.19$

Effective horizontal permeability: $k = 8.2$ md

Pay zone thickness: $h = 53$ ft

Reservoir pressure: p_e or $\bar{p} = 5651$ psia

Bubble-point pressure: $p_b = 50$ psia

Oil formation volume factor: $B_o = 1.1$

Oil viscosity: $\mu_o = 1.7$ cp

Total compressibility: $c_t = 0.0000129$ psi⁻¹

Drainage area: $A = 640$ acres ($r_e = 2980$ ft)

Wellbore radius: $r_w = 0.328$ ft

Skin factor: $S = 0$

SOLUTION

1) For transient flow at 30 days,

$$\begin{aligned}
 J^* &= \frac{kh}{162.6B_o\mu_o \left(\log t + \log \frac{k}{\phi\mu_o c_t r_w^2} - 3.23 \right)} \\
 &= \frac{(8.2)(53)}{162.6(1.1)(1.7) \left(\log [((30)(24))] + \log \frac{(8.2)}{(0.19)(1.7)(0.0000129)(0.328)^2} - 3.23 \right)} \\
 &= 0.2075 \text{ STB/d-psi}
 \end{aligned}$$

The calculated points are

p_{wf} (psi)	q_o (STB/day)
50	1,162
5,651	0

The transient IPR curve is illustrated in Figure 4–8.

2) For steady-state flow,

$$\begin{aligned}
 J^* &= \frac{kh}{141.2B_o\mu_o \left(\ln \frac{r_e}{r_w} + S \right)} \\
 &= \frac{(8.2)(53)}{141.2(1.1)(1.7) \ln \left(\frac{2980}{0.328} \right)} \\
 &= 0.1806 \text{ STB/d-psi}
 \end{aligned}$$

The calculated points are

p_{wf} (psi)	q_o (STB/day)
50	1,011
5,651	0

The steady-state IPR curve is illustrated in Figure 4–9.

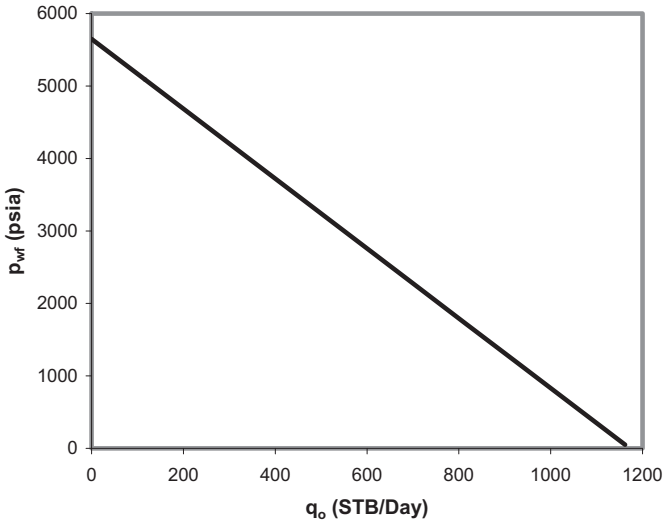


Figure 4–8 *Transient IPR curve for Sample Problem 4-2.*

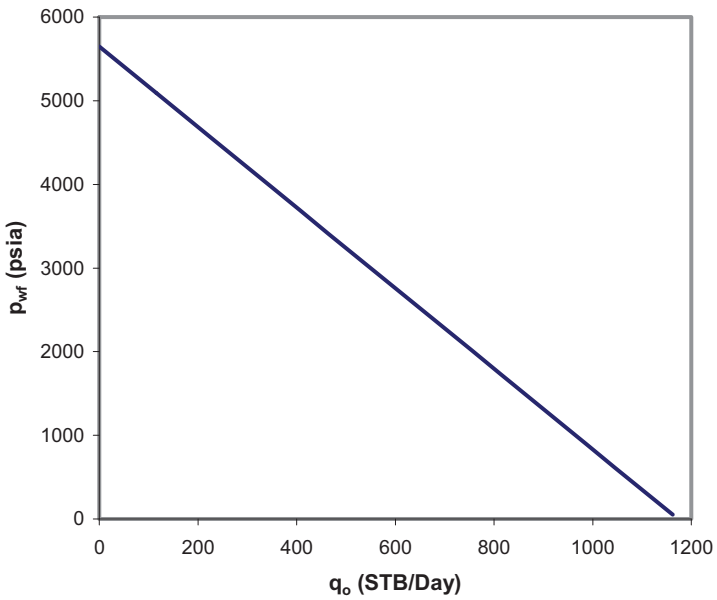


Figure 4–9 *Steady-state IPR curve for Sample Problem 4-2.*

3) For pseudosteady-state flow,

$$\begin{aligned}
 J^* &= \frac{kh}{141.2B_o\mu_o \left(\ln \frac{r_e}{r_w} - \frac{3}{4} + S \right)} \\
 &= \frac{(8.2)(53)}{141.2(1.1)(1.7) \left(\ln \frac{2980}{0.328} - 0.75 \right)} \\
 &= 0.1968 \text{ STB/d-psi}
 \end{aligned}$$

The calculated points are

p_{wf} (psi)	q_o (STB/day)
50	1,102
5,651	0

The pseudosteady-state IPR curve is illustrated in Figure 4–10.

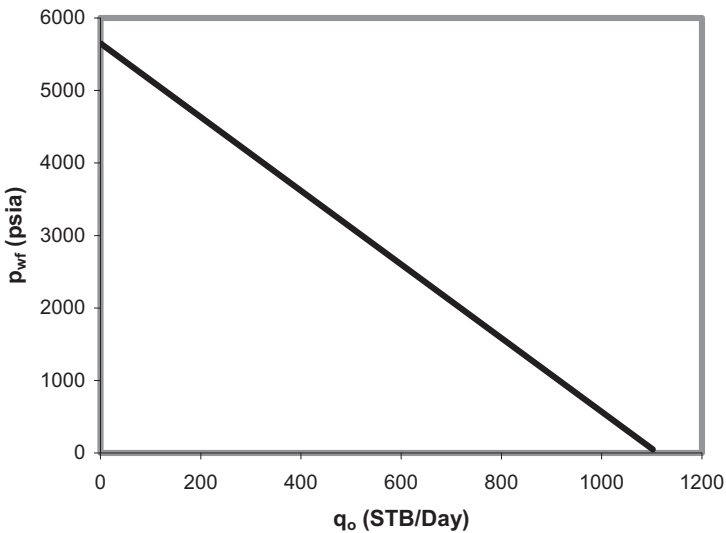


Figure 4–10 Pseudosteady-state IPR curve for Sample Problem 4-2.

4.5.2 IPR for Two-Phase Reservoirs

The linear IPR model presented in the last section is valid for pressure values as low as bubble-point pressure. At pressures less than the bubble-point pressure, some solution gas escapes from the oil and becomes free gas, which occupies some portion of available pore space. This reduces oil flow, both because of reduced relative permeability to the oil, and because oil viscosity increases as its solution gas content decreases. This combination of decreased relative permeability and increased viscosity results in a lower oil production rate at any given bottom-hole pressure. This causes the IPR curve to deviate from a linear trend at pressures less than the bubble-point pressure, as shown in Figure 4–7. The lower the pressure, the larger will be the deviation. If the reservoir pressure is less than the initial bubble-point pressure, two-phase oil and gas flow exists in the entire reservoir domain and it is referred to as a two-phase reservoir.

Only empirically-derived equations are available for modeling the IPR of two-phase reservoirs. These include the Vogel (1968) equation as extended by Standing (1971) and those of Fetkovich (1973), Bandakhlia and Aziz (1989), Chang (1992), and Retnanto and Economides (1998). Vogel's equation is still widely used in the industry, expressed as

$$q = q_{\max} \left[1 - 0.2 \left(\frac{p_{wf}}{\bar{p}} \right) - 0.8 \left(\frac{p_{wf}}{\bar{p}} \right)^2 \right] \quad (4.29)$$

or

$$p_{wf} = 0.125 \bar{p} \left[\sqrt{81 - 80 \left(\frac{q}{q_{\max}} \right)} - 1 \right] \quad (4.30)$$

where q_{\max} is an empirical constant that represents the maximum possible reservoir deliverability, or AOF. The value of q_{\max} can be estimated theoretically from reservoir pressure and the productivity index at the bubble-point pressure. For pseudosteady-state flow, it follows that

$$q_{\max} = \frac{J^* \bar{p}}{1.8} \quad (4.31)$$

The derivation of this relation is left to the reader for an exercise.

Fetkovich's equation is expressed as

$$q = q_{\max} \left[1 - \left(\frac{p_{wf}}{\bar{p}} \right)^2 \right]^n \quad (4.32)$$

or

$$q = C \left(\bar{p}^2 - p_{wf}^2 \right)^n \quad (4.33)$$

where C and n are empirical constants, and are related to q_{\max} by $C = q_{\max} / \bar{p}^{2n}$. As illustrated in Sample Problem 4-6, Fetkovich's equation using two constants is more conservative than Vogel's equation for IPR modeling.

Again, Equations (4.29) and (4.33) are valid if average reservoir pressure \bar{p} is at or less than the initial bubble-point pressure. Equation (4.33) is often used in gas reservoir applications.

4-3 SAMPLE PROBLEM

Calculate and graph the IPR for a vertical well in a saturated oil reservoir using Vogel's equation. The following data are given:

Porosity: $\phi = 0.19$

Effective horizontal permeability: $k = 8.2$ md

Pay zone thickness: $h = 53$ ft

Reservoir pressure: $\bar{p} = 5651$ psia

Bubble-point pressure: $p_b = 5651$ psia

Oil formation volume factor: $B_o = 1.1$

Oil viscosity: $\mu_o = 1.7$ cp

Total compressibility: $c_t = 0.0000129$ psi⁻¹

Drainage area: $A = 640$ acres ($r_e = 2980$ ft)

Wellbore radius: $r_w = 0.328$ ft

Skin factor: $S = 0$

SOLUTION

$$\begin{aligned}
 J^* &= \frac{kh}{141.2B_o\mu_o \left(\ln \frac{r_e}{r_w} - \frac{3}{4} + S \right)} \\
 &= \frac{(8.2)(53)}{141.2(1.1)(1.7) \left(\ln \frac{2980}{0.328} - 0.75 \right)} \\
 &= 0.1968 \text{ STB/d-psi}
 \end{aligned}$$

$$\begin{aligned}
 q_{\max} &= \frac{J^* \bar{p}}{1.8} \\
 &= \frac{(0.1968)(5651)}{1.8} \\
 &= 618 \text{ stb/day}
 \end{aligned}$$

The IPR curve is illustrated in Figure 4–11.

The points calculated using Equation (4.29) are

p_{wf} (psi)	q_o (STB/day)
5651	0
5000	122
4500	206
4000	283
3500	352
3000	413
2500	466
2000	512
1500	550
1000	580
500	603
0	618

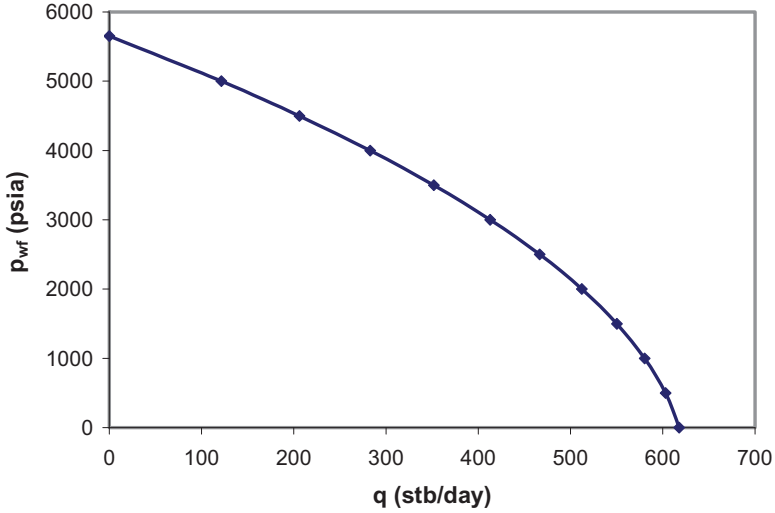


Figure 4–11 IPR curve for Sample Problem 4-3.

4.5.3 IPR for Partial Two-Phase Oil Reservoirs

If the reservoir pressure is greater than the bubble-point pressure and the flowing bottom-hole pressure is less than the bubble-point pressure, a generalized model of Vogel's IPR can be used. The model combines the straight-line IPR model for single-phase flow with Vogel's IPR model for two-phase flow. Figure 4–12 illustrates the curve derived using the two-part model.

According to the linear IPR model, the flow rate at the bubble-point pressure is

$$q_b = J^* (\bar{p} - p_b) \quad (4.34)$$

Based on Vogel's IPR model, the additional component of flow resulting from the pressure below the bubble-point pressure is expressed as

$$\Delta q = q_v \left[1 - 0.2 \left(\frac{p_{wf}}{p_b} \right) - 0.8 \left(\frac{p_{wf}}{p_b} \right)^2 \right] \quad (4.35)$$

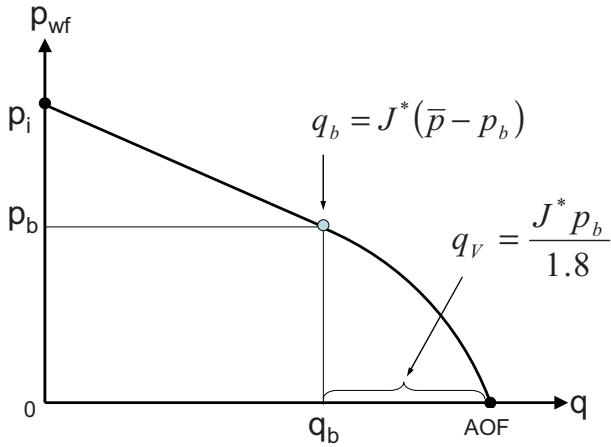


Figure 4–12 Generalized Vogel IPR model for partial two-phase reservoirs.

Thus the total flow rate at a given bottom-hole pressure that is less than the bubble-point pressure is expressed as

$$q = q_b + q_v \left[1 - 0.2 \left(\frac{p_{wf}}{p_b} \right) - 0.8 \left(\frac{p_{wf}}{p_b} \right)^2 \right] \quad (4.36)$$

Because

$$q_v = \frac{J^* p_b}{1.8} \quad (4.37)$$

Equation (4.36) becomes

$$q = J^* (\bar{p} - p_b) + \frac{J^* p_b}{1.8} \left[1 - 0.2 \left(\frac{p_{wf}}{p_b} \right) - 0.8 \left(\frac{p_{wf}}{p_b} \right)^2 \right] \quad (4.38)$$

4-4 SAMPLE PROBLEM

Calculate and graph the IPR of a vertical well in an undersaturated oil reservoir using the generalized Vogel's equation. The following data are given:

Porosity: $\phi = 0.19$

Effective horizontal permeability: $k = 8.2$ md

Pay zone thickness: $h = 53$ ft

Reservoir pressure: $\bar{p} = 5651$ psia

Bubble-point pressure: $p_b = 3000$ psia

Oil formation volume factor: $B_o = 1.1$

Oil viscosity: $\mu_o = 1.7$ cp

Total compressibility: $c_t = 0.0000129$ psi⁻¹

Drainage area: $A = 640$ acres ($r_e = 2980$ ft)

Wellbore radius: $r_w = 0.328$ ft

Skin factor: $S = 0$

SOLUTION

$$J^* = \frac{kh}{141.2B_o\mu_o \left(\ln \frac{r_e}{r_w} - \frac{3}{4} + S \right)}$$

$$= \frac{(8.2)(53)}{141.2(1.1)(1.7) \left(\ln \frac{2980}{0.328} - 0.75 \right)}$$

$$= 0.1968 \text{ STB/d-psi}$$

$$q_b = J^* (\bar{p} - p_b)$$

$$= (0.1968)(5651 - 3000)$$

$$= 522 \text{ stb/day}$$

$$\begin{aligned}
 q_v &= \frac{J^* p_b}{1.8} \\
 &= \frac{(0.1968)(3000)}{1.8} \\
 &= 328 \text{ stb/day}
 \end{aligned}$$

The points calculated using Equation (4.36) are

p_{wf}	q_o (STB/day)
0	850
565	828
1130	788
1695	729
2260	651
2826	555
3000	522
565	0

The IPR curve is illustrated in Figure 4–13.

4.6 Construction of IPR Curves Using Test Points

As shown in the last section, well IPR curves can be constructed using formation permeability, pay zone thickness, fluid viscosity, drainage area, wellbore radius, and well skin factor. These parameters determine the constants (such as the productivity index) used in the IPR model. However, actual values for these parameters are not always available in reality. Because of this, reservoir engineers frequently use measured values of production rate and flowing bottom-hole pressure, called test points, to construct IPR curves.

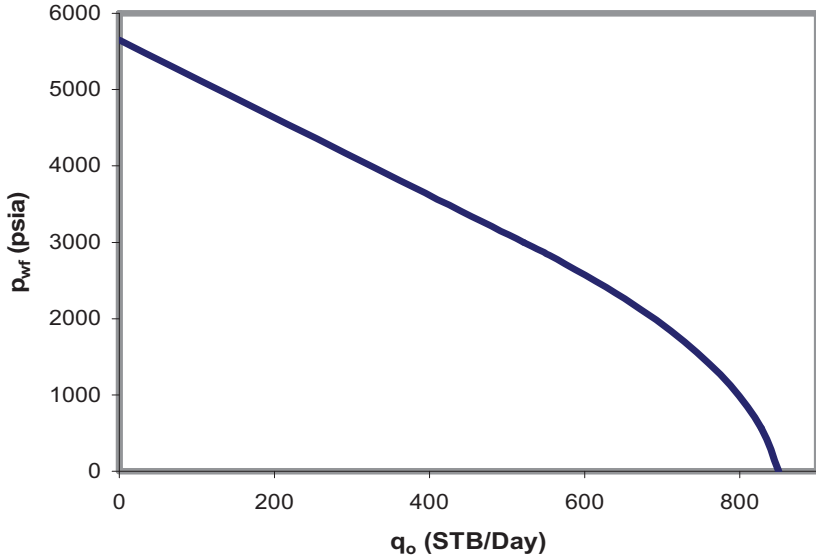


Figure 4-13 IPR curve for Sample Problem 4-4.

Constructing oil well IPR curves using test points requires the calculation of the productivity index J^* . For a single-phase (undersaturated oil) reservoir, the model constant J^* can be determined by

$$J^* = \frac{q_1}{(\bar{p} - p_{wf1})} \quad (4.39)$$

where q_1 is the tested production rate at actual flowing bottom-hole pressure p_{wf1} .

For a partial two-phase reservoir, the model constant J^* in the generalized Vogel's equation must be determined based on the pressure range in which the tested flowing bottom-hole pressure falls. If the tested flowing bottom-hole pressure is *greater than* the bubble-point pressure, the model constant J^* should be determined by

$$J^* = \frac{q_1}{(\bar{p} - p_{wf1})} \quad (4.40)$$

If the tested flowing bottom-hole pressure is *less than* bubble-point pressure, the model constant J^* should be determined using Equation (4.38)—that is,

$$J^* = \frac{q_1}{\left((\bar{p} - p_b) + \frac{p_b}{1.8} \left[1 - 0.2 \left(\frac{p_{wfl}}{p_b} \right) - 0.8 \left(\frac{p_{wfl}}{p_b} \right)^2 \right] \right)} \quad (4.41)$$

4-5 SAMPLE PROBLEM

Calculate and graph the IPR for two wells in an undersaturated oil reservoir using the generalized Vogel's model. The following data are given:

Reservoir pressure: $\bar{p} = 5000$ psia

Bubble-point pressure: $p_b = 3000$ psia

Tested flowing bottom-hole pressure in Well A: $p_{wfl} = 4000$ psia

Tested production rate from Well A: $q_1 = 300$ stb/day

Tested flowing bottom-hole pressure in Well B: $p_{wfl} = 2000$ psia

Tested production rate from Well B: $q_1 = 900$ stb/day

SOLUTION FOR WELL A

$$\begin{aligned} J^* &= \frac{q_1}{(\bar{p} - p_{wfl})} \\ &= \frac{300}{(5000 - 4000)} \\ &= 0.3000 \text{ stb/day-psi} \end{aligned}$$

The points calculated using Eq. (4.38) are

p_{wf} (psia)	q (stb/day)
0	1100
500	1072
1000	1022
1500	950
2000	856
2500	739
3000	600
5000	0

The IPR curve is illustrated in Figure 4–14.

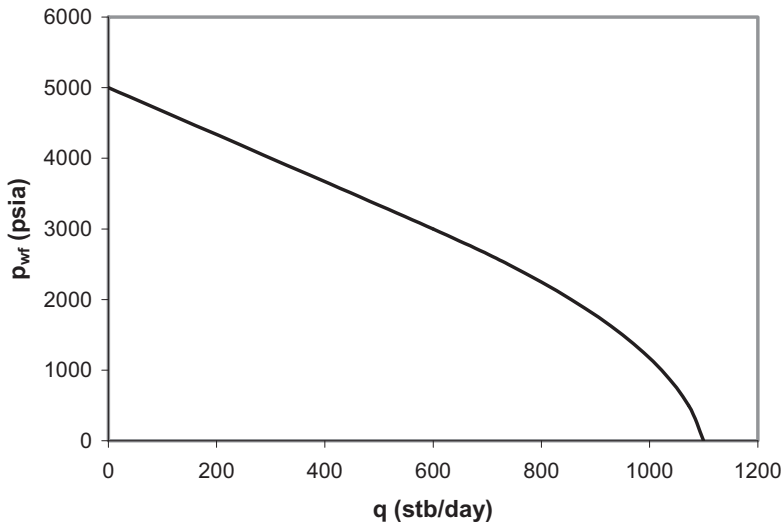


Figure 4–14 IPR curves for Sample Problem 4-5, Well A.

SOLUTION FOR WELL B

$$\begin{aligned}
 J^* &= \frac{q_1}{\left((\bar{p} - p_b) + \frac{p_b}{1.8} \left[1 - 0.2 \left(\frac{p_{wf1}}{p_b} \right) - 0.8 \left(\frac{p_{wf1}}{p_b} \right)^2 \right] \right)} \\
 &= \frac{900}{\left((5000 - 3000) + \frac{3000}{1.8} \left[1 - 0.2 \left(\frac{2000}{3000} \right) - 0.8 \left(\frac{2000}{3000} \right)^2 \right] \right)} \\
 &= 0.3156 \text{ stb/day-psi}
 \end{aligned}$$

The calculated points are

p_{wf} (psia)	q (stb/day)
0	1157
500	1128
1000	1075
1500	999
2000	900
2500	777
3000	631
5000	0

The IPR curve is illustrated in Figure 4-14.

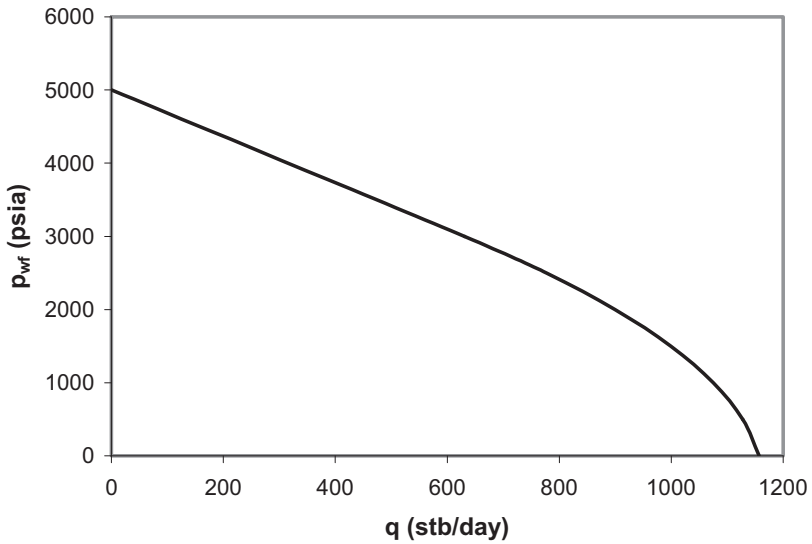


Figure 4-15 IPR curves for Sample Problem 4-5, Well B.

For a two-phase (saturated oil) reservoir, if Vogel's equation (Equation (4.29)) is used for constructing the IPR curve, the model constant q_{\max} can be determined by

$$q_{\max} = \frac{q_1}{1 - 0.2 \left(\frac{p_{wf1}}{\bar{p}} \right) - 0.8 \left(\frac{p_{wf1}}{\bar{p}} \right)^2} \quad (4.42)$$

The productivity index at and above reservoir pressure, if desired, can then be estimated by

$$J^* = \frac{1.8q_{\max}}{\bar{p}} \quad (4.43)$$

If Fetkovich's equation is used instead, two test points are required to determine the values of the two model-constants:

$$n = \frac{\log \left(\frac{q_1}{q_2} \right)}{\log \left(\frac{\bar{p}^2 - p_{wf1}^2}{\bar{p}^2 - p_{wf2}^2} \right)} \quad (4.44)$$

and

$$C = \frac{q_1}{\left(\bar{p}^2 - p_{wf1}^2 \right)^n} \quad (4.45)$$

where q_1 and q_2 are the tested production rates at the actual flowing bottom-hole pressures p_{wf1} and p_{wf2} respectively.

4-6 SAMPLE PROBLEM

Calculate and graph the IPR of a well in a saturated oil reservoir using both Vogel's and Fetkovich's equations. The following data are given:

Reservoir pressure: $\bar{p} = 3000$ psia

Tested flowing bottom-hole pressure: $p_{wf1} = 2000$ psia

Tested production rate at p_{wf1} : $q_1 = 500$ stb/day

Tested flowing bottom-hole pressure: $p_{wf2} = 1000$ psia

Tested production rate at p_{wf2} : $q_2 = 800$ stb/day

SOLUTION USING VOGEL'S EQUATION

$$\begin{aligned} q_{\max} &= \frac{q_1}{1 - 0.2 \left(\frac{p_{wf1}}{\bar{p}} \right) - 0.8 \left(\frac{p_{wf1}}{\bar{p}} \right)^2} \\ &= \frac{500}{1 - 0.2 \left(\frac{2000}{3000} \right) - 0.8 \left(\frac{2000}{3000} \right)^2} \\ &= 978 \text{ stb/day} \end{aligned}$$

The data points calculated using Equation (4.29) are

p_{wf} (psia)	q (stb/day)
0	978
500	924
1000	826
1500	685
2000	500
2500	272
3000	0

SOLUTION USING FETKOVICH'S EQUATION

$$\begin{aligned}
 n &= \frac{\log\left(\frac{q_1}{q_2}\right)}{\log\left(\frac{\bar{p}^2 - p_{wf1}^2}{\bar{p}^2 - p_{wf2}^2}\right)} \\
 &= \frac{\log\left(\frac{500}{800}\right)}{\log\left(\frac{(3000)^2 - (2000)^2}{(3000)^2 - (1000)^2}\right)} \\
 &= 1.0
 \end{aligned}$$

$$\begin{aligned}
 C &= \frac{q_1}{(\bar{p}^2 - p_{wf1}^2)^n} \\
 &= \frac{500}{((3000)^2 - (2000)^2)^{1.0}} \\
 &= 0.0001 \text{ stb/day-psi}^{2n}
 \end{aligned}$$

The data points calculated using Equation (4.33) are

p_{wf} (psia)	q (stb/day)
0	900
500	875
1000	800
1500	675
2000	500
2500	275
3000	0

The IPR curves are illustrated in Figure 4–16 and show that Fetkovich's equation with two constants yields more conservative results than Vogel's equation.

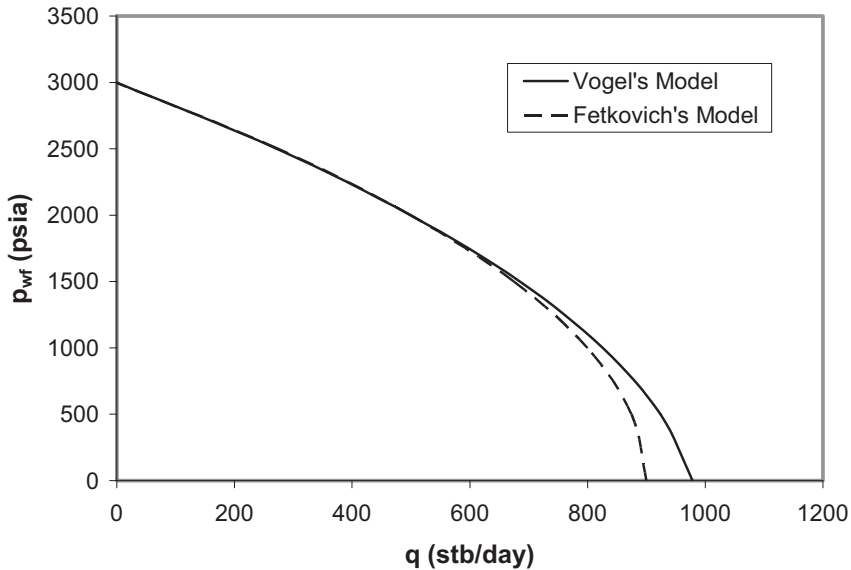


Figure 4–16 IPR curves for Sample Problem 4-6.

4.7 Composite IPR of Stratified Reservoirs

Nearly all producing formations are stratified to some extent. This means that the vertical borehole encounters different rock layers in the production zone with different reservoir pressures, permeabilities, and producing fluids. If there is no communication between these formations other than the wellbore, production will come mainly from the higher-permeability layers.

As the well's production rate is gradually increased, the less consolidated layers will begin to produce one after the other at progressively lower GOR's, and the overall GOR of production will decrease. If the most highly depleted layers themselves produce at high GOR's owing to high free gas saturations, however, the overall GOR will eventually start to rise as the production rate is increased, and this climb will continue even after the most permeable zone has come onto production. Thus, one can expect that a well producing from a stratified formation will exhibit minimum GOR as the rate of liquid production is increased.

One of the major concerns in multilayer systems is that inter-layer cross-flow may occur if reservoir fluids are produced from commingled layers of unequal potentials or pressures converted to the datum depth. This

cross-flow greatly affects the composite IPR of the well, which may result in an over-optimistic estimate of production rate from the commingled layers.

EI-Banbi and Wattenbarger (1996, 1997) investigated the productivity of commingled gas reservoirs based on matching history of production data. However, no information was given in their papers regarding the generation of IPR curves.

4.7.1 Composite IPR Models

The following assumptions are made in this section:

1. Pseudosteady-state flow prevails in all reservoir layers.
2. Fluids from/into all layers have similar properties.
3. Pressure losses in the wellbore sections between layers are negligible. (These pressure losses are considered when multi-lateral wells are addressed in Chapter 7.)
4. The IPR's of individual layers are known.

On the basis of assumption 1, under steady flow conditions, the principle of material balance dictates:

Net mass flow rate from layers to the well = Mass flow rate at well head

That is,

$$\sum_{i=1}^n m_i = m_{wh} \quad (4.46)$$

or

$$\sum_{i=1}^n \rho_i q_i = \rho_{wh} q_{wh} \quad (4.47)$$

where

m_i = mass flow rate from/into layer i

m_{wh} = mass flow rate at wellhead

ρ_i = density of fluid from/into layer i

q_i = flow rate from/into layer i

ρ_{wh} = density of fluid at wellhead

q_{wh} = flow rate at wellhead

n = number of layers

Fluid flow from the wellbore to reservoir is indicated by a negative value for q_i . Using assumption 2 and ignoring the density change from bottom-hole to well head, Equation (4.46) simplifies to

$$\sum_{i=1}^n q_i = q_{wh} \quad (4.48)$$

4.7.1.1 Single-Phase Liquid Flow

For reservoir layers that contain undersaturated oils, if the flowing bottom-hole pressure is greater than the bubble-point pressures of the oils in all layers, then we can expect single-phase flow in all layers. In that case, Equation (4.48) becomes

$$\sum_{i=1}^n J_i^* (\bar{p}_i - p_{wf}) = q_{wh} \quad (4.49)$$

where J_i^* is the productivity index of layer i at and greater than the bubble-point pressure, and \bar{p}_i and p_{wf} are converted to the datum depth. Thus Equation (4.49) represents a linear composite IPR of the well. A straight-line IPR can be drawn through two points at absolute open flow (AOF) and at stabilized shut-in bottom-hole pressure (p_{wfo}) at a datum depth. It is apparent from Equation (4.49) that

$$AOF = \sum_{i=1}^n J_i^* \bar{p}_i = \sum_{i=1}^n AOF_i \quad (4.50)$$

and

$$P_{wfo} = \frac{\sum_{i=1}^n J_i^* \bar{p}_i}{\sum_{i=1}^n J_i^*} \quad (4.51)$$

It should be borne in mind that p_{wfo} could be a dynamic bottom-hole pressure due to cross-flow between layers.

4.7.1.2 Two-Phase Flow

For reservoir layers that contain saturated oils, two-phase flow is expected. In that case Equation (4.49) becomes a polynomial of an order greater than 1. If Vogel's IPR model is used, Equation (4.49) becomes

$$\sum_{i=1}^n \frac{J_i^* \bar{p}_i}{1.8} \left[1 - 0.2 \left(\frac{P_{wf}}{\bar{p}_i} \right) - 0.8 \left(\frac{P_{wf}}{\bar{p}_i} \right)^2 \right] = q_{wh} \quad (4.52)$$

which gives

$$AOF = \sum_{i=1}^n \frac{J_i^* \bar{p}_i}{1.8} = \sum_{i=1}^n AOF_i \quad (4.53)$$

and

$$P_{wfo} = \frac{\sqrt{80 \sum_{i=1}^n J_i^* \bar{p}_i \sum_{i=1}^n \frac{J_i^*}{\bar{p}_i} + \left(\sum_{i=1}^n J_i^* \right)^2} - \sum_{i=1}^n J_i^*}{8 \sum_{i=1}^n \frac{J_i^*}{\bar{p}_i}} \quad (4.54)$$

Again, p_{wfo} could be a dynamic bottom-hole pressure at the datum depth due to cross-flow between layers.

4.7.1.3 Partial Two-Phase Flow

The generalized Vogel's IPR model can be used to describe well inflow from multi-layer reservoirs where the reservoir pressures are greater than oil bubble-point pressures, and the wellbore pressure is less. Equation (4.48) takes the form

$$\sum_{i=1}^n J_i^* \left\{ (\bar{p}_i - p_{bi}) + \frac{p_{bi}}{1.8} \left[1 - 0.2 \left(\frac{p_{wf}}{p_{bi}} \right) - 0.8 \left(\frac{p_{wf}}{p_{bi}} \right)^2 \right] \right\} = q_{wh} \quad (4.55)$$

where all pressures are converted to the datum depth. Equation (4.45) gives

$$AOF = \sum_{i=1}^n J_i^* (\bar{p}_i - 0.44 p_{bi}) = \sum_{i=1}^n AOF_i \quad (4.56)$$

and

$$p_{wfo} = \frac{\sqrt{147 \left[0.56 \sum_{i=1}^n J_i^* p_{bi} + \sum_{i=1}^n J_i^* (\bar{p}_i - p_{bi}) \right] \sum_{i=1}^n \frac{J_i^*}{p_{bi}} + \left(\sum_{i=1}^n J_i^* \right)^2 - \sum_{i=1}^n J_i^*}}{8 \sum_{i=1}^n \frac{J_i^*}{p_{bi}}} \quad (4.57)$$

Once again, p_{wfo} could be a dynamic bottom-hole pressure converted to the datum depth due to cross-flow between layers.

4.7.2 Applications

The equations presented in the previous section can be easily used to generate composite IPR curves if all values for J_i^* are known. Although numerous equations have been proposed to estimate J_i^* for different types of wells, it is always better to determine J_i^* based on actual flow tests of individual strata. If the tested flow rate (q_i) is obtained at a well-

bore pressure (p_{wfi}) that is *greater than* the bubble-point pressure in layer i , the productivity index J_i^* can be determined by

$$J_i^* = \frac{q_i}{\bar{p}_i - p_{wfi}} \quad (4.58)$$

If the tested rate (q_i) is obtained at a wellbore pressure (p_{wfi}) that is *less than* the bubble-point pressure in layer i , the productivity index J_i^* should be determined by

$$J_i^* = \frac{q_i}{(\bar{p}_i - p_{bi}) + \frac{p_{bi}}{1.8} \left[1 - 0.2 \left(\frac{p_{wfi}}{p_{bi}} \right) - 0.8 \left(\frac{p_{wfi}}{p_{bi}} \right)^2 \right]} \quad (4.59)$$

With J_i^* , \bar{p}_i and p_{bi} known, composite IPR can be generated using Equation (4.55).

4-7 SAMPLE PROBLEM

An exploration well in the South China Sea penetrated eight oil-bearing strata displaying unequal pressures within a short interval. These oil-bearing strata were tested in six groups. Strata B4 and C2 were tested together, and Strata D3 and D4 were tested together. The remaining four strata were tested individually. Test data and the calculated productivity indexes (J_i^*) are summarized in Table 4-1. All pressures are converted to a datum depth. The IPR curves of the individual strata are shown in Figure 4-17, which shows that the productivities of strata A4, A5, and B1 are significantly lower than the others. It is expected that wellbore cross-flow should occur if the bottom pressure (converted to datum depth) is greater than the lowest reservoir pressure of 2,254 psi. Strata B4, C1, and C2 should be the major thief zones because of their high injectivities (assumed to be equal to their productivities) and their relatively low pressures.

The composite IPR of these strata is shown in Figure 4-18, where the net production rate from the well is plotted against bottom-hole pressure. This figure shows that net oil production will not be available unless the bottom-hole pressure is reduced to less than 2,658 psi.

Table 4–1 Summary of Test Points for Eight Oil-Bearing Layers

Layer No.	D3-D4	C1	B4-C2	B1	A5	A4
Strata Pressure (psi)	3,030	2,648	2,606	2,467	2,302	2,254
Bubble Point (psi)	26.3	4.1	4.1	56.5	31.2	33.8
Test Rate (bopd)	3,200	3,500	3,510	227	173	122
Test Pressure (psi)	2,936	2,607	2,571	2,422	2,288	2,216
J* (bopd/psi)	34	85.4	100.2	5.04	12.4	3.2

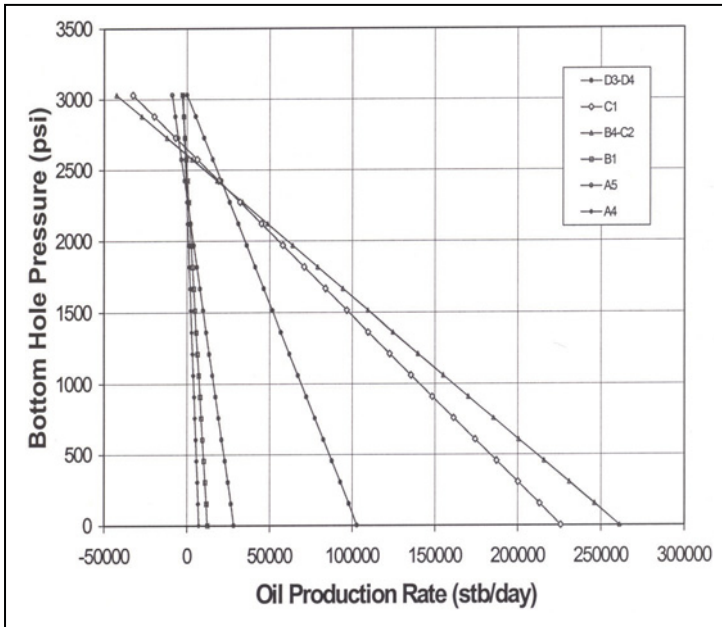


Figure 4–17 IPR curves of individual oil-bearing strata.

A reservoir engineer inspecting Figure 4–17 might suggest that the eight oil-bearing strata be produced separately in three groups:

Group 1: Strata D3 and D4

Group 2: Strata B4, C1, and C2

Group 3: Strata B1, A4, and A5

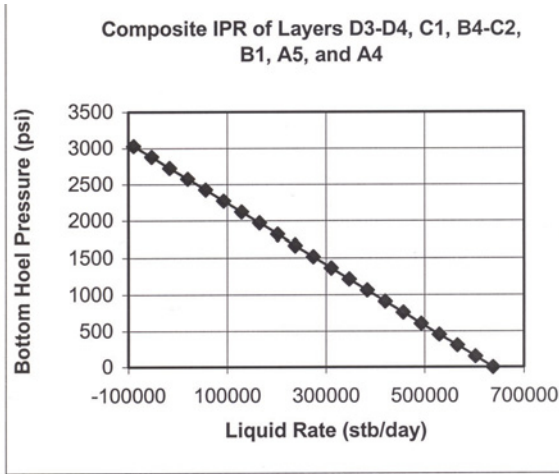


Figure 4-18 Composite IPR curve for all strata open to flow.

Use Table 4-2 to compare the production rates at several bottom-hole pressures. This comparison indicates that significant production from Group 1 can be achieved at bottom-hole pressures higher than 2658 psi, while Group 2 and Group 3 are shut in. A significant production from Group 1 and Group 2 can be achieved at bottom-hole pressures higher than 2625 psi, while Group 3 is shut in. The grouped-strata production can proceed until the bottom-hole pressure is decreased to less than 2335 psi, at which time Group 3 can be opened for production.

Table 4-2 Comparison of Commingled and Strata-Grouped Productions

Bottom-hole Pressure (psi)	Production Rate (stb/day)				
	All Strata Commingled	Grouped Strata			
		Group 1	Group 2	Group 3	Total
2,658	0	12,663	Shut in	Shut in	12,663
2,625	7,866	13,787	0	Shut in	13,787
2,335	77,556	23,660	53,896	0	77,556
2,000	158,056	35,063	116,090	6,903	158,056

4.8 Predicting Future IPR

Reservoir deliverability inevitably declines with time. During the transient flow period in single-phase reservoirs, this is because the overall pressure gradient in the reservoir drops with time. Graphically, this is because the radius of the pressure funnel, over which the pressure draw-down ($p_i - p_{wf}$) acts, increases with time. During pseudo-steady-state flow, reservoir deliverability decreases due to the depletion of reservoir pressure. In two-phase reservoirs, as the reservoir pressure is depleted, reservoir deliverability decreases due to the reduced relative permeability to oil and the increased oil viscosity. Reservoir engineers use both Vogel's and Fetkovich's methods to predict future IPR.

4.8.1 Using Vogel's Method to Predict Future IPR

Let J_p^* and J_f^* be the present and future productivity indices, respectively. The following relation can be derived:

$$\frac{J_f^*}{J_p^*} = \frac{\left(\frac{k_{ro}}{B_o \mu_o}\right)_f}{\left(\frac{k_{ro}}{B_o \mu_o}\right)_p} \quad (4.60)$$

or

$$J_f^* = J_p^* \frac{\left(\frac{k_{ro}}{B_o \mu_o}\right)_f}{\left(\frac{k_{ro}}{B_o \mu_o}\right)_p} \quad (4.61)$$

Thus,

$$q = \frac{J_f^* \bar{p}_f}{1.8} \left[1 - 0.2 \frac{p_{wf}}{\bar{p}_f} - 0.8 \left(\frac{p_{wf}}{\bar{p}_f} \right)^2 \right] \quad (4.62)$$

where \bar{p}_f is the reservoir pressure at the future time.

4-8 SAMPLE PROBLEM

Determine the IPR for a well at a future time when the average reservoir pressure has dropped to 1800 psig. The following data have been obtained from laboratory tests of well fluid samples.

Reservoir Properties	Present	Future
Average pressure (psig)	2250	1800
Productivity index J^* (stb/day-psi)	1.01	
Oil viscosity (cp)	3.11	3.59
Oil formation volume factor (rb/stb)	1.173	1.150
Relative permeability to oil	0.815	0.685

SOLUTION

$$\begin{aligned}
 J_f^* &= J_p^* \frac{\left(\frac{k_{ro}}{B_o \mu_o} \right)_f}{\left(\frac{k_{ro}}{B_o \mu_o} \right)_p} \\
 &= 1.01 \frac{\left(\frac{0.685}{3.59(1.150)} \right)}{\left(\frac{0.815}{3.11(1.173)} \right)} \\
 &= 0.75 \text{ stb/day-psi}
 \end{aligned}$$

Using Vogel's equation for future IPR

$$\begin{aligned}
 q &= \frac{J_f^* \bar{p}_f}{1.8} \left[1 - 0.2 \frac{p_{wf}}{\bar{p}_f} - 0.8 \left(\frac{p_{wf}}{\bar{p}_f} \right)^2 \right] \\
 &= \frac{(0.75)(1800)}{1.8} \left[1 - 0.2 \frac{p_{wf}}{1800} - 0.8 \left(\frac{p_{wf}}{1800} \right)^2 \right]
 \end{aligned}$$

Calculated data points:

Reservoir Pressure = 2250 psig		Reservoir Pressure = 1800 psig	
p_{wf} (psig)	q (stb/day)	p_{wf} (psig)	q (stb/day)
2250	0	1800	0
2025	217	1620	129
1800	414	1440	246
1575	591	1260	351
1350	747	1080	444
1125	884	900	525
900	1000	720	594
675	1096	540	651
450	1172	360	696
225	1227	180	729
0	1263	0	750

The present and future IPR curves are illustrated in Figure 4–19.

4.8.2 Using Fetkovich's Method to Predict Future IPR

The integral form of the reservoir inflow relationship for multi-phase flow is expressed as

$$q = \frac{0.007082kh}{\ln\left(\frac{r_e}{r_w}\right)} \int_{p_{wf}}^{p_e} f(p) dp \quad (4.63)$$

where $f(p)$ is a pressure function. The simplest case of two-phase flow is that of a constant pressure p_e at the outer boundary (r_e), with the value of p_e of less than the bubble-point pressure, so that two-phase flow occurs throughout the reservoir. Under these circumstances, $f(p)$ takes the value

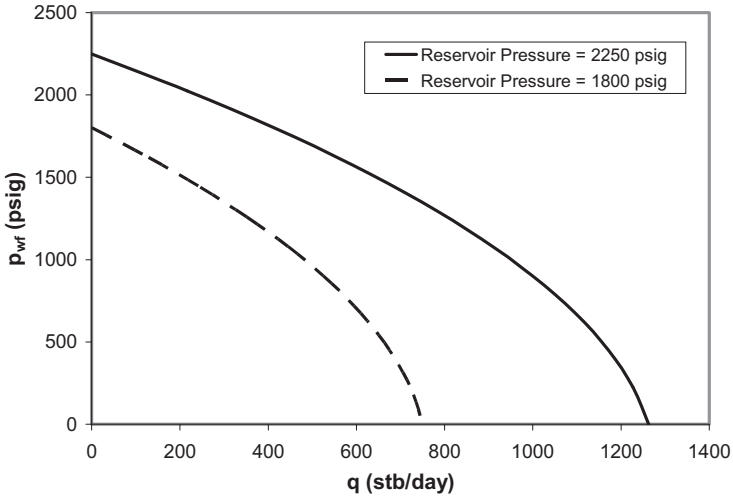


Figure 4-19 IPR curves for Sample Problem 4-8.

$$\frac{k_{ro}}{\mu_o B_o}$$

where k_{ro} is the relative permeability to oil at the saturation conditions in the formation, corresponding to the pressure p . The Fetkovich method makes the key assumption that the expression

$$\frac{k_{ro}}{\mu_o B_o}$$

is a good approximation of a linear function of p and passes through zero. If p_i is the initial formation pressure (i.e. $\sim p_e$), then the straight-line relationship is expressed as

$$\frac{k_{ro}}{\mu_o B_o} = \left(\frac{k_{ro}}{\mu_o B_o} \right)_i \frac{p}{p_i} \quad (4.64)$$

Substituting Equation (4.64) into Equation (4.63) and integrating the latter gives

$$q_o = \frac{0.007082kh}{\ln\left(\frac{r_e}{r_w}\right)} \left(\frac{k_{ro}}{\mu_o B_o}\right)_i \frac{1}{2p_i} (p_i^2 - p_{wf}^2) \quad (4.65)$$

or

$$q_o = J'_i (p_i^2 - p_{wf}^2) \quad (4.66)$$

where

$$J'_i = \frac{0.007082kh}{\ln\left(\frac{r_e}{r_w}\right)} \left(\frac{k_{ro}}{\mu_o B_o}\right)_i \frac{1}{2p_i} \quad (4.67)$$

The derivative of Equation (4.65) with respect to the flowing bottom-hole pressure is

$$\frac{dq_o}{dp_{wf}} = -2J'_i p_{wf} \quad (4.68)$$

This implies that the rate of change of q with respect to p_{wf} is lower at lower values of inflow pressure.

Next, we can modify Equation (4.63) to take into account the fact that in practice p_e is not constant, but decreases with cumulative production. The assumption made is that J'_i will decrease in proportion to the decrease in average reservoir (drainage area) pressure. Thus, when the static pressure is $p_e (< p_i)$, the IPR equation is

$$q_o = J'_i \frac{p_e}{p_i} (p_e^2 - p_{wf}^2) \quad (4.69)$$

or, alternatively,

$$q_o = J' (p_e^2 - p_{wf}^2) \quad (4.70)$$

where

$$J' = J_i \frac{p_e}{p_i} \quad (4.71)$$

These equations may be used to predict future IPR.

4-9 SAMPLE PROBLEM

Using Fetkovich's method, plot the IPR curves for a well in which p_i is 2000 psia and $J'_i = 5 \times 10^{-4}$ stb/day-psia². Predict the IPR's of the well at the well shut in static pressures of 1500 psia and 1000 psia.

SOLUTION

The value of J'_o at 1500 psia is

$$\begin{aligned} J'_o &= 5 \times 10^{-4} \left(\frac{1500}{2000} \right) \\ &= 3.75 \times 10^{-4} \text{ stb / day- (psia)}^2 \end{aligned}$$

And the value of J'_o at 1000 psia is

$$\begin{aligned} J'_o &= 5 \times 10^{-4} \left(\frac{1000}{2000} \right) \\ &= 2.5 \times 10^{-4} \text{ stb / day- (psia)}^2 \end{aligned}$$

Using the above values for J_o' and the accompanying p_e in Equation (4.54), the following data points can be calculated:

$p_e = 2000$ psig		$p_e = 1500$ psig		$p_e = 1000$ psig	
p_{wf} (psig)	q (stb/day)	p_{wf} (psig)	q (stb/day)	p_{wf} (psig)	q (stb/day)
2000	0	1500	0	1000	0
1800	380	1350	160	900	48
1600	720	1200	304	800	90
1400	1020	1050	430	700	128
1200	1280	900	540	600	160
1000	1500	750	633	500	188
800	1680	600	709	400	210
600	1820	450	768	300	228
400	1920	300	810	200	240
200	1980	150	835	100	248
0	2000	0	844	0	250

The IPR curves are illustrated in Figure 4–20.

4.9 Summary

This chapter presented and illustrated several mathematical models for estimating the deliverability of oil and gas reservoirs. Production engineers should choose between the models based on their best estimates of reservoir flow regimes and pressure levels. The selected models should be checked against actual well production rates and bottom-hole pressures. At least one test point is required to validate a straight-line (single-liquid flow) IPR model. At least two test points are required to validate a non-linear (single-gas flow or two-phase flow) IPR model.

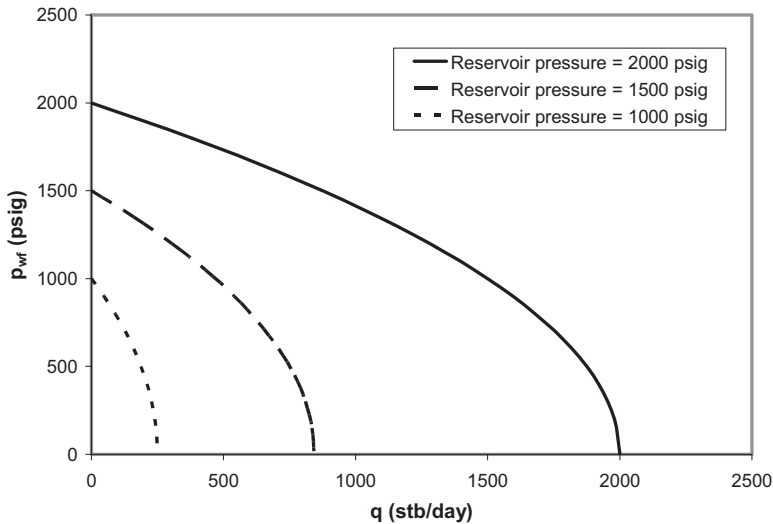


Figure 4-20 IPR curves for Sample Problem 4-9.

4.10 References

Argawal, R.G., Carter, R.D., and Pollock, C.B.: "Evaluation and Prediction of Performance of Low-Permeability Gas Wells Stimulated by Massive Hydraulic Fracturing," *Journal of Petroleum Technology* (March 1979), *Trans. AIME*, 267: 362–372.

Bandakhlia, H. and Aziz, K.: "Inflow Performance Relationship for Solution-Gas Drive Horizontal Wells," paper SPE 19823 presented at the 64th SPE Annual Technical Conference and Exhibition (8–11 October, 1989), San Antonio, Texas.

Cinco-Ley, H. and Samaniego, F.: "Transient Pressure Analysis for Fractured Wells," *Journal of Petroleum Technology* (September 1981): 1749–1766.

Dietz, D.N.: "Determination of Average Reservoir Pressure from Build-Up Surveys," *Journal of Petroleum Technology* (August 1965): 955–959.

Dake, L.P.: *Fundamentals of Reservoir Engineering*, Elsevier, New York (1978).

Earlougher, R.C.: *Advances in Well Test Analysis*, Society of Petroleum Engineers, Dallas (1977).

Economides, M.J., Deimbacher, F.X., Brand, C.W., and Heinemann, Z.E.: "Comprehensive Simulation of Horizontal Well Performance," SPEFE, (December 1991): 418–426.

El-Banbi, A.H. and Wattenbarger, R.A.: "Analysis of Commingled Tight Gas Reservoirs," paper SPE 36736 presented at the SPE Annual Technical Conference and Exhibition (6–9 October 1996), Denver, Colorado.

El-Banbi, A.H. and Wattenbarger, R.A.: "Analysis of Commingled Gas Reservoirs With Variable Bottom-Hole Flowing Pressure and Non-Darcy Flow," paper SPE 38866 presented at the SPE Annual Technical Conference and Exhibition (5–8 October 1997), San Antonio, Texas.

Fetkovich, M.J.: "The Isochronal Testing of Oil Wells," paper SPE 4529 presented at the SPE Annual Technical Conference and Exhibition (30 September–3 October 1973), Las Vegas, Nevada.

Guo, B. and Schechter, D.S.: "A Simple and Rigorous IPR Equation for Vertical and Horizontal Wells Intersecting Long Fractures," *Journal of Canadian Petroleum Technology* (July 1999): 46–54.

Guo, B., Zhou, J., Liu, Y. and Ghalambor, A.: "A Rigorous Analytical Model for Fluid Flow in Drain Holes of Finite Conductivity Applied to Horizontal and Multilateral Wells," paper SPE 106947 presented at the 2007 Production Operations Symposium (31 March–03 April 2007), Oklahoma City, OK.

Joshi, S.D.: "Augmentation of Well Productivity with Slant and Horizontal Wells," *Journal of Petroleum Technology* (June 1988): 729–739.

Retnanto, A. and Economides, M.: "Inflow Performance Relationships of Horizontal and Multibranch Wells in a Solution Gas Drive Reservoir," paper SPE 49054 presented at the 1998 SPE Annual Technical Conference and Exhibition (27–30 September 1998), New Orleans, Louisiana.

Standing, M.B.: "Concerning the Calculation of Inflow Performance of Wells Producing from Solution Gas Drive Reservoirs," paper SPE 3332, *Journal of Petroleum Technology* (September 1971): 1141–1142.

Vogel, J.V.: "Inflow Performance Relationships for Solution-Gas Drive Wells," *Journal of Petroleum Technology* (January 1968): 83–92.

Chang, M.: "Analysis of Inflow Performance Simulation of Solution-Gas Drive for Horizontal/Slant Wells," paper SPE 24352 presented at the SPE Rocky Mountain Regional Meeting (18–21 May 1992.), Casper, Wyoming.

4.11 Problems

- 4-1 Calculate and graph the IPR of a vertical well in an oil reservoir. Consider: 1) transient flow at 30 days, 2) steady state flow, and 3) pseudosteady state flow. The following data are given:

Porosity: $\phi = 0.28$

Effective horizontal permeability: $k = 12$ md

Pay zone thickness: $h = 52$ ft

Reservoir pressure: p_e or $\bar{p} = 5200$ psia

Bubble-point pressure: $p_b = 120$ psia

Fluid formation volume factor: $B_o = 1.2$

Fluid viscosity: $\mu_o = 1.6$ cp

Total compressibility: $c_t = 0.0000125$ psi⁻¹

Drainage area: $A = 640$ acres ($r_e = 2980$ ft)

Wellbore radius: $r_w = 0.328$ ft

Skin factor: $S = 8$

- 4-2 A gas reservoir has a permeability of 1.5 md. A vertical well with a radius of 0.328 ft drains the reservoir from the center of an area of 160 acres. If the well is hydraulically fractured to create a 2,500 ft long, 0.14 inch wide fracture of 220,000 md permeability around the center of the drainage area, what would be the factor of increase in reservoir deliverability?
- 4-3 Calculate and graph the IPR of a vertical well in a saturated oil reservoir using Vogel's equation, given the following data:

Porosity: $\phi = 0.24$

Effective horizontal permeability: $k = 84$ md

Pay zone thickness: $h = 58$ ft

Reservoir pressure: $\bar{p} = 4600$ psia
Bubble-point pressure: $p_b = 4600$ psia
Fluid formation volume factor: $B_o = 1.15$
Fluid viscosity: $\mu_o = 1.5$ cp
Total compressibility: $c_t = 0.000013$ psi⁻¹
Drainage area: $A = 640$ acres ($r_e = 2980$ ft)
Wellbore radius: $r_w = 0.328$ ft
Skin factor: $S = 6$

- 4-4 Calculate and graph the IPR of a vertical well in an unsaturated oil reservoir using the generalized Vogel's equation given the following data:

Porosity: $\phi = 0.22$
Effective horizontal permeability: $k = 110$ md
Pay zone thickness: $h = 53$ ft
Reservoir pressure: $\bar{p} = 5200$ psia
Bubble-point pressure: $p_b = 3400$ psia
Fluid formation volume factor: $B_o = 1.15$
Fluid viscosity: $\mu_o = 1.4$ cp
Total compressibility: $c_t = 0.000013$ psi⁻¹
Drainage area: $A = 640$ acres ($r_e = 2980$ ft)
Wellbore radius: $r_w = 0.328$ ft
Skin factor: $S = 5.1$

- 4-5 Calculate and graph the IPR of two wells in an unsaturated oil reservoir using generalized Vogel's equation, given the following data:

Reservoir pressure: $\bar{p} = 5600$ psia
Bubble-point pressure: $p_b = 3400$ psia
Tested flowing bottom-hole pressure in Well A: $p_{wfl} = 4100$ psia
Tested production rate from Well A: $q_I = 405$ stb/day
Tested flowing bottom-hole pressure in Well B: $p_{wfl} = 2200$ psia
Tested production rate from Well B: $q_I = 1100$ stb/day

- 4-6 Calculate and graph the IPR of a well in a saturated oil reservoir using both Vogel's and Fetkovich's equations, given the following data:

Reservoir pressure: $\bar{p} = 3600$ psia

Tested flowing bottom-hole pressure: $p_{wf1} = 2700$ psia

Tested production rate at p_{wf1} : $q_1 = 620$ stb/day

Tested flowing bottom-hole pressure: $p_{wf2} = 1550$ psia

Tested production rate at p_{wf2} : $q_2 = 940$ stb/day

- 4-7 Determine the IPR for a well at the time when the average reservoir pressure will be 1500 psig. The following data have been obtained from laboratory tests of well fluid samples:

Reservoir Properties	Present	Future
Average pressure (psig)	2210	1510
Productivity index J^* (stb/day-psi)	1.22	
Oil viscosity (cp)	3.05	3.55
Oil formation volume factor (rb/stb)	1.20	1.15
Relative permeability to oil	0.80	0.62

- 4-8 Using Fetkovich's method, plot the IPR curve for a well in which p_i is 3420 psia and $J_o' = 4 \times 10^{-4}$ stb/day- psia^2 . Predict the IPR's of the well at well shut in static pressures of 2500 psia, 2000 psia, 1500 psia, and 1000 psia.

This page intentionally left blank

Wellbore Performance

5.1 Introduction

Wellbores provide paths for both petroleum production and fluid injection. Oil and natural gas are usually produced through well strings such as tubing, and the higher the performance of the well strings, the higher the productivity of the wells. A well-designed well string ensures that the flow in the wellbore will not be a limiting factor, or “bottleneck,” during fluid production. This requires that both friction and flow stability (mixing of multiple phases) be considered.

The flow performance of well string depends on the geometry of the string and the properties of the fluids transported through it. The fluids in production wells are usually multiple phases: oil, water, and gas, sometimes with included sand.

Analyzing wellbore performance requires establishing a relationship between tubing size, wellhead and bottom-hole pressures, fluid properties, and fluid production rate. An understanding of wellbore flow performance is vitally important to engineers for designing production wells.

Although oil and natural gas can be produced through tubing, casing, or both, the use of tubing is more common. This is because a tubing string provides a better gas-lift effect than does casing in oil wells, assists in liquid removal in gas wells, and seals better than casing. The properties of American Petroleum Institute (API) tubing are presented in Appendix B. The traditional term *tubing performance relationship* (TPR) is used in this book and is equivalent to other terms from the literature, such as vertical lift performance. Mathematical models are valid for flow in all types of conduits. This chapter focuses on the determination of the pressure profile

along the well string and TPR. Both single and multiphase fluids will be considered. Calculation examples are illustrated using computer spreadsheets. Applications of the TPR will be discussed in Chapters 6 and 7 in well productivity analyses.

5.2 Single-Phase Liquid Flow

Single-phase oil flow exists in production oil wells only when the well-head pressure is greater than the bubble-point pressure of the oil. Consider a fluid flowing from point 1 to point 2 in a tubing string of length L and height Δz (Figure 5–1). The First Law of Thermodynamics yields the following equation for pressure drop:

$$\Delta P = P_1 - P_2 = \frac{g}{g_c} \rho \Delta z + \frac{\rho}{2g_c} \Delta u^2 + \frac{2f_F \rho u^2 L}{g_c D} \quad (5.1)$$

where

ΔP = pressure drop (lb_f/ft²)

P_1 = pressure at point 1 (lb_f/ft²)

P_2 = pressure at point 2 (lb_f/ft²)

g = gravitational acceleration (32.17 ft/s²)

g_c = unit conversion factor (32.17 lb_m-ft/lb_f-s²)

ρ = fluid density (lb_m/ft³)

Δz = elevation increase (ft)

u = fluid velocity (ft/s)

f_F = Fanning friction factor

L = tubing length (ft)

D = tubing inside diameter (ft)

The first, second, and third term in the right-hand-side of Equation (5.1) represent pressure decrease due to changes in elevation, kinetic energy, and friction, respectively.

The Fanning friction factor (f_F) can be evaluated based on the Reynolds number and the relative roughness of the tubing string interior. The Reyn-

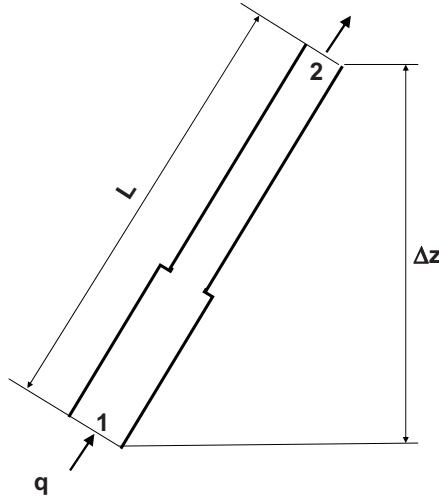


Figure 5–1 Parameters used to characterize flow along a tubing string.

olds number is defined as the ratio of inertial force to viscous force. The Reynolds number is expressed in consistent units as

$$N_{\text{Re}} = \frac{Du\rho}{\mu} \quad (5.2)$$

or in U.S. field units as

$$N_{\text{Re}} = \frac{1.48q\rho}{d\mu} \quad (5.3)$$

where

N_{Re} = Reynolds number

q = fluid flow rate (bbl/day)

ρ = fluid density (lb_m/ft^3)

d = tubing inside diameter (in)

μ = fluid viscosity (cp)

For laminar flow regimes, in which $N_{Re} < 2100$, the Fanning friction factor is inversely proportional to the Reynolds number, or

$$f_F = \frac{16}{N_{Re}} \quad (5.4)$$

For turbulent flow regimes, where $N_{Re} > 2100$, the Fanning friction factor can be estimated empirically. Among numerous correlations developed by different investigators, that developed by Chen (1979) has an explicit form and gives similar accuracy to the Colebrook-White equation (Gregory and Fogarasi 1985). The latter was used to generate the friction factor chart widely used in the petroleum industry. Chen's correlation takes the following form:

$$\frac{1}{\sqrt{f_F}} = -4 \log \left\{ \frac{\epsilon}{3.7065} - \frac{5.0452}{N_{Re}} \log \left[\frac{\epsilon^{1.1098}}{2.8257} + \left(\frac{7.149}{N_{Re}} \right)^{0.8981} \right] \right\} \quad (5.5)$$

where the relative roughness of the tubing string interior is defined as

$$\epsilon = \frac{\delta}{d}$$

and δ is the absolute roughness of pipe wall.

The Fanning friction factor can also be obtained from the Darcy-Wiesbach friction factor diagram shown in Figure 5–2. The Darcy-Wiesbach friction factor might also be referred to as the Moody friction factor (f_M) in the literature. The relationship between these factors is expressed as

$$f_F = \frac{f_M}{4} \quad (5.6)$$

5-1 SAMPLE PROBLEM

A well produces 1000 bbl/day of 40° API, 1.2 cp oil, through a 2 7/8-in., 8.6-lb_m/ft tubing in a bore-hole with a 15° average inclination angle. The tubing wall relative roughness is 0.001. Assuming that the tubing head

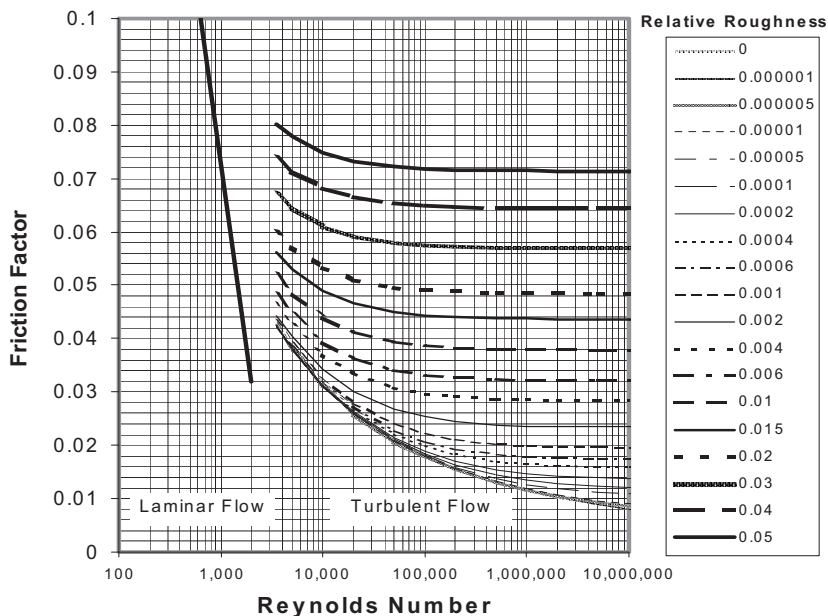


Figure 5–2 Darcy-Wiesbach friction factor diagram.

pressure is 2000 psia, and the oil bubble-point pressure is 1950 psia, calculate the pressure at the tubing shoe at 1000 ft measured depth.

SOLUTION

Determine the oil specific gravity:

$$\begin{aligned}\gamma_o &= \frac{141.5}{\text{oAPI} + 131.5} \\ &= \frac{141.5}{40 + 131.5} \\ &= 0.825\end{aligned}$$

Determine the approximate oil density in tubing:

$$\begin{aligned}\rho &= 62.4\gamma_o \\ &= (62.4)(0.825) \\ &= 51.57 \text{ lbm/ft}^3\end{aligned}$$

Determine the elevation increase:

$$\begin{aligned}\Delta Z &= \cos(\alpha)L \\ &= \cos(15)(1000) \\ &= 966 \text{ ft}\end{aligned}$$

Determine the tubing inside diameter in ft. The 2 7/8-in., 8.6-lb_m/ft tubing has an inside diameter of 2.259 in. Therefore,

$$D = \frac{2.259}{12} = 0.188 \text{ ft}$$

Determine the fluid velocity:

$$\begin{aligned}u &= \frac{4q}{\pi D^2} \\ &= \frac{4(5.615)(1000)}{\pi(0.188)^2(86400)} \\ &= 2.34 \text{ ft/s}\end{aligned}$$

Determine the Reynolds number:

$$\begin{aligned}N_{\text{Re}} &= \frac{1.48q\rho}{d\mu} \\ &= \frac{1.48(1000)(51.57)}{(2.259)(1.2)} \\ &= 28115 > 2100, \text{ indicating turbulent flow}\end{aligned}$$

Using Chen's correlation, the Fanning friction factor can be calculated by

$$\begin{aligned}\frac{1}{\sqrt{f_F}} &= -4 \log \left\{ \frac{\epsilon}{3.7065} - \frac{5.0452}{N_{\text{Re}}} \log \left[\frac{\epsilon^{1.1098}}{2.8257} + \left(\frac{7.149}{N_{\text{Re}}} \right)^{0.8981} \right] \right\} \\ &= 12.3255 \\ f_F &= 0.006583\end{aligned}$$

If Figure 5–2 is utilized instead, it gives a Moody friction factor of 0.0265. Thus the Fanning friction factor can then be estimated as

$$f_F = \frac{0.0265}{4}$$

$$= 0.006625$$

The pressure at the tubing shoe can be calculated by

$$P_1 = P_2 + \frac{g}{g_c} \rho \Delta z + \frac{\rho}{2g_c} \Delta u^2 + \frac{2f_F \rho u^2 L}{g_c D}$$

$$= (2000)(144) + \frac{32.17}{32.17} (51.57)(966) + \frac{2(0.006625)(51.57)(2.34)^2 (1000)}{(32.17)(0.188)}$$

$$= 338423 \text{ lbf/ft}^2$$

$$= 2350 \text{ psi}$$

5-2 SAMPLE PROBLEM

In a water injection well, 1000 bbl/day of water with a specific gravity of 1.05 is injected through a 2 7/8-in., 8.6-lb_m/ft tubing in a well that is 15° from vertical. The water viscosity is 1 cp. The tubing wall relative roughness is 0.001. Assuming that the pressure at the tubing shoe of 1000 ft is 2350 psia, calculate the necessary injection pressure at the tubing head.

SOLUTION

Determine the water density:

$$\rho = 62.4 \gamma_w$$

$$= (62.4)(1.05)$$

$$= 65.52 \text{ lb}_m/\text{ft}^3$$

Determine the elevation increase:

$$\Delta Z = \cos(\alpha)L$$

$$= \cos(15)(-1000)$$

$$= -966 \text{ ft}$$

Determine the inside diameter of the tubing in ft. The 2 7/8-in., 8.6-lb_m/ft tubing has an inside diameter of 2.259 in. Therefore,

$$D = \frac{2.259}{12}$$

$$= 0.188 \text{ ft}$$

Determine the fluid velocity:

$$u = \frac{4q}{\pi D^2}$$

$$= \frac{4(5.615)(1000)}{\pi(0.188)^2(86400)}$$

$$= 2.34 \text{ ft/s}$$

Determine the Reynolds number:

$$N_{\text{Re}} = \frac{1.48q\rho}{d\mu}$$

$$= \frac{1.48(1000)(65.52)}{(2.259)(1.0)}$$

$$= 42926 > 2100, \text{ indicating turbulent flow}$$

Using Chen's correlation, the Fanning friction factor can be calculated by

$$\frac{1}{\sqrt{f_F}} = -4 \log \left\{ \frac{\epsilon}{3.7065} - \frac{5.0452}{N_{\text{Re}}} \log \left[\frac{\epsilon^{1.1098}}{2.8257} + \left(\frac{7.149}{N_{\text{Re}}} \right)^{0.8981} \right] \right\}$$

$$= 12.7454$$

$$f_F = 0.006156$$

The pressure at the tubing shoe can be calculated by

$$P_1 = P_2 + \frac{g}{g_c} \rho \Delta z + \frac{\rho}{2g_c} \Delta u^2 + \frac{2f_F \rho u^2 L}{g_c D}$$

$$= (2,350)(144) + \frac{32.17}{32.17} (65.52)(-966) + \frac{2(0.006156)(65.52)(2.34)^2(1000)}{(32.17)(0.188)}$$

$$= 275838 \text{ lbf/ft}^2$$

$$= 1916 \text{ psi}$$

5.3 Multiphase Flow in Oil Wells

In addition to liquid oil, almost all oil wells produce some amount of water, gas, and occasionally sand. These wells are called multiphase oil wells, and the TPR equation for single-phase flow is not valid for them. To analyze the TPR of multiphase oil wells correctly, a multiphase flow model is required.

Multiphase flow is much more complicated than single-phase flow due to the variation of flow regime (or flow pattern). The fluid distribution changes greatly between different flow regimes, which significantly affects the pressure gradient in the tubing.

5.3.1 Flow Regimes

At least five flow regimes have been identified in gas-liquid two-phase flow. They are bubble, slug, churn, annular, and mist flow. These flow regimes occur in a progression displaying increasing gas flow rate for any fixed rate of liquid flow. In bubble flow, the gas phase is dispersed in the form of small bubbles within a continuous liquid phase. In slug flow, small gas bubbles coalesce into larger bubbles that eventually fill the entire pipe cross section. Between the large bubbles are slugs of liquid that contain smaller bubbles of entrained gas. In churn flow, the larger gas bubbles become unstable and collapse, resulting in a highly turbulent flow pattern with both phases dispersed. In annular flow, gas becomes the continuous phase, with liquid flowing in an annulus coating the surface of the pipe and as droplets entrained in the gas phase. In mist flow, dispersed liquid droplets move in the continuous gas phase, forming a relatively homogeneous fluid emulsion.

5.3.2 Liquid Holdup

In multiphase flow, the volume of pipe occupied by a particular phase is often different from its proportion of the total volumetric flow. This is due to density differences between phases. Gravity causes the denser phases to slip down within the upward flow—that is, the lighter phase rises faster than the denser phase. Because of this, the in-situ volume fraction of the denser phase will be greater than the input volume fraction of the denser

phase; the denser phase is “held up” in the pipe relative to the lighter phase. The term liquid “holdup” is defined as

$$y_L = \frac{V_L}{V} \quad (5.7)$$

where

y_L = liquid holdup (fractional)

V_L = volume of liquid phase in the pipe segment (ft³)

V = volume of the pipe segment (ft³)

Liquid holdup depends on the flow regime, fluid properties, pipe size, and pipe configuration. Its value can only be determined experimentally.

5.3.3 TPR Models

Numerous TPR models exist for analyzing multiphase flow in vertical pipes, reviewed by Brown (1977). TPR models for multiphase flow wells fall into two categories: homogeneous-flow and separated-flow. The homogeneous-flow models treat multiphases as a homogeneous mixture and do not consider the effects of liquid holdup (a no-slip assumption). Therefore, these models are less accurate and are usually calibrated against local operating conditions in field applications. Their major advantage comes from their deterministic nature. They can be constructed to describe gas-oil-water three-phase and gas-oil-water-sand four-phase systems. It is easy to code a deterministic model in computer programs.

The separated-flow models are usually presented in the form of empirical correlations developed experimentally. Because they incorporate the effects of liquid holdup (slip) and flow regime automatically, these models are more realistic than the homogeneous-flow models. Their major disadvantage is that it is difficult to code them in computer programs because most correlations are presented in graphic form.

5.3.3.1 Homogeneous-Flow Models

Numerous homogeneous-flow models have been developed for analyzing the TPR of multiphase wells since the pioneering works of Poettmann and

Carpenter (1952). Poettmann-Carpenter's model uses an empirical two-phase friction factor for friction pressure-loss calculations, without considering the effect of liquid viscosity. Liquid viscosity was considered by later researchers, including Cicchitti et al. (1960) and Dukler et al. (1964), and a comprehensive review of these models is given by Hasan and Kabir (2002). Recent work addressing gas-oil-water-sand four-phase flow was presented by Guo and Ghalambor (2005).

Assuming no-slip of the liquid phase, Poettmann and Carpenter (1952) presented a simplified gas-oil-water three-phase flow model to compute pressure losses in tubing by estimating mixture density and friction factor. According to Poettmann and Carpenter, the following equation can be used to calculate the pressure profile in vertical tubing when the acceleration term is neglected:

$$\Delta p = \left(\bar{\rho} + \frac{\bar{k}}{\bar{\rho}} \right) \frac{\Delta h}{144} \quad (5.8)$$

where

Δp = pressure increment (psi)

$\bar{\rho}$ = average mixture density (specific weight) (lb/ft³)

Δh = depth increment (ft)

and

$$\bar{k} = \frac{f_{2F} q_o^2 M^2}{7.4137 \times 10^{10} D^5} \quad (5.9)$$

where

f_{2F} = Fanning friction factor for two phase flow

q_o = oil production rate (stb/day)

M = total mass associated with 1 stb of oil

D = tubing inside diameter (ft)

The average mixture density $\bar{\rho}$ can be calculated by

$$\bar{\rho} = \frac{\rho_1 + \rho_2}{2} \quad (5.10)$$

where

ρ_1 = mixture density at top of tubing segment (lb/ft³)

ρ_2 = mixture density at bottom of segment (lb/ft³)

The mixture density at any given point can be calculated based on mass flow rate and volume flow rate, expressed as

$$\rho = \frac{M}{V_m} \quad (5.11)$$

where

$$M = 350.17(\gamma_o + WOR \gamma_w) + GOR \rho_{air} \gamma_g \quad (5.12)$$

and

$$V_m = 5.615(B_o + WOR B_w) + (GOR - R_s) \left(\frac{14.7}{p} \right) \left(\frac{T}{520} \right) \left(\frac{z}{1.0} \right) \quad (5.13)$$

where

γ_o = oil specific gravity (1 for fresh water)

WOR = producing water-oil ratio (bbl/stbv)

γ_w = water specific gravity (1 for fresh water)

GOR = producing gas-oil ratio (scf/stb)

ρ_{air} = density of air (lb_m/ft³)

γ_g = gas specific gravity (1 for air)

V_m = volume of mixture associated with 1 stb of oil (ft³)

B_o = formation volume factor of oil (rb/stb)

B_w = formation volume factor of water (rb/bbl)

R_s = solution gas-oil ratio (scf/stb)

p = in-situ pressure (psia)

T = in-situ temperature (°R)

z = gas compressibility factor at p and T

If data from direct measurements are not available, the solution gas-oil ratio and formation volume factor of oil can be estimated using Equations (2.2) and (2.7), respectively:

$$R_s = \gamma_g \left[\frac{p}{18} \frac{10^{0.0125API}}{10^{0.00091t}} \right]^{1.2048} \quad (5.14)$$

$$B_o = 0.9759 + 0.00012 \left[R_s \left(\frac{\gamma_g}{\gamma_o} \right)^{0.5} + 1.25t \right]^{1.2} \quad (5.15)$$

where t is the in-situ temperature in °F. The two-phase friction factor f_{2F} can be estimated graphically, as presented by Poettmann and Carpenter (1952). For easy coding in computer programs, Guo and Ghalambor (2002) developed the following correlation to approximate the chart values:

$$f_{2F} = 10^{1.444 - 2.5 \log(D\rho v)} \quad (5.16)$$

where $(D\rho v)$ is the numerator of the Reynolds number representing inertial force, expressed as

$$(D\rho v) = \frac{1.4737 \times 10^{-5} M q_o}{D} \quad (5.17)$$

Because Poettmann-Carpenter's model takes a finite-difference form, it is only accurate for a small depth incremental (Δh). For deep wells, therefore, this model should be used in a piecewise manner for accurate results. The tubing string should be divided into segments and the model applied separately to each segment.

Because iterations are required to solve the Equation (5.8) for pressure, a computer spreadsheet program **Poettmann-CarpenterBHP.xls** has been developed and is included in this book.

5-3 SAMPLE PROBLEM

For the following given data, calculate the tubing shoe pressure:

Tubing head pressure:	500 psia
Tubing head temperature:	100 °F
Tubing inside diameter:	1.66 in.
Tubing shoe depth:	5000 ft
Temperature at tubing shoe:	150 °F
Liquid production rate:	2000 stb/day
Water cut:	25 %
Producing GLR:	1000 scf/stb
Oil gravity:	30 °API
Water specific gravity:	1.05 1 for fresh water
Gas specific gravity:	0.65 1 for air

SOLUTION

This problem may be solved using spreadsheet program **Poettmann-CarpenterBHP.xls**, as shown in Table 5–1.

The gas-oil-water-sand four-phase flow model developed by Guo and Ghalambor (2005) assumes no-slip of the denser phases, but takes a closed (integrated) form, which makes it easy to use. It is expressed as follows:

$$\begin{aligned}
 & 144b(p_{ust} - p_{dst}) + \frac{1 - 2bM}{2} \ln \left| \frac{(144p_{ust} + M)^2 + N}{(144p_{dst} + M)^2 + N} \right| \\
 & - \frac{M + \frac{b}{c}N - bM^2}{\sqrt{N}} \left[\tan^{-1} \left(\frac{144p_{ust} + M}{\sqrt{N}} \right) - \tan^{-1} \left(\frac{144p_{dst} + M}{\sqrt{N}} \right) \right] \\
 & = a(\cos\theta + d^2e)L
 \end{aligned}
 \tag{5.18}$$

Table 5-1 Results given by Spreadsheet Program **Poettmann-CarpenterBHP.xls** for Sample Problem 5-3**Poettman-CarpenterBHP.xls**

Description: This spreadsheet calculates flowing bottom-hole pressure based on tubing head pressure and tubing flow performance using Poettmann-Carpenter Method.

Instruction: 1) Select a unit system; 2) Update parameter values in the “Input Data” section; 3) Click “Solution” button; and 4) View result in the Solution section.

Input Data:	US Field Units
Tubing ID:	1.66 in
Wellhead pressure:	500 psia
Liquid production rate:	2000 stb/d
Producing gas-liquid ratio (GLR):	1000 scf/stb
Water cut (WC):	25 %
Oil gravity:	30 °API
Water specific gravity:	1.05 fresh water =1
Gas specific gravity:	0.65 1 for air
N ₂ content in gas:	0 mole fraction
CO ₂ content in gas:	0 mole fraction
H ₂ S content in gas:	0 mole fraction
Formation volume factor for water:	1.2 rb/stb
Wellhead temperature:	100 °F
Tubing shoe depth:	5000 ft
Bottom hole temperature:	150 °F
Solution:	
Oil specific gravity =	0.88 fresh water =1
Mass associated with 1 stb of oil =	495.66 lb

Table 5-1 Results given by Spreadsheet Program **Poettmann-CarpenterBHP.xls** for Sample Problem 5-3 (Continued)

Solution gas ratio at wellhead =	78.42 scf/stb
Oil formation volume factor at wellhead =	1.04 rb/stb
Volume associated with 1 stb oil at wellhead =	45.12 cf
Fluid density at wellhead =	10.99 lb/cf
Solution gas-oil ratio at bottom hole =	301.79 scf/stb
Oil formation volume factor at bottom hole =	1.16 rb/stb
Volume associated with 1 stb oil at bottom hole =	17.66 cf
Fluid density at bottom hole =	28.07 lb/cf
The average fluid density =	19.53 lb/cf
Inertial force ($D\rho v$) =	79.21 lb/day-ft
Friction factor =	0.002
Friction term =	293.12 (lb/cf) ²
Error in depth =	0.00 ft
Bottom-hole pressure =	1699 psia

where p_{ust} and p_{dst} are the upstream and downstream pressures, respectively, and group parameters are defined as

$$a = \frac{0.0765\gamma_g q_g + 350\gamma_o q_o + 350\gamma_w q_w + 62.4\gamma_s q_s}{4.07T_{av} q_g} \quad (5.19)$$

$$b = \frac{5.615q_o + 5.615q_w + q_s}{4.07T_{av} q_g} \quad (5.20)$$

$$c = 0.00678 \frac{T_{av} q_g}{A} \quad (5.21)$$

$$d = \frac{0.00166}{A} (5.615q_o + 5.615q_w + q_s) \quad (5.22)$$

$$e = \frac{f_M}{2gD_H} \quad (5.23)$$

$$M = \frac{cde}{\cos\theta + d^2e} \quad (5.24)$$

$$N = \frac{c^2e \cos\theta}{(\cos\theta + d^2e)^2} \quad (5.25)$$

where

- A = cross-sectional area of conduit (ft²)
- D_H = hydraulic diameter (ft)
- f_M = Darcy-Wiesbach friction factor (Moody factor)
- g = gravitational acceleration (32.17 ft/s²)
- L = conduit length (ft)
- p = pressure (psia)
- p_{hf} = wellhead flowing pressure (psia)
- q_g = gas production rate (scf/d)
- q_o = oil production rate (bbl/d)
- q_s = sand production rate (ft³/day)
- q_w = water production rate (bbl/d)
- T_{av} = average temperature (°R)
- γ_g = specific gravity of gas (air =1)
- γ_o = specific gravity of produced oil (fresh water =1)
- γ_s = specific gravity of produced solid (fresh water =1)
- γ_w = specific gravity of produced water (fresh water =1)

The Darcy-Wiesbach friction factor (f_M) can be obtained graphically, as in Figure 5–2, or by calculating the Fanning friction factor (f_F), obtained from Equation (5.16). The required relation is $f_M = 4f_F$.

Because iterations are required to solve Equation (5.18) for pressure, Guo and Ghalambor developed a computer spreadsheet program, **Guo-GhalamborBHP.xls**.

5-4 SAMPLE PROBLEM

From the data given below, estimate the bottom-hole pressure using the Guo-Ghalambor method.

Total measured depth:	7000 ft
The average inclination angle:	20 deg
Tubing inside diameter:	1.995 in
Gas production rate:	1 MMscfd
Gas specific gravity:	0.7 air=1
Oil production rate:	1000 stb/d
Oil specific gravity:	0.85 H ₂ O=1
Water production rate:	300 bbl/d
Water specific gravity:	1.05 H ₂ O=1
Solid production rate:	1 ft ³ /d
Solid specific gravity:	2.65 H ₂ O=1
Tubing head temperature:	100 °F
Bottom-hole temperature:	224 °F
Tubing head pressure:	300 psia

SOLUTION

This sample problem is solved with the spreadsheet program **Guo-GhalamborBHP.xls**. The result is shown in Table 5–2.

5.3.3.2 Separated-Flow Models

Many models for separated-flow are available for TPR calculations, including the Lockhart-Martinelli correlation (1949), Duns-Ros Correlation (1963), and Hagedorn-Brown method (1965). Based on comprehensive comparisons, Ansari et al. (1994) and Hasan and Kabir (2002)

Table 5–2 Results given by Spreadsheet Program **Guo-GhalamborBHP.xls** for Sample Problem 5-4**Guo-GhalamborBHP.xls**

Description: This spreadsheet calculates flowing bottom-hole pressure based on tubing head pressure and tubing flow performance using Guo-Ghalambor Method.

Instruction: 1) Select a unit system; 2) Update parameter values in the “Input Data” section; 3) Click “Solution” button; and 4) View result in the Solution section.

Input Data:**US Field Units**

Total measured depth:	7,000 ft
Average inclination angle:	20 deg
Tubing I.D.:	1.995 in
Gas production rate:	1,000,000 scfd
Gas specific gravity:	0.7 air=1
Oil production rate:	1000 stb/d
Oil specific gravity:	0.85 H ₂ O=1
Water production rate:	300 bbl/d
Water specific gravity:	1.05 H ₂ O=1
Solid production rate:	1 ft ³ /d
Solid specific gravity:	2.65 H ₂ O=1
Tubing head temperature:	100 °F
Bottom hole temperature:	224 °F
Tubing head pressure:	300 psia

Solution:

A =	3.1243196 in ²
D =	0.16625 ft
T _{av} =	622 °R

Table 5–2 Results given by Spreadsheet Program **Guo-GhalamborBHP.xls** for Sample Problem 5-4 (Continued)

$\cos(\theta) =$	0.9397014
$(D\rho v) =$	40.908853
$f_M =$	0.0415505
$a =$	0.0001713
$b =$	2.884E-06
$c =$	1349785.1
$d =$	3.8942921
$e =$	0.0041337
$M =$	20447.044
$N =$	6.669E+09
Bottom-hole pressure, $p_{wf} =$	1,682 psia

recommended using the Hagedorn-Brown method with adjustments for near vertical flow.

The modified Hagedorn-Brown method (mH-B) is an empirical correlation based on the original work of Hagedorn and Brown (1965). The recommended modifications to it include assuming zero no-slip liquid holdup whenever the original correlation predicts a liquid holdup value less than the no-slip holdup, and using the Griffith correlation (Griffith and Wallis 1961) for the bubble flow regime.

The original Hagedorn-Brown correlation takes the following form:

$$\frac{dP}{dz} = \frac{g}{g_c} \bar{\rho} + \frac{2f_F \bar{\rho} u_m^2}{g_c D} + \bar{\rho} \frac{\Delta(u_m^2)}{2g_c \Delta z} \quad (5.26)$$

Expressed in U.S. field units as

$$144 \frac{dp}{dz} = \bar{\rho} + \frac{f_F M_i^2}{7.413 \times 10^{10} D^5 \bar{\rho}} + \bar{\rho} \frac{\Delta(u_m^2)}{2g_c \Delta z} \quad (5.27)$$

where

M_t = total mass flow rate (lb_m/d)

$\bar{\rho}$ = in-situ average density (lb_m/ft³)

u_m = mixture velocity (ft/s)

and

$$\bar{\rho} = y_L \rho_L + (1 - y_L) \rho_G \quad (5.28)$$

$$u_m = u_{SL} + u_{SG} \quad (5.29)$$

where

ρ_L = liquid density (lb_m/ft³)

ρ_G = in-situ gas density (lb_m/ft³)

u_{SL} = superficial velocity of liquid phase (ft/s)

u_{SG} = superficial velocity of gas phase (ft/s)

The superficial velocity of a given phase is defined as the volumetric flow rate of the phase divided by the pipe cross-sectional area. The third term in the right-hand-side of Equation (5.27) represents pressure change due to the change in kinetic energy, which is usually negligible for oil wells.

Obviously, determining the value for liquid holdup y_L is essential in calculating pressures. The mH-B correlation determines liquid holdup from three charts, using the following dimensionless numbers:

Liquid velocity number, N_{vL} :

$$N_{vL} = 1.938 u_{SL}^4 \sqrt{\frac{\rho_L}{\sigma}} \quad (5.30)$$

Gas velocity number, N_{vG} :

$$N_{vG} = 1.938 u_{SG}^4 \sqrt{\frac{\rho_L}{\sigma}} \quad (5.31)$$

Pipe diameter number, N_D :

$$N_D = 120.872 D \sqrt{\frac{\rho_L}{\sigma}} \quad (5.32)$$

Liquid viscosity number, N_L :

$$N_L = 0.15726 \mu_L^4 \sqrt[3]{\frac{1}{\rho_L \sigma^3}} \quad (5.33)$$

where

D = conduit inside diameter (ft)

σ = liquid-gas interfacial tension (dyne/cm)

μ_L = liquid viscosity (cp)

The first chart is used for determining parameter (CN_L) based on N_L . Guo et al. (2007) found that this chart can be replaced by the following correlation with acceptable accuracy:

$$(CN_L) = 10^Y \quad (5.34)$$

where

$$Y = -2.69851 + 0.15841X_1 - 0.55100X_1^2 + 0.54785X_1^3 - 0.12195X_1^4 \quad (5.35)$$

and

$$X_1 = \log(N_L) + 3 \quad (5.36)$$

Once the value of (CN_L) is determined, it can be used to calculate the value of the ratio:

$$\frac{N_{vL} P^{0.1} (CN_L)}{N_{vG}^{0.575} P_a^{0.1} N_D}$$

where p is the absolute pressure at the location where pressure gradient is to be calculated, and p_a is atmospheric pressure. The value of this ratio can then be used as an entry in the second chart to determine (y_L / ψ) .

Guo et al. (2007) found that the second chart can be represented by the following correlation with acceptable accuracy:

$$\left(\frac{y_L}{\psi}\right) = -0.10307 + 0.61777[\log(X_2) + 6] - 0.63295[\log(X_2) + 6]^2 + 0.29598[\log(X_2) + 6]^3 - 0.0401[\log(X_2) + 6]^4 \quad (5.37)$$

where

$$X_2 = \frac{N_{vL} P^{0.1} (CN_L)}{N_{vG}^{0.575} p_a^{0.1} N_D} \quad (5.38)$$

According to Hagedorn and Brown (1965), the value of parameter ψ can be determined from the third chart, using a value for the ratio:

$$\frac{N_{vG} N_L^{0.38}}{N_D^{2.14}}$$

Guo et al. (2007) found that where

$$\frac{N_{vG} N_L^{0.38}}{N_D^{2.14}} > 0.01$$

the third chart can be replaced by the following correlation with acceptable accuracy:

$$\psi = 0.91163 - 4.82176X_3 + 1232.25X_3^2 - 22253.6X_3^3 + 116174.3X_3^4 \quad (5.39)$$

where

$$X_3 = \frac{N_{vG} N_L^{0.38}}{N_D^{2.14}} \quad (5.40)$$

However, $\psi = 1.0$ should be used if

$$\frac{N_{vG} N_L^{0.38}}{N_D^{2.14}} \leq 0.01$$

Finally, the liquid holdup can be calculated by

$$y_L = \psi \left(\frac{y_L}{\psi} \right) \quad (5.41)$$

The Fanning friction factor in Equation (4.27) can be determined using either Chen's correlation Equation (5.5) or Equation (5.16). The appropriate Reynolds number for multiphase flow can be calculated by

$$N_{Re} = \frac{2.2 \times 10^{-2} m_t}{D \mu_L^{y_L} \mu_G^{(1-y_L)}} \quad (5.42)$$

where m_t is mass flow rate. The modified Hagedorn-Brown method (mH-B) uses the Griffith correlation for the bubble flow regime, which exists where

$$\lambda_G < L_B \quad (5.43)$$

where

$$\lambda_G = \frac{u_{sG}}{u_m} \quad (5.44)$$

and

$$L_B = 1.071 - 0.2218 \left(\frac{u_m^2}{D} \right) \quad (5.45)$$

which is valid for $L_B \geq 0.13$. When the L_B value given by Equation (5.45) is less than 0.13, $L_B = 0.13$ should be used.

Neglecting the kinetic energy pressure drop term, the Griffith correlation in U.S. field units may be expressed as

$$144 \frac{dp}{dz} = \bar{\rho} + \frac{f_F m_L^2}{7.413 \times 10^{10} D^5 \rho_L y_L^2} \quad (5.46)$$

where m_L is the mass flow rate of the liquid phase. The liquid holdup in Griffith correlation is given by the following expression:

$$y_L = 1 - \frac{1}{2} \left[1 + \frac{u_m}{u_s} - \sqrt{\left(1 + \frac{u_m}{u_s} \right)^2 - 4 \frac{u_{sG}}{u_s}} \right] \quad (5.47)$$

where $u_s = 0.8$ ft/s. The Reynolds number used to obtain the friction factor is based on the in-situ average liquid velocity, expressed as

$$N_{Re} = \frac{2.2 \times 10^{-2} m_L}{D \mu_L} \quad (5.48)$$

To simplify calculations, the Hagedorn-Brown correlation has been coded in the spreadsheet program **HagedornBrownCorrelation.xls**.

5-5 SAMPLE PROBLEM

From the data given below, calculate and graph the pressure profile in the tubing string:

Tubing shoe depth:	9,700 ft
Tubing inside diameter:	1.995 in
Oil gravity:	40 °API
Oil viscosity:	5 cp
Production GLR:	75 scf/bbl
Gas specific gravity:	0.7 air=1

Flowing tubing head pressure:	100 psia
Flowing tubing head temperature:	80 °F
Flowing temperature at tubing shoe:	180 °F
Liquid production rate:	758 stb/day
Water cut:	10 %
Interfacial tension:	30 dynes/cm
Specific gravity of water:	1.05 H ₂ O = 1

SOLUTION

This sample problem can be solved with the spreadsheet program **HagedornBrownCorrelation.xls**, as shown in Table 5–3 and Figure 5–3.

Table 5–3 Result Given by Spreadsheet Program **HagedornBrownCorrelation.xls** for Sample Problem 5-5

HagedornBrownCorrelation.xls

Description: This spreadsheet calculates flowing pressures in a single-diameter tubing string based on tubing head pressure using Hagedorn-Brown Correlation.

Instruction: 1) Select a unit system; 2) Update parameter values in the “Input Data” section; 3) Click “Solution” button; and 4) View result in the Solution section and charts.

Input Data:**US Field Units**

Depth (D):	9,700 ft
Tubing inner diameter (d_{ti}):	1.995 in
Oil gravity (API):	40 °API
Oil viscosity (μ_o):	5 cp
Production GLR (GLR):	75 scf/bbl
Gas specific gravity (γ_g):	0.7 air = 1

Table 5-3 Result Given by Spreadsheet Program
HagedornBrownCorrelation.xls for Sample Problem 5-5
 (Continued)

Flowing tubing head pressure (p_{hf}):	100 psia			
Flowing tubing head temperature (t_{hf}):	80 °F			
Flowing temperature at tubing shoe (t_{wfs}):	180 °F			
Liquid production rate (q_L):	758 stb/day			
Water cut (WC):	10 %			
Interfacial tension (σ):	30 dynes/cm			
Specific gravity of water (γ_w):	1.05 H ₂ O=1			
Solution:				
	Depth	Pressure		
	(ft)	(m)	(psia)	(MPa)
	0	0	100	0.68
	334	102	183	1.24
	669	204	269	1.83
	1,003	306	358	2.43
	1,338	408	449	3.06
	1,672	510	543	3.69
	2,007	612	638	4.34
	2,341	714	736	5.01
	2,676	816	835	5.68
	3,010	918	936	6.37

Table 5-3 Result Given by Spreadsheet Program
HagedornBrownCorrelation.xls for Sample Problem 5-5
 (Continued)

Depth		Pressure	
(ft)	(m)	(psia)	(MPa)
3,345	1,020	1,038	7.06
3,679	1,122	1,141	7.76
4,014	1,224	1,246	8.48
4,348	1,326	1,352	9.20
4,683	1,428	1,459	9.93
5,017	1,530	1,567	10.66
5,352	1,632	1,676	11.40
5,686	1,734	1,786	12.15
6,021	1,836	1,897	12.90
6,355	1,938	2,008	13.66
6,690	2,040	2,121	14.43
7,024	2,142	2,234	15.19
7,359	2,243	2,347	15.97
7,693	2,345	2,461	16.74
8,028	2,447	2,576	17.52
8,362	2,549	2,691	18.31
8,697	2,651	2,807	19.10
9,031	2,753	2,923	19.89
9,366	2,855	3,040	20.68
9,700	2,957	3,157	21.48

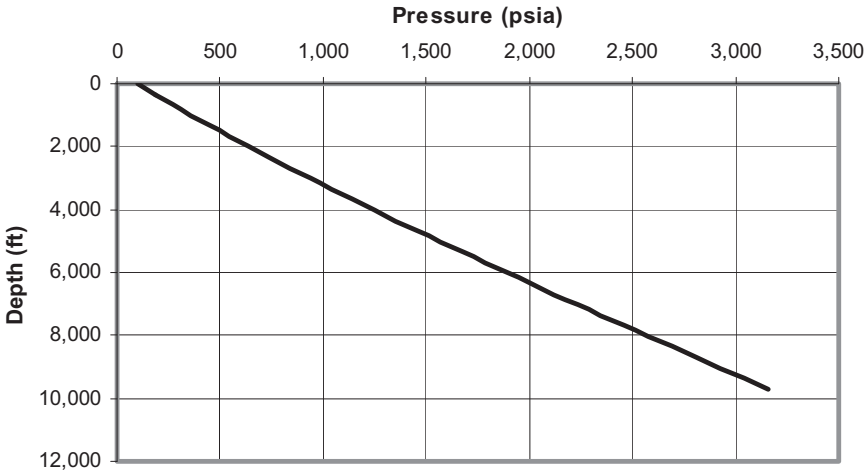


Figure 5–3 Pressure profile given by the spreadsheet program *HagedornBrownCorrelation.xls* for Sample Problem 5-5.

5.4 Single-Phase Gas Flow

The First Law of Thermodynamics (the conservation of energy) governs gas flow in tubing. The effects of kinetic energy changes are usually negligible because the variation in tubing diameter is insignificant in most gas wells. If no shaft work device is installed along the tubing string, the First Law of Thermodynamics yields the following mechanical balance equation:

$$\frac{dP}{\rho} + \frac{g}{g_c} dZ + \frac{f_M v^2 dL}{2g_c D_i} = 0 \quad (5.49)$$

Because $dZ = \cos\theta dL$, $\rho = \frac{29\gamma_g P}{ZRT}$, and $v = \frac{4q_{sc} z P_{sc} T}{\pi D_i^2 T_{sc} P}$, Equation (5.49) can be rewritten as

$$\frac{zRT}{29\gamma_g} \frac{dP}{P} + \left\{ \frac{g}{g_c} \cos\theta + \frac{8f_M Q_{sc}^2 P_{sc}^2}{\pi^2 g_c D_i^5 T_{sc}^2} \left[\frac{zT}{P} \right]^2 \right\} dL = 0 \quad (5.50)$$

which is an ordinary differential equation governing gas flow in tubing. Although the temperature T can be approximated as a linear function of length L through the geothermal gradient, the compressibility factor z is a function of pressure P and temperature T . This makes it difficult to solve the equation analytically. Fortunately, the pressure P at length L is not strongly affected by the temperature and the compressibility factor, and the petroleum industry has developed approximate solutions to Equation (5.50).

5.4.1 Average Temperature and Compressibility Factor Method

If we assume that the average values of temperature and compressibility factor can be obtained, Equation (5.50) becomes

$$\frac{\bar{z}R\bar{T}}{29\gamma_g} \frac{dP}{P} + \left\{ \frac{g}{g_c} \cos\theta + \frac{8f_M Q_{cs}^2 P_{sc}^2 \bar{z}^2 \bar{T}^2}{\pi^2 g_c D_i^5 T_{sc}^2 P^2} \right\} dL = 0 \quad (5.51)$$

By separating the variables, Equation (5.51) can be integrated over the full length of a single-diameter tubing to yield

$$P_1^2 = \text{Exp}(s)P_2^2 + \frac{8f_M[\text{Exp}(s)-1]Q_{cs}^2 P_{sc}^2 \bar{z}^2 \bar{T}^2}{\pi^2 g_c D_i^5 T_{sc}^2 \cos\theta} \quad (5.52)$$

where

$$s = \frac{58\gamma_g g L \cos\theta}{g_c R \bar{z} \bar{T}} \quad (5.53)$$

Equations (5.52) and (5.53) take the following forms when U.S. field units (q_{sc} in Mscf/d) are used (Katz et al. 1959):

$$P_1^2 = \text{Exp}(s)P_2^2 + \frac{6.67 \times 10^{-4} [\text{Exp}(s)-1] f_M q_{sc}^2 \bar{z}^2 \bar{T}^2}{d_i^5 \cos\theta} \quad (5.54)$$

where

$$s = \frac{0.0375\gamma_g L \cos\theta}{\bar{z}\bar{T}} \quad (5.55)$$

For downward flow in gas-injection wells, Equation (5.54) takes the following form:

$$p_2^2 = \text{Exp}(-s) \left[p_1^2 + \frac{6.67 \times 10^{-4} [\text{Exp}(s) - 1] f_M q_{sc}^2 \bar{z}^2 \bar{T}^2}{d_i^5 \cos\theta} \right] \quad (5.56)$$

The Darcy-Wiesbach (Moody) friction factor f_M can be determined in the conventional manner for a given tubing diameter, wall roughness, and Reynolds number. However, if one assumes fully-turbulent flow, which is the case for most gas wells, then a simple empirical relation may be used for typical tubing strings instead (Katz and Lee 1990):

$$f_M = \frac{0.01750}{d_i^{0.224}} \quad \text{for } d_i \leq 4.277 \text{ in} \quad (5.57)$$

$$f_M = \frac{0.01603}{d_i^{0.164}} \quad \text{for } d_i > 4.277 \text{ in} \quad (5.58)$$

Guo (2001) used the following Nikuradse (1933) friction factor correlation for fully turbulent flow in rough pipes:

$$f_M = \left[\frac{1}{1.74 - 2 \log\left(\frac{2\delta}{d_i}\right)} \right]^2 \quad (5.59)$$

Because the average compressibility factor is itself a function of pressure, a numerical technique such as the Newton-Raphson iteration is required to solve Equation (5.54) for bottom-hole pressure. This computation can be performed automatically with the spreadsheet program **AverageTZ.xls**.

5-6 SAMPLE PROBLEM

Suppose a vertical well produces 2 MMscf/d of 0.71 gas-specific gravity gas through a 2 7/8-in tubing set into the top of a gas reservoir at a depth of 10,000 ft. At the tubing head, the pressure is 800 psia and the temperature is 150°F. The bottom-hole temperature is 200°F. The relative roughness of tubing is about 0.0006. Calculate the pressure profile along the tubing length and plot the results.

SOLUTION

This sample problem may be solved with the spreadsheet program **AverageTZ.xls**, as shown in Table 5-4. This table shows the data input and result sections. The calculated pressure profile is illustrated in Fig. 5-4.

Table 5-4 Spreadsheet Program **AverageTZ.xls**—Data Input and Result Sections

AverageTZ.xls

Description: This spreadsheet calculates tubing pressure traverse for gas wells.

Instructions:

Step 1: Input your data in the “Input Data” section.

Step 2: Click “Solution” button to get results.

Step 3: View results in table and in graph sheet “Profile.”

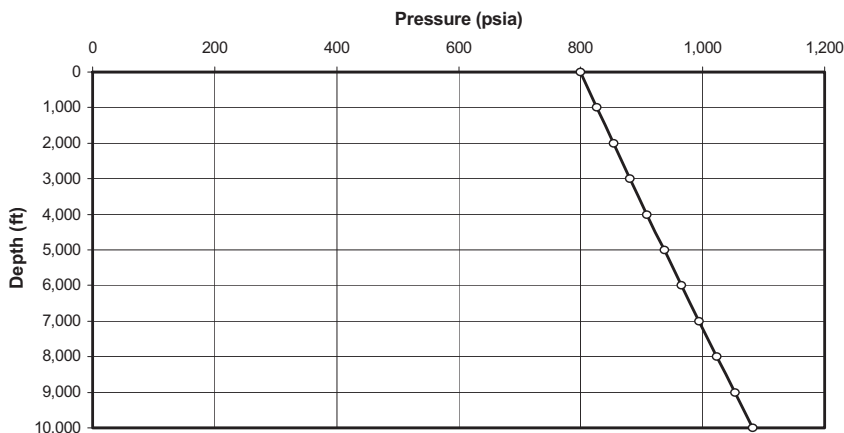
Input Data:

$\gamma_g =$	0.71
$d =$	2.259 in
$\varepsilon/d =$	0.0006
$L =$	10000 ft
$\theta =$	0 Deg
$P_{hf} =$	800 psia
$T_{hf} =$	150 °F
$T_{wf} =$	200 °F
$q_{sc} =$	2000 Mscf/d

Table 5-4 Spreadsheet Program **AverageTZ.xls**—Data Input and Result Sections (Continued)**Solution:**

$$f_M = 0.017396984$$

Depth (ft)	T ($^{\circ}\text{R}$)	p (psia)	Z_{av}
0	610	800	0.9028
1000	615	827	0.9028
2000	620	854	0.9027
3000	625	881	0.9027
4000	630	909	0.9026
5000	635	937	0.9026
6000	640	965	0.9026
7000	645	994	0.9026
8000	650	1023	0.9027
9000	655	1053	0.9027
10000	660	1082	0.9028

**Figure 5-4** Calculated tubing pressure profile for Sample Problem 5-6.

5.4.2 Cullender and Smith Method

Equation (5.50) can be solved for bottom pipe pressure using a quick numerical method originally developed by Cullender and Smith (Katz et al. 1959) by rearranging it as

$$\frac{\frac{P}{zT} dp}{\frac{g}{g_c} \cos \theta \left(\frac{P}{zT} \right)^2 + \frac{8f_M Q_{sc}^2 P_{sc}^2}{\pi^2 g_c D_i^5 T_{sc}^2}} = - \frac{29\gamma_g}{R} dL \quad (5.60)$$

That takes an integral form of

$$\int_{P_{wf}}^{P_{hf}} \left[\frac{\frac{P}{zT}}{\frac{g}{g_c} \cos \theta \left(\frac{P}{zT} \right)^2 + \frac{8f_M Q_{sc}^2 P_{sc}^2}{\pi^2 g_c D_i^5 T_{sc}^2}} \right] dp = \frac{29\gamma_g L}{R} \quad (5.61)$$

In U.S. field units (q_{msc} in MMscf/d), Equation (5.61) takes the following form:

$$\int_{P_2}^{P_1} \left[\frac{\frac{p}{zT}}{0.001 \cos \theta \left(\frac{p}{zT} \right)^2 + 0.6666 \frac{f_M q_{msc}^2}{d_i^5}} \right] dp = 18.75 \gamma_g L \quad (5.62)$$

If the integrant is denoted with symbol I —that is,

$$I = \frac{\frac{p}{zT}}{0.001 \cos \theta \left(\frac{p}{zT} \right)^2 + 0.6666 \frac{f_M q_{msc}^2}{d_i^5}} \quad (5.63)$$

Equation (5.62) becomes

$$\int_{p_2}^{p_1} Idp = 18.75\gamma_g L \quad (5.64)$$

Integrating Equation (5.64) results in

$$\frac{(p_m - p_2)(I_m + I_2)}{2} + \frac{(p_1 - p_m)(I_1 + I_m)}{2} = 18.75\gamma_g L \quad (5.65)$$

where p_m is the pressure at well mid-depth. The I_2 , I_m , and I_1 are integrant I 's evaluated at p_2 , p_m , and p_1 , respectively. Assuming the first and second terms in the right-hand side of Equation (5.65) each represent half of the integration—that is,

$$\frac{(p_m - p_2)(I_m + I_2)}{2} = \frac{18.75\gamma_g L}{2} \quad (5.66)$$

$$\frac{(p_1 - p_m)(I_1 + I_m)}{2} = \frac{18.75\gamma_g L}{2} \quad (5.67)$$

The following expressions are obtained:

$$p_m = p_2 + \frac{18.75\gamma_g L}{I_m + I_2} \quad (5.68)$$

$$p_1 = p_m + \frac{18.75\gamma_g L}{I_1 + I_m} \quad (5.69)$$

Because I_m itself is a function of pressure p_m , a numerical technique such as the Newton-Raphson iteration is required to solve Equation (5.68) for p_m . Once p_m is obtained, p_w can then be calculated from Equation (5.69). These computations can be performed automatically using the spreadsheet program **Cullender-Smith.xls**.

5-7 SAMPLE PROBLEM

Solve the problem in Sample Problem 5-6 using the Cullender and Smith method.

SOLUTION

This sample problem can be solved using the spreadsheet program **Cullender-Smith.xls**. Table 5-5 shows the data input and result sections. The pressures at depths of 5,000 ft and 10,000 ft are 937 psia and 1,082 psia, respectively. These results are exactly the same as that given by the **AverageTZ.xls**.

5.5 Mist Flow in Gas Wells

In addition to dry gas, almost all gas wells produce a certain amount of liquids, consisting of formation water and/or gas condensate (light oil). Depending on pressure and temperature, gas condensate may not be seen at the surface in some wells, but it exists in the wellbore. Some gas wells also produce sand and coal particles. All of these wells are called multi-phase gas wells. Guo and Ghalambor's (2005) four-phase flow model presented in section 5.3.3.1 can be applied to mist flow in gas wells. Its applications in liquid loading analysis will be shown in Chapter 6.

5.6 Summary

This chapter presented and illustrated different mathematical models for describing wellbore/tubing performance. Among many models, the modified Hagedorn-Brown (mHB) model has been found to give results with satisfactory accuracy for multiphase flow. Industry practice is to conduct flow gradient (FG) surveys to measure the actual flowing pressures along the tubing string. The FG data is then employed to validate one of the models and to tune the model, if necessary, before use in field applications.

5.7 References

Ansari, A.M. et al.: "A Comprehensive Mechanistic Model for Upward Two-Phase Flow in Wellbores," *SPE Production and Facilities* (May 1994) 143, *Trans.*, AIME: 297.

Table 5–5 Spreadsheet Program **Cullender-Smith.xls**—Data Input and Result Sections**Cullender-SmithBHP.xls**

Description: This spreadsheet calculates bottom-hole pressure with Cullender-Smith method.

Instructions:

Step 1: Input your data in the “Input Data” section.

Step 2: Click “Solution” button to get results.

Input Data:

$$\gamma_g = 0.71$$

$$d = 2.259 \text{ in}$$

$$\varepsilon/d = 0.0006$$

$$L = 10000 \text{ ft}$$

$$\theta = 0 \text{ Deg}$$

$$p_{hf} = 800 \text{ psia}$$

$$T_{hf} = 150 \text{ }^\circ\text{F}$$

$$T_{wf} = 200 \text{ }^\circ\text{F}$$

$$q_{msc} = 2 \text{ MMscf/d}$$

Solution:

$$f_M = 0.017397$$

Depth (ft)	T (°R)	p (psia)	Z	p/ZT	I
0	610	800	0.9028	1.45263	501.137
5000	635	937	0.9032	1.63324	472.581
10000	660	1082	0.9057	1.80971	445.349

Brown, K.E.: *The Technology of Artificial Lift Methods*, Vol. 1, PennWell Books, Tulsa, OK (1977): 104–58.

Chen, N.H.: “An Explicit Equation for Friction factor in Pipe,” *Ind. Eng. Chem. Fund* (1979)18: 296.

Cicchitti, A., et al.: “Two-Phase Cooling Experiments—Pressure Drop, Heat Transfer and Burnout Measurements,” *Energia Nucleare* (1960) 7, No. 6: 407.

Dukler, A.E., Wicks, M., and Cleveland, R.G.: “Frictional Pressure Drop in Two-Phase Flow: A Comparison of Existing Correlations for Pressure Loss and Hold-Up,” *AIChE Journal* (1964): 38–42.

Duns, H. and Ros, N.C.J.: “Vertical Flow of Gas and Liquid Mixtures in Wells,” Proceedings of the 6th World Petroleum Congress, Tokyo (1963): 451.

Goier, G.W. and Aziz, K.: *The Flow of Complex Mixtures in Pipes*, Robert E. Drieger Publishing Co., Huntington, New York (1977).

Guo, B. and Ghalambor, A.: *Gas Volume Requirements for Underbalanced Drilling Deviated Holes*, PennWell Corporation, Tulsa, OK (2002): 132–33.

Guo, B. and Ghalambor, A.: *Natural Gas Engineering Handbook*, Gulf Publishing Company, Houston (2005): 59–61.

Guo, B., Lyons, W.C., and Ghalambor, A.: *Petroleum Production Engineering*, Elsevier, Amsterdam (2007): 52–53.

Gregory, G.A. and Fogarasi, M.: “Alternate to Standard Friction Factor Equation,” *Oil and Gas Journal* (1 April 1985): 120–27.

Griffith, P. and Wallis, G.B.: “Two-Phase Slug Flow,” *Journal of Heat Transfer* (August 1961), *Trans. ASME*, Ser. C, 83: 307–320.

Hagedorn, A.R. and Brown, K.E.: “Experimental Study of Pressure Gradients Occurring During Continuous Two-Phase Flow in Small-Diameter Conduits,” *Journal of Petroleum Technology* (April 1965), *Trans. AIME*, 234: 475–484.

Hasan, A.R. and Kabir, C.S.: *Fluid Flow and Heat Transfer in Wellbores*, Society of Petroleum Engineers, Richardson, Texas (2002): 10–15.

Katz, D.L., Cornell, D., Kobayashi R., Poettmann, F. H., Vary, J. A., Elenbaas, J.R., and Weinaug, C.F.: *Handbook of Natural Gas Engineering*, McGraw-Hill Publishing Company, New York (1959).

Katz, D. L., and R. L. Lee. *Natural Gas Engineering—Production and Storage*, McGraw-Hill Publishing Company, New York (1990).

Lockhart, R.W. and Martinelli, R.C.: “Proposed Correlation of Data for Isothermal Two-Phase, Two-Component Flow in Pipes,” *Chem. Eng. Prog.* (1949): 39.

Nikuradse, J.: “A New Correlation for Friction Factor,” *Forschungshelb.* (October 1933): 301–307.

Poettmann, F.H. and Carpenter, P.G.: “The Multiphase Flow of Gas, Oil, and Water through Vertical Strings,” *API Dril. and Prod. Prac.* (1952): 257–263.

5.8 Problems

- 5-1 Suppose that 1,200 bbl/day of 18 °API, 5 cp oil is being produced through 2 7/8-in., 8.6-lb_m/ft tubing in a well that is 3° from vertical. If the tubing wall roughness is 0.003-in., assuming no free gas in tubing string, calculate the pressure drop over a 2,000 ft of tubing.
- 5-2 For the following given data, calculate bottom-hole pressure using Poettmann-Carpenter method:

Tubing head pressure:	400 psia
Tubing head temperature:	120°F
Tubing inside diameter:	1.66 in
Tubing shoe depth (near bottom-hole):	8,200 ft
Bottom-hole temperature:	170°F
Liquid production rate:	2,200 stb/day
Water cut:	32%
Producing GLR:	820 scf/stb
Oil gravity:	42 °API
Water specific gravity:	1.05 1 for fresh water
Gas specific gravity:	0.72 1 for air

- 5-3 From the data given below, estimate bottom-hole pressure with Guo-Ghalambor method:

Total measured depth:	8,200 ft
The average inclination angle:	3 deg
Tubing inside diameter	1.995 in
Gas production rate:	0.5 MMscfd
Gas specific gravity:	0.75 air = 1
Oil production rate:	2,500 stb/d
Oil specific gravity:	0.82 H ₂ O = 1
Water production rate:	550 bbl/d
Water specific gravity:	1.05 H ₂ O = 1
Solid production rate:	3 ft ³ /d
Solid specific gravity:	2.67 H ₂ O = 1
Tubing head temperature:	100°F
Bottom-hole temperature:	175°F
Tubing head pressure:	550 psia

- 5-4 From the data given below, calculate and plot pressure profile in the tubing string using Hagedorn-Brown correlation:

Tubing shoe depth:	6,200 ft
Tubing inside diameter:	1.995 in
Oil gravity:	30 °API
Oil viscosity:	2 cp
Production GLR:	550 scf/bbl
Gas specific gravity:	0.75 air = 1
Flowing tubing head pressure:	120 psia
Flowing tubing head temperature:	80°F
Flowing temperature at tubing shoe:	142 F
Liquid production rate:	1,520 stb/day
Water cut:	30 %
Interfacial tension:	30 dynes/cm
Specific gravity of water:	1.05 H ₂ O = 1

- 5-5 Suppose 3 MMscf/d of 0.70 specific gravity gas is produced through a 3 1/2-in tubing string set to the top of a gas reservoir at a depth of 8,300 ft. At tubing head, the pressure is 1,200 psia and the temperature is 125°F; the bottom-hole temperature is 185°F. The roughness of tubing is about 0.002-in. Calculate the

flowing bottom-hole pressure with three methods: (1) the average temperature and compressibility factor method; (2) the Cullender and Smith method; and (3) the four-phase flow method. Make comments on your results.

- 5-6 Solve problem 5.5 for gas production through a K-55, 17 lb/ft, 5 1/2-in casing.
- 5-7 Suppose 2 MMscf/d of 0.7 specific gravity gas is produced through a 2 7/8-in (2.259-in ID) tubing string set to the top of a gas reservoir at a depth of 5,200 ft. Tubing head pressure is 400 psia and the temperature is 100°F; the bottom-hole temperature is 155°F. The roughness of tubing is about 0.002-in. Calculate the flowing bottom pressure with the average temperature and compressibility factor method.

This page intentionally left blank

Productivity of Wells with Simple Trajectories

6.1 Introduction

Well productivity is defined as the deliverability of the well, rather than reservoir, although the latter affects the former. Well deliverability is determined by the combination of well inflow performance described in Chapter 4 and the wellbore flow performance described in Chapter 5. While the former describes reservoir deliverability, the latter introduces the resistance to flow by the production string. This chapter focuses on the prediction of achievable fluid production rates from various types of reservoirs with given production string characteristics. This technique is called NODAL analysis (a Schlumberger patent). Calculation examples are illustrated using computer spreadsheets.

6.2 Principles of Well Productivity Analysis

Fluid properties change with the location-dependent pressure and temperature in oil and gas production systems. To simulate the fluid flow in a particular system, it is necessary to “break” the system into discrete elements (equipment sections) by nodes. Fluid properties in the elements are then evaluated locally. In petroleum engineering, the techniques for predicting oil and gas production rates and pressure at a specified node are called NODAL analysis.

NODAL analysis is performed on the principle of pressure continuity—that is, there is only one pressure value at any given node no matter what

pressures are indicated by the performance of upstream or downstream equipment. For a given node, the pressure-flow rate relationship for upstream equipment is called the inflow performance relationship (IPR). The relationship for downstream equipment is called the outflow performance relationship (OPR). The equations representing IPR and OPR can be solved mathematically or graphically, and yield the operating flow rate and pressure at the specified node.

Although NODAL analysis can be performed using any point in the system as a solution node, it is usually conducted using bottom-hole or the wellhead as the solution node. This is because measured pressure data are normally available for these two points and these data can be used to validate the result of the analysis. This chapter illustrates the principle of NODAL analysis using bottom-hole as the solution node for predicting well productivity. Thus the IPR reflects the flow performance of reservoir from the reservoir boundary to bottom-hole and the OPR reflects the flow performance of the wellbore (tubing) from the bottom-hole to the wellhead (TPR).

6.3 Deliverability of Vertical Wells

The term *vertical well* in this section is defined as a wellbore penetrating nearly vertically into a nearly horizontal, non-hydraulically fractured pay zone. For multi-layer reservoirs, a composite IPR should be used. All IPR models used in this chapter were presented in Chapter 4.

6.3.1 Oil Wells in Volumetric Reservoirs

A volumetric reservoir is a reservoir surrounded by no-flow boundaries in all directions. As discussed in Chapter 4, the IPR of a vertical well can be described on the basis of flow pattern—that is, transient, steady-state, or pseudosteady-state flow.

6.3.1.1 Transient Production

During the transient production period, as determined using Equation (4.7) for a theoretical circular boundary, Equation (4.2) can be used to construct the IPR curve, and the mHB correlation described in Chapter 5 can be used to construct the TPR curve. The intersection of these two curves defines the operating point.

6-1 SAMPLE PROBLEM

From the data given below, assuming the tubing string is set directly above the pay zone, predict the transient production rate after 30 days:

Reservoir porosity (ϕ):	0.2
Effective horizontal permeability (k):	10 md
Pay zone thickness (h):	50 ft
Reservoir pressure (p_i):	5500 psia
Oil formation volume factor (B_o):	1.2 rb/stb
Total reservoir compressibility (c_t):	0.000013 psi^{-1}
Wellbore radius (r_w):	0.328 ft
Skin factor (S):	0
Well depth (H):	10000 ft
Tubing inner diameter (d):	2.441 in
Oil gravity (API):	30 API
Oil viscosity (μ_o):	1.5 cp
Producing GLR (GLR):	300 scf/bbl
Gas specific gravity (γ_g):	0.7 air = 1
Flowing tubing head pressure (p_{hf}):	800 psia
Flowing tubing head temperature (t_{hf}):	150 °F
Flowing temperature at tubing shoe (t_{wf}):	180 °F
Water cut (WC):	10 %
Oil-gas interfacial tension (σ):	30 dynes/cm
Specific gravity of water (γ_w):	1.05

SOLUTION

This sample problem can be solved using the spreadsheet program **Transient Production Forecast.xls**. Table 6–1 presents calculated data. Figure 6–1 shows the calculated IPR and TPR curves, which indicate an expected oil production rate of 640 stb/day at a flowing bottom-hole pressure of 2870 psia.

Table 6–1 Data Given by the Spreadsheet Program **Transient Production Forecast.xls**

q (stb/d)	p _{wf} (psia)	
	IPR	TPR
134	4,950	2,343
268	4,400	2,560
402	3,850	2,702
537	3,300	2,811
671	2,750	2,902
805	2,200	2,982
939	1,650	3,054
1,073	1,100	3,120
1,207	550	3,182
1,341	0	3,241

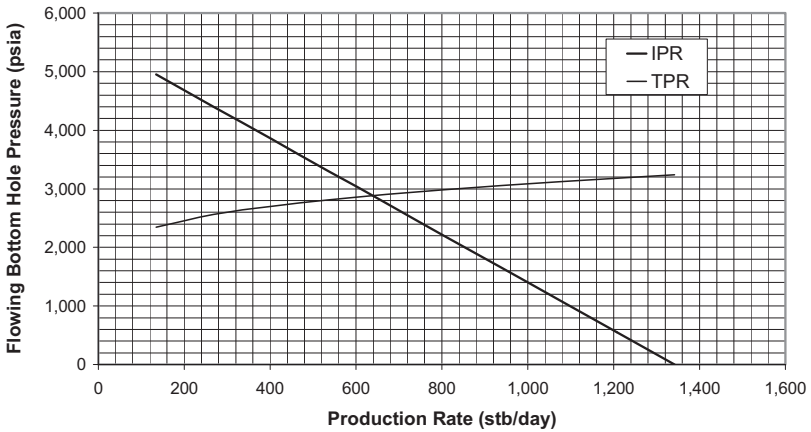


Figure 6–1 IPR and TPR curves given by the spreadsheet program **Transient Production Forecast.xls**.

6.3.1.2 Pseudosteady-State Production

During the pseudosteady-state production period as determined using Equation (4.7) for a theoretical circular boundary, Equation (4.9) can be used to construct the IPR curve, and the mHB correlation, to construct the TPR curve. The intersection of the two curves then defines the operating point.

6-2 SAMPLE PROBLEM

From the data given below, assuming the tubing string is set just above the pay zone, predict the pseudosteady-state production rate:

Initial oil bubble-point pressure (p_b):	4500 psia
Effective horizontal permeability (k):	10 md
Pay zone thickness (h):	50 ft
Average reservoir pressure (p_{bar}):	2500 psia
Oil formation volume factor (B_o):	1.2 rb/stb
Well drainage area (A):	320 acres
Wellbore radius (r_w):	0.328 ft
Skin factor (S):	0
Well depth (H):	8000 ft
Tubing inner diameter (d):	2.441 in
Oil gravity (API):	30 API
Oil viscosity (μ_o):	1.5 cp
Producing GLR (GLR):	440 scf/bbl
Gas specific gravity (γ_g):	0.7 air =1
Flowing tubing head pressure (p_{hf}):	800 psia
Flowing tubing head temperature (t_{hf}):	150 °F
Flowing temperature at tubing shoe (t_{wf}):	180 °F
Water cut (WC):	10 %
Oil-gas interfacial tension (σ):	30 dynes/cm
Specific gravity of water (γ_w):	1.05
Shape factor for drainage area (C_A):	31.6

SOLUTION

This sample problem can be solved using the spreadsheet program **Pseudosteady-2Phase Production Forecast.xls**. Table 6–2 summarizes some calculated data. Figure 6–2 presents the calculated IPR and TPR curves, which indicate a predicted oil production rate of 136 stb/day at a flowing bottom-hole pressure of 1890 psia.

6.3.1.3 Steady-State Production

Steady-state production occurs after a constant-pressure boundary is reached. Equation (4.5) can be used to construct the IPR curve, and the mHB correlation can be used to construct the TPR curve. The intersection of the two curves then defines the operating point.

Table 6–2 Data Generated by the Spreadsheet Program **Pseudosteady-2Phase Production Forecast.xls**

q (stb/d)	p _{wf} (psia)	
	IPR	TPR
34	2,358	1,650
68	2,207	1,752
102	2,047	1,823
136	1,875	1,878
170	1,688	1,924
204	1,483	1,963
239	1,250	1,998
273	976	2,030
307	625	2,058
341	0	2,085

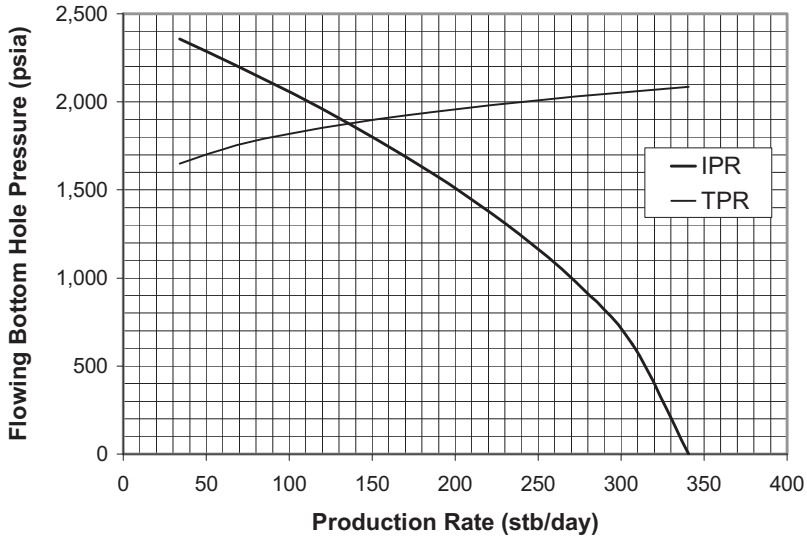


Figure 6–2 IPR and TPR curves given by the spreadsheet program *Pseudosteady-2Phase Production Forecast.xls*.

6-3 SAMPLE PROBLEM

From the data given below, assuming the tubing string is set just above the pay zone, predict the steady-state production rate:

Initial oil bubble-point pressure (p_b):	4000 psia
Effective horizontal permeability (k):	50 md
Pay zone thickness (h):	50 ft
Boundary reservoir pressure (p_e):	4000 psia
Oil formation volume factor (B_o):	1.2 rb/stb
Well drainage area (A):	640 acres
Wellbore radius (r_w):	0.328 ft
Skin factor (S):	0
Well depth (H):	7000 ft
Tubing inner diameter (d):	2.441 in

Oil gravity (API):	40 API
Oil viscosity (μ_o):	1.5 cp
Producing GLR (GLR):	500 scf/bbl
Gas specific gravity (γ_g):	0.7 air =1
Flowing tubing head pressure (p_{hf}):	1000 psia
Flowing tubing head temperature (t_{hf}):	120 °F
Flowing temperature at tubing shoe (t_{wf}):	170 °F
Water cut (WC):	10 %
Oil-gas interfacial tension (σ):	30 dynes/cm
Specific gravity of water (γ_w):	1.05

SOLUTION

This sample problem can be solved using the spreadsheet program **Steady-2Phase Production Forecast.xls**. Table 6–3 shows some calculated data. Figure 6–3 presents the calculated IPR and TPR curves, which indicate an operating oil production rate of 1350 stb/day at a flowing bottom-hole pressure of 2500 psia.

6.3.2 Oil Wells in Water/Gas-Coning Reservoirs

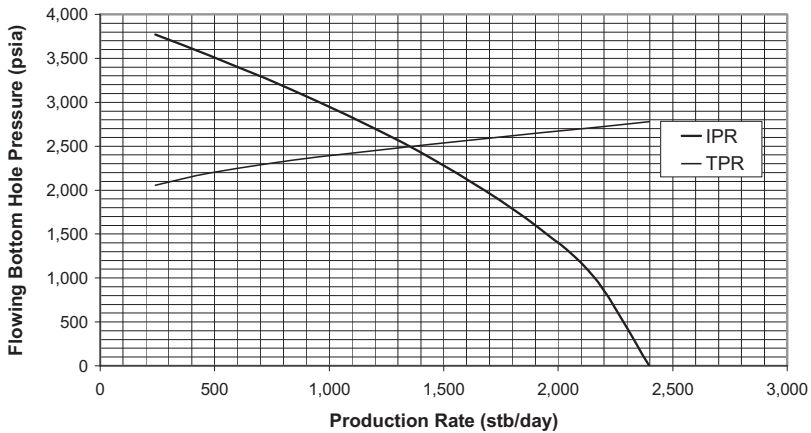
In some reservoirs, oil production rate is limited by water or gas-coning. Water breakthrough from the water cone is a result of excessive production drawdown. Reducing the oil production rate can minimize the problem of dealing with large amounts of produced water.

Excess gas production from a gas zone overlaying an oil pay zone can occur due to premature gas breakthrough from the gas cone, also due to excessive production drawdown. In order to avoid dealing with a large amount of produced gas, and to maintain reservoir pressure, the oil production rate should be reduced to lower levels.

There are a number of methods for predicting the maximum water-free and gas-free production rates (critical rates), including Craft-Hawkins (1959), Schols (1972), Meyer-Gardner-Pirson, (1977), Chaperon (1986), Joshi (1988), Hoyland-Papatzacos-Skjjaeveland (1989), and Guo-Lee (1994).

Table 6–3 Data Given by the Spreadsheet Program **Steady-2Phase Production Forecast.xls**

q (stb/d)	p _{wf} (psia)	
	IPR	TPR
240	3,772	2,053
480	3,531	2,196
719	3,275	2,296
959	3,000	2,378
1,199	2,702	2,451
1,439	2,372	2,520
1,679	2,000	2,586
1,919	1,562	2,651
2,158	1,000	2,716
2,398	0	2,781

**Figure 6–3** IPR and TPR curves given by the spreadsheet program **Steady-2Phase Production Forecast.xls**.

The Chaperon, Hoyland-Papatzacos-Skjaveland, and Guo-Lee methods take into account the effects of vertical permeability on the critical rates, with the Chaperon method giving the most optimistic value of critical rate.

The Chaperon method uses the following equation to predict the critical oil production rate:

$$q_o = 4.888 \times 10^{-4} \frac{k_H h^2 \Delta \rho}{B_o \mu_o} q_c^* \quad (6.1)$$

where

q_o = critical oil rate (STB/day)

k_H = horizontal permeability (md)

h = oil column thickness (ft)

B_o = oil formation volume factor (rb/STB)

μ_o = oil viscosity (cp)

Δ_r = density difference (gm/cc)

and

$$q_c^* = 0.7311 + 1.9434\alpha'' \quad (6.2)$$

$$\alpha'' = \frac{r_e}{h} \sqrt{\frac{k_v}{k_H}} \quad (6.3)$$

6-4 SAMPLE PROBLEM

Calculate the anticipated critical oil production rate using the following data:

Oil column thickness:	80 ft
Horizontal permeability:	70 md
Vertical permeability:	7 md
Oil viscosity:	0.42 cp

Oil density:	0.7 gm/cc
Oil formation volume factor:	1.1 rb/STB
Water or gas density:	1.05 gm/cc
Drainage area:	160 acres

SOLUTION

This problem can be solved using the spreadsheet program **Chap-eron Critical Oil Rate.xls**. The result is 176 stb/day.

6.3.3 Gas Wells in Volumetric Reservoirs

Most gas reservoirs are volumetric. As discussed in Chapter 4, the IPR of a vertical gas well depends on whether the flow pattern is transient or pseudosteady-state.

6.3.3.1 Transient Production

During the transient production period, Equation (4.10) should be used for IPR analysis. Due to the complexity of real-gas pseudopressure computations, however, more simplified IPR equations are frequently employed. At pressures lower than 2000 psia, the pseudopressure is proportional to the square of the pressure. The following equation is often adopted:

$$q_g = \frac{kh(p_i^2 - p_{wf}^2)}{1638\bar{\mu}_g \bar{z}T \left(\log t + \log \frac{k}{\phi\bar{\mu}_g c_t r_w^2} - 3.23 + 0.87S \right)} \quad (6.4)$$

At pressures greater than 3000 psia, the pseudopressure is proportional to pressure. The following equation is often utilized:

$$q_g = \frac{kh(p_i - p_{wf})}{141.2 \times 10^3 \bar{B}_g \bar{\mu}_g \left(\log t + \log \frac{k}{\phi\bar{\mu}_g c_t r_w^2} - 3.23 + 0.87S \right)} \quad (6.5)$$

Because Equation (6.4) yields a more conservative production rate than Equation (6.5), use of the former is recommended for pressures between 2000 psia and 3000 psia.

Equation (5.54) is frequently used for TPR analysis of dry-gas wells. Equation (5.18) can be used for TPR analysis of gas condensate wells and gas wells producing water and/or solids.

6-5 SAMPLE PROBLEM

From the data given below, assuming the tubing string is set just above the pay zone, predict the transient production rate of gas after 30 days:

Reservoir permeability (k):	20 md
Pay zone thickness (h):	5 ft
Well skin factor (S):	10
Porosity (ϕ):	0.2
Wellbore radius (r_w):	0.328 ft
Gas specific gravity (γ_g):	0.65
Gas viscosity (μ_g):	0.01 cp
Tubing inside diameter (D):	3.5 in
Tubing relative roughness (ϵ/D):	0.0006
Measured depth at tubing shoe (L):	5000 ft
Inclination angle (θ):	0 deg
Wellhead pressure (p_{hf}):	500 psia
Wellhead temperature (T_{hf}):	150 °F
Bottom-hole temperature (T_{wf}):	200 °F
Initial reservoir pressure (p_i):	2000 psia

SOLUTION

This problem can be solved using the spreadsheet program **Dry Gas Production Forecast.xls**. Table 6–4 shows some calculated data, and Figure 6–4 illustrates the calculated IPR and TPR curves, which indicate an operating gas production rate of 2371 Mscf/day at a flowing bottom-hole pressure of 565 psia.

Table 6–4 Data Given by the Spreadsheet Program **Dry Gas Production Forecast.xls**

q_{sc} (Mscf/d)	IPR	TPR
0	2000	556
258	1897	557
515	1789	557
773	1673	557
1031	1549	558
1289	1414	559
1546	1265	560
1804	1095	561
2062	894	563
2319	632	565
2448	447	566
2513	316	566
2545	224	566
2577	0	567
Operating flow rate =	2371	Mscf/d
Residual of objective function =	3.86463E-05	
Operating pressure =	565	psia

6.3.3.2 Pseudosteady-State Production

During the pseudosteady-state production period as determined by using Equation (4.7) for a theoretical circular boundary, the appropriate IPR equation is Equation (4.10). Again, due to the difficulty of pseudopressure computations, more simplified IPR equations are frequently used. At pressures lower than 2000 psia, the following equation is often employed:

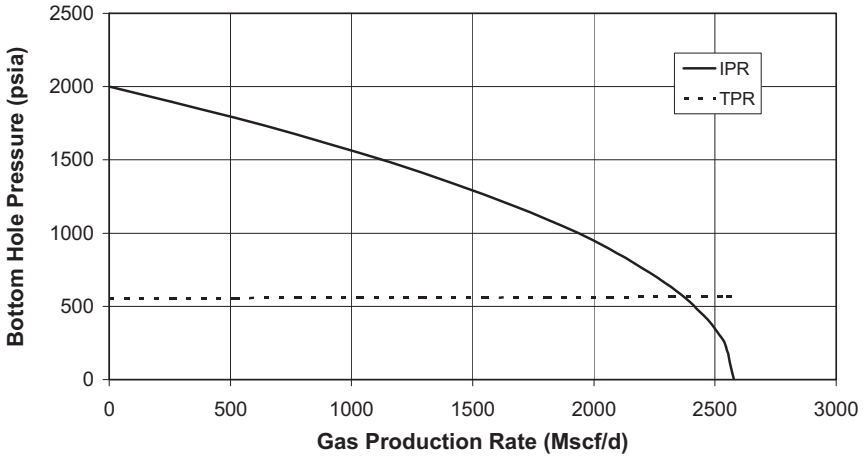


Figure 6-4 IPR and TPR curves given by the spreadsheet program *Dry Gas Production Forecast.xls*.

$$q_g = \frac{kh(\bar{p}^2 - p_{wf}^2)}{1424\bar{\mu}_g \bar{z} T \left(\ln \frac{r_e}{r_w} - \frac{3}{4} + S + Dq_g \right)} \quad (6.6)$$

At pressures higher than 3000 psia, the following equation is often utilized instead:

$$q_g = \frac{kh(\bar{p} - p_{wf})}{141.2 \times 10^3 \bar{B}_g \bar{\mu}_g T \left(\ln \frac{r_e}{r_w} - \frac{3}{4} + S + Dq_g \right)} \quad (6.7)$$

Because Equation (6.6) gives a more conservative production rate than Equation (6.7), use of the former is recommended for pressures between 2000 psia and 3000 psia.

Again, Equation (5.54) is used for the TPR analysis of dry-gas wells, and Equation (5.18) can be used for TPR analysis of gas-condensate wells and gas wells producing water and/or solids.

6-6 SAMPLE PROBLEM

From the data given below, assuming the tubing string is set just above the pay zone, predict the pseudosteady gas production rate:

Pay zone thickness:	78 ft
Permeability:	0.17 md
Wellbore radius:	0.328 ft
Darcy skin factor:	5
Non-Darcy skin coefficient:	0.001 Mscf/day
Reservoir pressure:	4613 psia
Total measured depth:	7,000 ft
Average inclination angle:	5 deg
Tubing I.D.:	1.995 in
Gas specific gravity:	0.65 air=1
Gas viscosity:	0.022 cp
Gas z-factor:	0.958
Oil production rate:	5 stb/day
Oil specific gravity:	0.85 H ₂ O=1
Water cut:	10 %
Water specific gravity:	1.05 H ₂ O=1
Solid production rate:	1 ft ³ /d
Solid specific gravity:	2.65 H ₂ O=1
Tubing head temperature:	100 °F
Bottom-hole temperature:	180 °F
Tubing head pressure:	1000 psia
Drainage area:	320 acres
Wall roughness:	0.01 in

SOLUTION

This problem can be solved using the spreadsheet program **Wet Gas Pseudosteady Production Forecast.xls**. Table 6–5 shows some calculated data, which indicates an operating gas production rate of 980 Mscf/day at a flowing bottom-hole pressure of 1189 psia.

Table 6–5 Data Given by the Spreadsheet Program **Wet Gas Pseudosteady Production Forecast.xls**

A =	3.1243196 in ²
D =	0.16625 ft
T _{av} =	600 °R
cos(θ) =	0.9961953
δ/D	0.0100251
f _M =	0.0303742
a =	2.114E-05
b =	1.346E-08
c =	1275763.4
d =	0.0171734
e =	0.0028505
M =	62.690286
N =	4.657E+09
Gas production rate, q =	980 Mscf/d
Bottom-hole pressure, p _{wf} =	1,189 psia

6.3.4 Liquid Loading in Gas Wells

Most gas wells produce wet gas—that is, natural gas carrying condensate and/or liquid water in the form of mist flow. As the gas flow velocity in the well decreases because of reservoir pressure depletion, the carrying capacity of the gas also decreases. When the gas velocity drops to a crit-

ical level, liquids begin to accumulate and undergo annular flow and slug flow in the tubing. This accumulation of liquids (liquid loading) increases the bottom-hole pressure and further reduces the gas production rate. The low-gas production rate will in turn cause gas velocity to drop further still. Eventually, the well will experience a bubbly flow regime and cease producing.

The liquid loading problem can be solved by using various measures. Artificially foaming the liquid water can enable the gas to lift the water from the well. Using narrower tubing or ensuring a lower wellhead pressure can sometimes maintain adequate mist flow. The well can also be unloaded by gas-lifting or by pumping the liquids out of the well. Heating the wellbore can prevent liquid condensation. Down-hole injection of water into an underlying disposal zone is yet another option.

Liquid loading is not always obvious, and recognizing the problem is not an easy task. A thorough diagnostic analysis of well data needs to be performed. The signs to look for include:

- Onset of liquid slugs at the surface of the well
- Increasing differential between tubing and casing pressures over time
- Sharp gradient changes on a flowing pressure survey
- Sudden decreases in a production decline curve

Two methods for predicting liquid loading are presented in this section.

6.3.4.1 Turner's Method

Turner et al. (1969) pioneered work in analyzing and predicting the minimum gas flow rate that can still prevent liquid loading. They presented two mathematical models describing the liquid loading problem: the film movement model and the entrained droplet movement model. Based on analyses of field data, they concluded that their film movement model did not represent the controlling liquid transport mechanism.

Turner et al.'s entrained drop movement model was derived from the terminal settling velocity of liquid droplets and the maximum droplet diameter

corresponding to the critical Weber number of 30. Turner et al.'s terminal slip velocity equation is expressed in U.S. field units as

$$v_{sl} = \frac{1.3\sigma^{1/4}(\rho_L - \rho_g)^{1/4}}{C_d^{1/4}\rho_g^{1/2}} \quad (6.8)$$

According to Turner et al.'s theory, gas will continuously remove liquids from the well until its velocity drops to below the terminal slip velocity. The minimum gas flow rate (in MMcf/D) for a particular pressure and conduit geometry can be calculated using Equations (6.8) and (6.9):

$$Q_{gstMM} = \frac{3.06pv_{sl}A}{Tz} \quad (6.9)$$

Turner et al. compared their model with actual field data and showed that it underestimated the required gas flow rate. They recommended adjusting the equation-derived values upward by approximately 20% to ensure removal of all droplets. Turner et al. believed that the discrepancy in their model could be attributed to the use of drag coefficients for solid spheres, an assumption of stagnation velocity, and that the critical Weber number was established for droplets falling in air, not in compressed natural gas.

The main problem complicating the use of Turner et al.'s entrained droplet model in gas wells comes from the difficulty of estimating fluid density and pressure accurately. Using an average value for gas specific gravity (0.6) and gas temperature (120°F), Turner et al. derived an estimate of gas density in lbm/ft³ as 0.0031 times the pressure in psi. However, they did not present a method for calculating the gas pressure in mist flow.

Turner et al.'s entrained droplet movement model was later modified by other researchers. Coleman et al. (1991) suggested using Equation (6.8) with a lower value of coefficient instead of 1.3. Nosseir et al. (2000) expanded Turner et al.'s entrained droplet model to more than one-flow regimes. Lea and Nickens (2004) made corrections to Turner et al.'s simplified equations. However, the drawbacks of Turner et al.'s original approach—neglected transport velocity and multiphase flow pressure—still remain unsolved.

6-7 SAMPLE PROBLEM

From the data given below, assuming the tubing string is set just above the pay zone, predict the minimum gas production rate that can prevent liquid loading:

Gas specific gravity (γ_g):	0.6
Tubing diameter (d):	2.441 in
Tubing shoe pressure (p_{wf}):	530 psia
Tubing shoe temperature (T_{wf}):	116 °F
Liquid density (ρ_l):	67.4 lbm/ft ³
Interfacial tension (σ):	60 dynes/cm

SOLUTION

This problem can be solved using the spreadsheet program **TurnerLoading.xls**. Table 6-6 shows some calculated data which indicates the minimum required gas production rate of 1004 Mscf/d.

Table 6-6 Result Given by the Spreadsheet Program **TurnerLoading.xls**

T =	576.00 °R
ρ_g =	1.49 lbm/ft ³
A =	0.0325 ft ²
p_{pc} =	672.50 psia
T_{pc} =	358.50 °R
T_{av} =	576.00 °R
p_{av} =	530.00 psia
p_{pr} =	0.79
T_{pr} =	1.61
Z =	0.94
v_{gm} =	10.37 ft/s
Q_{gm} =	1004 Mscf/d

6.3.4.2 Guo's Method

Building on Turner et al.'s entrained droplet model, Guo et al. (2006) determined the minimum kinetic energy of gas required to lift liquids. Applying the minimum kinetic energy criterion to the mist-flow model (see Chapter 5) results in a closed-form analytical equation that can be used to predict the minimum gas flow rate.

Kinetic energy per unit volume of gas can be expressed as

$$E_k = \frac{\rho_g v_g^2}{2g_c} \quad (6.10)$$

Substituting Equation (6.8) into Equation (6.10) gives an expression for the minimum kinetic energy required to keep liquid droplets in suspension in the gas:

$$E_{ksl} = 0.026 \sqrt{\frac{\sigma(\rho_L - \rho_g)}{C_d}} \quad (6.11)$$

If the value of the drag coefficient $C_d = 0.44$ recommended by Turner et al. is used, and the effects of gas density are neglected (a conservative assumption), Equation (6.11) then becomes

$$E_{ksl} = 0.04 \sqrt{\sigma \rho_L} \quad (6.12)$$

In gas wells that produce formation water, typical values for the water-gas interfacial tension and the water density are 60 dynes/cm and 65 lb_m/ft³, respectively. This yields the minimum kinetic energy value of 2.5 lb_f-ft/ft³. In gas wells that also produce condensate, typical values for the condensate-gas interfacial tension and condensate density are 20 dynes/cm and 45 lb_m/ft³, respectively. This yields the minimum kinetic energy value of 1.2 lb_f-ft/ft³. These results imply that the required minimum gas production rate in water-producing gas wells must be approximately twice that of condensate-producing gas wells.

The minimum gas velocity required for transporting the liquid droplets upward is equal to the minimum gas velocity required for floating the

liquid droplets (keeping the droplets in suspension) plus the transport velocity of the droplets, expressed as

$$v_{gm} = v_{sl} + v_{tr} \quad (6.13)$$

The transport velocity v_{tr} may be calculated from estimates of the liquid production rate, conduit geometry, and the liquid volume fraction, and is difficult to quantify. Instead of attempting to formulate an expression for the transport velocity v_{tr} , Guo et al. used v_{tr} as an empirical constant to combine the effects of non-stagnation velocity, drag coefficients for solid spheres, and the critical Weber number as established for droplets falling in air. On the basis of Turner et al.'s work, Guo et al. took the value of v_{tr} to be 20% of v_{sl} . Use of this value results in

$$v_{gm} \approx 1.2v_{sl} \quad (6.14)$$

Substituting Equations (6.8) and (6.14) into Equation (6.10) gives the expression for the minimum kinetic energy required for transporting the liquid droplets as

$$E_{km} = 0.0576\sqrt{\sigma\rho_L} \quad (6.15)$$

For typical gas wells producing water, this equation yields a minimum kinetic energy value of 3.6 lb_f-ft/ft³. For typical gas wells producing condensate, this equation results in a minimum kinetic energy value of 1.73 lb_f-ft/ft³. Again, these figures imply that the required minimum gas production rate in water-producing gas wells is approximately twice that of condensate-producing gas wells.

In order to evaluate the gas kinetic energy E_k in Equation (6.10) at a given gas flow rate and compare it with the minimum required kinetic energy E_{km} in Equation (6.15), the values of gas density ρ_g and gas velocity v_g need to be determined. Expressions for ρ_g and v_g can be obtained from the ideal gas law:

$$\rho_g = \frac{2.7S_g p}{T} \quad (6.16)$$

$$v_g = 4.71 \times 10^{-2} \frac{TQ_G}{A_i p} \quad (6.17)$$

Substituting Equations (6.16) and (6.17) into Equation (6.10) yields

$$E_k = 9.3 \times 10^{-5} \frac{S_g T Q_G^2}{A_i^2 p} \quad (6.18)$$

Equation (6.18) indicates that gas kinetic energy decreases with increased pressure. Therefore, the controlling conditions are those at bottom-hole, where the gas has the highest pressure and lowest kinetic energy. This analysis is consistent with observations from air-drilling operations, during which solid particles accumulate at bottom-hole rather than at the wellhead. However, this contradicts Turner et al.'s results, which indicated that the controlling conditions are generally at the wellhead.

Under the minimum unloaded condition (the last point of the mist-flow regime), Equation (6.18) becomes

$$E_{km} = 9.3 \times 10^{-5} \frac{S_g T_{bh} Q_{gm}^2}{A_i^2 p} \quad (6.19)$$

which gives

$$p = 9.3 \times 10^{-5} \frac{S_g T_{bh} Q_{gm}^2}{A_i^2 E_{km}} \quad (6.20)$$

Substituting Equation (6.20) into the mist-flow model of Equation (5.18) results in

$$144b\alpha_1 + \frac{1-2bM}{2} \ln \alpha_2 - \frac{M + \frac{b}{c}N - bM^2}{\sqrt{N}} \left[\tan^{-1} \beta_1 - \tan^{-1} \beta_2 \right] = \gamma \quad (6.21)$$

where

$$\alpha_1 = 9.3 \times 10^{-5} \frac{S_g T_{bh} Q_{gm}^2}{A_i^2 E_{km}} - p_{hf} \quad (6.22)$$

$$\alpha_2 = \frac{\left(1.34 \times 10^{-2} \frac{S_g T_{bh} Q_{gm}^2}{A_i^2 E_{km}} + M \right)^2 + N}{\left(144p_{hf} + M \right)^2 + N} \quad (6.23)$$

$$\beta_1 = \frac{1.34 \times 10^{-2} \frac{S_g T_{bh} Q_{gm}^2}{A_i^2 E_{km}} + M}{\sqrt{N}} \quad (6.24)$$

$$\beta_2 = \frac{144p_{hf} + M}{\sqrt{N}} \quad (6.25)$$

$$\gamma = a(1 + d^2 e)L \quad (6.26)$$

All parameters should be evaluated at Q_{gm} . The minimum required gas flow rate Q_{gm} can be determined from Equation (6.26) using trial-and-error or a numerical method such as the Bisection method. It can be shown that Equation (6.26) is a one-to-one function of Q_{gm} for Q_{gm} values greater than zero. Therefore, the Newton-Raphson iteration technique can also be used to determine Q_{gm} . Commercial software packages such as MS Excel with the Goal Seek function programmed in can be used to generate solutions. One such is the spreadsheet program **GasWellLoading.xls**.

6-8 SAMPLE PROBLEM

From the data given below, assuming a single-size tubing string is set just above the pay zone, use Guo's method to predict the minimum gas production rate that will prevent liquid loading:

Gas specific gravity:	0.6	air = 1
Hole inclination:	0	deg
Tubing shoe depth:	5555	ft
Wellhead pressure:	444	psi
Wellhead temperature:	60	°F
Producing zone temperature:	116	°F
Condensate gravity:	71	API
Condensate make:	1	bbl/MMscf
Water specific gravity:	1.08	water = 1
Water make:	50	bbl/MMscf
Solid specific gravity:	2.65	water = 1
Solid make:	0	ft ³ /MMscf
Conduit O.D.:	2.441	in
Conduit I.D.:	0	in
Conduit wall roughness:	0.000015	in
Liquid density:	67.4	lb/ft ³
Liquid-gas interfacial tension:	60	dyne/cm

SOLUTION

This problem can be solved using the spreadsheet program **Gas-WellLoading.xls**. Table 6–7 shows some calculated data which indicates that a minimum gas production rate of 1178 Mscf/d is required. Comparing this and Turner's result (1004 Mscf/d in Sample Problem 6-7) indicates that the Turner method may underestimate the minimum gas flow rate by 17.4%.

Table 6–7 Results Given by the Spreadsheet Program **GasWellLoading.xls**

Hydraulic diameter:	0.2034	ft
Conduit cross-sectional area:	0.0325	ft ²
Average temperature:	547.775	°R
Minimum kinetic energy:	3.6627	lbf-ft/ft ³
a =	2.91508E-05	
b =	1.2839E-07	
c =	936406.3493	
d =	0.1202439	
e =	0.000571676	
f =	0.007481992	
M =	64.36851023	
N =	501269364.5	
Critical gas production rate =	1178	Mscf/day
Pressure at tubing shoe =	530	psia

6.4 Deliverability of Fractured Wells

The deliverability of hydraulically-fractured wells is determined by their individual fracture characteristics. This section addresses productivity of wells with a single fracture. The productivity of wells completed with multiple fractures is discussed in Chapter 7.

6.4.1 Single-Fractured Oil Wells

For steady-state production of a single-fractured oil well, Equation (4.12) can be used to predict the production index and construct an IPR curve. For pseudosteady-state production, Equation (4.18) can be employed. The mHB correlation can be used to construct the TPR curve. The intersection of the two curves defines the operating point.

6-9 SAMPLE PROBLEM

From the data given below, assuming that tubing string is set just above the pay zone, predict the pseudosteady-state production rate:

Fracture half length (x_f):	600 ft
Fracture permeability (k_f):	50000 md
Oil bubble-point pressure (p_b):	5000 psia
Effective horizontal permeability (k):	10 md
Pay zone thickness (h):	50 ft
Average reservoir pressure ($p_{\text{-bar}}$):	4000 psia
Oil formation volume factor (B_o):	1.2 rb/stb
Well drainage area (A):	320 acres
Wellbore radius (r_w):	0.328 ft
Fracture width (w):	0.2 in
Well depth (H):	8000 ft
Tubing inner diameter (d):	2.441 in
Oil gravity (API):	30 API
Oil viscosity (μ_o):	1.5 cp
Producing GLR (GLR):	440 scf/bbl
Gas specific gravity (γ_g):	0.7 air = 1
Flowing tubing head pressure (p_{hf}):	800 psia
Flowing tubing head temperature (t_{hf}):	150 °F
Flowing temperature at tubing shoe (t_{wf}):	180 °F
Water cut (WC):	10 %
Oil-gas interfacial tension (s):	30 dynes/cm
Specific gravity of water (γ_w):	1.05
Shape factor for drainage area (C_A):	31.6

SOLUTION

This problem can be solved using the spreadsheet program **Pseudosteady Production of Single-Fractured Well.xls**. Table 6–8 shows some calculated data. Figure 6–5 presents the calculated IPR and TPR curves which indicate an operating oil production rate of 1300 stb/day at a flowing bottom-hole pressure of 2520 psia.

Table 6–8 Data Given by the Spreadsheet Program **Pseudosteady Production of Single-Fractured Well.xls**

q (stb/d)	p _{wf} (psia)	
	IPR	TPR
235	3,772	1,994
469	3,531	2,171
704	3,275	2,293
939	3,000	2,394
1,173	2,702	2,484
1,408	2,372	2,568
1,643	2,000	2,648
1,878	1,562	2,727
2,112	1,000	2,805
2,347	0	2,883

6.4.2 Single-Fractured Gas Wells

For the pseudosteady-state production of a single-fractured gas well, Equation (4.10) can be used to construct the IPR curve. However, the total skin factor ($S+Dq_g$) should be replaced by the equivalent fracture skin factor S_f . That is,

$$q_g = \frac{kh(\bar{p}^2 - p_{wf}^2)}{1424\bar{\mu}\bar{z}T \left(\ln \frac{r_e}{r_w} - \frac{3}{4} + S_f \right)} \quad (6.27)$$

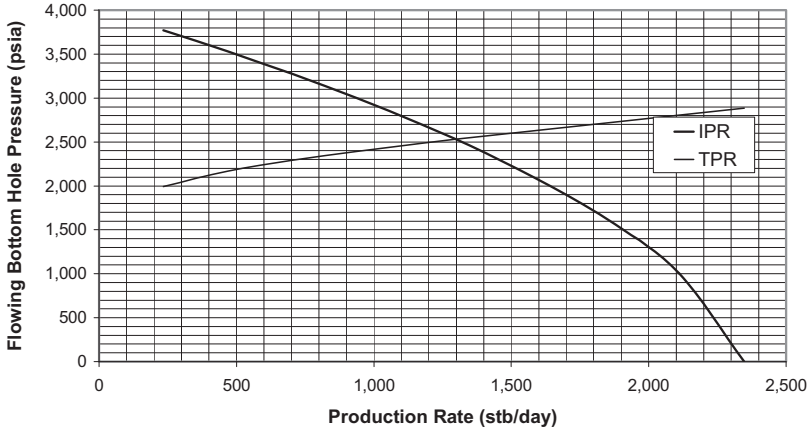


Figure 6-5 Curves given by the spreadsheet program *Pseudosteady Production of Single-Fractured Well.xls*.

Use Equation (5.54) for TPR analysis of dry-gas wells, and Equation (5.18) for TPR analysis of gas condensate wells and gas wells with accompanying water and/or solid production.

6-10 SAMPLE PROBLEM

From the data given below, assuming that the tubing string is set just above the pay zone, predict the pseudosteady-state gas production rate:

Pay zone thickness:	78 ft
Permeability:	0.17 md
Wellbore radius:	0.328 ft
Fracture half length:	600 ft
Fracture width:	0.3 in
Fracture permeability:	50000 md
Reservoir pressure:	4613 psia
Total measured depth:	7,000 ft
Average inclination angle:	5 deg
Tubing I.D.:	1.995 in

Gas specific gravity:	0.65	air=1
Gas viscosity:	0.022	cp
Gas z-factor:	0.958	
Oil production rate:	5	stb/day
Oil specific gravity:	0.85	H ₂ O=1
Water cut:	10	%
Water specific gravity:	1.05	H ₂ O=1
Solid production rate:	1	ft ³ /d
Solid specific gravity:	2.65	H ₂ O=1
Tubing head temperature:	100	°F
Bottom-hole temperature:	180	°F
Tubing head pressure:	1000	psia
Drainage area:	320	acres
Wall roughness:	0.01	in

SOLUTION

This problem can be solved using the spreadsheet program **Fractured Gas Well Production Forecast.xls**. Table 6–9 shows the calculated results which indicate an operating gas production rate of 8798 Mscf/day at a flowing bottom-hole pressure of 2705 psia.

6.5 Deliverability of Horizontal Wells

Predicting the deliverability of horizontal wells requires considering the hydraulics in the vertical, curved, and horizontal sections. While the hydraulics in the vertical and curved sections can be modeled using the mHB correction (for oil wells) and Guo's mist-flow model (for gas wells), the hydraulics in the horizontal section must be modeled based on reservoir-wellbore cross-flow.

Table 6–9 Data Given by the Spreadsheet Program **Fractured Gas Well Production Forecast.xls**

$S_f =$	-6.9220407
$A =$	3.1243196 in ²
$D =$	0.16625 ft
$T_{av} =$	600 °R
$\cos(\theta) =$	0.9961953
δ/D	0.0100251
$f_M =$	0.0303742
$a =$	2.045E-05
$b =$	1.498E-09
$c =$	11456002
$d =$	0.0171734
$e =$	0.0028505
$M =$	562.9414
$N =$	3.755E+11
Gas production rate, $q =$	8,798 Mscf/d
Bottom-hole pressure, $p_{wf} =$	2,705 psia

6.5.1 Oil Wells in Volumetric Reservoirs

For horizontal oil wells, use Equation (4.20) to construct the IPR curve. The mHB correlation described in Chapter 5 can be used to construct the TPR curve. The intersection of the two curves defines the operating point. Because Equation (4.20) incorporates the correction factor F_o (which depends on production rate itself), the following iterative procedure is recommended:

1. Perform NODAL analysis to predict oil production rate, assuming that $F_o = 1$.
2. Use the predicted operating pressure at heel to calculate F_o value.

3. Perform NODAL analysis to predict the oil production rate using the calculated F_o value.
4. Repeat steps 2 and 3 until the calculated oil production rates converge.

6-11 SAMPLE PROBLEM

A horizontal well is to be produced through a 4-in. screen. From the data given below, and assuming that the tubing string is set just above the screen, predict pseudosteady-state oil production rate:

Pay zone thickness (h):	48 ft
Effective horizontal permeability (k_h):	68 md
Effective vertical permeability (k_v):	17 md
Reservoir pressure (p_r):	4053 psia
Oil formation volume factor (B_o):	1.1 rb/stb
Well drainage area (A):	640 acres
Horizontal wellbore length (L):	2000 ft
Radius of curvature (ROC):	1000 ft
Total measured well depth (H):	8500 ft
Tubing inner diameter (d):	2.441 in
Oil gravity (API):	42 API
Oil viscosity (μ_o):	1.5 cp
Producing GLR (GLR):	550 scf/bbl
Gas specific gravity (γ_g):	0.7 air =1
Flowing tubing head pressure (p_{hf}):	500 psia
Flowing tubing head temperature (t_{hf}):	125 °F
Flowing temperature at tubing shoe (t_{wf}):	210 °F
Water cut (WC):	10 %
Oil-gas interfacial tension (σ):	30 dynes/cm
Specific gravity of water (γ_w):	1.07
Wellbore radius (r_w):	0.328 ft

SOLUTION

This problem can be solved using the spreadsheet programs **Pseudosteady-2Phase Horizontal Well Production Forecast.xls** and **Correction Factor Fo.xls**.

Assuming $F_o = 1.0$, the spreadsheet program **Pseudosteady-2Phase Horizontal Well Production Forecast.xls** gave IPR and TPR data shown in Table 6–10. Figure 6–6 presents the calculated IPR and TPR curves which indicate an operating oil production rate of 5600 stb/day at a flowing pressure at heel of 3200 psia.

1. Using the pressure at heel of 3200 psia as an input parameter value, the spreadsheet program **Correction Factor Fo.xls** gives a correction factor $F_o = 0.9048$.
2. Substituting $F_o = 0.9048$, the spreadsheet program **Pseudosteady-2Phase Horizontal Well Production Forecast.xls** gives an operating oil production rate of 5500 stb/day at a flowing pressure at heel of 3100 psia.
3. Utilizing this pressure at heel of 3100 psia as an input parameter value, the spreadsheet program **Correction Factor Fo.xls** gives a correction factor $F_o = 0.9003$.
4. Substituting $F_o = 0.9003$, the spreadsheet program **Pseudosteady-2Phase Horizontal Well Production Forecast.xls** gives an operating oil production rate of 5510 stb/day, which is only 0.2% higher than the previous value of 5500 stb/day. Thus, the procedure is completed.

6.5.2 Oil Wells in Water/Gas-Coning Reservoirs

The deliverability of horizontal oil wells in reservoirs with bottom water and/or gas caps is often limited by water and/or gas-coning. Several methods are available for predicting the critical oil production rate, including Efros (1963), Chaperon (1986), Giger-Karcher (1986, 1989), Joshi (1988), and Guo-Lee (1992). The Chaperon and Guo-Lee methods incorporate the effects of vertical permeability on the critical rates with the Chaperon method giving the most optimistic value.

Table 6–10 Data Given by the Spreadsheet Program **Pseudosteady-2Phase Horizontal Well Production Forecast.xls**

q (stb/d)	p _{wf} (psia)	
	IPR	TPR
1,573	3,822	1,658
3,146	3,578	2,165
4,719	3,318	2,765
6,293	3,040	3,465
7,866	2,737	4,264
9,439	2,404	5,161
11,012	2,027	6,154
12,585	1,582	7,244
14,158	1,013	8,430
15,732	0	9,713

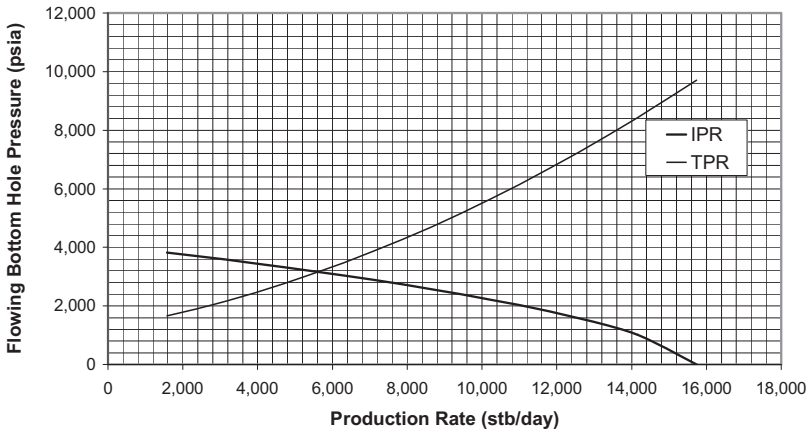


Figure 6–6 Curves given by the spreadsheet program **Pseudosteady-2Phase Horizontal Well Production Forecast.xls**.

The Chaperon method employs the following equation for predicting the critical oil production rate:

$$q_o = 4.888 \times 10^{-4} \frac{Lk_h h^2 \Delta\rho}{B_o \mu_o y_e} F \quad (6.28)$$

where

q_o = critical oil rate (STB/day)

L = horizontal wellbore length (ft)

k_h = horizontal permeability (md)

h = effective oil column thickness (ft)

$\Delta\rho$ = density difference (gm/cc)

B_o = oil formation volume factor (rb/STB)

μ_o = oil viscosity (cp)

y_e = half drainage length perpendicular to horizontal wellbore (ft)

and

$$F = 3.9624955 + 0.0616438\alpha^n - 0.000540\alpha^{n^2} \quad (6.29)$$

$$\alpha^n = \frac{y_e}{h} \sqrt{\frac{k_v}{k_h}} \quad (6.30)$$

6-12 SAMPLE PROBLEM

Calculate the anticipated critical oil production rate using following data:

Oil column thickness:	80 ft
Horizontal permeability:	70 md
Vertical permeability:	7 md
Oil viscosity:	0.42 cp
Oil density:	0.7 gm/cc
Oil formation volume factor:	1.1 rb/STB

Water or gas density:	1.05 gm/cc
Drainage area:	160 acres
Horizontal well placement from the no-flow boundary:	8 ft
Horizontal wellbore length:	1640 ft

SOLUTION

This sample problem is solved with the spreadsheet program **Chaperon Critical Oil Rate.xls**. The result is 718 stb/day.

All the methods mentioned in the beginning of this section assume that water/gas approaches the horizontal wellbore uniformly along the horizontal wellbore direction with a crest-shaped phase-interface. This is not true in reality partially due to the pressure variation in the wellbore. It is generally believed that water/gas reaches the horizontal wellbore at the heel of the horizontal well first due to the low-pressure at heel. Prediction of the water-free production rate requires a numerical model coupling the unevenly distributed reservoir inflow and wellbore hydraulics.

An effective means of delaying water production in horizontal wells is to install inflow control devices (ICD) along the production string in the horizontal section. The ICDs need to be sized and distributed following a careful design in order to achieve a uniform pressure distribution along the sandface. The following section provides equations that are necessary for developing a numerical simulator to perform design of production strings with ICD installations.

Reservoir Influx Model. It is generally believed that the reservoir influx is not uniformly distributed along the horizontal wellbore, even for a frictionless wellbore. This is due to the fact that the wellbore sections near the well toe and heel drain more oil from larger areas compared to sections of the same length near the mid-point of the horizontal wellbore. Theoretical studies have shown that the reservoir influx takes a U-shaped distribution with uniform distribution of pressure in the horizontal wellbore (Economides et al. 1996; Ozkan et al. 1999). Based on the result of Papatzacos' (1987) investigation, the author developed the following function for the specific productivity index of horizontal well:

$$J_{sp}(x) = J_{sp}^m \left[1 + 0.005e^{6.7122\left(\frac{x}{L/2}\right)} \right] \quad x \leq L/2 \quad (6.31)$$

where J_{sp}^m is the specific productivity index at the mid-point of the horizontal wellbore and x is the distance from the mid-point. One way of estimating the value of J_{sp}^m is to use Furuï's (2003) pseudo-linear flow model expressed as

$$J_{sp}^m = \frac{7.08 \times 10^{-3} k_H}{\mu_o B_o \left\{ I_{ani} \ln \left[\frac{h I_{ani}}{r_w (I_{ani} + 1)} \right] + \frac{\pi y_b}{h} - I_{ani} (1.224 - s) \right\}} \quad (6.32)$$

where

$$I_{ani} = \sqrt{\frac{k_H}{k_V}} \quad (6.33)$$

$$y_b = \sqrt{a^2 - (L/2)^2} \quad (6.34)$$

$$a = \left(\frac{L}{2} \right) \left\{ 0.5 + \left[0.25 + \left(\frac{2r_{eH}}{L} \right)^4 \right]^{0.5} \right\}^{0.5} \quad (6.35)$$

Another way of estimating the value of J_{sp}^m is to derive a relation from a pseudo 3-D model. According to Economides (1991), the average specific productivity index is expressed as

$$J_{sp}^J = \frac{7.08 \times 10^{-3} k_H h}{\mu_o B_o L \left\{ \ln \left[\frac{a + \sqrt{a^2 - (L/2)^2}}{(L/2)} \right] + \frac{I_{ani} h}{L} \ln \left[\frac{I_{ani} h}{r_w (I_{ani} - 1)} \right] + s \right\}} \quad (6.36)$$

Volume balance gives

$$2 \int_0^{L/2} J_{sp}(x) dx = J_{sp}^J L . \quad (6.37)$$

Substituting Equation (6.31) into Equation (6.37) gives

$$2 \int_0^{L/2} J_{sp}^m \left[1 + 0.005 e^{6.7122 \left(\frac{x}{L/2} \right)} \right] dx = J_{sp}^J L \quad (6.38)$$

which yields

$$J_{sp}^m L \left[1 + \frac{0.005}{6.7122} \left(e^{6.7122} - 1 \right) \right] = J_{sp}^J L \quad (6.39)$$

or

$$J_{sp}^m = 0.62 J_{sp}^J \quad (6.40)$$

ICD Model. Different types of ICDs are used in the industry, including orifice type, nozzle type, and helical channel type. The performance of the orifice type and nozzle type ICDs is affected by fluid density and port size. The pressure drop of a liquid across an orifice type or a nozzle type ICD can be estimated by

$$\Delta p = \frac{1.534 \times 10^{-8} \rho q^2}{C_D^2 d_p^4} \quad (6.41)$$

where

- ρ = fluid density, lbm/ft³
- Δp = pressure drop, psi
- q = flow rate, bbl/d
- d_p = port diameter, in
- C_D = discharge coefficient

The discharge coefficient C_D can be determined based on Reynolds number and choke/pipe diameter ratio from charts or correlations (Guo et al. 2007). The performance of helical channel type ICDs is affected by fluid density, viscosity, and channel design. Their performance curves normally obey the following model:

$$\Delta p = Aq^B \quad (6.42)$$

where the constants A and B are experimentally determined for each ICD design by manufacturers.

6-13 SAMPLE PROBLEM

The following data are given for a horizontal well. Calculate pressure and influx distributions in the annulus without ICD (production through screen) and with ICD installations. Assume 20 equal-size nozzles ($C_D = 1.0$) to be installed along the production string with even spacing.

Pay zone thickness:	131.2 ft
Drainage area:	160 acres
Horizontal permeability:	456 md
Vertical permeability:	114 md
Skin factor:	0
Oil density:	58 lbm/ft ³
Oil viscosity:	0.7 cp
Oil formation volume factor:	1.12 rb/stb
Reservoir pressure:	2,533 psi
Drain hole radius to sand face:	0.354 ft
Production string inner diameter:	5.5 in
Bottom-hole pressure at heel:	2,500 psi
Horizontal wellbore length:	2,438 ft
String wall roughness:	0.0024 in

SOLUTION

This sample problem was solved with a spreadsheet program that is not attached to the book and is available from the author upon request. The results are shown in Figures 6–7 and 6–8. ICD designed ICD sizes and locations are shown in Table 6–11. The total well production rates are predicted to be 10,962 stb/d and 10,699 stb/d for the wells without and with ICD, respectively.

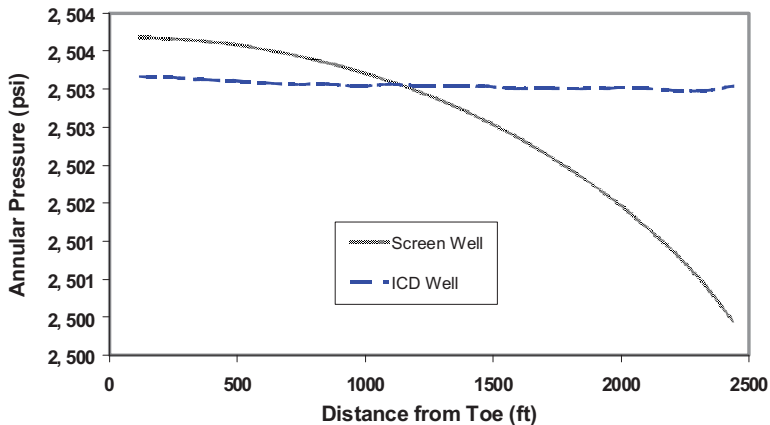


Figure 6–7 Calculated annular pressure distributions with and without ICD installations.

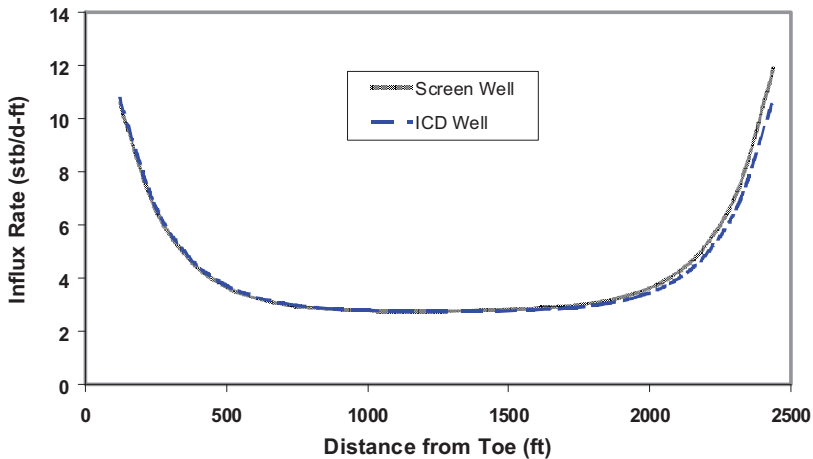


Figure 6–8 Calculated oil influx distributions with and without ICD installations.

Table 6–11 Designed ICD Locations and Sizes

Nozzle No.	Segment Center from Toe (ft)	Nozzle Diameter (in.)
1	60.95	4.00
2	182.85	3.00
3	304.75	2.50
4	426.65	1.50
5	548.55	1.20
6	670.45	1.00
7	792.35	0.85
8	914.25	0.78
9	1036.15	0.70
10	1158.05	0.66
11	1279.95	0.62
12	1401.85	0.59
13	1523.75	0.57
14	1645.65	0.55
15	1767.55	0.54
16	1889.45	0.54
17	2011.35	0.56
18	2133.25	0.61
19	2255.15	0.70
20	2377.05	0.84

6.5.3 Gas Wells in Volumetric Reservoirs

For horizontal gas wells, use Equation (4.21) to construct the IPR curve and use the mist-flow model of Guo et al. (described in Chapter 5) to construct the TPR curve. The intersection of the two curves defines the operating point. Because Equation (4.21) involves the correction factor F_g , which depends on production rate itself, the following procedure is recommended:

1. Perform NODAL analysis to predict the gas production rate, assuming $F_g = 1$.
2. Use the predicted pressure at heel to calculate the F_g value.
3. Perform NODAL analysis to predict gas production rate using the calculated F_g value.
4. Repeat steps 2 and 3 until the calculated gas production rates converge.

6-14 SAMPLE PROBLEM

For the data given below, assuming tubing string is set right above the pay zone, predict pseudosteady-state gas production rate:

Pay zone thickness (h):	20 ft
Horizontal permeability (k_h):	5 md
Vertical permeability (k_v):	1 md
Reservoir pressure (p_e):	3458 psia
Reservoir temperature (T):	200 °F
Gas specific gravity (γ_g):	0.71
Gas viscosity (μ_g):	0.02 cp
Drainage area (A):	320 acre
Wellbore radius (r_w):	0.328 ft
Horizontal wellbore length (L):	1000 ft
Total well depth (TD):	9000 ft

Kick-off-point (KOP):	6000 ft
Tubing diameter (d):	2.441 in
Tubing relative roughness (ϵ/d):	0.0006
Tubing head pressure (p_{hf}):	1500 psia
Tubing head temperature (T_{hf}):	150 °F

SOLUTION

This sample problem was solved with the spreadsheet programs **Horizontal Dry Gas Well Production Forecast.xls** and **Correction Factor Fg.xls**.

1. Assuming $F_g = 1.0$, the spreadsheet program **Horizontal Dry Gas Well Production Forecast.xls** gave the IPR and TPR data shown in Table 6–12. Figure 6–9 presents the calculated IPR and TPR curves which indicate an operating gas production rate of 13,700 Mscf/day at a flowing pressure at heel of 2,600 psia.
2. Using the pressure at heel of 2600 psia as an input parameter value, the spreadsheet program **Correction Factor Fg.xls** gives a correction factor $F_g = 0.9931$, which is very close to the assumed value of 1.0. Thus, no more computation is necessary.

6.6 Summary

This chapter demonstrated methods for predicting the productivities of oil and gas wells with simple trajectories: vertical wells, single-fractured vertical wells, and horizontal wells. The productivities of oil wells with water/gas-coning and gas wells with liquid loading were also discussed. The productivity of oil and gas wells with more complex trajectories will be discussed in Chapter 7.

Table 6–12 Data Given by the Spreadsheet Program **Horizontal Dry Gas Well Production Forecast.xls**

Flow Rate (Mscf/day)	Bottom-hole Pressure (psia)	
	IPR	TPR
0	3,458	1,792
3,231	3,281	1,847
6,462	3,093	2,005
9,693	2,893	2,241
12,924	2,679	2,533
16,155	2,445	2,863
19,386	2,187	3,224
22,617	1,894	3,608
25,848	1,546	4,014
29,080	1,094	4,441
32,310	19	4,888

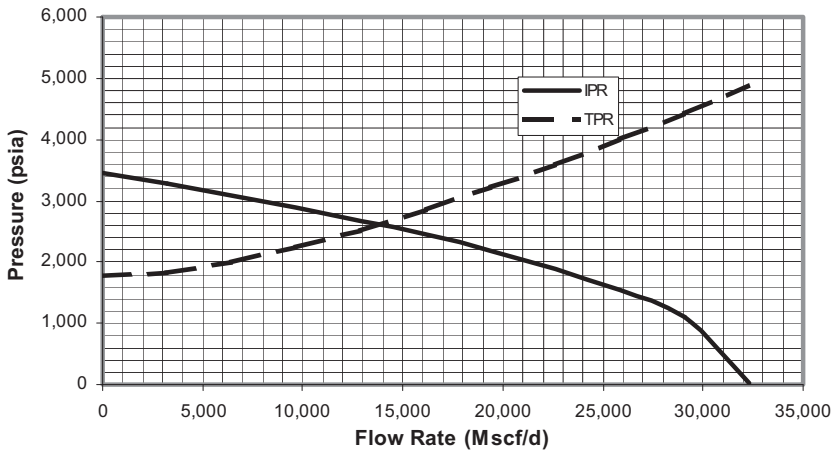


Figure 6–9 Curves given by the spreadsheet program **Horizontal Dry Gas Well Production Forecast.xls**.

6.7 References

Chaperon, I.: “Theoretical Study of Coning Toward Horizontal and Vertical Wells in Anisotropic Formations: Subcritical and Critical Rates,” paper SPE 15377, presented at the SPE Annual Technical Conference and Exhibition (5–8 October 1986), New Orleans, Louisiana.

Coleman, S.B., Clay H.B., McCurdy, D.G., and Norris III, L.H.: “A New Look at Predicting Gas Well Loading-Up,” *Journal of Petroleum Technology* (March 1991) *Trans. AIME*, 291: 329.

Craft, B.C. and Hawkins, M.F.: *Applied Petroleum Reservoir Engineering*, Prentice-Hall, Englewood Cliffs, New Jersey (1959).

Economides, M.J., Brand, C.W., and Frick, T.P.: “Well Configurations in Anisotropic Reservoirs,” *SPE Formation Evaluation* (December 1996): 257.

Economides, M.J., Deimbacher, F.X., Brand, C.W., and Heinemann, Z.E.: “Comprehensive Simulation of Horizontal Well Performance,” *SPEFE* (December 1991): 418.

Efros, D.A.: “Study of Multiphase Flows in Porous Media,” *Gas-toptexizdat*, Leningrad (1963).

Furui, K., Zhu, D., and Hill, A.D.: “A Rigorous Formation Damage Skin Factor and Reservoir Inflow Model for a Horizontal Well,” *SPEFE* (August 2003): 151.

Giger, F.M.: “Analytic 2-D Models for Water Cresting before Breakthrough for Horizontal Wells,” *SPE Reservoir Engineering* (1989): 409–416.

Karcher, B.J., Giger, F.M., and Combe, J.: “Some Practical Formulas to Predict Horizontal Well Behavior,” paper SPE 15430, presented at the SPE Annual Technical Conference and Exhibition (5–8 October 1986), New Orleans, Louisiana.

Guo, B. and Ghalambor, A., and Xu, C.: A Systematic Approach to Predicting Liquid Loading in Gas Well, *SPE Production & Operations J.* (February 2006).

Guo, B., Lyons, W.C. and Ghalambor, A.: *Petroleum Production Engineering—A Computer-Assisted Approach*, Elsevier, Amsterdam (2007).

- Horne, R.N.: *Modern Well Test Analysis: A Computer-Aided Approach*, Petroway Publishing, New York (1995).
- Hoyland, L.A., Papatzacos, P., and Skjaeveland, S.M.: "Critical Rate for Water Coning: Correlation and Analytical Solution," *SPE Reservoir Engineering* (November 1989): 495–502.
- Joshi, S.D.: "Augmentation of Well Productivity Using Slant and Horizontal Wells," *Journal of Petroleum Technology* (June 1988): 729–739.
- Lea, J.F. and Nickens, H.V.: "Solving Gas-Well Liquid-Loading Problems," *SPE Prod. & Facilities* (April 2004): 30.
- Lee, J.W., Rollins, J.B., and Spivey, J.P.: *Pressure Transient Testing*, Society of Petroleum Engineers, Richardson, Texas (2003).
- Meyer, H.L. and Gardner, A.O.: "Mechanics of Two Immiscible Fluids in Porous Media," *Journal of Applied Physics* (November 1954), Vol. 25, No. 11: 1400.
- Nosseir, M.A., Darwich, T.A., Sayyoub, M.H., and Sallaly, M.E.: "A New Approach for Accurate Prediction of Loading in Gas Wells Under Different Flowing Conditions," *SPE Prod. & Facilities* (Nov. 2000), Vol. 15, No. 4: 245.
- Ozkan, E., Sarica, C., and Haci, M.: "Influence of Pressure Drop Along the Wellbore on Horizontal-Well Productivity," *SPE Journal* (September 1999): 288.
- Papatzacos, P.: "Exact Solutions for Infinite-Conductivity Wells," *SPE Reservoir Engineering* (May 1987): 217.
- Pirson, S.J.: *Oil Reservoir Engineering*, Robert E. Krieger Publishing Company, Huntington, New York (1977).
- Schols, R.S.: "An Empirical Formula for the Critical Oil Production Rate," *Erdoel Erdgas, Z.* (January 1972), Vol. 88, No. 1: 6–11.
- Turner, R.G., Hubbard, M.G., and Dukler, A.E.: "Analysis and Prediction of Minimum Flow Rate for the Continuous Removal of Liquids from Gas Wells," *Journal of Petroleum Technology* (November 1969), *Trans. AIME*, 246: 1475.

6.8 Problems

- 6-1 From the data given below, assuming the tubing string is set just above the pay zone, predict production rate after 10 days:

Reservoir porosity (ϕ):	0.25
Effective horizontal permeability (k):	50 md
Pay zone thickness (h):	60 ft
Reservoir pressure (p_i):	5200 psia
Oil formation volume factor (B_o):	1.3 rb/stb
Total reservoir compressibility (c_i):	0.00001 psi ⁻¹
Wellbore radius (r_w):	0.328 ft
Skin factor (S):	5
Well depth (H):	9000 ft
Tubing inner diameter (d):	2.441 in
Oil gravity (API):	35 API
Oil viscosity (μ_o):	1.2 cp
Producing GLR (GLR):	500 scf/bbl
Gas specific gravity (γ_g):	0.7 air =1
Flowing tubing head pressure (p_{hf}):	500 psia
Flowing tubing head temperature (t_{hf}):	120 °F
Flowing temperature at tubing shoe (t_{wf}):	160 °F
Water cut (WC):	15 %
Oil-gas interfacial tension (σ):	35 dynes/cm
Specific gravity of water (γ_w):	1.04

- 6-2 From the data given below, assuming the tubing string is set just above the pay zone, predict the pseudosteady-state production rate:

Initial oil bubble-point pressure (p_b):	4300 psia
Effective horizontal permeability (k):	35 md
Pay zone thickness (h):	40 ft
Average reservoir pressure (p_{bar}):	2800 psia
Oil formation volume factor (B_o):	1.25 rb/stb
Well drainage area (A):	160 acres
Wellbore radius (r_w):	0.328 ft
Skin factor (S):	6
Well depth (H):	8200 ft
Tubing inner diameter (d):	2.441 in
Oil gravity (API):	40 API
Oil viscosity (μ_o):	1.45 cp
Producing GLR (GLR):	560 scf/bbl
Gas specific gravity (γ_g):	0.7 air = 1
Flowing tubing head pressure (p_{hf}):	600 psia
Flowing tubing head temperature (t_{hf}):	120 °F
Flowing temperature at tubing shoe (t_{wf}):	160 °F
Water cut (WC):	15 %
Oil-gas interfacial tension (σ):	40 dynes/cm
Specific gravity of water (γ_w):	1.06
Shape factor for drainage area (C_A):	31.6

- 6-3 From the data given below, assuming the tubing string is set just above the pay zone, predict the steady-state production rate:

Initial oil bubble-point pressure (p_b):	4200 psia
Effective horizontal permeability (k):	70 md
Pay zone thickness (h):	55 ft
Boundary reservoir pressure (p_e):	4200 psia
Oil formation volume factor (B_o):	1.3 rb/stb
Well drainage area (A):	320 acres
Wellbore radius (r_w):	0.328 ft
Skin factor (S):	3
Well depth (H):	7200 ft
Tubing inner diameter (d):	2.441 in
Oil gravity (API):	45 API
Oil viscosity (μ_o):	2.5 cp
Producing GLR (GLR):	700 scf/bbl
Gas specific gravity (γ_g):	0.75 air = 1
Flowing tubing head pressure (p_{hf}):	900 psia
Flowing tubing head temperature (t_{hf}):	130 °F
Flowing temperature at tubing shoe (t_{wf}):	180 °F
Water cut (WC):	20 %
Oil-gas interfacial tension (σ):	40 dynes/cm
Specific gravity of water (γ_w):	1.03

6-4 Calculate the anticipated critical oil production rate, using the following data:

Oil column thickness:	50 ft
Horizontal permeability:	60 md
Vertical permeability:	9 md
Oil viscosity:	0.45 cp
Oil density:	0.8 gm/cc
Oil formation volume factor:	1.2 rb/STB
Water or gas density:	1.06 gm/cc
Drainage area:	320 acres

6-5 From the data given below, assuming the tubing string is set just above the pay zone, predict the transient production rate after 10 days:

Reservoir permeability (k):	30 md
Pay zone thickness (h):	5 ft
Well skin factor (S):	10
Porosity (ϕ):	0.2
Wellbore radius (r_w):	0.328 ft
Gas specific gravity (γ_g):	0.65
Gas viscosity (μ_g):	0.01 cp
Tubing inside diameter (D):	3.5 in
Tubing relative roughness (ϵ/D):	0.0006
Measured depth at tubing shoe (L):	5000 ft
Inclination angle (θ):	0 Deg
Wellhead pressure (p_{hf}):	500 psia
Wellhead temperature (T_{hf}):	150 °F
Bottom hole temperature (T_{wf}):	200 °F
Initial reservoir pressure (p_i):	2000 psia

- 6-6 From the data given below, assuming the tubing string is set just above the pay zone, predict the pseudosteady gas production rate:

Pay zone thickness:	50 ft
Permeability:	0.5 md
Wellbore radius:	0.328 ft
Darcy skin factor:	5
Non-Darcy skin coefficient:	0.001 day/Mscf
Reservoir pressure:	4620 psia
Total measured depth:	7,100 ft
Average inclination angle:	0 deg
Tubing I.D.:	2.441 in
Gas specific gravity:	0.70 air=1
Gas viscosity:	0.02 cp
Gas z-factor:	0.96
Oil production rate:	4 stb/day
Oil specific gravity:	0.8 H ₂ O=1
Water cut:	12 %
Water specific gravity:	1.04 H ₂ O=1
Solid production rate:	0.5 ft ³ /d
Solid specific gravity:	2.65 H ₂ O=1
Tubing head temperature:	110 °F
Bottom-hole temperature:	190 °F
Tubing head pressure:	900 psia
Drainage area:	160 acres
Wall roughness:	0.005 in.

6-7 From the data given below, assuming a single-size tubing string is set just above the pay zone, use Guo's method to predict the minimum gas production rate that prevents liquid loading:

Gas specific gravity:	0.66	air = 1
Hole inclination:	0	Deg
Tubing shoe depth:	5600	ft
Wellhead pressure:	400	psi
Wellhead temperature:	90	°F
Producing zone temperature:	130	°F
Condensate gravity:	70	API
Condensate make:	2	bbl/MMscf
Water specific gravity:	1.05	water = 1
Water make:	40	bbl/MMscf
Solid specific gravity:	2.65	water = 1
Solid make:	1	ft ³ /MMscf
Conduit OD:	1.995	in
Conduit ID:	0	in
Conduit wall roughness:	0.00015	in
Liquid density:	64	lb/ft ³
Liquid-gas interfacial tension:	55	dyne/cm

- 6-8 From the data given below, assuming the tubing string is set just above the pay zone, predict the pseudosteady-state production rate:

Fracture half length (x_f):	800 ft
Fracture permeability (k_f):	60000 md
Oil bubble-point pressure (p_b):	5200 psia
Effective horizontal permeability (k):	10 md
Pay zone thickness (h):	50 ft
Average reservoir pressure ($p_{\text{-bar}}$):	4500 psia
Oil formation volume factor (B_o):	1.25 rb/stb
Well drainage area (A):	160 acres
Wellbore radius (r_w):	0.328 ft
Fracture width (w):	0.25 in
Well depth (H):	8200 ft
Tubing inner diameter (d):	2.441 in
Oil gravity (API):	35 API
Oil viscosity (μ_o):	2.2 cp
Producing GLR (GLR):	600 scf/bbl
Gas specific gravity (γ_g):	0.75 air =1
Flowing tubing head pressure (p_{hf}):	850 psia
Flowing tubing head temperature (t_{hf}):	140 °F
Flowing temperature at tubing shoe (t_{wf}):	170 °F
Water cut (WC):	15 %
Oil-gas interfacial tension (σ):	35 dynes/cm
Specific gravity of water (γ_w):	1.04
Shape factor for drainage area (C_A):	31.6

6-9 From the data given below, assuming the tubing string is set just above the pay zone, predict the pseudosteady-state gas production rate:

Pay zone thickness:	70 ft
Permeability:	0.22 md
Wellbore radius:	0.328 ft
Fracture half length:	800 ft
Fracture width:	0.25 in
Fracture permeability:	80000 md
Reservoir pressure:	4655 psia
Total measured depth:	7,200 ft
Average inclination angle:	0 deg
Tubing I.D.:	2.441 in
Gas specific gravity:	0.75 air=1
Gas viscosity:	0.025 cp
Gas z-factor:	0.97
Oil production rate:	3 stb/day
Oil specific gravity:	0.75 H ₂ O=1
Water cut:	15 %
Water specific gravity:	1.06 H ₂ O=1
Solid production rate:	1 ft ³ /d
Solid specific gravity:	2.65 H ₂ O=1
Tubing head temperature:	120 °F
Bottom-hole temperature:	180 °F
Tubing head pressure:	900 psia
Drainage area:	160 acres
Wall roughness:	0.001 in

- 6-10 A horizontal well is to be produced through a 4-in. screen. For the data given below, assuming the tubing string is set just above the screen, predict the pseudosteady-state oil production rate:

Pay zone thickness (h):	460	ft
Effective horizontal permeability (k_h):	80	md
Effective vertical permeability (k_v):	20	md
Reservoir pressure (p_r):	4080	psia
Oil formation volume factor (B_o):	1.15	rb/stb
Well drainage area (A):	320	acres
Horizontal wellbore length (L):	1800	ft
Radius of curvature (ROC):	1200	ft
Total measured well depth (H):	8700	ft
Tubing inner diameter (d):	2.441	in
Oil gravity (API):	46	API
Oil viscosity (μ_o):	0.8	cp
Producing GLR (GLR):	550	scf/bbl
Gas specific gravity (γ_g):	0.75	air =1
Flowing tubing head pressure (p_{hf}):	400	psia
Flowing tubing head temperature (t_{hf}):	120	°F
Flowing temperature at tubing shoe (t_{wf}):	200	°F
Water cut (WC):	15	%
Oil-gas interfacial tension (σ):	35	dynes/cm
Specific gravity of water (γ_w):	1.05	
Wellbore radius (r_w):	0.328	ft

- 6-11 Calculate the anticipated critical oil production rate, using the following data:

Oil column thickness:	60 ft
Horizontal permeability:	75 md
Vertical permeability:	15 md
Oil viscosity:	0.40 cp
Oil density:	0.65 gm/cc
Oil formation volume factor:	1.2 rb/STB
Water or gas density:	1.065 gm/cc
Drainage area:	320 acres
Horizontal well placement from the no-flow boundary:	10 ft
Horizontal wellbore length:	1500 ft

- 6-12 For the data given below, assuming the tubing string is set right above the pay zone, predict the pseudosteady-state gas production rate:

Pay zone thickness (h):	40 ft
Horizontal permeability (k_h):	10 md
Vertical permeability (k_v):	3 md
Reservoir pressure (p_e):	34708 psia
Reservoir temperature (T):	210 °F
Gas specific gravity (γ_g):	0.76
Gas viscosity (μ_g):	0.015 cp
Drainage area (A):	320 acre
Wellbore radius (r_w):	0.328 ft
Horizontal wellbore length (L):	1200 ft
Total well depth (TD):	9200 ft
Kick-off-point (KOP):	6500 ft

Tubing diameter (d):	2.441 in
Tubing relative roughness (ϵ/d):	0.001
Tubing head pressure (p_{hf}):	1200 psia
Tubing head temperature (T_{hf}):	120 °F

Productivity of Wells with Complex Trajectories

7.1 Introduction

More and more wells are completed using new technologies that enhance well production. These include multi-fractured horizontal wells, multi-lateral wells, and intelligent wells. This chapter focuses on the prediction of fluid production rates from multi-fractured horizontal wells and multi-lateral wells. The productivities of intelligent wells will be addressed in Chapter 8. Sample problems are solved with computer spreadsheet programs.

7.2 Multi-Fractured Horizontal Wells

Some horizontal wells are purposely drilled in parallel to the direction of the minimum horizontal stress in the formation. This specific wellbore orientation allows multiple transverse fractures to be hydraulically created for enhancing productivity. Linear flow may exist initially before fractures begin to influence each other. Radial flow may prevail later if the drainage area is sufficiently large compared to the fractured region of the reservoir.

Raghavan and Joshi (1993) presented a mathematical model that can predict the productivities of horizontal wells with multiple transverse fractures. The model uses the effective wellbore radius (in radial flow) to simulate fluid flow toward the fractured well. Flow within the fracture itself was not considered.

Li et al. (1996) presented an analytical model for predicting productivities of horizontal wells with multiple transverse fractures. The model incorporates:

- Linear flow from the fractured reservoir region to the fractures
- Linear flow within the fractures
- Radial flow within the fractures to the horizontal wellbore
- Flow from the fractured region directly to the horizontal wellbore

Most fractured horizontal wells are drilled in low-permeability reservoirs in which fluid flow from the unfractured regions directly to the horizontal wellbore is often negligible. As demonstrated by Guo and Yu (2008), predictions of the long-term productivity of multi-fractured horizontal wells must consider the following sequence:

1. Reservoir radial flow within the drainage boundary to the fractured region of reservoir
2. Reservoir linear flow between fractures in the reservoir to the fracture faces
3. Fracture linear flow in the fracture to the near-wellbore region
4. Wellbore radial flow in the fracture to the wellbore, where a “choking” effect occurs

Figure 7–1 shows two regions of the reservoir. The inner region is the fractured region, and the outer region is the non-fractured region. Figure 7–2 illustrates flow in the fracture.

7.2.1 Oil Wells

Consider a reservoir characterized by pseudosteady-state radial flow in the outer region (Figure 7–1). The total oil flow rate can then be described by:

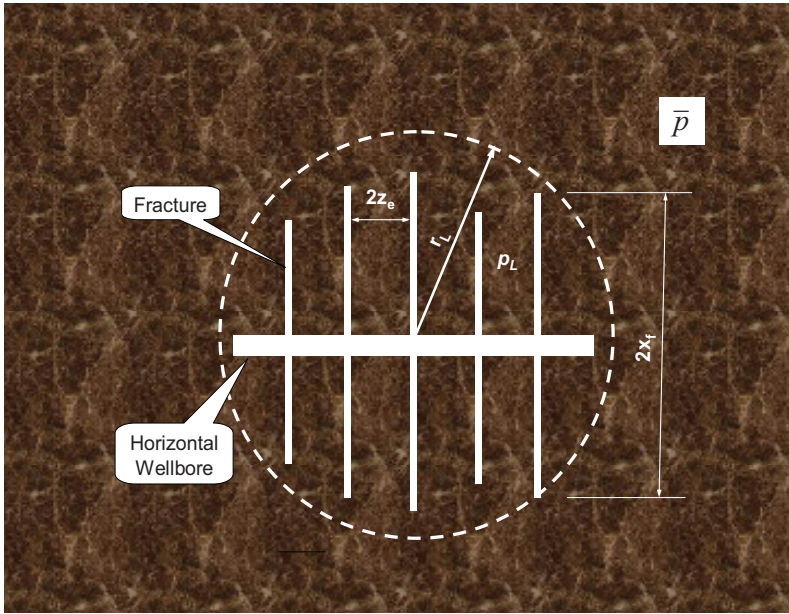


Figure 7-1 A reservoir section drained by a multi-fractured horizontal wellbore.

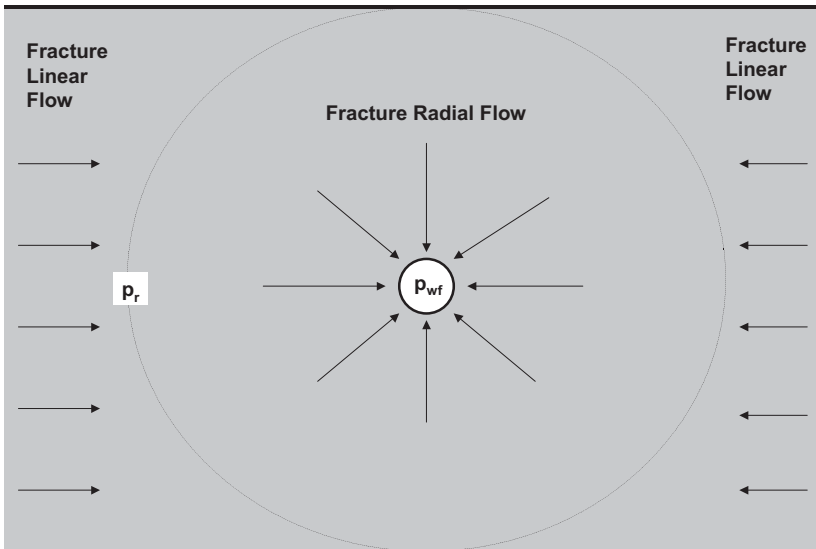


Figure 7-2 Fluid flow in a fracture to a horizontal wellbore.

$$q = \frac{7.08 \times 10^{-3} k_H h (\bar{p} - p_L)}{B_o \mu_o \left(\frac{1}{2} \ln \frac{4A}{\gamma C_A r_L^2} \right)} \quad (7.1)$$

where p_L is defined as the pressure at the outer boundary of the inner region, and r_L is the equivalent radius of the inner region that can be estimated by

$$r_L = \sqrt{\frac{4n\bar{z}_e\bar{x}_f}{\pi}} \quad (7.2)$$

where \bar{z}_e and \bar{x}_f are the average half-distances between fractures and the average fracture half-length, respectively.

If the multi-fractured well is used to drain an entire reservoir characterized by physical no-flow boundaries, the drainage area shape factor C_A can be estimated based on reservoir shape and the location of the reservoir's inner region. If the multi-fractured well is employed to drain a portion of a reservoir, then the C_A should be estimated based on the shape of the drainage area, with the location of the inner region centered in the drainage area. The aspect ratio (length to width) of the drainage area may be taken as

$$R_A = \frac{n\bar{z}_e}{\bar{x}_f}$$

and the shape factor may be estimated as $C_A = 39.51 - 8.5214R_A$.

The reservoir-fracture cross-flow model of Guo and Schechter (1997) links reservoir linear flow and fracture linear flow. For uniformly distributed fractures, according to this model, the deliverability of n fractures can be expressed as

$$q = \sum_{i=1}^n \frac{4.5 \times 10^{-3} h}{B_o \mu \sqrt{c_i} \left[\frac{(z_{ei} - z_{si})}{k_H} + \frac{z_{si}}{k_{si}} \right]} \left(1 - e^{-\sqrt{c_i} x_{fi}} \right) (p_L - p_r) \quad (7.3)$$

where

$$c_i = \frac{24}{k_{fi} w_i \left[\frac{(z_{ei} - z_{si})}{k_H} + \frac{z_{si}}{k_{si}} \right]} \quad (7.4)$$

z_{ei} is half the distance between the i^{th} and $(i+1)^{\text{th}}$ fractures, z_{si} is the depth of the altered zone near the surface of fracture i , k_{si} is the permeability of the altered zone near the surface of fracture i , and p_r represents the pressure in the fracture before the onset of flow convergence to wellbore (Figure 7-2).

The linear-radial flow model of Furui et al. (2003) can be used to couple the fracture linear flow and the fracture radial flow. According to this model, well deliverability through n uniformly distributed fractures can be expressed as

$$q = \sum_{i=1}^n \frac{5.9 \times 10^{-4} k_{fwi} w_{wi} (p_r - p_{wf})}{\mu_o B_o \left\{ \ln \left[\frac{h}{2r_{wi}} \right] + \pi - (1.224 - s_i - Dq) \right\}} \quad (7.5)$$

where p_{wf} is the flowing bottom-hole pressure. The k_{fwi} is fracture permeability in the near-wellbore region, and w_{wi} is the width of the i^{th} fracture in the near-wellbore region. These two parameters, plus the non-Darcy flow coefficient D , can be used to simulate choked fractures.

Combining Equations (7.1) through (7.5) gives the reservoir deliverability equation:

$$q = \frac{1}{\left(\frac{1}{J_R} + \frac{1}{J_L} + \frac{1}{J_r} \right)} (\bar{p} - p_{wf}) \quad (7.6)$$

where

$$J_R = \frac{7.08 \times 10^{-3} k_H h}{B_o \mu_o \left(\frac{1}{2} \ln \frac{4A}{\gamma C_A r_L^2} \right)} \quad (7.7)$$

$$J_L = \sum_{i=1}^n \frac{4.5 \times 10^{-3} h}{B_o \mu \sqrt{c_i} \left[\frac{(z_{ei} - z_{si})}{k_H} + \frac{z_{si}}{k_{si}} \right]} \left(1 - e^{-\sqrt{c_i} x_{fi}} \right) \quad (7.8)$$

$$J_r = \sum_{i=1}^n \frac{5.9 \times 10^{-4} k_{fwi} W_{wi}}{\mu_o B_o \left\{ \ln \left[\frac{h}{2r_{wi}} \right] + \pi - (1.224 - s_i - Dq) \right\}} \quad (7.9)$$

The tubing performance relationship of multi-fractured wells can be modeled using different correlations, depending on the fluid type. The Hagedorn-Brown correlation will be used in the following sample calculations.

7-1 SAMPLE PROBLEM

From the data given below, assuming no formation damage near the fractures, and that the tubing string is set just above the pay zone, predict the pseudosteady-state production rate:

Fracture spacing ($2z_c$):	1000 ft
Fracture half-length (x_f):	1000 ft
Fracture permeability (k_f):	50000 md
Oil bubble-point pressure (p_b):	5000 psia
Effective horizontal permeability (k):	10 md
Pay zone thickness (h):	60 ft
Average reservoir pressure ($p_{\text{-bar}}$):	4000 psia
Oil formation volume factor (B_o):	1.2 rb/stb

Well drainage area (A):	320 acres
Well radius (r_w):	0.328 ft
Fracture width (w):	0.3 in
Well vertical depth (H):	8000 ft
Tubing inner diameter (d):	4 in
Oil gravity (API):	40 API
Oil viscosity (μ_o):	1.5 cp
Producing GLR (GLR):	500 scf/bbl
Gas specific gravity (γ_g):	0.7 air =1
Flowing tubing head pressure (p_{hf}):	800 psia
Flowing tubing head temperature (t_{hf}):	150 °F
Flowing temperature at tubing shoe (t_{wf}):	180 °F
Water cut (WC):	10 %
Near-wellbore fracture width (w_w):	0.2 in
Total skin factor (S):	0
Number of fractures (n):	4
Near-wellbore fracture permeability (k_{fw}):	50000 md

SOLUTION

This problem can be solved using the spreadsheet program **Pseudosteady Production of Multi-Fractured Well.xls**. Figure 7–3 indicates that the expected liquid production rate is 1700 stb/day at a flowing bottom-hole pressure of 1900 psia.

It can be shown that the productivity of multi-fractured wells does not increase in proportion to the number of fractures. This is left to the reader to determine as an exercise using the spreadsheet.

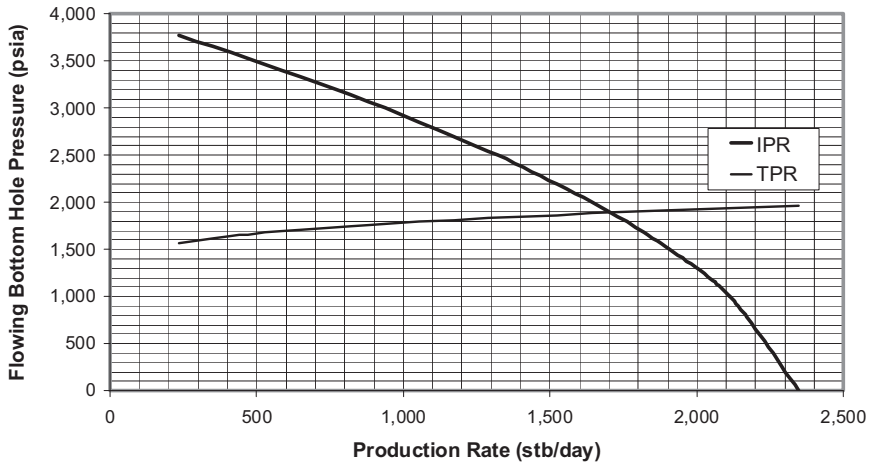


Figure 7–3 Curves given by spreadsheet program *Pseudosteady Production of Multi-Fractured Well.xls*.

7.2.2 Gas Wells

The mathematical model for multi-fractured horizontal gas wells is similar to that for oil wells. The pseudosteady-state radial flow in the outer region of the reservoir (Figure 7–1) can be described by

$$q = \frac{k_H h (\bar{p}^2 - p_L^2)}{1424 \bar{z} \bar{\mu}_g T \left(\frac{1}{2} \ln \frac{4A}{\gamma C_A r_L^2} \right)} \tag{7.10}$$

When applied to gas reservoirs, the reservoir-fracture cross-flow model of Guo and Schechter (1997) gives

$$q = \sum_{i=1}^n \frac{4.475 \times 10^{-4} h}{\bar{\mu}_g \bar{z} T \sqrt{c_i} \left[\frac{(z_{ei} - z_{si})}{k_H} + \frac{z_{si}}{k_{si}} \right]} \left(1 - e^{-\sqrt{c_i} x_{fi}} \right) (p_L^2 - p_r^2) \tag{7.11}$$

When the linear-radial flow model of Furui et al. (2003) is used, the well deliverability through n uniformly distributed fractures can be expressed as

$$q = \sum_{i=1}^n \frac{5.85 \times 10^{-5} k_{fwi} w_{wi} (p_r^2 - p_{wf}^2)}{\bar{z} \bar{\mu}_g T \left\{ \ln \left[\frac{h}{2r_{wi}} \right] + \pi - (1.224 - s_i - Dq) \right\}} \quad (7.12)$$

Combining Equations (7.10) through (7.12) yields a reservoir deliverability equation, expressed as

$$q = \frac{1}{\left(\frac{1}{J_R} + \frac{1}{J_L} + \frac{1}{J_r} \right)} (\bar{p}^2 - p_{wf}^2) \quad (7.13)$$

where

$$J_R = \frac{k_H h}{1424 \bar{z} \bar{\mu}_g T \left(\frac{1}{2} \ln \frac{4A}{\gamma C_A r_L^2} \right)} \quad (7.14)$$

$$J_L = \sum_{i=1}^n \frac{4.475 \times 10^{-4} h}{\bar{\mu}_g \bar{z} T \sqrt{c_i} \left[\frac{(z_{ei} - z_{si})}{k_H} + \frac{z_{si}}{k_{si}} \right]} \left(1 - e^{-\sqrt{c_i} x_{fi}} \right) \quad (7.15)$$

$$J_r = \sum_{i=1}^n \frac{5.85 \times 10^{-5} k_{fwi} w_{wi}}{\bar{z} \bar{\mu}_g T \left\{ \ln \left[\frac{h}{2r_{wi}} \right] + \pi - (1.224 - s_i - Dq) \right\}} \quad (7.16)$$

The tubing performance relationship of multi-fractured wells can be modeled using different correlations appropriate to the fluid type. Guo-Ghalambor's four-phase flow model may be used.

7.3 Multilateral Wells

A multilateral well is defined, in general, as a well with multiple branches in the lower bore hole targeting oil and gas reserves in the same or in different strata. These branches are called “laterals.” The primary, or main wellbore, from which the laterals are drilled out can be vertical or horizontal. Lateral bores extending from vertical wellbores are usually used to reach different pay zones, while the laterals drilled out from horizontal wellbores are usually intended to reach different areas of the same pay zone. In this book, multilateral wells with laterals drilled from vertical main wellbores are called “root wells” (Figure 7–4). Multilateral wells with the laterals drilled out from horizontal main wellbores are called “fishbone wells” (Figure 7–5). The prediction of fishbone well productivity is relatively simple because all laterals (rib holes) share approximately the same pressure in the main wellbore (backbone hole). Prediction of root well productivity is more complicated because the pressures in the laterals can be significantly different and wellbore hydraulics plays an important role.

7.3.1 Fishbone Wells

The initial flow regime in a fishbone well may be pseudolinear before the rib holes begin to interfere with each other. Radial flow may prevail later if the drainage area is large in proportion to the drilled region of the reservoir.

Raghavan and Joshi (1993) presented a mathematical model that can be used to predict the productivities of root wells. The model uses effective wellbore radius (horizontal radial flow) to simulate fluid flow to the horizontal drain holes. Retnanto and Economides (1996) published a simple formulation of multilateral well productivity for pseudosteady-state flow. They derived their formulation by combining a one-dimensional linear-flow model with a two-dimensional radial flow model to cover the whole drainage area. Larsen (1996) proposed a mathematical model similar to that of Raghavan and Joshi (1993) in the sense that horizontal drain holes are simulated by vertical wellbores located at the midpoints of the well elements.

A pseudolinear-radial-combined model is described in this section. The model assumes two regions within the reservoir—an inner drilled region and an outer non-drilled region. The model assumes the inner region to be dominated by pseudosteady-state pseudolinear flow between the rib holes, and the outer region to be dominated by pseudosteady-state radial flow.

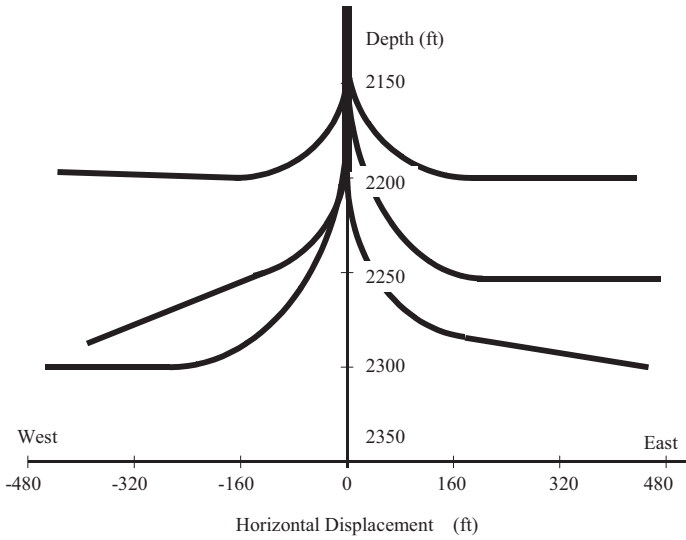


Figure 7-4 Schematic of a typical root well.

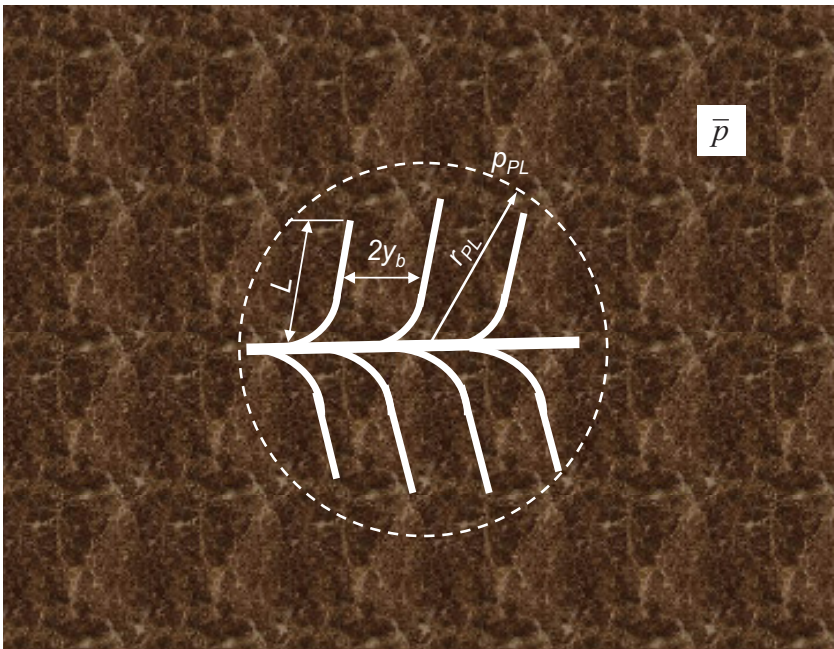


Figure 7-5 Schematic of a reservoir section drained by a fishbone well.

Following Furui et al. (2003), for uniformly distributed rib holes in the inner region, the deliverability of n rib holes is expressed as

$$q = \sum_{i=1}^n \frac{7.08 \times 10^{-3} k_H L_i (p_{PL} - p_{wf})}{\mu_o B_o \left\{ I_{ani} \ln \left[\frac{h I_{ani}}{r_{wi} (I_{ani} + 1)} \right] + \frac{\pi y_{bi}}{h} - I_{ani} (1.224 - s_i) \right\}} \quad (7.17)$$

for **oil reservoirs**, where L_i , r_{wi} , y_{bi} and s_i are length, radius, drainage distance, and skin factor of rib hole i , respectively. For **gas reservoirs**:

$$q = \sum_{i=1}^n \frac{k_H L_i (p_{PL}^2 - p_w^2)}{1424 \bar{\mu}_g \bar{z} T \left\{ I_{ani} \ln \left[\frac{h I_{ani}}{r_{wi} (I_{ani} + 1)} \right] + \frac{\pi y_{bi}}{h} - I_{ani} (1.224 - (s_i + Dq)) \right\}} \quad (8)$$

The permeability anisotropy I_{ani} is defined as

$$\sqrt{\frac{k_H}{k_V}}$$

The p_{PL} is defined as the average pressure at the edge of the inner region. The radial flow in the outer region can be described by

$$q = \frac{k_H h (\bar{p} - p_{PL})}{141.2 B_o \mu_o \left(\frac{1}{2} \ln \frac{4A}{\gamma C_A r_{PL}^2} \right)} \quad (7.19)$$

for **oil reservoirs**, and

$$q = \frac{k_H h (\bar{p}^2 - p_{PL}^2)}{1424 \bar{\mu}_g \bar{z} T \left(\frac{1}{2} \ln \frac{4A}{\gamma C_A r_{PL}^2} \right)} \quad (7.20)$$

for **gas reservoirs**. Solving these equations for production rates gives

$$q = \frac{1}{\left(\frac{1}{J_{PL}} + \frac{1}{J_R}\right)} (\bar{p} - p_{wf}) \quad (7.21)$$

for **oil reservoirs**, and

$$q = \frac{1}{\left(\frac{1}{J_{PL}} + \frac{1}{J_R}\right)} (\bar{p}^2 - p_{wf}^2) \quad (7.22)$$

for **gas reservoirs**, where

$$J_{PL} = \sum_{i=1}^n \frac{7.08 \times 10^{-3} k_H L_i}{\mu_o B_o \left\{ I_{ani} \ln \left[\frac{h I_{ani}}{r_{wi} (I_{ani} + 1)} \right] + \frac{\pi y_{b_i}}{h} - I_{ani} (1.224 - s_i) \right\}} \quad (7.23)$$

for **oil reservoirs**, and

$$J_{PL} = \sum_{i=1}^n \frac{k_H L_i}{1424 \bar{\mu}_g \bar{z} T \left\{ I_{ani} \ln \left[\frac{h I_{ani}}{r_{wi} (I_{ani} + 1)} \right] + \frac{\pi y_{b_i}}{h} - I_{ani} (1.224 - (s_i + Dq)) \right\}}$$

for **gas reservoirs**, and

$$J_R = \frac{k_H h}{141.2 B_o \mu_o \left(\frac{1}{2} \ln \frac{4A}{\gamma C_A r_{PL}^2} \right)} \quad (7.25)$$

for **oil reservoirs**, and

$$J_R = \frac{k_H h}{1424 \bar{\mu}_g \bar{z} T \left(\frac{1}{2} \ln \frac{4A}{\gamma C_A r_{PL}^2} \right)} \quad (7.26)$$

for **gas reservoirs**. The equivalent radius of the inner region may be estimated by

$$r_{PL} = \sqrt{\frac{2(n+1)\bar{y}_b\bar{L}}{\pi}}$$

where \bar{y}_b and \bar{L} are the average rib hole drainage distance and rib hole length, respectively. If the fishbone well is used to drain an entire reservoir with physical no-flow boundaries, the drainage area shape factor C_A can be estimated based on the reservoir shape and the location of the inner region in the reservoir. If the fishbone well is employed to drain only a portion of a reservoir, the C_A should be estimated based on the shape of the drainage area, with the location of the inner region at the center of the drainage area. The aspect ratio (length to width) of the drainage area may be taken as

$$R_A = \frac{(n+1)\bar{y}_b}{2\bar{L}}$$

The shape factor may be estimated by $C_A = 39.51 - 8.5214R_A$. Because all the above equations are deterministic, they can be used for predicting actual well IPR.

The tubing performance relationship of fishbone wells can be modeled using different correlations that depend on the fluid type. The Hagedorn-Brown correlation is used in the following examples.

7-2 SAMPLE PROBLEM

For the data given below, assuming the tubing string is set just above the pay zone, predict the pseudosteady-state liquid production rate:

Average rib hole spacing ($2y_b$):	1000 ft
Average rib hole length (L):	1000 ft
Average rib hole skin factor (s):	5
Oil bubble-point pressure (p_b):	5000 psia
Effective horizontal permeability (k_H):	10 md
Pay zone thickness (h):	50 ft
Average reservoir pressure (p_{bar}):	4000 psia
Oil formation volume factor (B_o):	1.2 rb/stb
Well drainage area (A):	320 acres
Average rib hole radius (r_w):	0.328 ft
Vertical permeability (k_V):	2 md
Well vertical depth (H):	8000 ft
Tubing inner diameter (d):	4 in
Oil gravity (API):	30 API
Oil viscosity (μ_o):	1.5 cp
Producing GLR (GLR):	500 scf/bbl
Gas specific gravity (γ_g):	0.7 air = 1
Flowing tubing head pressure (p_{hf}):	800 psia
Flowing tubing head temperature (t_{hf}):	150 °F
Flowing temperature at tubing shoe (t_{wf}):	180 °F
Water cut (WC):	10 %
Oil-gas interfacial tension (σ):	30 dynes/cm
Specific gravity of water (γ_w):	1.05
Number of rib holes (n):	7
Drainage area shape factor (C_A) based on aspect ratio:	5.38

SOLUTION

This problem can be solved using the spreadsheet program **Pseudosteady Production of Fishbone Oil Well.xls**. Figure 7–6 indicates that the expected liquid production rate is 1540 stb/day at a flowing bottom-hole pressure of 1905 psia.

Using this spreadsheet, it can be shown that the productivity of fishbone wells does not increase in proportion to the number of rib holes. The solution to the problem is left to the reader as an exercise in using the spreadsheet.

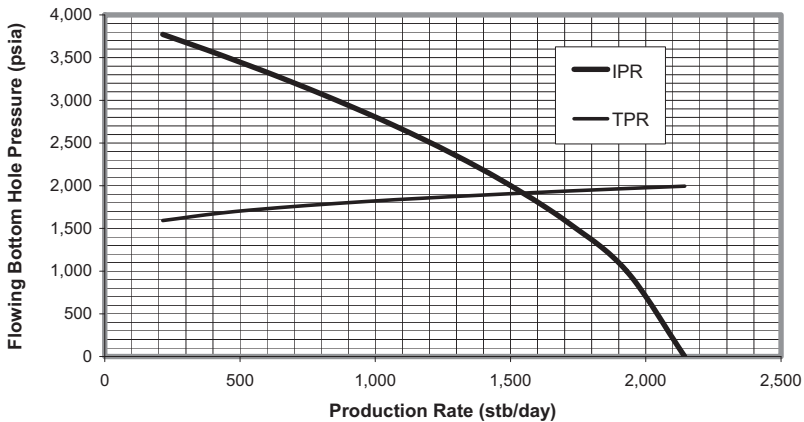


Figure 7–6 Curves given by the spreadsheet program *Pseudosteady Production of Fishbone Oil Well.xls*.

7-3 SAMPLE PROBLEM

For the data given below, assuming tubing string is set just above the pay zone, predict the pseudosteady-state gas production rate:

Pay zone thickness:	30 ft
Horizontal permeability:	1 md
Wellbore radius:	0.328 ft
Average Darcy skin factor:	5
Non-Darcy skin coefficient:	0.001 day/Mscf

Reservoir pressure:	4613	psia
Total measured depth:	7,000	ft
Average inclination angle:	0	deg
Tubing I.D.:	3.5	in
Gas specific gravity:	0.65	air=1
Gas viscosity:	0.022	cp
Gas z-factor:	0.958	
Oil production rate:	1	stb/day
Oil specific gravity:	0.85	H ₂ O=1
Water cut:	10	%
Water specific gravity:	1.05	H ₂ O=1
Solid production rate:	1	ft ³ /d
Solid specific gravity:	2.65	H ₂ O=1
Tubing head temperature:	100	°F
Bottom-hole temperature:	180	°F
Tubing head pressure:	2000	psia
Drainage area:	640	acres
Average wall roughness:	0.01	in
Number of rib holes:	4	
Average rib hole length:	500	ft
Average rib hole spacing (2y _b):	1000	ft
Vertical permeability:	0.25	md

SOLUTION

This problem is solved using the spreadsheet program **Pseudosteady Production of Fishbone Gas Well.xls**. Table 7-1 indicates that the expected liquid production rate is 12,092 Mscf/d at a flowing bottom-hole pressure of 2427 psia.

Table 7-1 Results Given by Spreadsheet Program **Pseudosteady Production of Fishbone Gas Well.xls**

$f_M =$	2.58E-02	$I_{ana} =$	2
$a =$	2.04E-05	$r_{PL} =$	892 ft
$b =$	2.45E-10	$J_{PL} =$	0.00115 Mscf/d-psi ²
$c =$	5.12E+06	$J_R =$	0.00250 Mscf/d-psi ²
$d =$	1.25E-03	$J =$	0.00079 Mscf/d-psi ²
$e =$	1.37E-03		
$M =$	8.82E+00		
$N =$	3.60E+10		
	Gas production rate, $q =$	12,092	Mscf/d
	Bottom-hole pressure, $p_{wf} =$	2,427	psia

7.3.2 Root Wells

The lower section of a root well is an integration of several horizontal wells. However, because of pressure drops in the wellbore sections, the productivity of a root well is not simply the sum of the productivities of the individual laterals, unless the inflow performance relationships of all the laterals are properly integrated with an understanding of the wellbore hydraulics.

Figure 7-7 shows a generalized root well structure. The root well can be viewed as a few well branches linked in series, each having three sections: vertical, curved, and horizontal sections. The symbols H , R , and L stand for the vertical length, the radius-of-curvature, and the horizontal length of the vertical, curved, and horizontal sections, respectively.

Figure 7-8 illustrates the parameters used to characterize a root well. The notations K , h , and \bar{p} represent the respective permeability, thickness, and the average pressure in the reservoir area drained by a lateral branch. The pressures at heel and kick-out point are denoted by P_{wf} and P_{kf} respectively. The symbols P_{hf} and q represent wellhead pressure and well production rate. The following trial-and-error procedure can be used to predict the productivity of a root well with n roots.

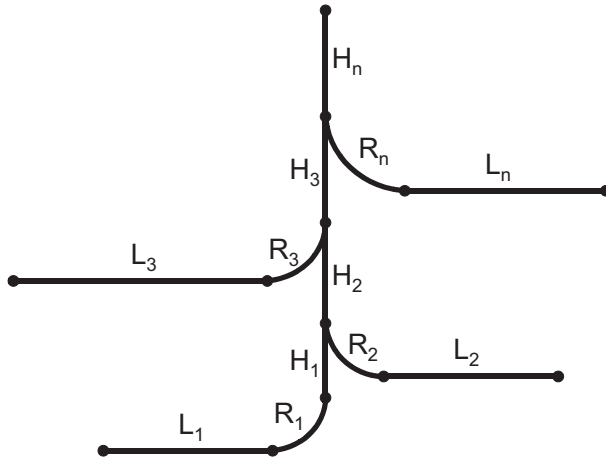


Figure 7-7 A simplified multilateral well structure.

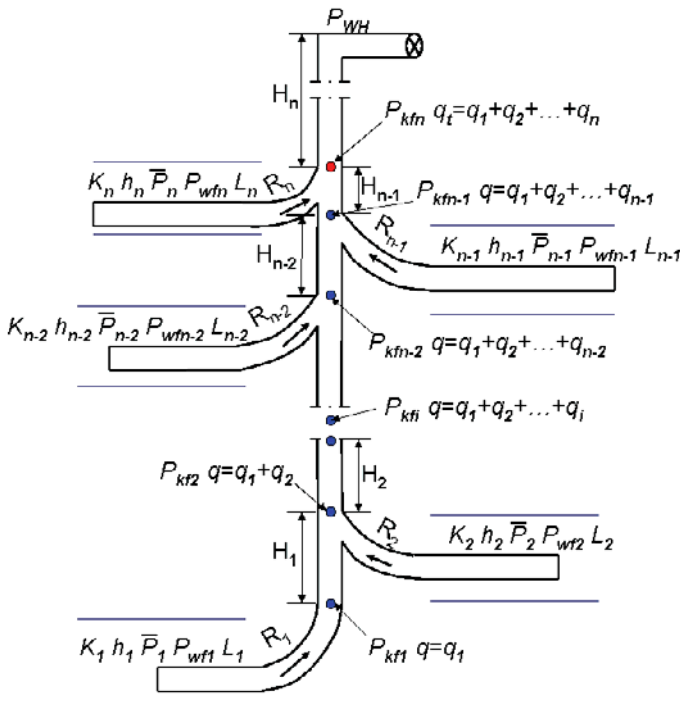


Figure 7-8 Symbols used to describe a multilateral well.

1. At the given wellhead flowing pressure p_{hf_n} , assume a value of the total well flow rate q_t , and calculate the pressure at the kick-out point of lateral n and p_{kf_n} using the tubing performance relationship (TPR) function \mathfrak{S}_n :

$$p_{kf_n} = \mathfrak{S}_n(p_{hf_n}, q_t) \quad (7.27)$$

2. Perform an inflow-outflow analysis for lateral n to calculate the production rate. Do this by combining the TPR of the curved section and the IPR of the horizontal section by solving for q_n from the following two relations:

$$p_{wfn} = \mathfrak{K}_n(\bar{p}_n, q_n) \quad (7.28)$$

$$p_{wfn} = \mathfrak{K}_n(p_{kf_n}, q_n) \quad (7.29)$$

where \mathfrak{K}_n and \mathfrak{K}_n are IPR and TPR (curved section) functions for the lateral n .

3. Calculate the flowing pressure at the kick-out point of lateral $n-1$ and $p_{kf_{n-1}}$ using the TPR function of the vertical section with flow rate $(q_t - q_n)$, that is:

$$p_{kf_{n-1}} = \mathfrak{S}_{n-1}(p_{kf_n}, q_t - q_n) \quad (7.30)$$

4. Perform an inflow-outflow analysis for lateral $n-1$ to calculate the production rate from that lateral. This is done by combining the TPR of the curved section and the IPR of the horizontal section, and then solving for q_{n-1} from the following two relations:

$$p_{wfn-1} = \mathfrak{K}_{n-1}(\bar{p}_{n-1}, q_{n-1}) \quad (7.31)$$

$$p_{wfn-1} = \mathfrak{K}_{n-1}(p_{kf_{n-1}}, q_{n-1}) \quad (7.32)$$

5. Calculate the flowing pressure at the kick-out point of lateral $n-2$ and $p_{kf\,n-2}$ using the TPR function of the vertical section with flow rate $(q_t - q_n - q_{n-1})$ —that is,

$$p_{kf\,n-2} = \mathfrak{S}_{n-2} \left(p_{kf\,n-1}, q_t - q_n - q_{n-1} \right) \quad (7.33)$$

6. Perform an inflow-outflow analysis for lateral $n-2$ to calculate the production rate from that lateral. Do this by combining the TPR of the curved section and the IPR of the horizontal section by solving for q_{n-2} from the following two relations:

$$p_{wf\,n-2} = \mathfrak{K}_{n-1} \left(\bar{p}_{n-2}, q_{n-2} \right) \quad (7.34)$$

$$p_{wf\,n-2} = \mathfrak{R}_{n-2} \left(p_{kf\,n-2}, q_{n-2} \right) \quad (7.35)$$

7. Repeat the procedure shown in steps 3 through 6 until the flow rate from lateral 1 (q_1) is calculated.

Compare the calculated total flow rate $(q_1 + q_2 + \dots + q_n)$ with the assumed total flow rate q_t . If the $(q_1 + q_2 + \dots + q_n) - q_t$ is greater than the specified tolerance, use the value of $(q_1 + q_2 + \dots + q_n)$ as a new assumption for the total flow rate q_t and repeat steps 1 to 6. If $(q_1 + q_2 + \dots + q_n) - q_t$ is less than the specified tolerance, exit the loop. Then the q_t is a prediction of production rate of the root well.

For oil wells, the Hagedorn-Brown correlation presented in Chapter 5 can be employed to generate the tubing performance functions \mathfrak{S} and \mathfrak{R} . The lateral inflow performance relationship function \mathfrak{K} can be chosen from different IPR models, including Equation (4.20).

For gas wells, Guo's mist flow model presented in Chapter 5 can be employed to generate the tubing performance functions \mathfrak{S} and \mathfrak{R} . The lateral inflow performance relationship function \mathfrak{K} can be chosen from different IPR models, including Equation (4.21).

One of the difficulties in predicting the productivity of root wells lies in accommodating the mixed properties of fluids (oil, water, and gas) from all roots in the hydraulics computations for different wellbore sections.

The mixing rule can be applied to all stages of the trial-and-error procedure.

7-4 SAMPLE PROBLEM

A planned root well has 10 roots penetrating 10 reservoir sections. From the data given in Tables 7–2 through 7–6, predict the pseudosteady-state oil production rate.

SOLUTION

This problem can be solved using the spreadsheet program **Guo's Multilateral Well.xls**. The result is presented in Table 7–7.

Table 7–2 Reservoir Property Data

Lateral No.	Reservoir Pressure (psia)	Temp. (°F)	Horizontal Permeability (md)	Vertical Permeability (md)	Thickness (ft)
1	1200	120	5	1.67	50
2	1400	125	6	2.00	51
3	1600	130	7	2.33	52
4	1800	135	8	2.67	53
5	2000	140	9	3.00	54
6	2200	145	10	3.33	55
7	2400	150	11	3.67	56
8	2600	155	12	4.00	57
9	2800	160	13	4.33	58
10	3000	165	14	4.67	59

Table 7–3 Fluid Property Data

Lateral No.	Oil Gravity (API)	Oil Viscosity (cp)	Oil Formation Volume Factor (rb/stb)	Solution Gas Ratio (scf/stb)	Water Cut (%)
1	65	0.5	1.4	5000	33
2	60	1	1.35	4000	34
3	55	1.5	1.3	3000	35
4	50	2	1.25	2000	36
5	45	2.5	1.2	1000	37
6	40	3	1.15	500	38
7	35	3.5	1.13	300	39
8	30	4	1.1	200	40
9	25	4	1.07	100	60
10	20	4	1.05	50	80

Table 7–4 Well Data for Vertical Sections

Lateral No.	Kick-off Point (ft)	Inclination Angle (deg)	Tubing Diameter (in)	Wall Roughness (in)
1	3000	0	9	0.0001
2	3500	0	6	0.0001
3	4000	0	6	0.0001
4	4500	0	6	0.0001
5	5000	0	6	0.0001
6	5500	0	6	0.0001
7	6000	0	6	0.0001
8	6500	0	6	0.0001
9	7000	0	6	0.0001
10	7500	0	6	0.0001

Table 7-5 Well Data for Curved Sections

Lateral No.	Radius of Curvature (ft)	Plane Inclination Angle (deg)	Tubing Diameter (in)	Wall Roughness (in)
1	500	0	4	0.0001
2	550	0	4	0.0001
3	600	0	4	0.0001
4	650	0	4	0.0001
5	700	0	4	0.0001
6	750	0	4	0.0001
7	800	0	4	0.0001
8	850	0	4	0.0001
9	900	0	4	0.0001
10	950	0	4	0.0001

Table 7-6 Well Data for Horizontal Sections

Lateral No.	Lateral Length (ft)	Inclination Angle (deg)	Tubing Diameter (in)	Wall Roughness (in)	Openhole Radius (ft)	Drainage Area (acre)
1	2000	90	4	0.0001	0.328	160
2	1900	90	4	0.0001	0.328	160
3	1800	90	4	0.0001	0.328	160
4	1700	90	4	0.0001	0.328	160
5	1600	90	4	0.0001	0.328	160
6	1500	90	4	0.0001	0.328	160
7	1400	90	4	0.0001	0.328	160
8	1300	90	4	0.0001	0.328	160
9	1200	90	4	0.0001	0.328	160
10	1100	90	4	0.0001	0.328	160

Table 7-7 Summary of Calculated Lateral and Well Production Rates

Lateral No.	Heel Pressure (psi)	Liquid Production Rate (stb/day)	Oil Production Rate (stb/day)	Water Production Rate (bbl/day)	Gas Production Rate (Mscf/day)
1	808	743	498	245	2,489
2	1,020	443	292	151	1,170
3	1,224	346	225	121	675
4	1,424	298	191	107	381
5	1,623	265	167	98	167
6	1,842	227	141	86	70
7	2,065	182	111	71	33
8	2,299	132	79	53	16
9	2,556	104	42	62	4
10	2,818	56	11	45	1
Total:		2,796	1,756	1,040	5,006

7.4 Summary

This chapter presented practical methods for predicting the productivities of wells with complex trajectories. These wells are multi-fractured horizontal wells, fishbone wells, and root wells. The IPR's of multi-fractured wells and fishbone wells can be estimated using simple models that allow solutions be obtained by hand calculation. The productivity prediction of root wells requires computer programs due to the complex procedure of coupling the root inflow and wellbore hydraulics.

7.5 References

Furui, K., Zhu, D., and Hill, A.D.: "A Rigorous Formation Damage Skin Factor and Reservoir Inflow Model for a Horizontal Well," *SPE* (August 2003): 151.

Guo, B. and Schechter, D.S.: “A Simple and Rigorous Mathematical Model for Estimating Inflow Performance of Wells Intersecting Long Fractures,” paper SPE 38104 presented at the SPE Asia Pacific Oil and Gas Conference and Exhibition (14–16 April 1997), Kuala Lumpur, Malaysia.

Guo, B. and Yu, X.: “A Simple and Accurate Mathematical Model for Predicting Productivity of Multifractured Horizontal Wells,” paper SPE 114452 presented at the CIPC/SPE Gas Technology Symposium 2008 Joint Conference (16–19 June 2008), Calgary, Canada.

Larsen, L.: “Productivity Computations for Multilateral, Branched, and Other Generalized and Extended Well Concepts,” paper SPE 36754 presented at the SPE Annual Technical Conference & Exhibition (6–9 October 1996), Denver, Colorado.

Li, H., Jia, Z., and Wei, Z.: “A New Method to Predict Performance of Fractured Horizontal Wells,” paper SPE 37051 presented at the SPE International Conference on Horizontal Well Technology (18–20 November 1996), Calgary, Canada.

Raghavan, R. and Joshi, S.D.: “Productivity of Multiple Drainholes or Fractured Horizontal Wells,” SPE Formation Evaluation (March 1993): 11–16.

Retnanto, A. and Economides, M.J.: “Performance of Multilateral Horizontal Well laterals in Low- to Medium-Permeability Reservoirs,” SPE Reservoir Engineering (May 1996): 7–77.

7.6 Problems

7-1 From the data given below, and assuming that the tubing string is set just above the pay zone, predict the pseudosteady-state production rate:

Fracture spacing ($2z_e$):	1200 ft
Fracture half length (x_f):	800 ft
Fracture permeability (k_f):	40000 md
Oil bubble-point pressure (p_b):	4000 psia

Effective horizontal permeability (k):	20 md
Pay zone thickness (h):	40 ft
Average reservoir pressure (p_{bar}):	3000 psia
Oil formation volume factor (B_o):	1.2 rb/stb
Well drainage area (A):	320 acres
Well radius (r_w):	0.328 ft
Fracture width (w):	0.3 in
Well vertical depth (H):	6000 ft
Tubing inner diameter (d):	3.5 in
Oil gravity (API):	40 API
Oil viscosity (μ_o):	1.2 cp
Producing GLR (GLR):	800 scf/bbl
Gas specific gravity (γ_g):	0.65 air = 1
Flowing tubing head pressure (p_{hf}):	600 psia
Flowing tubing head temperature (t_{hf}):	120 °F
Flowing temperature at tubing shoe (t_{wf}):	150 °F
Water cut (WC):	15 %
Near-wellbore fracture width (w_w):	0.2 in
Total skin factor (S):	1
Number of fractures (n):	5
Near-wellbore fracture permeability (k_{fw}):	50000 md

7-2 A planned fishbone well will have 10 laterals penetrating 10 reservoir sections. From the data given in the following tables, predict the pseudosteady-state oil production rate:

Reservoir Property Data

Lateral No.	Reservoir Pressure (psia)	Temp. (°F)	Horizontal Permeability (md)	Vertical Permeability (md)	Thickness (ft)
1	1200	120	5	2	50
2	1400	125	5	2	50
3	1600	130	5	2	50
4	1800	135	5	2	50
5	2000	140	5	2	50
6	2200	145	10	4	55
7	2400	150	10	4	55
8	2600	155	10	4	55
9	2800	160	10	4	55
10	3000	165	10	4	55

Fluid Property Data

Lateral No.	Oil Gravity (API)	Oil Viscosity (cp)	Oil Formation Volume Factor (rb/stb)	Solution Gas Ratio (scf/stb)	Water Cut (%)
1	65	0.5	1.4	5000	30
2	60	1	1.35	4000	30
3	55	1.5	1.3	3000	35
4	50	2	1.25	2000	35
5	45	2.5	1.2	1000	35
6	40	3	1.15	500	38
7	35	3.5	1.13	300	38
8	30	4	1.1	200	40
9	25	4	1.07	100	50
10	20	4	1.05	50	60

Well Data for the Vertical Sections

Lateral No.	Kick-off Point (ft)	Inclination Angle (deg)	Tubing Diameter (in)	Wall Roughness (in)
1	3000	0	7	0.0001
2	3500	0	4	0.0001
3	4000	0	4	0.0001
4	4500	0	4	0.0001
5	5000	0	4	0.0001
6	5500	0	4	0.0001
7	6000	0	4	0.0001
8	6500	0	4	0.0001
9	7000	0	4	0.0001
10	7500	0	4	0.0001

Data for the Curve Sections

Lateral No.	Radius of Curvature (ft)	Plane Inclination Angle (deg)	Tubing Diameter (in)	Wall Roughness (in)
1	500	0	4	0.0001
2	500	0	4	0.0001
3	600	0	4	0.0001
4	600	0	4	0.0001
5	700	0	4	0.0001
6	700	0	4	0.0001
7	800	0	4	0.0001
8	800	0	4	0.0001
9	900	0	4	0.0001
10	900	0	4	0.0001

Well Data for the Horizontal Sections

Lateral No.	Lateral Length (ft)	Inclination Angle (deg)	Tubing Diameter (in)	Wall Roughness (in)	Openhole Radius (ft)	Drainage Area (acre)
1	2100	90	4	0.0001	0.328	160
2	2000	90	4	0.0001	0.328	160
3	1900	90	4	0.0001	0.328	160
4	1800	90	4	0.0001	0.328	160
5	1700	90	4	0.0001	0.328	160
6	1600	90	4	0.0001	0.328	160
7	1500	90	4	0.0001	0.328	160
8	1400	90	4	0.0001	0.328	160
9	1300	90	4	0.0001	0.328	160
10	1200	90	4	0.0001	0.328	160

Productivity of Intelligent Well Systems

8.1 Introduction

An Intelligent Well System (IWS) enables operators to control well production or injection remotely through using down-hole valves without additional well entry, optimizing well production and reservoir management. Different tool manufacturers focus on different aspects of intelligent completion, but the key properties of intelligent completion include the ability to monitor and control injection and production at down-hole remotely, and the ability to respond quickly to unexpected changes in reservoir performance. This chapter provides a comprehensive description of IWS and IWS well productivity.

8.2 IWS Description

The basic components of the intelligent well system (Figure 8–1) include:

- Remote-controlled down-hole flow control valves (On-Off/Choking valves)
- Down-hole pressure and temperature gauges
- Down-hole isolation tools (packers with hydraulic/electric-cable lines feed-through)
- Surface data acquisition and control systems
- Communication and power cable

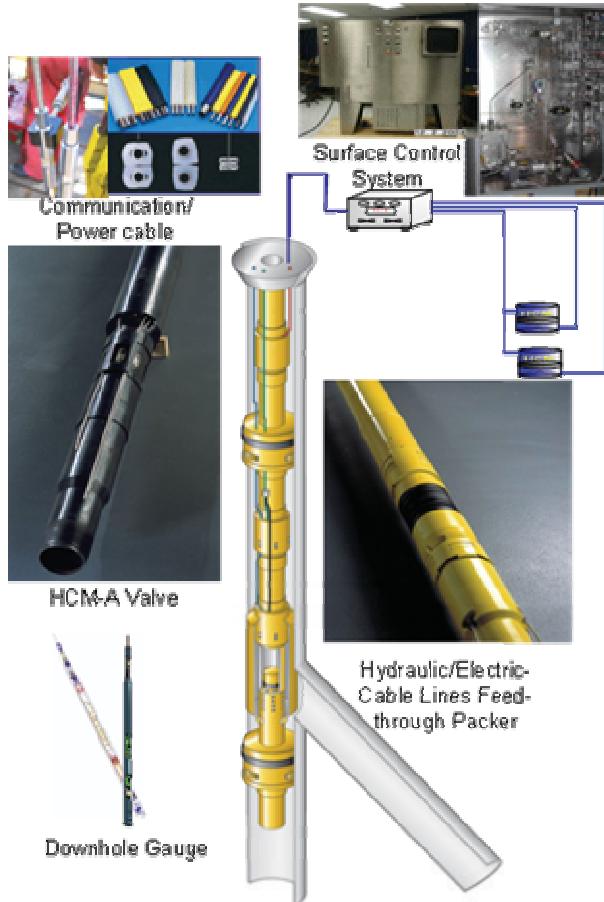


Figure 8–1 *Intelligent well system components.* (Courtesy Baker Oil Tools)

The down-hole flow control and isolation tools provide the ability to control each production zone of the reservoir separately. The down-hole valves (On-Off/Choking) can be remotely-controlled to adjust the production or injection rates for each zone, where control and optimization of commingled production is important. The down-hole valve and gauges are controlled through the surface data acquisition and control system and hydraulic/electrical lines.

Depending upon production optimization purposes, the economic value of an intelligent well installation could be summarized as:

- Accelerated and maximized commingled hydrocarbon production
- Reduced well operating costs because of simplified surface facilities and decreased well intervention
- Increased ultimate recovery
- Improved reservoir knowledge and ability to adapt to changing conditions

Figure 8–2 compares a cash flow profile of an intelligent well system to a conventional completion system. Intelligent completion can directly decrease capital investment during exploration by requiring fewer wells and fewer surface facilities, especially when zonal isolation and commingled production is anticipated. Once the wells are in operation, the obvious benefits of commingled production are accelerated and maximized production. Down-hole monitoring also helps to understand reservoir performance, and down-hole choking permits optimizing production and injection of each isolated zone to increase ultimate recovery. In addition, remotely-controlled valves decrease the frequency of well intervention, which in turn decreases operating costs, especially for offshore wells.

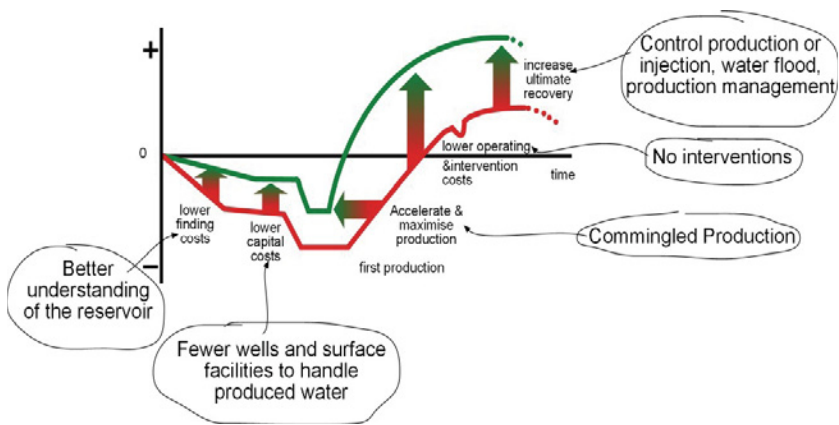


Figure 8–2 Cash flow profile of IWS versus conventional. (Courtesy Baker Oil Tools)

The first intelligent well was installed in 1997 in Scandinavia. To date (2007), there have been approximately 500 to 600 intelligent well completions globally. Depending upon completion configuration and purpose, intelligent well systems can be classified as follows:

- Single tubing string selectively controlling multiple zone production/injection
- Single tubing string selectively controlling multiple lateral production/injection
- Intelligent completion with sand control selectively controlling multiple zone/lateral production/injection
- Intelligent completion with Electric Submerge Pump (ESP) selectively controlling multiple zone/lateral production
- Intelligent completion utilizing an in-situ gas zone for auto-gas lift
- Intelligent completion utilizing an in-situ water zone for dump-flooding

Figure 8–3 illustrates a single tubing string intelligent completion with selective control of production/injection in multiple zones. Each production unit along the wellbore is isolated by packers and control valves. The production/injection of each separated zone can be controlled individually by operating on-off and choking valves remotely.

Figure 8–4 illustrates a single tubing string intelligent completion with selective control of production/injection in multiple laterals. The isolated feed-through packers and control valves are installed along the main bore to control production/injection of both the main bore and each side bore.

The shroud-unshroud valve configuration is very common in intelligent well system design (Figure 8–5). This configuration separates the hydrocarbon production flow paths from a two-lateral IWS production well. The upper control valve controls the production fluid rate from the sidebore, while the lower control valve controls the production fluid rate from the mainbore. The lower zone control valve is shrouded, and its lower tubular side is plugged to separate the production fluid of both zones. The two lateral production fluids flow separately through the two flow paths before they commingle at the upper valve choke port. The production fluid of the sidebore flows through the annulus between the

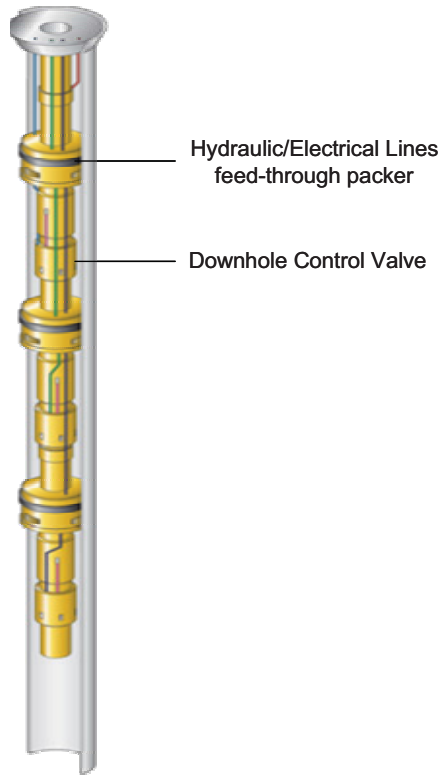


Figure 8–3 *Single tubing string with selective control of production/injection in multiple zones.* (Courtesy Baker Oil Tools)

casing and tubing strings and is controlled by the upper valve. The production fluid in the mainbore flows through the tubing string and into the shroud, and is controlled by the lower control valve. Figure 8–6 illustrates the shrouded valve configuration and the flow directions of production fluid.

Both Figures 8–3 and 8–7 illustrate intelligent completion with sand control, selectively controlling production/injection in two zones/laterals. As shown in Figure 8–7, an upper fluid loss control device is located in the upper zone gravel pack completion and isolates the upper sand. When the upper completion string (including tubing, packers, and control valves) is landed, the seal assembly below the shrouded valve locates in a polished bore between the zones and isolates the upper and lower zones during production. Production from the upper zone passes between the OD of the

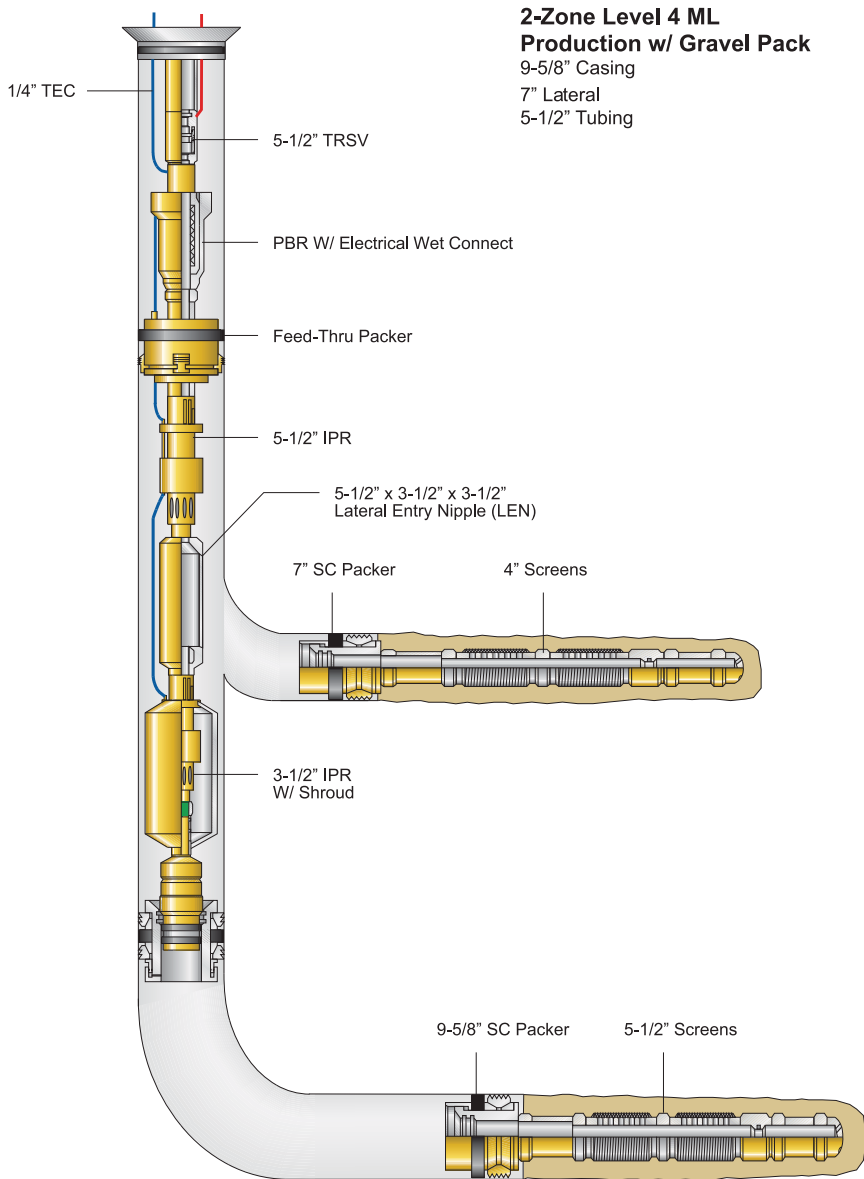


Figure 8-4 Single tubing string with selective control of production/injection in multi-laterals. (Courtesy Baker Oil Tools)

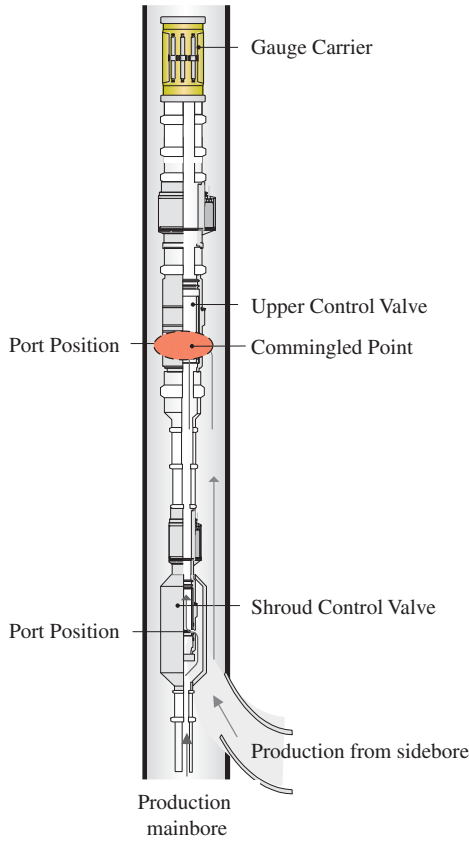


Figure 8–5 Flow paths of a two-lateral IWS production well with shroud-unshroud valve configuration. (Courtesy Baker Oil Tools)

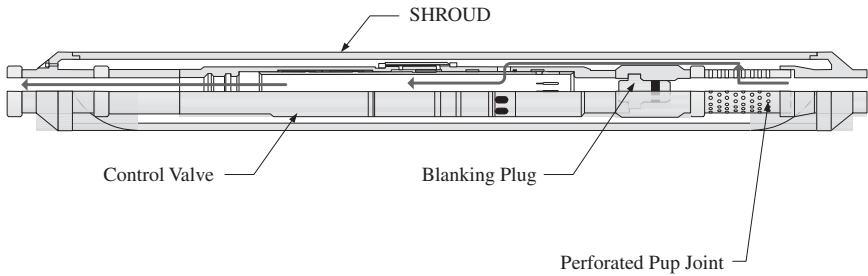


Figure 8–6 Flow direction in shrouded control valve. (Courtesy Baker Oil Tools)

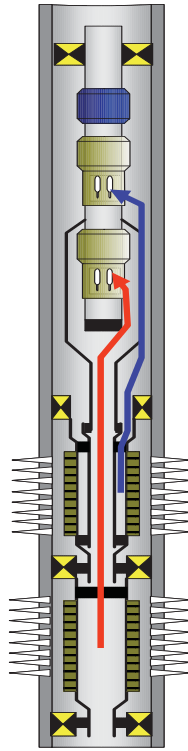


Figure 8–7 *Intelligent completion with sand control to selectively control production in multiple zones.* (Courtesy Baker Oil Tools)

concentric tub and the ID of the fluid loss control device out into the casing/tubing annulus space, and is controlled by the upper control valve. Production from the lower zone passes through the ID of the concentric tub and into the shroud, and is controlled by the lower control valve. The two arrows show the flow directions of the production fluids for the upper and lower zones, respectively.

To accelerate oil production, an Electric Submerge Pump (ESP) can be integrated with an intelligent well system to control production selectively in multiple zones or laterals (Figure 8–8). A shroud-unshroud valve configuration is used to control production from two zones. Production fluid from the upper zone passes through the annulus between the casing and tubular string, and is controlled by the upper valve; the production from lower zone flows through the tubing string and into the shroud, and is con-

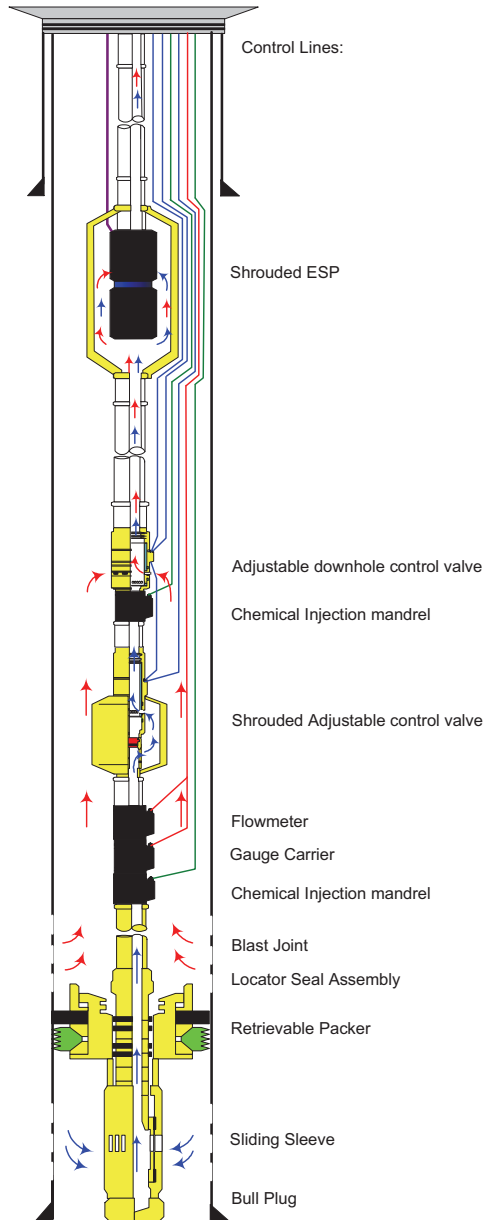


Figure 8–8 Intelligent completion with Electric Submerge Pump (ESP) to selectively control production in multiple zones/laterals. (Courtesy Baker Oil Tools)

trolled by the lower control valve. The ESP is installed above the commingled point (the upper control valve) to increase flowing pressure and accelerate oil production.

If a gas cap is available above the oil zone, an intelligent well system called auto-gas-lift can be designed to optimize hydrocarbon production (Figure 8–9). Initial oil production is maintained by opening the lower valve fully and choking the upper valve. The upper valve has pre-designed small orifices to control gas entry into the tubing to lift the lower zone oil. This IWS system can be switched from oil to gas production when the lower zone oil production becomes uneconomic. This is done by fully opening the upper valve and closing the lower valve.

Intelligent completions also can be used for dump-flooding of in-situ water zones (Figure 8–10). The water from a deep aquifer is produced and injected back into the upper injection zone. The adjustable control valve regulates the water flow rates from the lower zone remotely, and therefore controls the water injection rate into the upper zone. The injected water helps increase oil recovery from the upper zone.

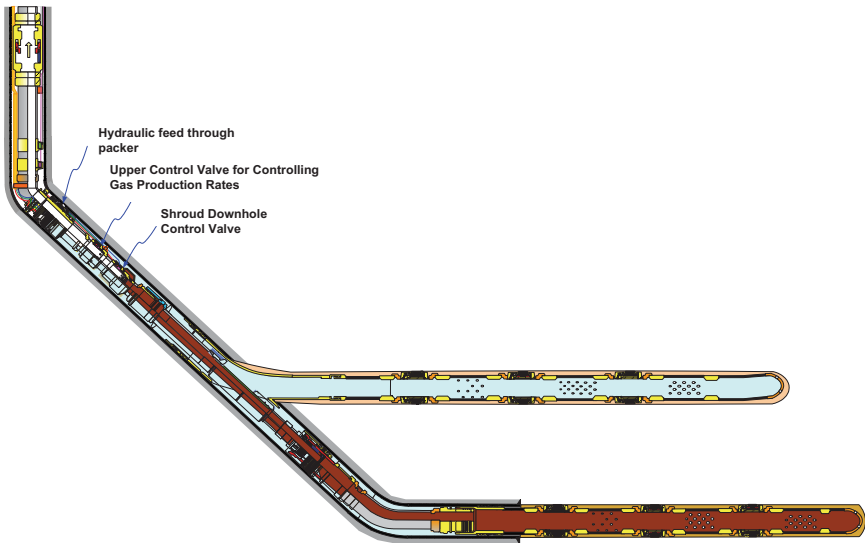


Figure 8–9 Intelligent completion utilizing in-situ gas zone for auto-gas-lift. (Courtesy Baker Oil Tools)

Sequence No. 4
Dump Flood Deep Aquifer to Injection Zone

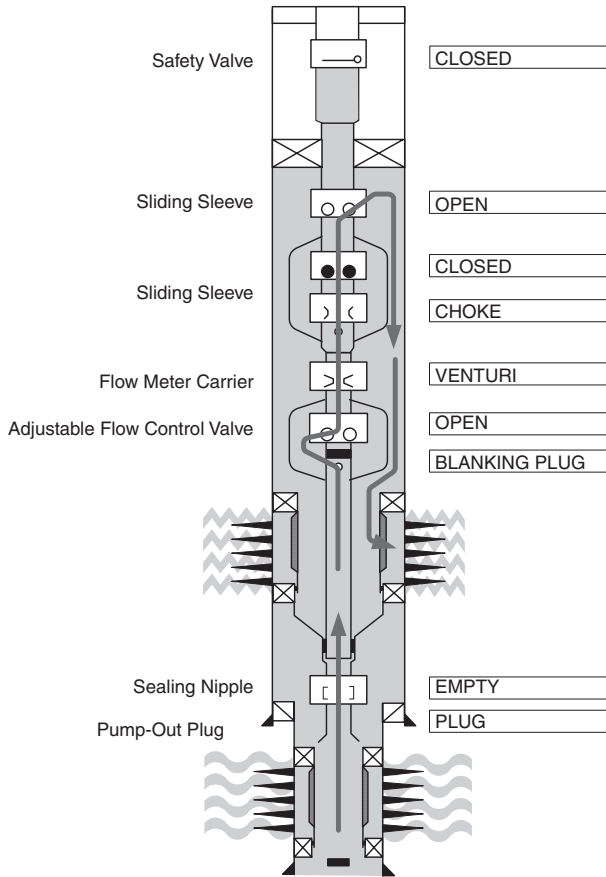


Figure 8–10 Intelligent completion utilizing in-situ water zone for dump-flooding. (Courtesy Baker Oil Tools)

8.3 Performance of Down-Hole Flow Control Valves

Intelligent Well Systems are normally used for commingled production/injection in multiple zones. Down-hole flow control valves, as the key components of IWS systems, are installed for distinct purposes:

- To control the fluid communications between the annulus and tubing
- To isolate production from each zone
- To limit zonal production rates for regulation compliance or optimization
- To adjust the wellbore pressure profile
- To avoid cross-flow, unexpected reservoir conditions, or sand problems due to high drawdown
- To control the zonal flow rate and avoid water or gas coning

Depending upon the functions of the valves, the down-hole flow control valve can be one of two types:

- On/Off, where the control valve is only used to isolate zonal flow-in/flow-out
- Choking, where the control valve not only isolates the zonal flow-in/flow-out, but also adjusts the wellbore pressure profile and zonal flow rates to optimize well production and reservoir management

The choking down-hole control valve also can be one of two types: In the first, the choking position can be adjusted remotely to any open percentage, with infinite choke positions. In the other, the choking positions are pre-designed with a fixed-open valve. The fixed-open control valves are normally controlled hydraulically. Figures 8–11 and 8–12 show this type of valve port shape when the valve is partially open.

Placing the control valve down-hole requires setting a constraint for each production zone's reservoir inflow. Working with the surface wellhead choke, the wellbore pressure profile can be adjusted by choking the down-hole control valve, thus regulating the production profile from each zone.

8.3.1 Sonic and Subsonic Flow

Pressure drop across the down-hole control valve is usually very significant. No universal equation can predict the pressure drop across the chokes for all types of production fluids. Different choke flow models are

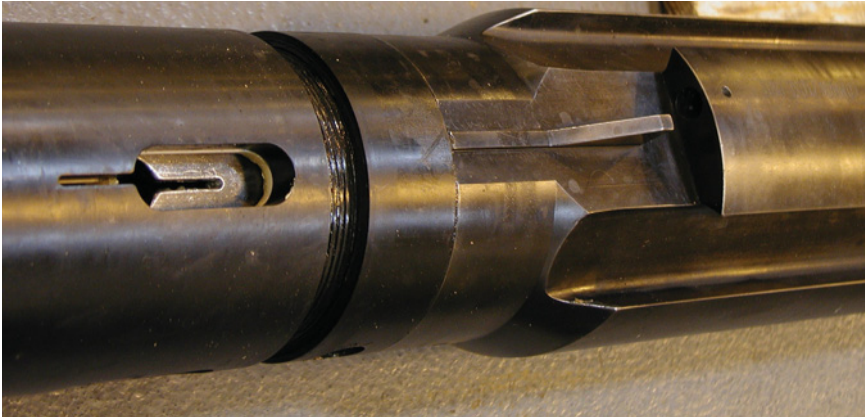


Figure 8–11 *Down-hole control valve at fixed-open position. (Courtesy Baker Oil Tools)*



Figure 8–12 *Down-hole control valve at fixed-open position. (Courtesy WellDynamics)*

available, and they must be chosen based upon the gas fraction in the fluid and flow regimes—that is, subsonic or sonic flow.

When the fluid flow velocity in a choke reaches the velocity of sound in the fluid under the localized temperature and pressure, the flow is called

“sonic flow.” Under sonic conditions, the pressure wave downstream of the choke cannot travel upstream through the choke because the fluid medium is traveling in the opposite direction at the same velocity. A pressure discontinuity therefore exists at the choke, and the downstream pressure cannot affect the upstream pressure. Because of the pressure discontinuity, any changes in the downstream pressure cannot be detected from the upstream pressure gauge. Of course, any changes in the upstream pressure cannot be detected from the downstream pressure gauge, either. Sonic flow provides a unique choke feature that stabilizes the well production rate and separates operation regimes.

Whether sonic flow exists through a choke depends on the downstream-to-upstream pressure ratio. If this ratio is less than a critical value, sonic, or critical flow, exists. If the pressure ratio is greater than or equal to the critical pressure ratio, subsonic, or subcritical flow, exists. The critical pressure ratio through a choke is expressed as

$$\left(\frac{P_{outlet}}{P_{up}} \right)_c = \left(\frac{2}{k+1} \right)^{\frac{k}{k-1}} \quad (8.1)$$

where P_{outlet} is the pressure at choke outlet, P_{up} is the upstream pressure, and k is the specific heat ratio. The value of k depends upon the composition of the natural gas and can be estimated from the mixing rule. Normally, $k = 1.28$ is used in cases in which there is insufficient information on gas composition. The critical pressure ratio of natural gas is, therefore, about 0.55. Figure 8–13 shows the typical choke flow performance of gas through a down-hole control valve.

8.3.2 Single-Phase Liquid Flow

The single-phase liquid flow choking equation requires the following assumptions:

- The pressure drop across a choke is due to kinetic energy change
- The liquid is incompressible

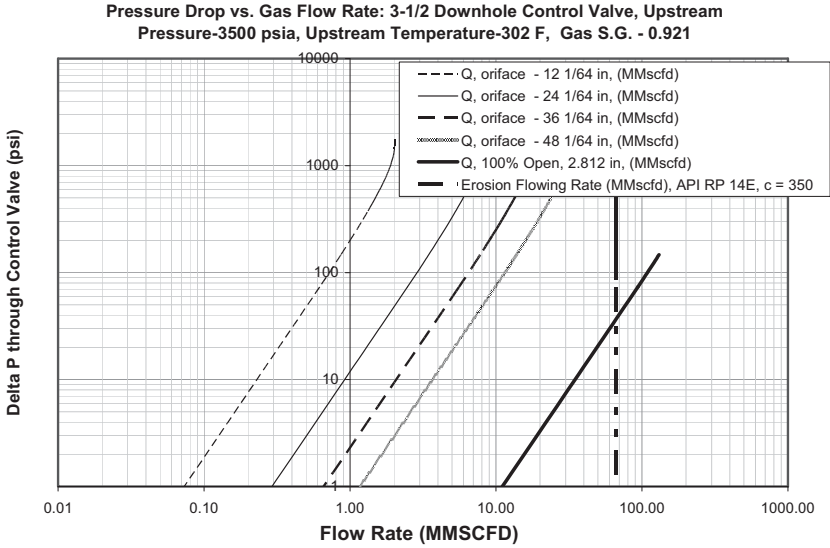


Figure 8–13 Typical choke flow performance of a down-hole control valve. (Courtesy Baker Oil Tools)

The equation can be written as

$$M = \frac{c_d A}{\sqrt{1 - \beta^4}} \sqrt{2g_c \rho \Delta P} \tag{8.2}$$

where

M = liquid mass flow rate (lbm/sec)

c_d = choke discharge coefficient (dimensionless)

A = choke port area (ft²)

g_c = unit conversion factor (32.17 lbm-ft/lbf-s²)

ρ = liquid fluid density (lbm/ft³)

ΔP = differential pressure through choke port (lbf/ft²)

where

$$\beta = \frac{d_{choke}}{d_1} \quad (8.3)$$

d_{choke} = choke port ID (in/ft)

d_1 = upstream hydraulic ID (in/ft)

If U.S. field units are used, Equation (8.2) is expressed as

$$Q = \frac{1.48 \times 10^6 c_d A}{\sqrt{1 - \beta^4}} \sqrt{\frac{\Delta p}{\rho}} \quad (8.4)$$

Q = liquid flow rate (bbl/d)

Δp = differential pressure through choke throat (psi)

If the choke port inside diameter is small, the term $\sqrt{1 - \beta^4}$ is close to 1. Equations (8.2) and (8.4) can be written as the following forms:

$$M = c_d A \sqrt{2g_c \rho \Delta P} \quad (8.5)$$

and

$$Q = 1.48 \times 10^6 c_d A \sqrt{\frac{\Delta p}{\rho}} \quad (8.6)$$

The control valve coefficient (C_v) is also commonly used to characterize the performance of control valves, relating pressure drop across the valve to the liquid flow rate through the valve at a given valve opening. The coefficient C_v is defined by the following equation for single-phase liquid flow:

$$C_v = \frac{Q_{gpm}}{\sqrt{\frac{\Delta p}{\gamma}}} \quad (8.7)$$

where

Q_{gpm} = liquid flow rate (gallon/min)

γ = specific gravity of the liquid relative to water (water = 1)

Then, the relationship of c_d and C_v can be expressed as

$$C_v = 5468.65Ac_d \quad (8.8)$$

8.3.3 Choke Discharge Coefficient (c_d)

For fluid flow through restrictions, it is common to use a discharge coefficient (c_d) as a final modifying factor in the flow rate equation. Its use should counteract errors due to assumptions made while developing a model. A theoretically “perfect” choke model will have $c_d = 1$. The laws of thermodynamics imply that the value of c_d less than unity should result in the real world. Various researchers, including Sachdeva et al. (1986), Husu et al. (1994), and Guo et al. (2007), indicate that the value of c_d is not a constant. Often, c_d is correlated with factors such as Reynolds number, pressure differential, gas expansion factor, choke shape, etc.

Down-hole flow control valves are used to control flow communication between the tubing and annulus. The design of a control valve choke is different from that of other chokes in valve open area, moving mechanisms, and erosion considerations. Figures 8–11, 8–12, and 8–14 illustrate typical choking control valve shapes from some major product suppliers at various fixed-open positions. The choke shapes of the down-hole valve are very different at different open positions and between different manufacturers.

Many flow tests have established values for the discharge coefficients (c_d) of down-hole flow control valves. The choke discharge coefficients (c_d) vary with different open-choke values, and the Reynolds numbers through the choke throat also have some impact on the discharge

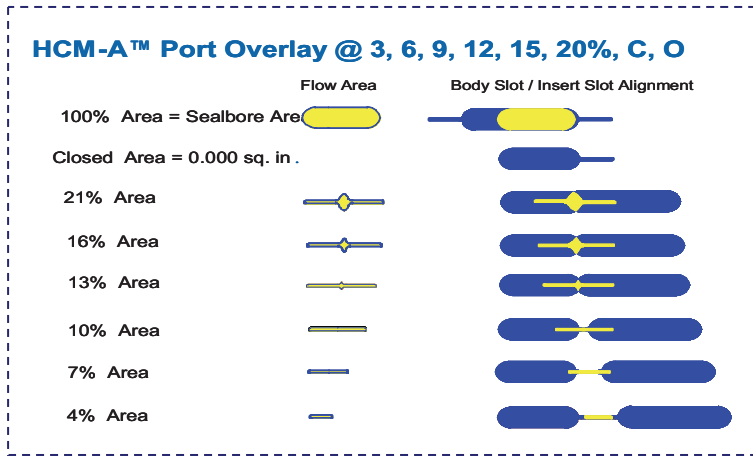


Figure 8–14 Typical choke shapes at various open positions. (Courtesy Baker Oil Tools)

coefficient (c_d). Therefore, when applying choking models to predict down-hole valve performance, it is important to estimate the discharge coefficient (c_d) correctly.

8.3.4 Single-Phase Gas Flow

Equations for gas flow through a choke assume isentropy, where there is no transfer of heat energy (adiabatic) in a reversible process-- that is, no energy losses occur due to friction or dissipative effects. Equation (8.9) represents this process:

$$p_1 V_{G1}^k = p_2 V_{G2}^k = p V_G^k = c \quad (8.9)$$

where

V_{G1} = upstream gas-specific volume (ft³/lbm)

V_{G2} = downstream gas-specific volume (ft³/lbm)

p_1 = upstream pressure (psi)

p_2 = downstream pressure (psi)

c = polytropic constant

k = heat specific ratio (c_p/c_v)

c_p = specific heat of gas at constant pressure

c_v = specific heat of gas at constant volume

8.3.4.1 Subsonic Flow

Under subsonic flow conditions, the rate of gas flow through a down-hole flow control valve can be expressed as

$$Q_{US} = 1242.5c_d A_{in} p_1 \sqrt{\left(\frac{k}{k-1}\right) \left(\frac{1}{z_{up} T_{up} \gamma_g}\right) \left[\left(\frac{p_2}{p_1}\right)^{\left(\frac{2}{k}\right)} - \left(\frac{p_2}{p_1}\right)^{\left(\frac{k+1}{k}\right)}\right]} \quad (8.10)$$

where

Q_{US} = flow rate in volume (Mscf/day)

A_{in} = choke port area (in²)

z_{up} = upstream gas compressibility factor

T_{up} = upstream gas temperature (°R)

γ_g = specific gravity of the gas relative to air

In calculating down-hole control valve flow performance, it is sometimes more convenient to calculate the flow rates in mass flux (lbm/sec) to avoid having to insert a P - v - T correction. In the unit of mass rate (lbm/sec), Equation (8.10) can be expressed as

$$M_g = 1.098c_d A_{in} p_1 \sqrt{\left(\frac{k}{k-1}\right) \left(\frac{\gamma_g}{z_{up} T_{up}}\right) \left[\left(\frac{p_2}{p_1}\right)^{\left(\frac{2}{k}\right)} - \left(\frac{p_2}{p_1}\right)^{\left(\frac{k+1}{k}\right)}\right]} \quad (8.11)$$

The gas velocities (ft/sec) at upstream and downstream loci can be calculated separately by the equations:

$$u = \frac{144M_g}{\rho A_m} \quad (8.12)$$

where the gas densities are estimated by

$$\rho_{G1} = \frac{2.7\gamma_g p_1}{z_{up} T_{up}} \quad (8.13)$$

$$\rho_{G2} = \rho_{G1} \left(\frac{p_2}{p_1} \right)^{\left(\frac{1}{k} \right)} \quad (8.14)$$

where

u = gas in-situ velocity (ft/sec)

ρ = gas in-situ density (lbm/ft³)

ρ_{G1} = upstream gas in-situ density (lbm/ft³)

ρ_{G2} = downstream gas in-situ density (lbm/ft³)

8.3.4.2 Sonic Flow

Under sonic flow conditions, the gas passage rate reaches its maximum value. The gas passage rate is expressed in the following equation by replacing the downstream-to-upstream pressure ratio with the ideal gas critical pressure ratio, Equation (8.1):

$$Q_{US} = 1242.5c_d A_m p_1 \sqrt{\left(\frac{k}{k-1} \right) \left(\frac{1}{z_1 T_1 \gamma_g} \right) \left(\left(\frac{2}{k+1} \right)^{\left(\frac{2}{k-1} \right)} - \left(\frac{2}{k+1} \right)^{\left(\frac{k+1}{k-1} \right)} \right)} \quad (8.15)$$

$$M_g = 1.098c_d A_{in} p_1 \sqrt{\left(\frac{k}{k-1} \right) \left(\frac{\gamma_g}{z_{up} T_{up}} \right) \left[\left(\frac{2}{k+1} \right)^{\frac{2}{k-1}} - \left(\frac{2}{k+1} \right)^{\frac{k+1}{k-1}} \right]} \quad (8.16)$$

Gas velocity under sonic flow can be estimated by

$$u = \frac{144M_g}{A_{in} \rho_{G1} \left(\frac{2}{k+1} \right)^{\frac{1}{k-1}}} \quad (8.17)$$

or

$$u \approx 44.76 \sqrt{T_{up}} \quad (8.18)$$

8.3.4.3 Temperature at Valve

In addition to pressure drop across the chokes, another concern in managing gas wells is the temperature drop associated with choke flow, because hydrates may form that can plug flow lines.

Depending upon the downstream-to-upstream pressure ratio, the temperature at the valve may be much lower than expected. This low temperature is due to the Joule-Thomson cooling effect—that is, a sudden gas expansion downstream the choke throat causes a significant temperature decrease. The temperature can drop to below the ice point, resulting in ice-plugging if there is water in the fluids. Even though the temperature can be still above ice point, gas hydrates can form and cause plugging problems.

Assuming isentropic conditions for ideal gas flow through valves, the temperature at the valve downstream can be predicted using the following equation:

$$T_{dn} = T_{up} \frac{z_{up}}{z_{outlet}} \left(\frac{P_{outlet}}{P_{up}} \right)^{\frac{k-1}{k}} \quad (8.19)$$

The outlet pressure will be equal to the downstream pressure in subsonic flow conditions.

Alternatively, the downstream temperature can be estimated by determining the average Joule-Thomson coefficient. The Joule-Thomson Effect is defined as a process in which the temperature of a real gas is either decreased or increased by letting the gas expand freely at constant enthalpy (meaning that no heat is transferred to or from the gas, and no external work is extracted). Choking can be assumed as a constant enthalpy process, where Joule-Thomson coefficient is defined as

$$\mu_J = \left(\frac{\partial T}{\partial P} \right)_h \quad (8.20)$$

To express Equation (8.20) in terms of P - V - T behavior, Sonntag et al. (1998) presented the following relation:

$$\mu_J = \frac{RT^2}{Pc_p} \left(\frac{\partial Z}{\partial T} \right)_P \quad (8.21)$$

In Equations (8.20) and (8.21), μ_J is the Joule-Thomson coefficient, T is the temperature, P is the pressure, R is the universal gas constant, c_p is the specific heat of gas at constant pressure, and z is the gas compressibility factor. The unit system of Equations (8.20) and (8.21) may be either SI units or US field units. The calculation procedure is summarized as:

1. Assume a downstream temperature and estimate the gas compressibility factors for both upstream and downstream temperatures under constant upstream pressure.
2. Calculate μ_J using Equation (8.21) to determine an average Joule-Thomson coefficient.
3. Apply the calculated average μ_J into Equation (8.20) to calculate a new downstream temperature, where

$$T_{up} - T_{down} = \mu_{J(av)} \cdot (P_{up} - P_{outlet})$$

4. Compare the calculated downstream temperature with the assumed one. If they are within acceptable tolerances, then accept the assumed value. If they are outside specifications, then use the calculated temperature as a new assumed downstream temperature to repeat the procedure.

8.3.4.4 Applications of Single-Phase Choke Flow

Equations (8.1) through (8.21) can be used for estimating the:

- Liquid/gas passage rate through the down-hole valve at given upstream and downstream pressures
- Upstream pressure at the down-hole valve at given downstream pressure and liquid/gas passage
- Downstream pressure at the down-hole valve at given upstream pressure and liquid/gas passage
- Critical pressure ratio of ideal gas flow through the down-hole valve
- Downstream temperature

To estimate the gas passage rate at given upstream and downstream pressures, the procedures can be summarized as:

1. Calculate the critical pressure ratio using Equation (8.1).
2. Calculate the downstream-to-upstream pressure ratio.
3. If the downstream-to-upstream pressure ratio is greater than the critical pressure ratio, use Equation (8.10) to calculate gas passage rate. Otherwise, use Equation (8.15) to calculate gas passage rate.

8-1 SAMPLE PROBLEM

A 3-1/2-in. shrouded down-hole control valve is installed to restrict water injection to a single pay zone. At full open flow, the valve cross-sectional area is 6.21 in². It is opened remotely to 12%. The specific gravity of the injected water is 1.03. A down-hole venturi flow meter measured the in-situ water injection rate through the valve as 12,000 bpd. After compensating

for hydrostatic pressure drop, the in-situ downstream pressure measured by the down-hole gauge was 2520 psi. The measured downstream fluid temperature was 75°F. Given a valve discharge coefficient of 0.841 derived from flow testing, estimate the pressure differential through the valve, and the valve upstream pressure.

SOLUTION

Use Equation (8.6) to estimate the valve differential pressure and the upstream pressure. Before applying this equation, the in-situ injection fluid density must be estimated, as the fluid pressure/temperature will have an effect upon it. The correlation of Gould (1974) can be used to estimate the water formation volume factor (B_w):

$$\begin{aligned} B_w &= 1 + 0.00012 \times (75 - 60) + 0.000001 \times (75 - 60)^2 - 0.00000333 \times 2520 \\ &= 0.994 \text{ rb/STB} \end{aligned}$$

Next, water in-situ density can be calculated by

$$\begin{aligned} \rho_w &= 1.03 \times \frac{62.4259}{0.994} \\ &= 64.687 \text{ lbm/ft}^3 \end{aligned}$$

The differential pressure through the valve can be calculated by applying Equation (8.6):

$$12000 = 1.48 \times 10^6 \times 0.841 \times \left(\frac{6.21 \times 12\%}{144} \right) \times \sqrt{\frac{\Delta p}{64.687}}$$

Yielding:

$$\Delta p = 225 \text{ psi}$$

The valve upstream pressure is

$$p_{up} = 2520 + 225 = 2745 \text{ psi}$$

8-2 SAMPLE PROBLEM

A 4-1/2-in. down-hole control valve is installed to control oil production from one pay zone. The full open flow area of the valve is 10.68 in², and the valve is opened remotely to 3%. The specific gravity of the oil is 0.87 (water = 1). The solution gas-oil ratio at $p \geq p_b$ is $R_{sb} = 285$ scf/STB. The solution gas-specific gravity is 0.83 (air = 1). The static reservoir temperature is 192°F. After compensating for the hydrostatic/frictional pressure drop, the in-situ upstream/downstream pressures measured by the down-hole gauges were 2810 psi and 2690 psi, respectively. The measured fluid temperature through the valve was 185°F. If the valve discharge coefficient is given as 0.826 from flow test, estimate the oil production rate and the flow velocity through the valve. The oil properties are assumed to be exactly represented by Standing's correlation.

SOLUTION

The in-situ hydrocarbon properties are estimated by Standing (1947) correlations:

The oil API gravity is

$$\begin{aligned} API &= \frac{141.5 - 131.5\gamma_o}{\gamma_o} \\ &= \frac{141.5 - 0.87 \times 131.5}{0.87} \\ &= 31.1 \end{aligned}$$

The oil bubble-point pressure is

$$\begin{aligned} p_b &= 18 \times \left(\frac{R_{sb}}{\gamma_g} \right)^{0.83} \times 10^{(0.00091 \times T_r - 0.0125 API)} \\ &= 18 \times \left(\frac{285}{0.83} \right)^{0.83} \times 10^{(0.00091 \times 192 - 0.0125 \times 31.1)} \\ &= 1399 \text{ psi} \end{aligned}$$

Because the flowing pressure of interest is higher than p_b , the oil of interest is an undersaturated oil. Neglecting the oil isothermal

compressibility (psi^{-1}), the oil formation volume factor is estimated as

$$\begin{aligned} B_o &= 0.972 + 0.000147 \left(R_{sb} \left(\frac{\gamma_g}{\gamma_o} \right)^{0.5} + 1.25T \right)^{1.175} \\ &= 0.972 + 0.000147 \times \left(285 \times \left(\frac{0.83}{0.87} \right)^{0.5} + 1.25 \times 185 \right)^{1.175} \\ &= 1.196 \text{ rb/STB} \end{aligned}$$

Neglecting the oil isothermal compressibility (psi^{-1}), the oil density (lbm/ft^3) of interest can be calculated as

$$\begin{aligned} \rho_o &= \frac{350\gamma_o + 0.0764\gamma_g R_{sb}}{5.615B_o} \\ &= \frac{350 \times 0.87 + 0.0764 \times 0.83 \times 285}{5.615 \times 1.196} \\ &= 48 \text{ lbm/ft}^3 \end{aligned}$$

Applying Equation (8.6), the production rate can be estimated as

$$\begin{aligned} Q &= 1.48 \times 10^6 \times 0.826 \times \left(\frac{10.68 \times 0.03}{144} \right) \times \sqrt{\frac{(2810 - 2690)}{48}} \\ &= 4301 \text{ bpd} \end{aligned}$$

When converted to the standard conditions (STP) will result in

$$Q_{STB} = \frac{4301}{1.196} = 3596 \text{ STB/day}$$

The flow velocity through the valve throat is

$$\begin{aligned} v &= \frac{4301 \times 5.615}{24 \times 60 \times 60 \times \left(\frac{10.68 \times 0.03}{144} \right)} \\ &= 126 \text{ ft/sec} \end{aligned}$$

8-3 SAMPLE PROBLEM

A 3-1/2-in. down-hole auto-gas-lift control valve is installed to control the gas production rate from a gas zone to optimize production in another zone containing oil. The valve is opened remotely to a position in which the tubing and annulus communication is a 1/4" port. The specific gravity of the gas is 0.696 (air = 1). After compensating for the hydrostatic/frictional pressure drop, the in-situ upstream/downstream pressures measured by the down-hole gauges are 3150 psi and 2880 psi respectively. The monitored fluid temperature at the upstream of the valve is 205°F. If the valve discharge coefficient is given as 0.893, estimate the gas rate through the valve, fluid velocity through the valve, and outlet temperature. The gas heat specific ratio is assumed to be 1.28. The gas C_p is assumed to be 7691 ft-lbf/(lb-mol-R).

SOLUTION

1) Gas rate prediction

The downstream-to-upstream pressure ratio is

$$\left(\frac{P_2}{P_1}\right) = \left(\frac{2880}{3150}\right) = 0.914 < 0.55, \text{ indicating subsonic flow.}$$

The Brill and Beggs (1974) correlation is used to estimate the upstream gas compressibility factor (z_{up}) to get $z_{up} = 0.891$.

The gas density will be estimated based on the port area, given by

$$A_m = \frac{3.14159 \times 0.25^2}{4} = 0.0491 \text{ in}^2$$

The mass flux (lbm/sec) of the gas through the control valve can be estimated using Equation (8.11):

$$\begin{aligned} M_g &= 1.098 \times 0.893 \times 0.0491 \times 3150 \times \\ &\sqrt{\left(\frac{1.28}{1.28-1}\right) \left(\frac{0.696}{0.891 \times (205 + 459.67)}\right) \left(0.914^{\left(\frac{2}{1.28}\right)} - 0.914^{\left(\frac{1.28+1}{1.28}\right)}\right)} \\ &= 1.388 \text{ lbm/sec} \end{aligned}$$

The gas rate in standard condition can be estimated as

$$\begin{aligned}
 Q_{us} &= \frac{24 \times 60 \times 60 \times M_g}{\frac{2.7 \gamma_g p_s}{z_s T_s} \times 1000000} \\
 &= \frac{24 \times 60 \times 60 \times 1.388}{\frac{2.7 \times 0.696 \times 14.7}{1 \times (60 + 459.67)} \times 1000000} \\
 &= 2.256 \text{ MMSCFD}
 \end{aligned}$$

2) Gas velocity through the valve

The average gas pressure through the valve is:

$$\begin{aligned}
 p_{avg} &= \frac{p_1 + p_2}{2} \\
 &= \frac{3150 + 2880}{2} \\
 &= 3015 \text{ psi}
 \end{aligned}$$

The Brill and Beggs (1974) correlation is used to estimate average z-factor as the average gas pressure, to obtain $z_{avg} = 0.888$.

The average fluid density passing through the valve can be estimated by

$$\begin{aligned}
 \rho_{avg} &= \frac{2.7 \gamma_g p_{avg}}{z_{avg} T} \\
 &= \frac{2.7 \times 0.696 \times 3015}{0.888 \times (205 + 459.67)} \\
 &= 9.599 \text{ lbm/ft}^3
 \end{aligned}$$

The gas velocity through the valve can be estimated as

$$\begin{aligned} u_{avg} &= \frac{144M_g}{\rho_{avg}A_{in}} \\ &= \frac{144 \times 1.388}{9.599 \times 0.0491} \\ &= 424 \text{ ft/sec} \end{aligned}$$

3) Outlet temperature prediction

Assuming the acceptable tolerance value to be 0.1°F, Equations (8.20) and (8.21) can be used to estimate the outlet temperature. In fact, combining Equations (8.20) and (8.21) gives the equation:

$$\frac{T_2 - T_1}{p_2 - p_1} = \frac{RT_1^2}{Pc_p} \cdot \frac{(z_2 - z_1)_{p_1}}{(T_2 - T_1)}$$

where the outlet temperature T_2 is the only unknown parameter. Solve by substituting the Brill and Beggs (1974) z-factor correlation. A spreadsheet program can be made to yield the outlet temperature of:

$$T_{outlet} = 199.3^\circ\text{F}$$

8.3.5 Multiphase Flow

When the upstream pressure is below the bubble-point pressure of the oil, free gas exists in the fluid stream flowing through the down-hole control valve. Fluid behavior at the down-hole control valve will depend upon gas content and whether the flow regime is sonic or subsonic flow.

Mathematical modeling of multiphase flow through choke has been controversial for decades. Fortunati (1972) was the first investigator to present a model that can be used to calculate critical and subcritical two-phase flow through chokes. Ashford (1974) also developed a relation for two-phase critical flow based on the work of Ros (1960). Gould (1974)

plotted the critical-subcritical boundary defined by Ashford, showing that different values of the polytropic exponents yield different boundaries. Ashford and Pierce (1975) derived an equation to predict the critical pressure ratio. Their model assumes that the derivative of flow rate with respect to the downstream pressure is zero at critical conditions. They recommended a single set of equations for both critical and subcritical flow conditions. Pilehvari (1980, 1981) also studied choke flow under subcritical conditions. Sachdeva (1986) extended the work of Ashford and Pierce (1975) and proposed a relationship to predict critical pressure ratio. Surbey et al. (1988, 1989) discussed the application of multiple orifice valve chokes for both critical and subcritical flow conditions. Empirical relations were developed for gas and water systems. Al-Attar and Abdul-Majeed (1988) made a comparison of existing choke flow models based on data from 155 well tests. They indicated that the best overall comparison was obtained using the Gilbert correlation, which predicts measured production rates with an average error of 6.19%. On the basis of energy equations, Perkins (1990) derived relationships that described isentropic flow of multiphase mixtures through chokes. Osman and Dokla (1990) applied the least-squares method to field data to develop empirical correlations for gas condensate choke flow. Gilbert-type relationships were generated. Applications of these choke flow models can be found elsewhere (Wallis 1969, Perry 1973, Brown and Beggs 1977, Brill and Beggs 1978, Ikoku 1980, Nind 1981, Bradley 1987, Beggs 1991, Guo et al. 2007).

The Sachdeva and Perkins models are typical of most of these works and have been coded in commercial network modeling software to characterize flow behavior for both surface and down-hole chokes. The first step in applying these models is to predict the downstream-to-upstream pressure ratio at the critical flow transition. Both Sachdeva and Perkins developed equations to estimate this ratio. Sachdeva's work assumed that the derivative of mixture mass flow rate with respect to the choke throat downstream pressure is zero at the critical flow condition, which means the mass flux reaches a maximum with respect to the downstream pressure. By assuming the gas phase at the choke entrance contracts isentropically, but expands polytropically, they developed equations to predict critical pressure ratio and mass flow rate at both critical and subcritical conditions. Perkins' work is derived from the general energy equation by assuming polytropic processes, and an important feature is that Perkins assumed the gas compressibility factors at both the choke throat upstream

and downstream were the same. This assumption may be reasonable at low differential pressures, but is not applicable at high differential pressures. By assuming that the derivative of mixture mass flow rate with respect to downstream-to-upstream-pressure ratio is zero, which is similar to Sachdeva's (1986) work, an equation to predict critical pressure ratio was developed. Both models used a constant discharge coefficient (C_d) to correct errors resulting from various assumptions. However, the down-hole control valves normally operate at high temperature and pressures, and the control valve choke shape varies with different choke positions. Therefore, these models must be modified by incorporating down-hole pressure and temperature conditions, correlated choke discharge coefficients, and upstream/downstream completion geometries.

8.3.5.1 Sachdeva's Model

Sachdeva provided the following equation to calculate the critical-subcritical ratio at the critical flow transition:

$$y_c = \left(\frac{\frac{k}{k-1} + \frac{(1-x_1)V_L(1-y_c)}{x_1V_{G1}}}{\frac{k}{k-1} + \frac{n}{2} + \frac{n(1-x_1)V_L}{x_1V_{G2}} + \frac{n}{2} \left(\frac{(1-x_1)V_L}{x_1V_{G2}} \right)^2} \right)^{\frac{k}{k-1}} \quad (8.22)$$

where

y_c = critical pressure ratio

k = heat specific ratio, (c_p/c_v)

n = polytropic exponent for gas

x_1 = free gas quality at upstream (mass fraction)

V_L = upstream liquid specific volume (ft³/lbm)

V_{G1} = upstream gas-specific volume (ft³/lbm)

V_{G2} = downstream gas-specific volume (ft³/lbm)

The polytropic exponent (n) was calculated by

$$n = 1 + \frac{x_1(c_p - c_v)}{x_1c_v + (1 - x_1)c_L} \quad (8.23)$$

where c_L = specific heat of liquid.

The gas-specific volume at upstream can be determined using the gas law, based on upstream pressure and temperature. By assuming isentropic gas expansion, Equation (8.9) can be used to estimate the gas-specific volume downstream (V_{G2}) as

$$V_{G2} = V_{G1}y_c^{\left(-\frac{1}{k}\right)} \quad (8.24)$$

When the upstream pressure, temperature, physical gas properties, and free gas mass fraction are known, the only unknown parameter in Equation (8.22) is the critical pressure ratio (y_c). It can be solved mathematically.

The actual pressure ratio can be calculated by

$$y_a = \frac{p_2}{p_1} \quad (8.25)$$

where

y_a = actual downstream-to-upstream pressure ratio

p_1 = upstream pressure (psi)

p_2 = downstream pressure (psi)

If $y_a < y_c$, **critical flow exists**, and the y_c should be used ($y = y_c$) to calculate flow rates. Otherwise, **subcritical flow exists**, and y_a should be used ($y = y_a$).

The mixture mass rate (lbm/sec) is usually calculated first when applying multiphase choke model. The total mixture mass flux equation given by Sachdeva has the following form:

$$G_2 = c_d \left(288 g_c p_1 \rho_{m2}^2 \left(\frac{(1-x_1)(1-y)}{\rho_L} + \frac{x_1 k}{k-1} (V_{G1} - y V_{G2}) \right) \right)^{0.5} \quad (8.26)$$

where

G_2 = mass flux downstream (lbm/ft²/sec)

c_d = choke discharge coefficient

y = downstream-to-upstream pressure ratio ($\frac{p_2}{p_1}$)

ρ_{m2} = mixture density downstream (lbm/ft³)

ρ_L = liquid density (lbm/ft³)

By assuming the liquid phase is incompressible, and that gas expansion is isentropic, the downstream gas-specific volume (V_{G2}) can be calculated using Equation (8.24). Then the mixture density downstream (ρ_{m2}) can be calculated using the following equation:

$$\frac{1}{\rho_{m2}} = x_1 V_{G1} y^{-\frac{1}{k}} + (1-x_1) V_L \quad (8.27)$$

The mixture mass rate can be calculated by multiplying the mass flux by the choke port area as

$$M_2 = G_2 A \quad (8.28)$$

where

A = choke port area (ft²)

M_2 = mixture mass flow rate downstream (lbm/sec)

Assuming there is no time for phase changes as when mixture fluid flows through the choke port ($x_1 = x_2$), the mass rates for liquid and gas phase can be estimated by

$$M_{L2} = (1 - x_1)M_2 \quad (8.29)$$

$$M_{G2} = x_1M_2 \quad (8.30)$$

M_{G2} = gas phase mass flow rate downstream (lbm/sec)

M_{L2} = liquid phase mass flow rate downstream (lbm/sec)

The gas volumetric flow rate at the downstream choke can be determined using the gas law given the downstream pressure and temperature. The oil volumetric flow rate can be determined using oil P - V - T data or black oil correlations.

8.3.5.2 Perkins' Model

Perkins' model was based on the general energy equation. One important assumption that Perkins made is that the gas compressibility factor is constant at both upstream and downstream points. The Perkins model takes into account gas-oil-water three-phase flow. An equation to predict critical-subcritical ratio at the critical flow transition was provided as

$$\begin{aligned} & [2\lambda(1 - y_c^{(n-1)/n}) + 2\alpha_1(1 - y_c)] \left\{ \left[1 - \left(\frac{A_2}{A_1} \right)^2 \left(\frac{x_g + \alpha_1}{x_g y_c^{-1/n} + \alpha_1} \right)^2 \right] + \left(\frac{x_g}{n} y_c^{-(1+n)/n} \right) + \left(\frac{A_2}{A_1} \right)^2 \left(\frac{x_g}{n} \right) \frac{(x_g + \alpha_1)^2 y_c^{-(1+n)/n}}{(x_g y_c^{-1/n} + \alpha_1)^2} \right\} \\ & = \left[1 - \left(\frac{A_2}{A_1} \right) \left(\frac{x_g + \alpha_1}{x_g y_c^{-1/n} + \alpha_1} \right)^2 \right] (x_g y_c^{-1/n} + \alpha_1) \left[\lambda \left(\frac{n-1}{n} \right) y_c^{-1/n} + \alpha_1 \right] \end{aligned} \quad (8.31)$$

where

y_c = critical downstream-to-upstream pressure ratio

n = polytropic exponent for gas

x_g = free gas in-situ quality at upstream (mass fraction)

A_1 = upstream hydraulic flow area (ft²)

A_2 = downstream hydraulic flow area (ft²)

The polytropic exponent (n) was calculated using the same method as Sachdeva:

$$n = \left(\frac{x_g k c_{vg} + x_o c_{vo} + x_w c_{vw}}{x_g c_{vg} + x_o c_{vo} + x_w c_{vw}} \right) \quad (8.32)$$

where

k = heat specific ratio (c_p/c_v)

x_o = oil in-situ quality at upstream (mass fraction)

x_w = water in-situ quality at upstream (mass fraction)

c_{vg} = gas heat capacity at constant volume

c_{vo} = oil heat capacity at constant volume

c_{vw} = water heat capacity at constant volume

Both λ and α_1 are group parameters, and can be expressed as

$$\lambda = x_g + \frac{(x_g c_{vg} + x_o c_{vo} + x_w c_{vw}) M_w}{zR} \quad (8.33)$$

$$\alpha_1 = \frac{1}{V_{G1}} \left(\frac{x_o}{\rho_o} + \frac{x_w}{\rho_w} \right) \quad (8.34)$$

where

z = gas compressibility factor

R = universal gas constant, 10.73 psi-ft³/mole-R,
8.3145 kJ/kmol-K

M_w = molecular weight of gas

V_{G1} = upstream gas-specific volume (ft³/lbm)

ρ_o = oil density upstream (lbm/ft³)

ρ_w = water density upstream (lbm/ft³)

The downstream mixture fluid velocity (ft/sec) can be calculated by

$$u_2 = \sqrt{\frac{288g_c \left\{ \lambda p_1 V_{G1} \left[1 - y^{(n-1)/n} \right] + \left(\frac{x_o}{\rho_o} + \frac{x_w}{\rho_w} \right) p_1 (1 - y) \right\}}{1 - \left(\frac{A_2}{A_1} \right)^2 \left[\frac{(x_g + \alpha_1)}{(x_g y^{-1/n} + \alpha_1)} \right]^2}} \quad (8.35)$$

where

y = downstream-to-upstream pressure ratio (p_2 / p_1), if

$y < y_c$ then $y = y_c$

u_2 = mixture fluid velocity downstream (ft/sec)

The downstream mixture mass flow rate (lbm/sec) then is given by

$$M_2 = A_2 \rho_2 u_2 \quad (8.36)$$

where

ρ_2 = mixture fluid density downstream (lbm/ft³)

By assuming that the liquid phase (water and oil) is incompressible, the downstream mixture fluid density can be calculated as

$$\rho_2 = \frac{1}{x_g V_{G2} + \left(\frac{x_o}{\rho_o}\right) + \left(\frac{x_w}{\rho_w}\right)} \quad (8.37)$$

The downstream gas-specific volume (V_{G2}) is given by assuming the process is polytropic:

$$V_{G2} = V_{G1} y^{\left(-\frac{1}{n}\right)} \quad (8.38)$$

8.3.5.3 Sun et al.'s Modified Model

Sun et al. (2006) extended Sachedeva's work in order to make the model more suitable for down-hole conditions. This work is based upon assumptions similar to most of the published multiphase choke models:

- Horizontal flow through the choke throat
- No slippage and negligible frictional effect at the choke throat
- No time for phase changes at the choke throat
- Liquid is incompressible
- All phases are at the same temperature

Compared to Sachedeva's work, the improved model is extended by taking into account of oil-gas-water three-phase flow through the choke port. Polytropic processes were assumed, and the upstream-downstream geometry impact on choking flow was taken into account.

The polytropic exponent at gas-oil-water flow can be calculated using Equation (8.32), as Equation (8.39) permits calculating the upstream-downstream velocity ratio. This equation was developed based on material balance:

$$\beta = \frac{A_2}{A_1} \left(\frac{V_{G1} x_g + \frac{x_o}{\rho_o} + \frac{x_w}{\rho_w}}{V_{G1} y^{-\frac{1}{n}} x_g + \frac{x_o}{\rho_o} + \frac{x_w}{\rho_w}} \right) \quad (8.39)$$

where

β = upstream-downstream fluid velocity ratio (u_1 / u_2)

u_1 = mixture fluid velocity at upstream (ft/sec)

u_2 = mixture fluid velocity downstream (ft/sec)

A_1 = upstream hydraulic flow area (ft²)

A_2 = downstream hydraulic flow area (ft²)

The equation to predict the critical-subcritical ratio at the critical flow transition has the following form:

$$\frac{V_{G1} y_c^{-\frac{1}{n}} x_g \left(\frac{n}{n-1} \right) \left[1 - \left(\frac{1}{y_c} \right)^{\frac{n-1}{n}} \right] + \left(\frac{x_o}{\rho_o} + \frac{x_w}{\rho_w} \right) \left(1 - \frac{1}{y_c} \right)}{n(\beta^2 - 1) \left[x_g \left(V_{G1} y_c^{-\frac{1}{n}} - \left[\frac{x_o \rho_w + x_w \rho_o}{\rho_o \rho_w (x_o + x_w)} \right] \right) + \left(\frac{x_o \rho_w + x_w \rho_o}{\rho_o \rho_w (x_o + x_w)} \right) \right]^2} = 0 \quad (8.40)$$

The mixture mass flow rate (lbm/sec) can be calculated by

$$M_2 = A_2 c_d \left\{ \frac{288 g_c P_1 \left[V_{G1} y_c^{-\frac{1}{n}} x_g \left(\frac{n}{n-1} \right) \left(y - y_c^{-\frac{1}{n}} \right) + \left(\frac{x_o \rho_w + x_w \rho_o}{\rho_o \rho_w (x_o + x_w)} \right) (1 - x_g) (y - 1) \right]}{(\beta^2 - 1) \left[x_g \left(V_{G1} y_c^{-\frac{1}{n}} - \left(\frac{x_o \rho_w + x_w \rho_o}{\rho_o \rho_w (x_o + x_w)} \right) \right) + \left(\frac{x_o \rho_w + x_w \rho_o}{\rho_o \rho_w (x_o + x_w)} \right) \right]^2} \right\}^{\frac{1}{2}} \quad (8.41)$$

8.3.5.4 Applications of Multiphase Choke Flow

Whether using the Sachedeva's and Perkins' models, or that of Sun et al., the major drawback of these multiphase choke flow models is that they require free gas quality (the mass fraction of gas within the mixture) as an input parameter to determine the flow regime and flow rates. This param-

eter is usually unknown before production data such as GOR and WOR is available. In addition, as the down-hole flow control valve is normally working at high down-hole pressure and temperature conditions, the hydrocarbon phase behavior properties must be taken into account. Even with good production data, this feature makes estimation of the in-situ free gas quality more difficult.

Depending upon available information, two different approaches can be used to estimate the in-situ free gas quality, oil quality and water quality upstream of the down-hole valve. One method is to apply surface production data, while another is to use data from hydrocarbon P - V - T relations.

Figure 8–15 shows the calculation flow charts proposed by Sun et al. (2006) for the in-situ x_g , x_o , and x_w , when surface production data, that is, the gas-oil ratio (GOR), water-oil ratio (WOR), oil API and gas-specific gravity, are available. The oil API and gas-specific gravity (γ_g) can be used to estimate the in-situ oil solution gas ratio (R_s), oil formation volume factor (B_o) and oil density (ρ_{o1}) at the valve upstream by applying the black oil correlations of Standing (1947) or Vasquez-Beggs (1980). The water in-situ properties (water viscosity, volume factor B_w , and water density) can be estimated using the correlations of Gould (1974) and Van Wingen (1950), or to simplify calculation by using a constant value. Knowing the gas components or gas-specific gravity at surface (γ_g), the pseudoreduced pressure (P_{pr}) and pseudoreduced temperature (T_{pr}) can be calculated per Guo-Ghalambor (2005). The gas compression factor can be calculated from the Brill-Beggs z-factor correlation (1974) or the Hall-Yarborough z-factor correlation (1973). Then, the in-situ free gas, oil, and water qualities can be estimated using the equations below:

$$x_g = \frac{\xi}{\xi + 5.615\rho_{o1}B_o + 350.52\gamma_w WOR} \quad (8.42)$$

$$x_o = \frac{5.615\rho_{o1}B_o}{\xi + 5.615\rho_{o1}B_o + 350.52\gamma_w WOR} \quad (8.43)$$

$$x_w = 1 - x_o - x_g \quad (8.44)$$

$$\xi = 0.0765\gamma_g (GOR \times 10^6 - R_s) \quad (8.45)$$

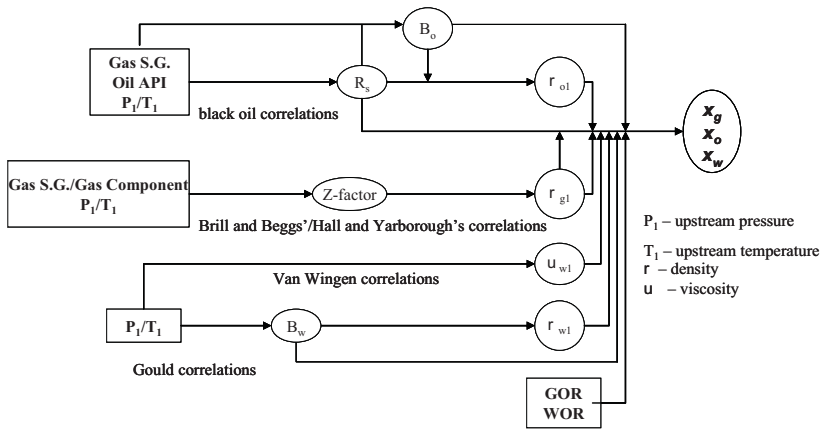


Figure 8–15 Procedure for calculating free gas quality.

where

GOR = gas-oil ratio (MMscf/stb)

WOR = water oil ratio (stb/stb)

R_s = solution gas-oil ratio (scf/stb)

B_w = water in-situ volume factor (bbl/stb)

B_o = oil in-situ volume factor (bbl/stb)

γ_w = water specific gravity (pure water = 1)

γ_g = gas-specific gravity (air = 1)

ρ_{oi} = oil in-situ density at valve upstream (lbm/ft³)

ξ = parameters group (lbm/STB)

8-4 SAMPLE PROBLEM

A 5-1/2-in shrouded down-hole control valve is installed to control hydrocarbon production from one pay zone. Oil, water and gas are measured at the surface, where the GOR and the WOR from this pay zone are 0.00286 MMSCF/STB and 0.1 STB/STB. The oil, water and gas properties are listed in Table 8–1. The valve has a full open flow area equal to 16.34 in², and is opened remotely to 4%. The upstream hydraulic flow area of the

Table 8–1 Fluid Property Data

Oil API Gravity	30 API
	0.848 (pure water = 1)
Oil Bubble point, p_b	3500 psi
Water Specific Gravity	1.020 (pure water = 1)
Gas Specific Gravity	0.872 (air = 1)
Cvo (heat capacity of oil)	0.430 BTU/(lbm-R)
Cvw (heat capacity of water)	1.000 BTU/(lbm-R)
Cvg (heat capacity of gas)	0.583 BTU/(lbm-R)
k (heat specific gravity of gas)	1.254

valve is calculated as 22.3 in². After compensating for the hydrostatic/frictional pressure drop, the in-situ upstream/downstream pressures measured by the down-hole gauges are 2920 psi and 2810 psi, respectively. The measured fluid temperature through the valve is 185°F. If the valve discharge coefficient is given as 0.843, estimate the mixture production rate and flowing velocity through the valve. The oil properties are assumed to be represented by Standing's correlation.

SOLUTION

1) Gas quality, water quality and oil quality calculations

The pressure of interest (upstream choke pressure) is less than the oil bubble pressure, and solution gas is also released at the point of interest. Applying Standing's correlation to estimate R_s and formation volume factor B_o at the upstream choke gives

$$\begin{aligned}
 R_s &= \gamma_g \left(\frac{p}{18 \times 10^{(0.00091T - 0.0125\gamma_{API})}} \right)^{1.204} \\
 &= 0.872 \times \left(\frac{2920}{18 \times 10^{(0.00091 \times 185 - 0.0125 \times 30)}} \right)^{1.204} \\
 &= 708 \text{ SCF/STB}
 \end{aligned}$$

$$\begin{aligned}
 B_o &= 0.972 + 0.000147 \left(R_s \left(\frac{\gamma_g}{\gamma_o} \right)^{0.5} + 1.25T \right)^{1.175} \\
 &= 0.972 + 0.000147 \times \left(708 \times \left(\frac{0.872}{0.848} \right)^{0.5} + 1.25 \times 185 \right)^{1.175} \\
 &= 1.429 \text{ rb/STB}
 \end{aligned}$$

Gould (1974) correlation is used for water density and water formation volume factor:

$$\begin{aligned}
 B_w &= 1 + 0.00012 \times (185 - 60) + 0.000001 \times (185 - 60)^2 - 0.00000333 \times 2920 \\
 &= 1.021 \text{ rb/STB}
 \end{aligned}$$

Water density (lbm/ft³) at the valve is

$$\rho_w = 1.02 \times \frac{62.4259}{1.021} = 62.37 \text{ lbm/ft}^3$$

Brill and Beggs (1974) correlation is used to estimate z-factor at 2920 psi and 185°F:

$$z_1 = 0.792$$

Gas density at the valve is estimated by

$$\begin{aligned}
 \rho_{G1} &= \frac{2.7\gamma_g p_1}{z_1 T_1} \\
 &= \frac{2.7 \times 0.872 \times 2920}{0.792 \times (185 + 459.67)} \\
 &= 13.465 \text{ lbm/ft}^3
 \end{aligned}$$

Oil density at the valve is estimated by

$$\begin{aligned}\rho_{ol} &= \frac{350\gamma_o + 0.0764\gamma_g R_s}{5.615B_o} \\ &= \frac{350 \times 0.848 + 0.0764 \times 0.872 \times 708}{5.615 \times 1.429} \\ &= 44.11 \text{ lbm/ft}^3\end{aligned}$$

Apply Equations (8.42), (8.43), and (8.44) to give

$$\begin{aligned}x_g &= \frac{0.0765 \times 0.872 \times (0.00286 \times 10^6 - 708)}{0.0765 \times 0.872 \times (0.00286 \times 10^6 - 708) + 5.615 \times 44.11 \times 1.429 + 350.376 \times 62.37 \times 1.021 \times 0.1} \\ &= 0.269\end{aligned}$$

$$\begin{aligned}x_o &= \frac{5.615 \times 44.11 \times 1.429}{0.0765 \times 0.872 \times (0.00286 \times 10^6 - 708) + 5.615 \times 44.11 \times 1.429 + 350.376 \times 62.37 \times 1.021 \times 0.1} \\ &= 0.664\end{aligned}$$

$$\begin{aligned}x_w &= 1 - x_g - x_o \\ &= 1 - 0.269 - 0.664 \\ &= 0.067\end{aligned}$$

2) Gas polytropic exponent calculations

Apply Equation (8.32) to calculate the gas polytropic exponent (n):

$$\begin{aligned}n &= \left(\frac{x_g k c_{vg} + x_o c_{vo} + x_w c_{vw}}{x_g c_{vg} + x_o c_{vo} + x_w c_{vw}} \right) = \left(\frac{0.269 \times 1.254 \times 0.538 + 0.664 \times 0.43 + 0.067 \times 1}{0.269 \times 0.538 + 0.664 \times 0.43 + 0.076 \times 1} \right) \\ &= 1.074\end{aligned}$$

3) Using Equations (8.39) and (8.40) to determine the critical-subcritical ratio

The upstream-downstream fluid velocity ratio (β) is

$$\beta = \frac{A_2}{A_1} \left(\frac{V_{G1} x_g + \frac{x_o}{\rho_o} + \frac{x_w}{\rho_w}}{V_{G1} y^{-\frac{1}{n}} x_g + \frac{x_o}{\rho_o} + \frac{x_w}{\rho_w}} \right)$$

$$= \frac{16.34 \times 0.04}{22.3} \left(\frac{\frac{1}{13.465} \times 0.269 + \frac{0.664}{44.11} + \frac{0.067}{62.37}}{\frac{1}{13.465} \times y^{\left(-\frac{1}{1.074}\right)} \times 0.269 + \frac{0.664}{44.11} + \frac{0.067}{62.37}} \right)$$

The critical-subcritical ratio is involved in

$$\frac{1}{13.465} y_c^{-\frac{1}{1.074}} 0.269 \left(\frac{1.074}{1.074-1} \right) \left[1 - \left(\frac{1}{y_c} \right)^{\frac{1.074-1}{1.074}} \right] + \left(\frac{0.664}{44.11} + \frac{0.067}{62.37} \right) \left(1 - \frac{1}{y_c} \right)$$

$$= \frac{1.074(\beta^2 - 1) \left[0.269 \left(\frac{1}{13.465} y_c^{-\frac{1}{1.074}} - \left[\frac{0.664 \times 62.37 + 0.067 \times 44.11}{62.37 \times 44.11 \times (0.664 + 0.067)} \right] \right) + \left(\frac{0.664 \times 62.37 + 0.067 \times 44.11}{62.37 \times 44.11 \times (0.664 + 0.067)} \right) \right]^2}{2 \times 0.269 \times \frac{1}{13.465} y_c^{-\frac{1}{1.074}}}$$

= 0

The critical-subcritical ratio (y_c) can be solved numerically to yield $y_c = 0.509$ and $\beta = 0.020$.

4) Calculating the liquid and gas rates

Because $\left(\frac{2810}{2920} \right) = 0.962 > 0.506$, subcritical flow exists and

Equation (8.41) is used to calculate mass rate:

$$M_2 = \left(\frac{16.34 \times 0.04}{144} \right) \times (0.843) \times$$

$$\left\{ \frac{288 \times (32.17) \times 2920 \left[\frac{1}{13.465} (0.962)^{\left(\frac{1}{1.074}\right)} 0.269 \left(\frac{1.074}{1.074-1} \right) \left(0.962 - 0.962^{\left(\frac{1}{1.074}\right)} \right) + \left(\frac{0.664 \times 62.37 + 0.067 \times 44.11}{62.37 \times 44.11 \times (0.664 + 0.067)} \right) (1 - 0.269)(0.962 - 1) \right]}{(0.020^2 - 1) \left[0.269 \left(\frac{1}{13.465} \times 0.962^{-\frac{1}{1.074}} - \left(\frac{0.664 \times 62.37 + 0.067 \times 44.11}{62.37 \times 44.11 \times (0.664 + 0.067)} \right) \right) + \left(\frac{0.664 \times 62.37 + 0.067 \times 44.11}{62.37 \times 44.11 \times (0.664 + 0.067)} \right) \right]^2} \right\}^{\frac{1}{2}}$$

which gives $M_2 = 18.34$ lbm/s. Thus,

$$M_g = M_2 \times x_g = 18.34 \times 0.269 = 4.93 \text{ lbm/s}$$

$$M_o = M_2 \times x_o = 18.34 \times 0.664 = 12.18 \text{ lbm/s}$$

$$M_w = M_2 \times x_w = 18.34 \times 0.067 = 1.23 \text{ lbm/s}$$

In field units, the free gas, oil, and water flow rates through the valve are

$$Q_g = \frac{M_g \times 24 \times 60 \times 60}{\rho_{G1}} = \frac{4.93 \times 24 \times 60 \times 60}{13.465 \times 1,000,000} \approx 0.032 \text{ MMcf/D}$$

$$Q_o = \frac{M_o \times 24 \times 60 \times 60}{\rho_{o1} \times 5.615 \times B_o} = \frac{12.18 \times 24 \times 60 \times 60}{44.11 \times 5.615 \times 1.429} \approx 2973 \text{ STBD}$$

$$Q_w = \frac{M_w \times 24 \times 60 \times 60}{\rho_{w1} \times 5.615 \times B_w} = \frac{1.23 \times 24 \times 60 \times 60}{62.37 \times 5.615 \times 1.021} \approx 297 \text{ STBD}$$

5) Calculating fluid velocities

Equation (8.37) can be used to calculate mixture fluid density:

$$\begin{aligned} \rho_{m2} &= \frac{1}{x_g V_{G2} + \left(\frac{x_o}{\rho_o}\right) + \left(\frac{x_w}{\rho_w}\right)} \\ &= \frac{1}{0.269 \times \left(\frac{1}{13.465}\right) (0.962)^{\left(\frac{-1}{1.074}\right)} + \left(\frac{0.664}{44.11}\right) + \left(\frac{0.067}{62.37}\right)} \\ &= 27.15 \text{ lbm/ft}^3 \end{aligned}$$

Then the mixture fluid velocity through the valve is estimated:

$$\begin{aligned}u_2 &= \frac{M_2}{A_2 \rho_{m2}} \\ &= \frac{18.34}{\frac{16.34 \times 0.04}{144}} \times 27.15 \\ &\approx 149 \text{ ft/sec}\end{aligned}$$

If reservoir fluid P - V - T data is available, the in-situ free gas quality can be estimated by calculating the released gas volume and assuming that the gas-liquid phase is moving at the same velocity in the wellbore.

Note: The introduced method assumed that the gas and liquid phases are moving at the same velocity along the production string, which in many situations is not true. Therefore, the above method can be used as a rough estimate for the liquid-gas flow rate through the down-hole valve. To make the estimation more accurate, liquid holdup in the tubular string must be taken into account.

8.4 Well Deliverability

Well deliverability is determined by the combination of well inflow performance and wellbore flow performance. The former describes the deliverability of the reservoir; the latter is a function of the resistance of the production string to the outflow. This section focuses on the prediction of achievable fluid production rates from multiple zone intelligent well systems.

8.4.1 NODAL Analysis Approach

NODAL Analysis (a Schlumberger patent) is the commonly accepted technology for analyzing well deliverabilities. Fluid properties change with location-dependent pressure and temperature changes in an oil and gas production system. To simulate the fluid flow in a system, it is necessary to “break” the system into discrete nodes that separate the system

elements (equipment sections). Fluid properties at the elements can then be evaluated locally. The analysis determines fluid production rates and pressures at specified nodes. NODAL analysis is performed assuming pressure continuity—that is, there will be only one unique pressure value at a given node regardless of whether the pressure is evaluated from the performance of upstream or downstream equipment. The performance curve (pressure-rate relation) of the upstream equipment is called the “inflow performance curve”; the performance curve of downstream equipment is called the “outflow performance curve.” The intersection of the two performance curves defines the operating point—that is, the operating flow rate and pressure at the specified node. NODAL analysis is usually conducted using the bottom-hole or wellhead as the solution node. For specific purposes, the solution node may be chosen at any place along the production string.

8.4.2 Integrated IPR Approach

Intelligent wells are normally operated with multiple-zone production/injection in a commingled completion, which makes it difficult to predict the effect of wellbore pressure on well and zonal deliverability. This is because

- The production string, down-hole control equipment and isolation tools separate the production fluids into different flow paths. The different flow paths show different resistance to each zone’s outflow—that is, the control valve operation and the varied hydraulic inside diameters along each path.
- The reservoir and fluid properties such as pressure, temperature, reservoir deliverability, solution gas-oil ratio, bubble-point pressure, etc., of individual zones are normally different. These varying properties will cross-impact the outflow of the other zones when the fluids are commingled.
- Down-hole choke operations will affect the wellbore pressure profile, thus affecting the production profile from each zone.

For example, in Figure 8–16, the upper sand production fluid flows through the annulus between casing and tubing string and then passes into the upper control valve; the lower sand production fluid flows inside the

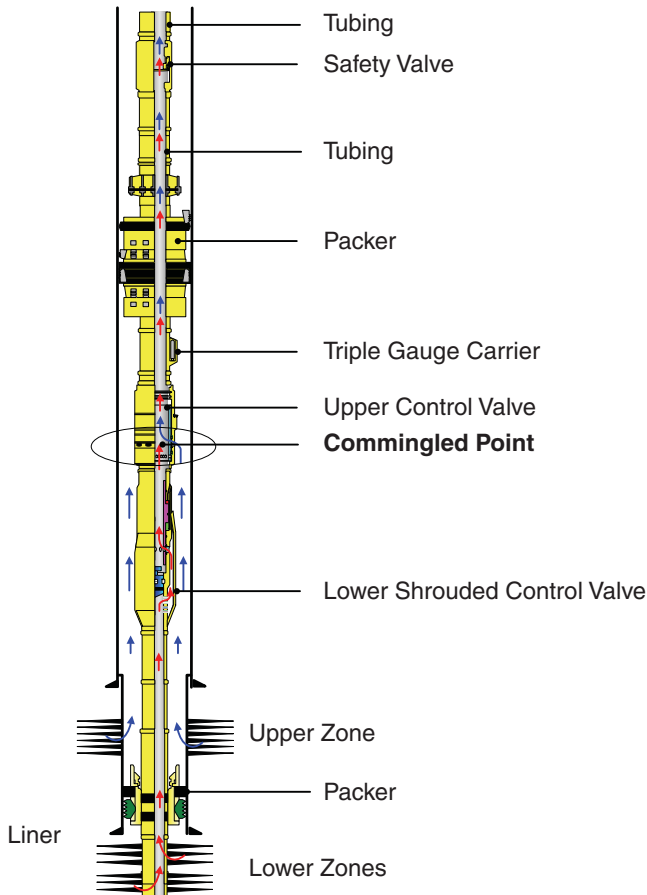


Figure 8–16 A typical two-zone IWS system. (Courtesy Baker Oil Tools)

tubing string and is controlled by the lower shrouded valve. Therefore, before commingled production, except for heat transfer, the two zone fluids flow independently through isolated paths. The flow port position of the upper control valve at the downstream side is the commingled production point, when both zones produce at the same time. Because the two production fluids flow in separate paths and are controlled by separate control valves, choking the two control valves affects the outflow capability of the two zones. The depths of the two reservoir zones and the different hydraulic inside diameters of the two flow paths create different hydrostatic and frictional pressure drops, also affecting the outflow capability of the two zones.

A technique called “integrated” IPR is used to account for each flow path’s impact on each zone’s outflow, and to model the cross-impact of each zone. A basic assumption of this technique is the pressure-system-balance, meaning that when the two zone’s production fluids are commingled, the pressure system at the commingled point is balanced at steady-state flow. The key of this technique is to integrate each zone’s inflow performance relationship (IPR) with each flow path and down-hole control valve’s flow performance to generate pressure versus flow-rate relationships that correspond to the commingled production point. Based upon the assumption of pressure-system-balance at the commingled point, the generated pressure versus flow-rate relationships can be combined. The well production rate, zonal production allocations and wellbore pressure profile can then be predicted using conventional NODAL analysis by choosing the commingled point as the solution node. In fact, the concept of integrated IPR is used in Chapter 7 for multilateral wells.

Figures 8–17 through 8–21 illustrate the analysis process using the integrated IPR technique for a two-zone intelligent well system (Figure 8–16). This system can be simplified as a NODAL network (Figure 8–17) for further analysis. Each zone’s reservoir deliverability can be expressed by an IPR model. This IPR model can be integrated with tubing flow models and choke flow models to generate pressure versus flow-rate relationships that correspond to the position of the upper control valve port (commingle point). Figure 8–18 shows the integrated inflow performance relationship of the upper zone with the upper control valve 3% open. Figure 8–19 is the integrated inflow performance relationship of the lower zone with the lower shrouded control valve 100% open. When the flowing pressure is lower than the oil bubble point, multiphase flow models must be applied to generate the integrated IPR curves. Then, the two pressure versus flow-rate relationships can be combined with the same series of pressures, as illustrated in Figure 8–20, yielding a combined inflow curve. By choosing the commingled point as the solution node, the outflow curve within the tubular segment from the upper control valve port (commingle point) to the wellhead can then be generated. The intersection of the two performance curves defines the operating point as the commingle point—that is, the point defined by the coordinates of the total expected production rate and the pressure at the commingle point. Thus, the production allocations of each zone can be predicted by reading each zone’s integrated pressure versus flow-rate relationship curve. This analysis is illustrated in Figure 8–21.

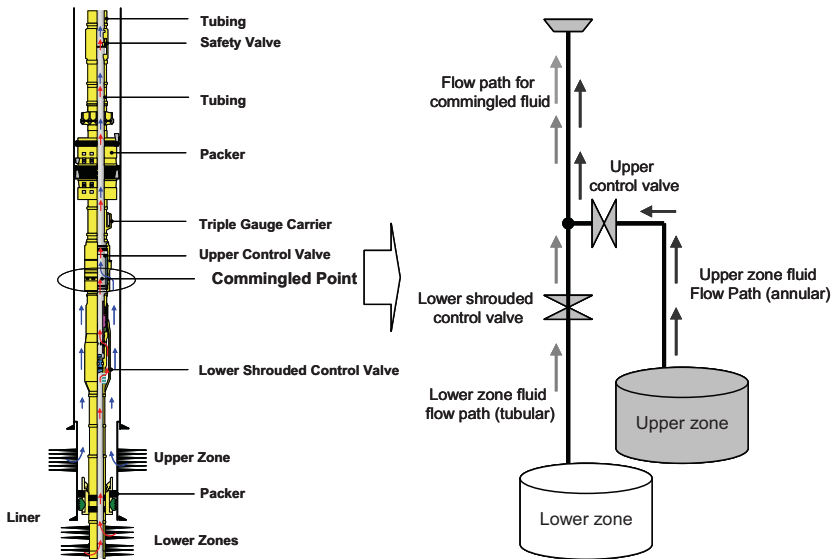


Figure 8–17 Simplified node network of the two-zone IWS system.

The IPR of individual zones can be described using the generalized Vogel model (see Chapter 4). The flow in the well tubing or annulus can be described by the flow models (see Chapter 5). Figure 8–18 shows the upper-zone IPR and the integrated IPR of the upper zone that corresponds to the commingle point with the upper control valve 3% open. Figure 8–19 presents the lower-zone IPR and the integrated IPR of the lower zone corresponding to the commingle point with the lower control valve 100% open. The combination of these two integrated IPR curves is illustrated in Figure 8–20, which indicates that zonal cross-flow occurs when the pressure at the commingle point is greater than 3300 psi. Figure 8–21 plots the integrated IPR and outflow performance curves to determine the operating point and production allocations from the upper and lower zones.

One concern in using the analysis method is that the properties of the mixture production fluid—such as temperature, density, viscosity, solution gas-oil ratio, water cut, etc.—are not known because production fluid allocations from each zone are not known for calculating the tubing outflow curve. Therefore, the mixture fluid properties must be assumed and an operating point predicted initially as an approximate value. To address this issue, an iterative calculation method can be used.

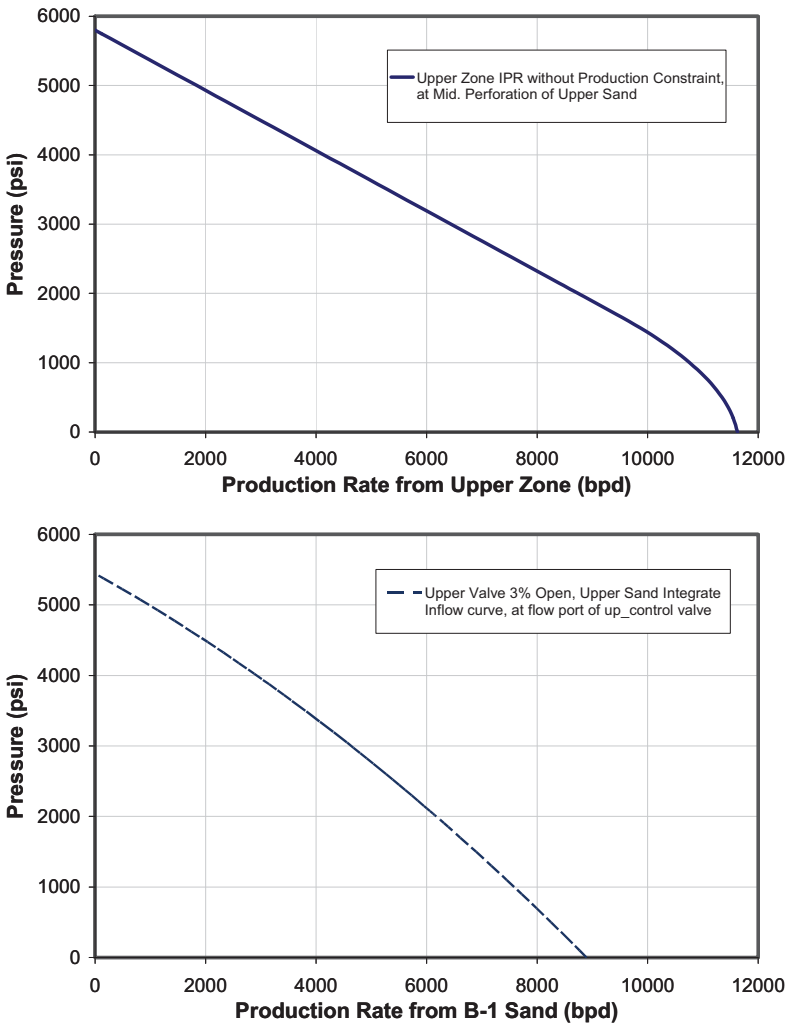


Figure 8–18 Integrated IPR of upper zone corresponding to the commingled production with the upper control valve 3% open.

8.4.3 Cross-Flow Control

Although cross-flow is seldom seen in intelligent well systems, one of the concerns about commingled production is the risk of potential cross-flow when the zonal reservoir properties are different. The integrated IPR procedure provides a way to predict potential cross-flow in commingled

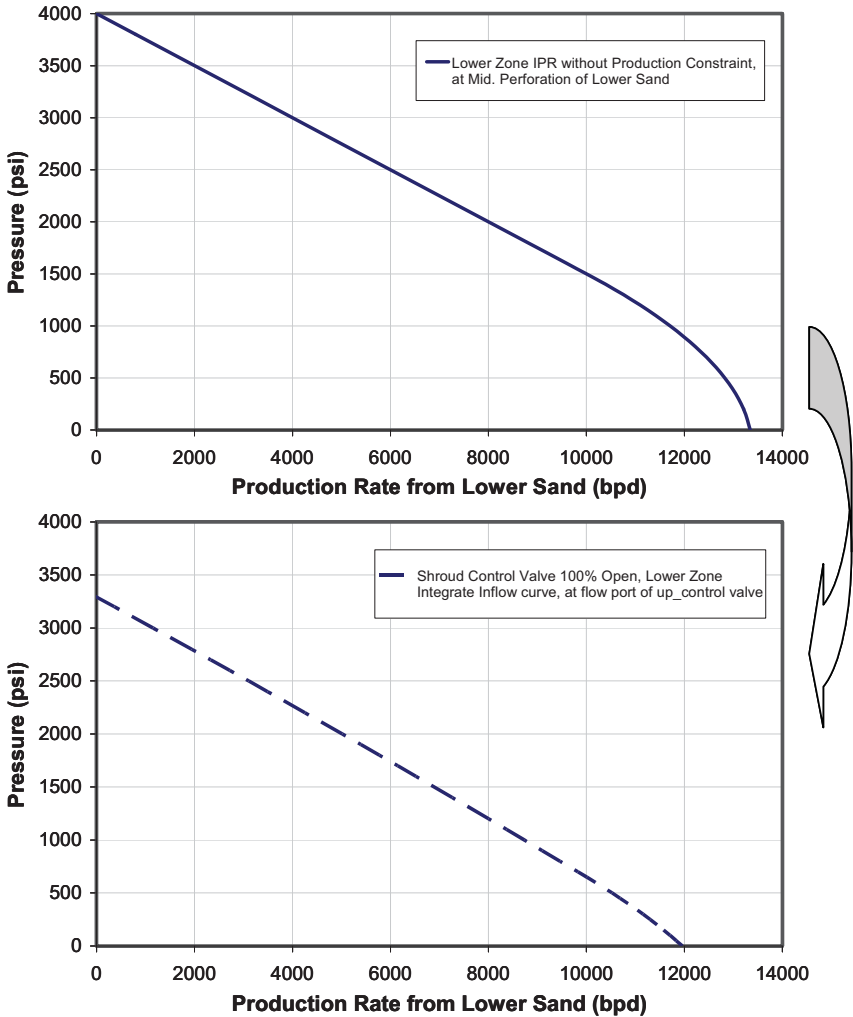


Figure 8–19 Integrated IPR of lower zone corresponding to the commingle point with the lower shrouded control valve 100% open.

production. The integrated IPR curve of the upper zone in Figure 8–18 shows that the commingle-point pressure should not be allowed to be higher than 5400 psi. If the pressure is higher than this, the flow rate of the upper zone will be negative. Figure 8–19 shows that the flow rate from the lower zone will be negative if the commingle-point pressure is higher than 3300 psi. Therefore, for this intelligent well system, 3300 psi is the

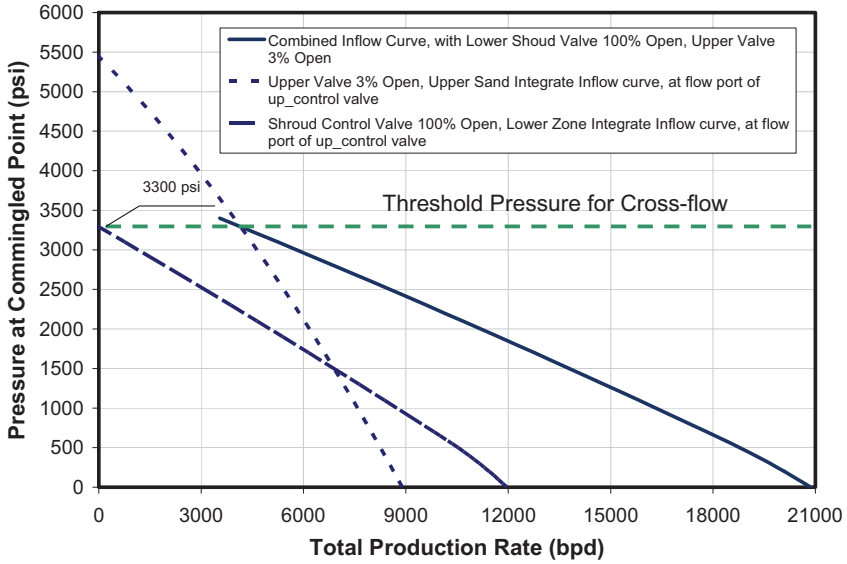


Figure 8-20 Combined inflow curve at the commingle point (upper control valve port).

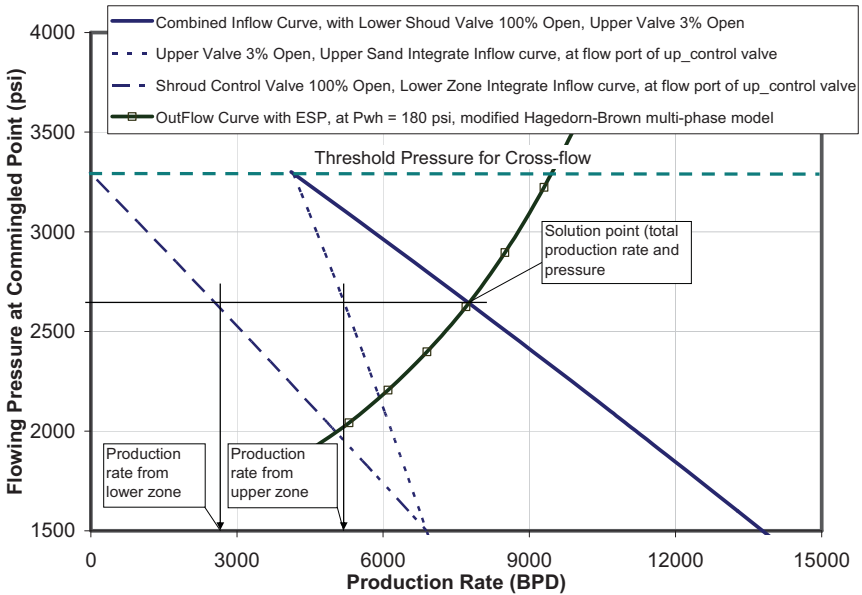


Figure 8-21 Operating point and production allocations.

threshold commingle-point pressure. When the pressure at the commingle point is higher than this value, no oil is produced from the lower zone; instead, production fluid from the upper zone will cross-flow into the lower zone. Both Figures 8–20 and 8–21 illustrate how to use the integrated IPR method to determine this threshold pressure. To ensure that oil from both zones is produced, the commingle-point pressure should be controlled to be lower than this threshold pressure. For example, the wellhead choke can be opened up to decrease backpressure and to decrease the commingle-point pressure. Down-hole-choking the high-pressure zone can also decrease the downstream pressure to avoid cross-flow.

In an intelligent well system, down-hole gauges are normally installed close to the commingle point to monitor the in-situ pressure and temperature at this position. The monitoring data can be compared with the calculated threshold pressure to determine if there is a possibility of inter-layer cross-flow.

8-5 SAMPLE PROBLEM

A deep-water two-zone IWS producer is illustrated in Figure 8–7. The water depth is 8325 ft. The reservoir information is provided in Table 8–2. The upper zone has a higher productivity index of 1.553 bpd/psi and a higher water cut of 50%. The lower zone has productivity index of 0.873 bpd/psi and water cut of 5%. The upper zone is controlled by a 4 1/2-in valve and the lower zone is controlled by a 3 1/2-in shrouded valve. The wellhead pressure is regulated to 8,000 psi. Since the lower zone has a lower water cut, it is preferable to produce more oil from the lower zone. Based on the zonal reservoir and productivity index information, upper valve choking is necessary to maximize oil production. The upper valve is 1.4% open. The lower shrouded valve is 100% open. Calculate the flow contributions from each zone and the tool's working conditions in this operation scenario. Analyze the impact of various down-hole choking operations on flow contribution. The well completion information is shown in Table 8–3.

SOLUTION

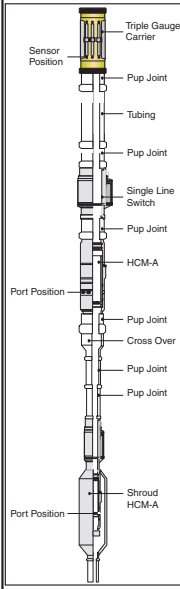
A computer program was developed to analyze the well performance under various down-hole-choking operations. As the target wellhead pressure was much higher than the oil bubble point, single phase liquid flow was assumed.

Table 8–2 Reservoir and Production Target Data

Reservoir Information	
Upper Zone	1.553 bdp/psi
Reservoir Pressure	19700 psi
Temp (mainbore)	257 °F
Solution GOR	175 scf/std
Oil Bubble Point	1200 psi
Oil Viscosity	13 cp
Oil Gravity	21.5 API
Gas S.G.	0.8 (air=1)
Initial WCUT	50.00%
Mid. Perf (TVD)	24200 ft
Lower Zone	0.873 bdp/psi
Reservoir Pressure	19700 psi
Temp. (sidebore)	258 °F
Solution GOR	205 scf/std
Oil Bubble Point	1200 psi
Oil Viscosity	21 cp
Oil Gravity	23 API
Gas S.G.	0.8 (air=1)
Initial WCUT	5.00%
Mid. Perf (TVD)	24721 ft
Operation Information	
WHP	8000 psi
Completion string roughness	0.0018
Water Specific Heat	1.00 BTU/lbm-R
Oil Specific Heat	0.43 BTU/lbm-R
Gas Specific Heat	0.525 BTU/lbm-R

Table 8–3 Completion String and Reservoir/Operation Data of a Full Wellbore Model

Reservoir Information		Wellhead	Tub str. OD (in)	Tub str. ID (in)	Casing OD (in)	Casing ID (in)	Wellbore ID (in)	MD Top (ft)	MD Bot. (ft)	Item Len. (ft)	TVD Top (ft)	TVD Bot. (ft)
Upper Zone	1,553 bpd/psi	Sea Floor	--	--	--	--	8325	8325	--	--	--	8325
Reservoir Pressure	19700 psi	4-1/2" tubing	4.500	3.826	9.875	8.625	12	8325	11500	3175	8325	11258
Temp (mainbore)	257 F	4-1/2" Safety Valve	7.125	3.740	9.875	8.625	12	11500	11510	10	11258	11268
Solution GOR	175 scf/std	tubing	4.500	3.826	9.875	8.625	12	11510	24600	13090	11268	23399
Oil Bubble Point	1200 psi	Packer	8.625	3.875	9.875	8.625	12	24600	24612	12	23399	23410
Oil viscosity	13 cp	tubing	4.500	3.826	9.875	8.625	12	24612	24643	31	23410	23439
Oil Gravity	21.5 API	Gauge mandrel:	5.800	3.875	9.875	8.625	12	24643	24651	8	23439	23446
Gas S.G	0.8 (air=1)	Pup Joint:	4.500	3.826	9.875	8.625	12	24651	24657	6	23446	23452
Initial WCUT	50.00%	Tubing:	4.500	3.826	9.875	8.625	12	24657	24712	55	23452	23503
Mid. Perf (TVD)	24721 ft	Pup Joint:	4.500	3.826	9.875	8.625	12	24712	24718	6	23503	23508
		Stepper Carrier	5.000	3.826	9.875	8.625	12	24718	24723	5	23508	23513
Lower Zone	0.873 bpd/psi	4-1/2 Valve:	7.125	3.688	9.875	8.625	12	24723	24735	12	23513	23524
Reservoir Pressure	19700 psi	Choke Port Pos.:	5.855	3.688	9.875	8.625	12	24731	--	--	23520	--
Temp. (sidebore)	258 F	FlowPath to Up_Zone (annulus flow)	Tub str. OD (in)	Tub str. ID (in)	Casing OD (in)	Casing ID (in)	Wellbore ID (in)	MD Top (ft)	MD Bot. (ft)	Item Len. (ft)	TVD Top (ft)	TVD Bot. (ft)
Solution GOR	205 scf/std	Frac-pack packer	--	--	--	--	8.625	12	25050	--	--	--
Oil Bubble Point	1200 psi	Valve Choke Port Pos.:	5.855	3.688	9.875	8.625	12	24731	--	--	23520	--
Oil viscosity	21 cp	Valve Assembly Bottom	5.855	3.688	9.875	8.625	12	--	24735	--	--	23524
Oil Gravity	23 API	Pup joint:	4.500	3.826	9.875	8.625	12	24735	24750	15	23524	23538
Gas S.G	0.8 (air=1)	Cross-Over upper side:	4.500	3.826	9.875	8.625	12	24750	24751	1	23538	23539
Initial WCUT	5.00%	Cross-Over lower side:	3.500	3.826	9.875	8.625	12	24751	24752	1	23539	23540
Mid. Perf (TVD)	24721 ft	Pup joint:	3.500	2.992	9.875	8.625	12	24752	24767	15	23540	23554
Operation Information	WHP 8000 psi	3-1/2 Shroud Valve:	7.000	2.812	9.875	8.625	12	24767	24788	21	23554	23573
		3-1/2 Valve Port Position:	7.000	2.812	9.875	8.625	12	24767	24777	10	23554	23563
		3-1/2 Valve Port-Bot:	7.000	2.812	9.875	8.625	12	24777	24782	5	23563	23568
		Shroud/Perf. Pup	7.000	2.812	9.875	8.625	12	24782	24787	5	23568	23572
		Crossover 7.625 x 4 1/2	7.000	2.812	9.875	8.625	12	24787	24788	1	23572	23573
		Tubing to Up Frac-Pack Packer	3.500	2.812	9.875	8.625	12	24788	25050	262	23573	23816
		GP Item	Centub OD	Centub ID	GP As. OD	GP Ass. ID	Wellbore ID (in)	MD (top)	MD (Bot)	Item length	TVD Top	TVD Bot
		Snap Latch seal Assembly	3.500	2.992	6.5	4.875	12	25050	25066	16	23816	23831
		Extention	3.500	2.992	6.5	5.500	12	25066	25076	10	23831	23840
		6-5/8x5-1/2x3-1/2 SAF-1	3.500	2.992	6.5	4.61	12	25076	25081	4.5	23840	23844
		Blank Pipe/Tub	3.500	2.992	6.5	4.67	12	25081	25190	109	23844	23945
		Sand Screen Length	3.500	2.992	6.5	4.892	12	25190	25600	410	23945	24325
		FlowPath to low_Zone (tubing flow)	Tub str. OD (in)	Tub str. ID (in)	Casing OD (in)	Casing ID (in)	Wellbore ID (in)	MD Top (ft)	MD Bot. (ft)	Item Len. (ft)	TVD Top (ft)	TVD Bot. (ft)
		Valve Choke Port Pos.:	5.855	3.688	9.875	8.625	12	24731	--	--	23520	--
		Valve assembly Bottom	5.855	3.688	9.875	8.625	12	--	24735	--	--	23524
		Pup joint:	4.500	3.826	9.875	8.625	12	24735	24750	15	23524	23538
		Cross-Over upper side:	4.500	3.826	9.875	8.625	12	24750	24751	1	23538	23539
		Cross-Over lower side:	3.500	3.826	9.875	8.625	12	24751	24752	1	23539	23540
		Pup joint:	3.500	2.992	9.875	8.625	12	24752	24767	15	23540	23554
		3-1/2 Shroud Valve:	7.000	2.812	9.875	8.625	12	24767	24788	21	23554	23573
		3-1/2 Valve Port Position:	4.280	2.812	7.000	6.004	12	24767	24777	10	23554	23563
		3-1/2 Valve Port-Bot:	4.280	2.812	7.000	6.004	12	24777	24782	5	23563	23568
		Shroud/Perf. Pup	3.500	2.812	7.000	6.004	12	24782	24787	5	23568	23572
		Crossover 7.625 x 4 1/2	7.000	2.812	9.875	8.625	12	24787	24788	1	23572	23573
		Tubing to Up Frac-Pack Packer	3.500	2.812	9.875	8.625	12	24788	25050	262	23573	23816
		GP Item	Centub OD	Centub ID	GP As. OD	GP Ass. ID	Wellbore ID (in)	MD (top)	MD (Bot)	Item length	TVD Top	TVD Bot
		Centre tub pup	3.500	2.992	7.840	4.875	12	25050	25066	16	23816	23831
		Extention	3.500	2.992	7.840	5.500	12	25066	25076	10	23831	23840
		6-5/8x5-1/2x3-1/2 SAF-1	3.500	2.992	6.500	4.610	12	25076	25081	5	23840	23844
		Blank Pipe/Tub	3.500	2.992	6.050	4.670	12	25081	25190	109	23844	23945
		Up Sand Screen Length	3.500	2.992	6.500	4.892	12	25190	25600	410	23945	24325
		3.5 Tub Pup to CMP	3.500	2.992	6.500	4.892	12	25600	26100	500	24325	24721
		Valve Choking Information	Sealbore ID (in)	Choke Open	Choke Open	Choke Open	Choke Open	Choke Open	Choke Open	Choke Open	Choke Open	Choke Open
		Upper 4-1/2 Valve	3.688	1.4%	20.0%	15.0%	10.0%	7.0%	5.0%	3.0%	1.5%	0.5%
		Lower Shroud 3-1/2 Valve	2.812	100.0%	100.0%	15.0%	10.0%	7.0%	5.0%	3.0%	1.5%	1.0%



1) Integrated IPR and Operating Point Determination

The commingle point (the upper control valve port) was chosen as the solution node. Figure 8–22 shows the integrated inflow performance relationship of each zone, the combined inflow performance relationship at the solution node, and the outflow performance curve.

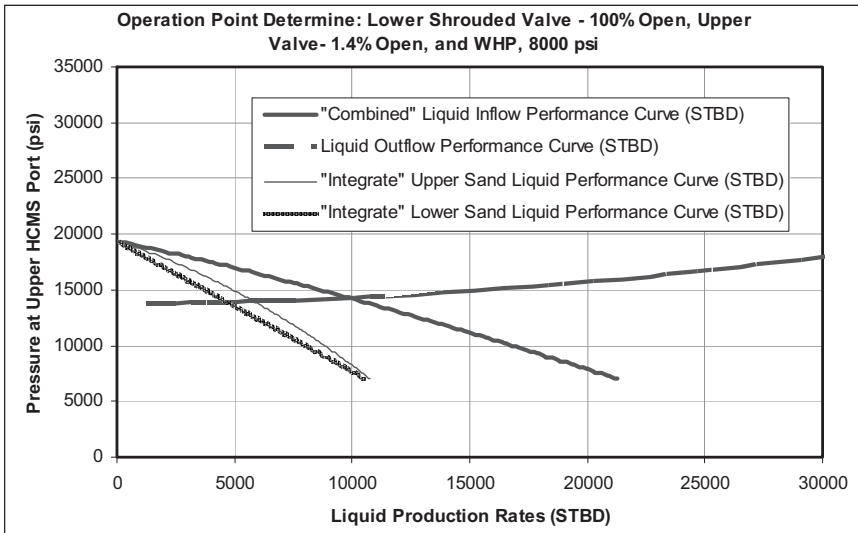


Figure 8–22 Determination of operating point using the integrated IPR approach.

2) Flow Contributions and Wellbore Conditions

Flow contributions: The intersection of the two performance curves (the “Combined” inflow performance relationship and the outflow performance curve) defines the operating point at the commingle point—that is, the total production rate and the pressure at the commingle point. The predicted total liquid rate was about 9950 STBD, the mixture water liquid ratio (WLR) was about 30.3%, and the commingle-point pressure was about 14235 psi. The production contributions of each zone can be predicted by reading each zone’s integrated pressure versus flow-rate relationship. Figure 8–23 shows the predicted production contributions from each zone. The liquid production contribution from the upper zone is about 5600 STBD. The liquid production contribution from the lower zone is about 4350 STBD. Thus, the lower zone contributes 44% of liquid production.

Tool’s working condition: The flowing profile, pressure profile, temperature profile, fluid properties and zonal reservoir deliverability for any choking scenario can be simulated by the computer model. Figure 8–24 uses the simulated flowing pressure profile at the operating point (upper valve 1.4%, lower valve 100%, WHP

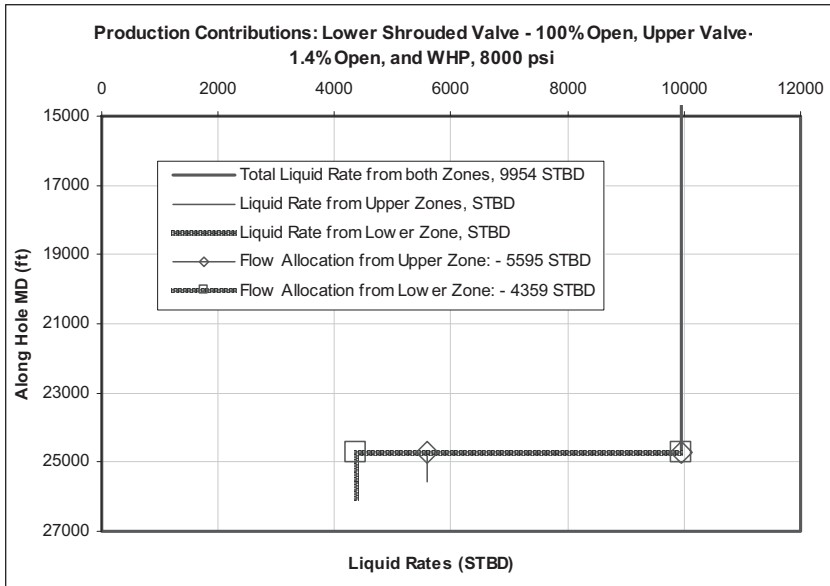


Figure 8-23 Flow contributions at the operating point (upper valve 1.4%, lower valve 100%, WHP 8000psi).

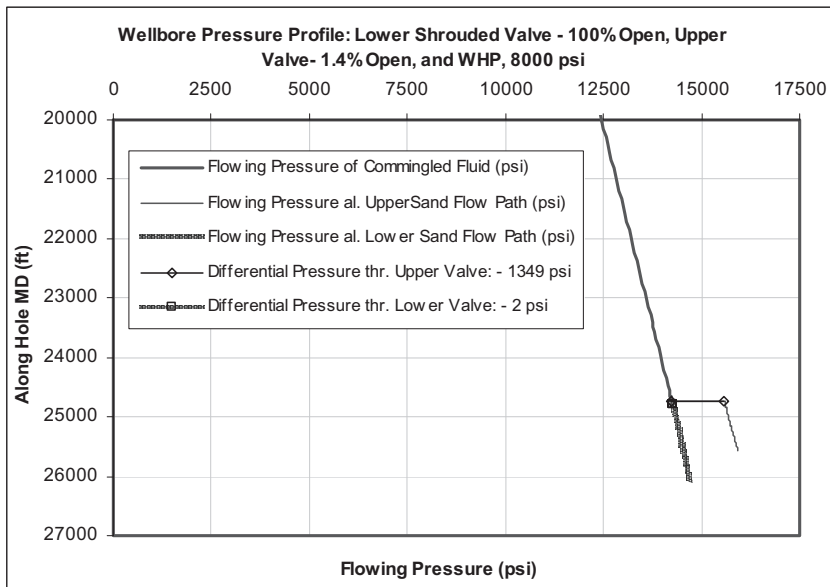


Figure 8-24 Wellbore flowing pressure profile at the recommended operating point.

8000psi) to illustrate the valve's differential pressure and tool's working pressures. Figure 8–25 presents the simulated flowing temperature profile. Figure 8–26 shows the production fluid velocity profile, which can be used for quick evaluation of erosion potential along the wellbore.

3) Compare with the Case of No Down-Hole Control

When both valves are 100% open, the condition is similar to a conventional completion, without down-hole control. Figure 8–27 illustrates the simulated result with both valves 100% open. It shows that to produce the same amount of liquid (about 9950 STB/d), the wellhead pressure needs to be increased to 8800 psi, the WLR would be 33.6%, and the contribution from the lower zone would be about 36%, thus less oil would be produced.

4) Multi-Scenario Analysis of Down-Hole Choking

To determine the effects of other upper valve choking operations on flow contribution, a multi-scenario analysis was performed. Figure 8–28 shows the results of various choking simulations (lower valve 100% open and upper valve choked) on production fluid distribution. Neglecting water production, Figure 8–29 shows the oil production contributions from each zone for the same choking operations. If 10,000 bpd is the separator's limit, then opening the lower valve fully and opening the upper valve 1.4% will maximize the total oil production rate.

8.5 Summary

This chapter gives an introduction to intelligent well systems and reviews intelligent well types. The choke equations for single liquid-phase flow, single gas-phase flow and multiphase flow are provided. The down-hole valve choke discharge coefficient is discussed. To accurately predict down-hole valve performance relationships, the values of the discharge coefficient are important, as the down-hole control valves have multi-position chokes, and different suppliers have different valve port shapes/geometries. To predict the wellbore behavior and production allocations of a multiple zone intelligent well system, a technique called integrated IPR is introduced. This concept simplifies calculation and is appropriate not only for intelligent well systems but also for multi-lateral well systems.

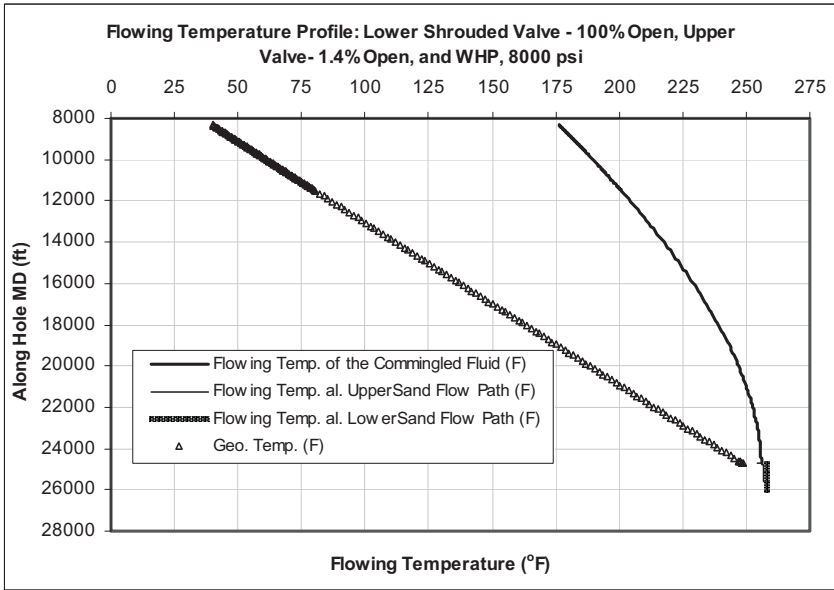


Figure 8–25 Wellbore flowing temperature profile at the recommended operating point.

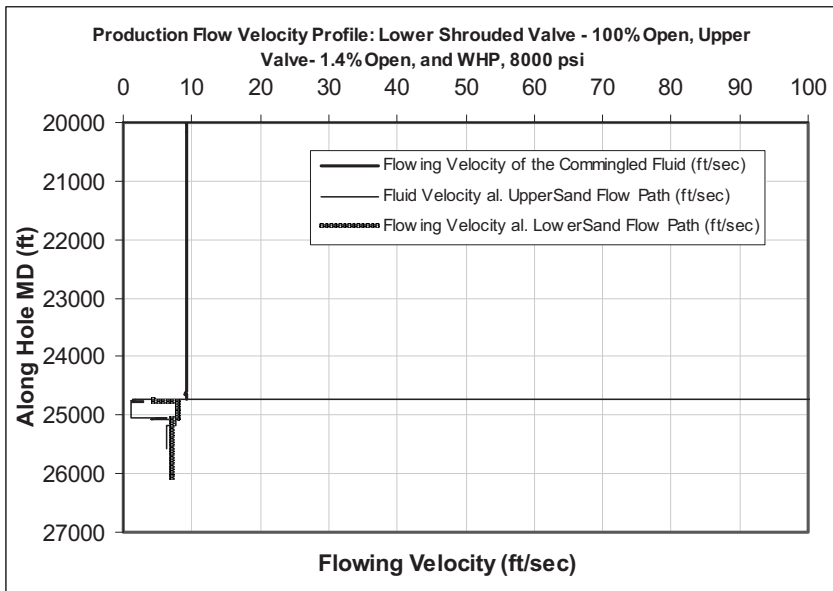


Figure 8–26 Wellbore flowing velocity profile at the recommended operating point.

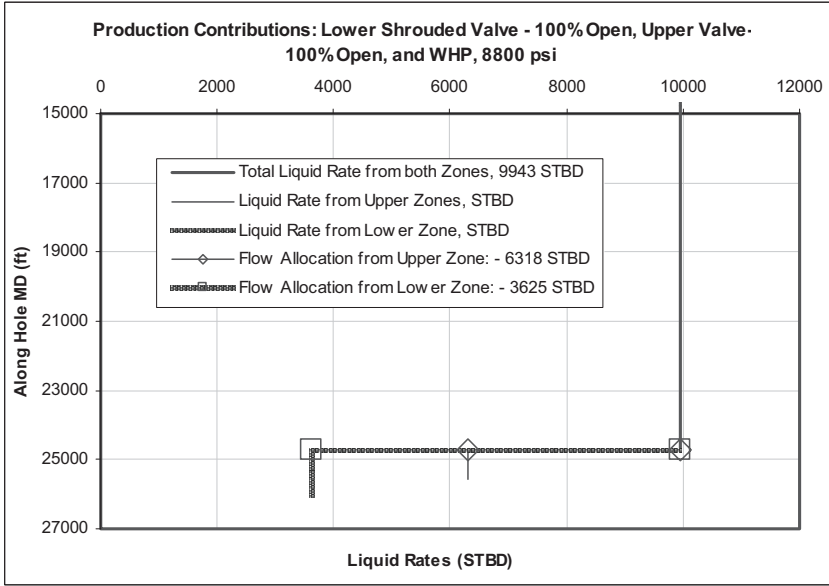


Figure 8-27 Flow contributions with both valves 100% open (WHP 8800 psi).

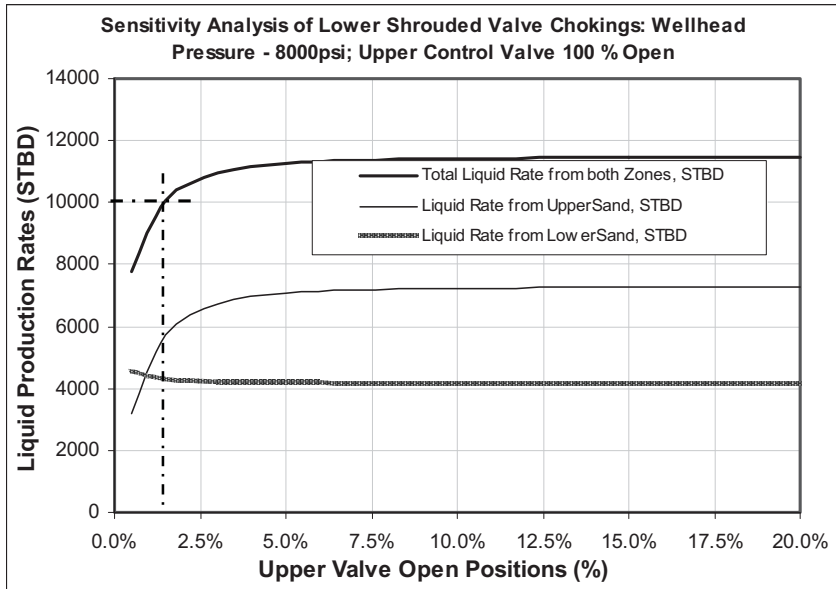


Figure 8-28 The effect of choking operations on liquid production contributions from individual zones.

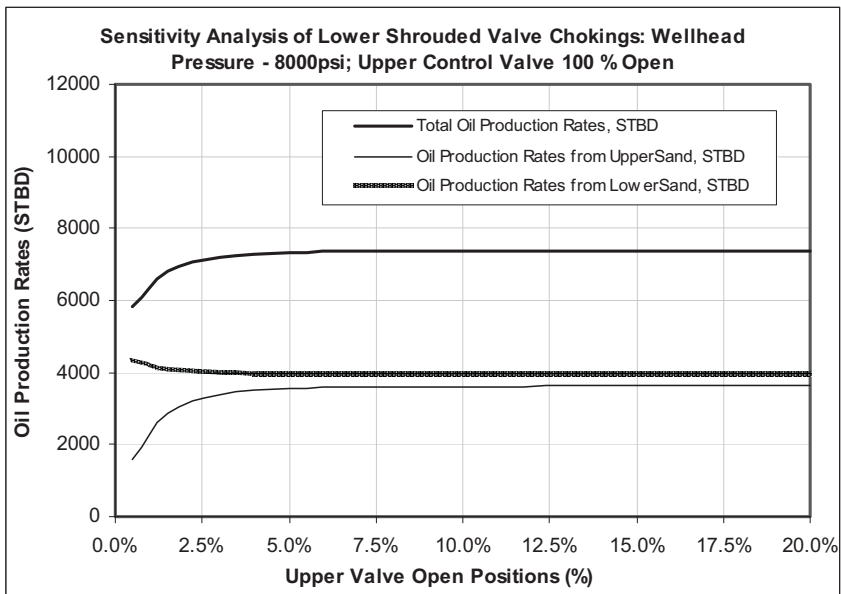


Figure 8–29 The effect of choking operation on oil contributions from individual zones.

8.6 References

Al-attar, H.H. and Abdul-Majeed, G.: “Revised Bean Performance Equation for East Baghdad Oil Wells,” *SPE Production Eng.* (February 1988): 127–131.

Ashford, F.E.: “An Evaluation of Critical Multiphase Flow Performance Through Wellhead Chokes,” *Journal of Petroleum Technology* (August 1974): 843–848.

Ashford, F.E. and Pierce, P.E.: “Determining Multiphase Pressure Drop and Flow Capabilities in Down-hole Safety Valves,” *Journal of Petroleum Technology* (September 1975): 1145–1152.

Beggs, H.D.: *Production Optimization Using NODAL Analysis*, OGTC Publications, Tulsa, OK (1991).

Bradley, H.B.: *Petroleum Engineering Handbook*, Society of Petroleum Engineers, Richardson, Texas (1987).

Brill, J.P. and Beggs, H.D.: *Two-Phase Flow in Pipes*, The University of Tulsa Press, Tulsa, OK (1978).

Brown, K.E. and Beggs, H.D.: *The Technology of Artificial Lift Methods*, PennWell Books, Tulsa, OK (1977).

Sachdeva, R., Schmidt, Z., Brill, J.P., and Blais, R.M.: "Two-Phase Flow through Chokes," paper SPE 15657 presented at the SPE Annual Technical Conference and Exhibition (5–8 October 1986), New Orleans, Louisiana.

Fortunati, F.: "Two-Phase Flow through Wellhead Chokes," paper SPE 3742 presented at the SPE European Spring Meeting (16–18 May 1972), Amsterdam, the Netherlands.

Gould, T.L.: "Discussion of an Evaluation of Critical Multiphase Flow Performance through Wellhead Chokes," *Journal of Petroleum Technology* (August 1974): 849–850.

Gould, T.L.: "Vertical Two-Phase Steam-Water Flow in Geothermal Wells," *Journal of Petroleum Technology* (August 1974): 833–42.

Guo, B. and Ghalambor, A.: *Natural Gas Engineering Handbook*, Gulf Publishing Company, Houston, Texas (2005).

Guo, B., Lyons, W., and Ghalambor, A.: *Petroleum Production Engineering—A Computer-Assisted Approach*, Elsevier, Amsterdam (2007).

Hall, K.R. and Yarborough L.: "A New Equation of State for Z-Factor Calculations," *Oil & Gas Journal* (18 June 1973): 82.

Husu, M., Niemela, I., Pyotsia J., and Simula, M.: *Flow Control Manual*, Neles-Jamesbury, Helsinki, Finland (1994).

Ikoku, C.U.: *Natural Gas Engineering*, PennWell Books, Tulsa, OK (1980).

Nind, T.E.W.: *Principles of Oil Well Production*, 2nd Edition, McGraw-Hill Book Co., New York (1981).

Osman, M.E. and Dokla, M.E.: "Gas Condensate Flow through Chokes," paper SPE 20988 presented at SPE Production Operations Symposium (23 April 1990), Oklahoma City.

Perkins, T.K.: "Critical and Subcritical Flow of Multiphase Mixtures through Chokes," paper SPE 20633 presented at the SPE 65th Annual Technical Conference and Exhibition (23–26 September 1990), New Orleans, Louisiana.

Perry, R.H.: *Chemical Engineers' Handbook*, 5th Edition, McGraw-Hill Book Co., New York (1973).

Pilehvari, A.A.: "Experimental Study of Critical Two-Phase Flow through Wellhead Chokes," University of Tulsa Fluid Flow Projects Report, Tulsa, OK (1980).

Pilehvari, A.A.: "Experimental Study of Critical Two-Phase Flow through Wellhead Chokes," University of Tulsa Fluid Flow Projects Report, Tulsa, OK (1981).

Ros, N.C.J.: "An Analysis of Critical Simultaneous Gas/Liquid Flow through a Restriction and Its Application to Flow Metering," *Applied Sci. Res.* (1960), section A (9): 374–389.

Sachdeva, R., Schmidt, Z., Brill, J.P., and Blais, R.M.: "Two-Phase Flow through Chokes," paper SPE 15657 presented at the SPE 61st Annual Technical Conference and Exhibition (5–8 October 1986), New Orleans, Louisiana.

Standing, M.B.: "A Pressure-Volume-Temperature Correlation for Mixtures of California Oils and Gases," *Drill. and Prod. Prac.*, API (1947).

Sonntag, R., Borgnakke, C., Van Wylen, G.J.: *Fundamentals of Thermodynamics*, John Wiley & Sons, New York (1998).

Sun, K., Coull, C., Constantine, J., Albrecht, K., Tirado, R. "Modeling the Downhole Choking's Impacts on Well Flow Performance and Production Fluid Allocations of a Multiple-Zone Intelligent Well System," paper SPE 113416 presented at the 2008 SPE Europec/EAGE Annual Conference and Exhibition (9–12 June 2008), Rome, Italy.

Sun, K., Konopczynski, M.R. and Ajayi, A.: "Using Down-hole Real-time Data to Estimate Zonal Production in a Commingled-Multiple-Zones Intelligent System," paper SPE 102743 presented at the 2006 SPE Annual Technical Conference and Exhibition (24–27 September 2006), San Antonio, TX.

Surbey, D.W., Kelkar, B.G. and Brill, J.P.: "Study of Subcritical Flow through Wellhead Chokes," *SPE Production Eng.* (May 1989): 103–108.

Van Wingen, N.: “Viscosity of Oil, Water, Natural Gas, and Crude Oil at Varying Pressures and Temperatures,” *Secondary Recovery of Oil in the United States*, American Petroleum Institute (1950).

Vasquez, M. and Beggs, H.D.: “Correlations for Fluid Physical Property Prediction.” *Journal of Petroleum Technology* (June 1980): 968–970.

Wallis, G.B.: *One Dimensional Two-Phase Flow*, McGraw-Hill Book Co., New York (1969).

This page intentionally left blank

Appendix A

Unit Conversion Factors

Quantity	US Field Unit	To SI Unit	To US Field Unit	SI Unit
Length	feet (ft)	0.3084	3.2808	meter (m)
	mile (mi)	1.609	0.6214	kilometer (km)
	inch (in)	25.4	0.03937	millimeter (mm)
Mass	ounce (oz)	28.3495	0.03527	gram (g)
	pound (lb)	0.4536	2.205	kilogram (kg)
	lbm	0.0311	32.17	slug
Volume	gallon (gal)	0.003785	264.172	meter ³ (m ³)
	cu.ft. (ft ³)	0.028317	35.3147	meter ³ (m ³)
	barrel (bbl)	0.15899	6.2898	meter ³ (m ³)
	Mcf (1,000 ft ³ , 60°F, 14.7psia)	28.317	0.0353	Nm ³ (15°C, 101.325kPa)
	sq.ft (ft ²)	9.29×10^{-2}	10.764	meter ² (m ²)
Area	acre	4.0469×10^3	2.471×10^{-4}	meter ² (m ²)
	sq.mile	2.59	0.386	(km) ²

Quantity	US Field Unit	To SI Unit	To US Field Unit	SI Unit
Pressure	lb/in ² (psi)	6.8948	0.145	kPa (1000 Pa)
	psi	0.068	14.696	atm
	psi/ft	22.62	0.0442	kPa/m
	inch Hg	3.3864×10^3	0.2953×10^{-3}	Pa
Temp.	F	$0.5556(F-32)$	$1.8C+32$	C
	Rankine (°R)	0.5556	1.8	Kelvin (K)
Energy (work)	Btu	252.16	3.966×10^{-3}	cal
	Btu	1.0551	0.9478	kilojoule (kJ)
	ft-lbf	1.3558	0.73766	joule (J)
	hp-hr	0.7457	1.341	kW-hr
Viscosity (μ)	cp	0.001	1,000	Pa·s
	lb/ft·sec	1.4882	0.672	kg/(m·sec) or (Pa·s)
	lbf·s/ft ²	479	0.0021	dyne·s/cm ² (poise)
Density (ρ)	lbm/ft ³	16.02	0.0624	kg/m ³
Permeability (k)	md	0.9862	1.0133	mD (=10 ⁻¹⁵ m ²)
	md (=10 ⁻³ darcy)	9.8692×10^{-16}	1.0133×10^{15}	m ²

Minimum Performance Properties of API Tubing

Nom. In.	O.D. In.	Grade	Wt. Per Ft. With Couplings, Lb.		Inside Diameter In.	Drift Diameter, In	O.D. of Upset, In.	O.D. of Cplg., In.		Collapse Resistance psi.	Internal Yield Pressure, psi	Joint Yield Strength, Lb.	
			Non-Upset	Upset				Non-Upset	Upset			Non-Upset	Upset
3/4	1.050	F-25	—	1.20	0.824	0.730	1.315	—	1.660	5,960	4,710	—	8,320
		H-40	—	1.20	0.824	0.730	1.315	—	1.660	7,680	7,530	—	13,300
		J-55	—	1.20	0.824	0.730	1.315	—	1.660	10,560	10,360	—	18,290
		C-75	1.14	1.20	0.824	0.730	1.315	1.313	1.660	14,410	14,120	11,920	24,950
		N-80	—	1.20	0.824	0.730	1.315	—	1.660	15,370	15,070	—	26,610
1	1.315	F-25	—	1.80	1.049	0.955	1.469	—	1.900	5,540	4,430	—	12,350
		H-40	—	1.80	1.049	0.955	1.469	—	1.900	7,270	7,080	—	19,760
		J-55	—	1.80	1.049	0.955	1.469	—	1.900	10,000	9,730	—	27,160
		C-75	1.70	1.80	1.049	0.955	1.469	1.660	1.900	13,640	13,270	20,540	37,040
		N-80	—	1.80	1.049	0.955	1.469	—	1.900	14,650	14,160	—	39,510
1 1/4	1.660	F-25	—	2.40	1.380	1.286	1.812	—	2.200	4,400	3,690	—	16,710
		H-40	—	2.40	1.380	1.286	1.812	—	2.200	6,180	5,910	—	26,740
		J-55	—	2.40	1.380	1.286	1.812	—	2.200	8,490	8,120	—	36,770
		C-75	2.30	2.40	1.380	1.286	1.812	2.054	2.200	11,580	11,070	29,120	50,140
		N-80	—	2.40	1.380	1.286	1.812	—	2.200	12,360	11,800	—	53,480
1 1/2	1.900	F-25	2.75	2.90	1.610	1.516	2.094	2.200	2.500	3,920	3,340	11,930	19,900
		H-40	2.75	2.90	1.610	1.516	2.094	2.200	2.500	5,640	5,350	19,090	31,980
		J-55	2.75	2.90	1.610	1.516	2.094	2.200	2.500	7,750	7,350	26,250	43,970
		C-75	2.75	2.90	1.610	1.516	2.094	2.200	2.500	10,570	10,020	35,800	59,960
		N-80	2.75	2.90	1.610	1.516	2.094	2.200	2.500	11,280	10,680	38,180	63,960

Nom. In.	O.D. In.	Grade	Wt. Per Ft. With Couplings, Lb.		Inside Diameter In.	Drift Diameter, In	O.D. of Upset, In.	O.D. of Cplg., In.		Collapse Resistance psi.	Internal Yield Pressure, psi	Joint Yield Strength, Lb.	
			Non-Upset	Upset				Non-Upset	Upset			Non-Upset	Upset
2	2.375	F-25	4.00		2.041	1.947		2.875		3,530	3,080	18,830	
		F-25	4.60	4.70	1.995	1.901	2.594	2.875	3.063	4,160	3,500	22,480	32,600
		H-40	4.00		2.041	1.947		2.875		5,230	4,930	30,130	
		H-40	4.60	4.70	1.995	1.901	2.594	2.875	3.063	5,890	5,600	35,960	52,170
		J-55	4.00		2.041	1.947		2.875		7,190	6,770	41,430	
		J-55	4.60	4.70	1.995	1.901	2.594	2.875	3.063	8,100	7,700	49,440	71,730
		C-75	4.00		2.041	1.947		2.875		9,520	9,230	56,500	
		C-75	4.60	4.70	1.995	1.901	2.594	2.875	3.063	11,040	10,500	67,430	97,820
		C-75	5.80	5.95	1.867	1.773	2.594	2.875	3.063	14,330	14,040	96,560	126,940
		N-80	4.00		2.041	1.947		2.875		9,980	9,840	60,260	
		N-80	4.60	4.70	1.995	1.901	2.594	2.875	3.063	11,780	11,200	71,920	104,340
		N-80	5.80	5.95	1.867	1.773	2.594	2.875	3.063	15,280	14,970	102,980	135,400
		P-105	4.60	4.70	1.995	1.901	2.594	2.875	3.063	15,460	14,700	94,400	136,940
		P-105	5.80	5.95	1.867	1.773	2.594	2.875	3.063	20,060	19,650	135,170	177,710
2 1/2	2.875	F-25	6.40	6.50	2.441	2.347	3.094	3.500	3.668	3,870	3,300	32,990	45,300
		H-40	6.40	6.50	2.441	2.347	3.094	3.500	3.668	5,580	5,280	52,780	72,480
		J-55	6.40	6.50	2.441	2.347	3.094	3.500	3.668	7,680	7,260	72,570	99,660
		C-75	6.40	6.50	2.441	2.347	3.094	3.500	3.668	10,470	9,910	98,970	135,900
		C-75	8.60	8.70	2.259	2.165	3.094	3.500	3.668	14,350	14,060	149,360	186,290
		N-80	6.40	6.50	2.441	2.347	3.094	3.500	3.668	11,160	10,570	105,560	144,960
		N-80	8.60	8.70	2.259	2.165	3.094	3.500	3.668	15,300	15,000	159,310	198,710
		P-105	6.40	6.50	2.441	2.347	3.094	3.500	3.668	14,010	13,870	138,550	190,260
		P-105	8.60	8.70	2.259	2.165	3.094	3.500	3.668	20,090	19,690	209,100	260,810

Nom. In.	O.D. In.	Grade	Wt. Per Ft. With Couplings, Lb.		Inside Diameter In.	Drift Diameter, In	O.D. of Upset, In.	O.D. of Cplg., In.		Collapse Resistance psi.	Internal Yield Pressure, psi	Joint Yield Strength, Lb.	
			Non-Upset	Upset				Non-Upset	Upset			Non-Upset	Upset
3	3.500	F-25	7.70		3.068	2.943		4.250		2,970	2,700	40,670	
		F-25	9.20	9.3	2.992	2.867	3.750	4.250	4.500	3,680	3,180	49,710	64,760
		F-25	10.20		2.922	2.797		4.250		4,330	3,610	57,840	
		H-40	7.70		3.068	2.943		4.250		4,630	4,320	65,070	
		H-40	9.20	9.3	2.992	2.867	3.750	4.250	4.500	5,380	5,080	79,540	103,610
		H-40	10.20		2.922	2.797		4.250		6,060	5,780	92,550	
		J-55	7.70		3.068	2.943		4.250		5,970	5,940	89,470	
		J-55	9.20	9.3	2.992	2.867	3.750	4.250	4.500	7,400	6,980	109,370	142,460
		J-55	10.20		2.922	2.797		4.250		8,330	7,940	127,250	
		C-75	7.70		3.068	2.943		4.250		7,540	8,100	122,010	
		C-75	9.20	9.3	2.992	2.867	3.750	4.250	4.500	10,040	9,520	149,140	194,260
		C-75	10.20		2.922	2.797		4.250		11,360	10,840	173,530	
		C-75	12.70	12.95	2.750	2.625	3.750	4.250	4.500	14,350	14,060	230,990	276,120
		N-80	7.70		3.068	2.943		4.250		7,870	8,640	130,140	
		N-80	9.20	9.3	2.992	2.867	3.750	4.250	4.500	10,530	10,160	159,080	207,220
		N-80	10.20		2.922	2.797		4.250		12,120	11,560	185,100	
		N-80	12.70	12.95	2.750	2.625	3.750	4.250	4.500	15,310	15,000	246,390	294,530
		P-105	9.20	9.3	2.992	2.867	3.750	4.250	4.500	13,050	13,340	208,790	271,970
P-105	12.70	12.95	2.750	2.625	3.750	4.250	4.500	20,090	19,690	323,390	386,570		

Nom. In.	O.D. In.	Grade	Wt. Per Ft. With Couplings, Lb.		Inside Diameter In.	Drift Diameter, In	O.D. of Upset, In.	O.D. of Cplg., In.		Collapse Resistance psi.	Internal Yield Pressure, psi	Joint Yield Strength, Lb.	
			Non-Upset	Upset				Non-Upset	Upset			Non-Upset	Upset
3 1/2	4.000	F-25	9.50		3.548	3.423		4.750		2,630	2,470	15,000	
		F-25		11.00	3.476	3.351	4.250		5.000	3,220	2,870		76,920
		H-40	9.50		3.548	3.423		4.750		4,060	3,960	72,000	
		H-40		11.00	3.476	3.351	4.250		5.000	4,900	4,580		123,070
		J-55	9.50		3.548	3.423		4.750		5,110	5,440	99,010	
		J-55		11.00	3.476	3.351	4.250		5.000	6,590	6,300		169,220
		C-75	9.50		3.548	3.423		4.750		6,350	7,420	135,010	
		C-75		11.00	3.476	3.351	4.250		5.000	8,410	8,600		230,760
		N-80	9.50		3.548	3.423		4.750		6,590	7,910	144,010	
N-80		11.00	3.476	3.351	4.250		5.000	8,800	9,170		246,140		
4	4.500	F-25	12.60	12.75	3.958	3.833	4.750	5.200	5.563	2,870	2,630	65,230	90,010
		H-40	12.60	12.75	3.958	3.833	4.750	5.200	5.563	4,500	4,220	104,360	144,020
		J-55	12.60	12.75	3.958	3.833	4.750	5.200	5.563	5,720	5,790	143,500	198,030
		C-75	12.60	12.75	3.958	3.833	4.750	5.200	5.563	7,200	7,900	195,680	270,030
		N-80	12.60	12.75	3.958	3.833	4.750	5.200	5.563	7,500	8,440	208,730	288,040

This page intentionally left blank

Mathematical Model for Obtaining Oil Rate Correction Factor F_o

The oil rate correction factor for wellbore friction is defined as

$$F_o = \frac{Q_{oH,Friction}}{Q_{oH,No-friction}} \quad (C.1)$$

where $Q_{oH,Friction}$ and $Q_{oH,No-friction}$ are the oil production rates predicted by mathematical models with and without considering wellbore friction. The $Q_{oH,No-friction}$ can be estimated using the inflow model of Furui et al. (2003) that was derived assuming a fully-penetrated box-shape reservoir:

$$Q_{oH,No-friction} = J_{sp,o} L(p_e - p_{wf}) \quad (C.2)$$

where

$$J_{sp,o} = \frac{7.08 \times 10^{-3} k_H}{\mu_o B_o \left\{ I_{ani} \ln \left[\frac{h I_{ani}}{r_w (I_{ani} + 1)} \right] + \frac{\pi y_b}{h} - I_{ani} (1.224 - s) \right\}} \quad (C.3)$$

and

$$I_{ani} = \sqrt{\frac{k_H}{k_V}} \quad (C.4)$$

where

L = length of drain hole, ft

p_e = reservoir pressure, psi

p_{wf} = flowing bottom-hole pressure psi

h = pay zone thickness, ft

k_H = horizontal permeability, md

k_V = vertical permeability, md

y_b = distance of boundary from drain hole, ft

s = skin face, dimensionless

B_o = oil formation volume factor, rb/stb

μ_o = oil viscosity, cp

The $Q_{oH,Friction}$ for a fully-penetrated box-shape reservoir was presented by Guo et al. (2007):

$$Q_{oH,Friction} = Q_{oc} + \frac{J_{sp,o}}{2b} \left[\frac{1}{(a + bx_c)^2} - \frac{1}{(a + bL)^2} \right] \quad (C.5)$$

where

$$Q_{oc} = 1351.34 \frac{\mu_o d_h}{\rho_o} \quad (C.6)$$

$$a = \frac{1}{\sqrt[3]{p_r - p_{wH}}} + 0.2752 C_1^{\frac{2}{3}} L \quad (C.7)$$

$$b = -0.2752 C_1^{\frac{2}{3}} \quad (C.8)$$

$$C_1 = \frac{2C_1'}{\sqrt{\frac{6g_c d_h}{f_f \rho_o}}} \quad (\text{C.9})$$

$$C_1' = \frac{0.012J_{sp.o}}{d_h^2} \quad (\text{C.10})$$

where

p_{wH} = pressure at the heel of drain hole, psi

d_h = equivalent diameter of the drain hole, in

f_f = Fanning friction factor, dimensionless

g_c = gravitational conversion factor, 32.17 lbf-ft/lbf-s²

ρ_o = oil density, lb_m/ft³

C.1 Reference

Guo, B., Zhou, J., Liu, Y., and Ghalambor, A., 2007: "A Rigorous Analytical Model for Fluid Flow in Drain Holes of Finite Conductivity Applied to Horizontal and Multilateral Wells," paper SPE 106947, presented at the SPE 2007 Production Operations Symposium in Oklahoma City, OK, held 31 March–03 April 2007.

This page intentionally left blank

Mathematical Model for Obtaining Gas Rate Correction Factor F_g

The gas rate correction factor for wellbore friction is defined as

$$F_g = \frac{Q_{gH,Friction}}{Q_{gH,No-friction}} \quad (D.1)$$

where $Q_{gH,Friction}$ and $Q_{gH,No-friction}$ are the gas production rates predicted by mathematical models with and without considering wellbore friction. The $Q_{gH,No-friction}$ can be estimated using the inflow model of Furui et al. (2003), that was derived assuming a fully-penetrated box-shape reservoir:

$$Q_{gH,No-friction} = J_{sp,g} L (p_e^2 - p_{wf}^2) \quad (D.2)$$

where

$$J_{sp,g} = \frac{k_H}{1424 \bar{\mu}_g \bar{z} T \left\{ I_{ani} \ln \left[\frac{h}{r_w (I_{ani} + 1)} \right] + \frac{\pi y_b}{h} - I_{ani} (1.224 - s) \right\}} \quad (D.3)$$

and

$$I_{ani} = \sqrt{\frac{k_H}{k_V}} \quad (D.4)$$

where

- L = length of drain hole, ft
- p_e = reservoir pressure, psi
- p_{wf} = flowing bottom-hole pressure psi
- h = pay zone thickness, ft
- k_H = horizontal permeability, md
- k_V = vertical permeability, md
- y_b = distance of boundary from drain hole, ft
- s = skin face, dimensionless
- T = reservoir temperature, °R
- \bar{z} = gas compressibility factor, dimensionless
- $\bar{\mu}_g$ = gas viscosity, cp

The $Q_{gH,Friction}$ for a fully-penetrated box-shape reservoir was presented by Guo et al. (2007):

$$Q_{gH,Friction} = \frac{3J_{sp}p_r}{\left(\frac{3}{C}\right)^{2/3}} \left\{ 2[F_1(z_0) - F_1(z)] - [F_2(z_0) - F_2(z)] \right\} \quad (D.5)$$

where

$$z = \frac{p_e}{3} \left[C_2 - \left(\frac{3}{C}\right)^{2/3} L \right] \quad (D.6)$$

$$z_0 = \frac{p_e C_2}{3} \quad (D.7)$$

$$F_1(z) = 3^{-1/3} \left\{ \begin{aligned} &\log(z + 3^{-1/3}) - \frac{1}{2} \log(z^2 - 3^{-1/3}z + 3^{-2/3}) \\ &+ 3^{1/2} \arctan \left[\frac{3^{1/2}}{3} (2 \times 3^{1/3}z - 1) \right] \end{aligned} \right\} \quad (D.8)$$

$$F_1(z_0) = 3^{-1/3} \left\{ \begin{aligned} &\log(z_0 + 3^{-1/3}) - \frac{1}{2} \log(z_0^2 - 3^{-1/3}z_0 + 3^{-2/3}) \\ &+ 3^{1/2} \arctan \left[\frac{3^{1/2}}{3} (2 \times 3^{1/3}z_0 - 1) \right] \end{aligned} \right\} \quad (D.9)$$

$$F_2(z) = 2F_1(z) + \frac{3z}{3z^3 + 1} \quad (D.10)$$

$$F_2(z_0) = 2F_1(z_0) + \frac{3z_0}{3z_0^3 + 1} \quad (D.11)$$

$$C = \frac{140.86}{J_{sp}} \sqrt{\frac{p_{wH} d_h^5}{f_f \gamma_g T}} \quad (D.12)$$

$$C_2 = \left(\frac{3}{C} \right)^{2/3} L + \frac{3}{p_e} \left(\frac{p_e - \frac{1}{3}(p_e - p_{wH})}{p_e - p_{wH}} \right)^{1/3} \quad (D.13)$$

where

p_{wH} = pressure at the heel of drain hole, psi

d_h = equivalent diameter of the drain hole, in

f_f = Fanning friction factor, dimensionless

g_c = gravitational conversion factor, 32.17 lbf-ft/lbf-s²

γ_g = gas specific gravity, air = 1.

D.1 Reference

Guo, B., Zhou, J., and Ghalambor, A, 2007: “Effects of Friction in Drain Hole on Productivity of Horizontal and Multilateral Wells,” paper SPE 106948, presented at the SPE 2007 Asia Pacific Oil and Gas Conference & Exhibition (APOGCE) in Jakarta, Indonesia, held 30 October–01 November 2007.

Index

C

- Choking valve 250, 263
- Christmas Tree 8–9
- Commingled production 249, 293–300
- Cullender and Smith method (1959) 152–153
Katz et al. (1959) 152

D

- Darcy's law 48, 67
- Darcy-Wiesbach (Moody) friction factor 149
- Discharge coefficient 263, 264
- Down-hole-choking 300

F

- Fanning friction factor 120–122, 135, 142
Chen (1979) 122
- First Law of Thermodynamics 120, 147
- Flow regimes 50, 127, 226, 275
diagnostic derivatives 54
horizontal linear flow 51, 53

- horizontal pseudo-linear flow 52
- horizontal pseudo-radial flow 52
- horizontal radial flow 50
- vertical radial flow 52

- Formation water 180
- Four-phase flow 132, 225
- Fractured wells 70, 73
Argawal et al. (1979) 71
bilinear flow 75
Cinco-Ley and Samaniego (1981) 71, 72, 73
fracture conductivity 72
Guo and Schechter (1999) 75
Valko et al. (1997) 73
- Free gas quality 285

G

- Gas cap 256
- Gas compressibility 38
- Gas compressibility factor 280
Brill and Beggs's correlation (1974) 32–34
deviation factor 30
z-factor 30–35, 285
- Gas density 35

Gas expansion factor 38
Gas viscosity 28
 Carr, Kobayashi, and
 Burrows (1954) 28
 Dean-Stiel (1958) 30
 Dempsey (1965) 29
 dynamic viscosity 28
 kinematic viscosity 28
 Lee-Gonzalez-Eakin (1966)
 30
Griffith correlation 143
Guo's mist-flow model 237

H

Hagedorn-Brown correlation
 222, 237
Hagedorn-Brown method
 (1965) 138, 142,
 144, 158
Horizontal wells 76, 189
 Economides et al. (1991) 76
 gas wells in volumetric
 reservoirs 201
 Guo et al. (2007) 76
 ICD model 197
 inflow control devices 195
 Joshi (1988) 76
 oil wells in volumetric
 reservoirs 190
 oil wells in water or gas-
 coning reservoirs
 192

I

Inflow performance relationship
 36, 63, 77, 78, 90,
 162, 230, 234, 292,
 295
 composite IPR 99
 Fetkovich's equation 95
 future IPR 106
 Fetkovich's method 108
 Vogel's method 106
 integrated IPR 293, 295,
 297
 partial two-phase oil
 reservoir 87, 91
 productivity index 91, 100,
 103
 reservoir inflow models 78
 single phase reservoir 78,
 80
 stratified reservoir 98
 test points 78, 90
 two-phase reservoir 84, 95
 Bandakhlia and Aziz
 (1989) 84
 Chang (1992) 84
 Fetkovich (1973) 84, 85
 Retnanto and
 Economides (1998)
 84
 Standing (1971) 84
 Vogel (1968) 84, 85
 Vogel's IPR model 87, 95,
 101
Intelligent well system
 auto-gas-lift 256
 basic components 247

cash flow profile 249
 choke discharge coefficient
 263
 classifications 250
 control valve coefficient 262
 cross-flow 297
 down-hole flow control
 valves 247, 248,
 257–258, 263, 275,
 277
 economic value 249
 electric submerge pump 254
 multiphase choke flow 284
 multiphase flow 275–277
 Gilbert correlation 276
 See also Perkins' model
 (1990)
 See also Sachdeva's
 model (1986)
 See also Sun et al.'s
 modified model
 (2006)
 pressure drop 258
 single-phase choke flow
 269
 single-phase gas flow 264
 single-phase liquid flow
 260
 temperature drop 267
See also shroud-unshroud
 valve configuration

J

Joule-Thomson cooling effect
 267–268

K

Klinkenberg effect 48

L

Linear flow 217, 218, 221
 Liquid loading 176–183
 annular flow 177
 entrained droplet movement
 model 177–178
 Guo's method (2006)
 180–181
 slug flow 177
 solutions 177
 transport velocity 181
 Turner et al. (1969) 177

M

Mass flux 265
 Mist flow in gas wells 154
 Multi-fractured horizontal wells
 217–218
 drainage area shape 220
 Furui (2003) 221, 225
 gas wells 224
 Guo and Schechter (1997)
 224
 Guo and Yu (2008) 218
 Li et al. (1996) 218
 oil wells 218
 Raghavan and Joshi (1993)
 217

Multilateral wells 226
fishbone wells 226–230
Furui et al.(2003) 228
mixed properties of fluids
237
pseudolinear-radial-
combined model
226
root wells 226, 234–237

Multiphase flow 127
Brown (1977) 128
Guo and Ghalambor (2002)
131
liquid holdup 127, 138–142
models 295
Poettmann and Carpenter
(1952) 129, 131
through down-hole flow
control valves 275
TPR models 128
homogeneous-flow
models 128
separated-flow models
128, 136
See also flow regimes

N

Natural gas properties 22–39
gas compressibility 38
gas compressibility factor
30
gas density 35
gas formation volume factor
36
gas expansion factor 38

gas pseudocritical pressure
and temperature
24–27
Wichert-Aziz (1972)
correction 27
gas specific gravity 22
mixing rule 24
gas viscosity 28
NODAL analysis 11, 161, 162,
292, 293
Non-Darcy flow coefficient 221

O

Oil properties 16–22
compressibility 21
density 18–19
formation volume factor
19–20
solution gas-oil ratio 16–18
viscosity 20–21, 84
gas-saturated crude oil
21
undersaturated crude oil
21
Outflow performance
relationship 162

P

Perkins' model (1990) 276,
280–283
Permeability 98
Petroleum fluids, hydrocarbons
15

Pressure continuity 161
Pressure discontinuity 260
Pressure drop 262
Pressure funnel 66, 67, 68, 106
Produced water properties
 39–41
 compressibility 41
 density 39
 formation volume factor 40
 salinity 39
 specific gravity 39
 viscosity 40
Pseudopressure 171
Pseudosteady-state flow 67, 69,
 76, 84

R

Radial flow 217, 218, 221, 226
Reservoir 1–5
 dissolved-gas drive 4
 gas-cap drive 3
 segment 1
 simulators 10
 water-drive 2
Reservoir deliverability 63, 77,
 106
Reservoir influx model 195
 Economides (1991) 196
 Furui (2003) 196
 Papatzacos (1987) 195
Reservoir properties 45
 lithology 45
 carbonate rocks 46
 igneous rocks 46
 metamorphic rocks 46

 sedimentary rocks 45
 pay zone 45, 162, 168, 226
 porosity 46
 reservoir permeability 48
 effective permeability
 48, 50
 relative permeability 49,
 50
 total compressibility 47

S

Sachdeva's model (1986)
 276–280
Shroud-unshroud valve
 configuration 250,
 254
Single-phase flow 2, 3, 67, 87,
 100, 120, 260
 gas 147
Skin factor 56, 73
Sonic flow 260, 266, 276
Standard temperature and
 pressure 16, 17
Steady-state flow 67, 76
Subsonic flow 260, 265, 276
Sun et al.'s modified model
 (2006) 283

T

Three-phase flow 280, 283
Transient flow 64, 76
 Dake (1978) 64
 Earlougher (1977) 66

Tubing performance relationship
119, 222, 225, 230,
236
Tubing string 6, 8, 147, 149,
250
Katz and Lee (1990) 149
temperature and
compressibility 148
Two-phase flow 2, 84, 101, 108
partial 102

V

Vertical well 64, 162

W

Wellbore 5, 11, 226
lateral bores 226, 234

performance 119, 292
Well deliverability 292
Well productivity 10, 11, 12,
50, 161, 162, 205,
226, 247
Chaperon (1986) 170, 192
gas wells in volumetric
reservoirs 171
nodes 161, 162, 293
oil wells in volumetric
reservoirs 162
oil wells in water or gas-
coning reservoirs
168
single-fractured wells
185–188
transient production 171
See also horizontal wells
Well string 119
Wellhead 6, 11
See also Christmas Tree